

Heterocyclic-Based 1,2-Dithiolate Ligands and Their Coordination Complexes with Transition Metals: Synthesis, Characterization and Functional Properties

**A Thesis Submitted for the degree of
Doctor of Philosophy**

By

Ramababu Bolligarla



**University of Hyderabad
Hyderabad 500 046
Andhra Pradesh
India**

June, 2011

అమ్మ, నాన్న

మరియు

గురువులకి అంకితం.....

CERTIFICATE

Certified that the work contained in the thesis entitled **“Heterocyclic-Based 1,2–Dithiolate Ligands and Their Coordination Complexes with Transition Metals: Synthesis, Characterization and Functional Properties”** has been carried out by Mr. Ramababu Bolligarla under my supervision and the same has not been submitted elsewhere for a degree.

Prof. Samar K. Das
(Supervisor)

Dean
School of Chemistry

University of Hyderabad
June, 2001

Statement

I hereby declare that the matter embodied in the thesis is the result of investigation carried out by me in the School of Chemistry, University of Hyderabad, Hyderabad, India, under the supervision of **Prof. Samar K. Das**.

In keeping with the general practice of reporting scientific observations, due acknowledgements have been made wherever the work described is based on the findings of other investigators. Any omission, which might have occurred by oversight or error, is regretted.

Ramababu Bolligarla

University of Hyderabad

June, 2011

Acknowledgements

I express my deep sense of gratitude and profound thanks to my supervisor **Prof. Samar K. Das** for his valuable guidance, patience, encouragement, and for the freedom he gave me in carrying out research. His optimistic approach towards every aspect was admirable and inspiring. Throughout my Ph.D tenure, he is always approachable, helpful, friendly and extremely tolerant. I consider my association with him as a cherishable memory in my life.

I take this opportunity to thank Prof. M. V. Rajasekharan, Dean, School of Chemistry for providing us the facilities needed for our research. I extend my sincere thank to former Deans Prof. D. Basavaiah and Prof. M. Periasamy, and all the faculty members, School of Chemistry for their co-operation on various aspects.

I am deeply indebted to Prof. S. Pal for his suggestions and allowing me to perform studies using the electrochemical facilities for my doctoral work.

It is great pleasure to thank my lab seniors Dr. V. Shivaiah, Dr. S. Supriya, Dr. V. Madhu (for initiating my work and valuable suggestions), Dr. Raghavaiah, Dr. C. H. Pradeep, Dr. Prabhakar, Dr. Arumuganathan, and Dr. Tanmay for their help, pleasant company, and cooperation during my Ph.D. tenure. From the bottom of my heart I thank to my friends and labmates Srinivas, GDP garu, Bharat (baru), Kishore for their support throughout the tenure. Without their help and encouragement it is not possible to complete the work. I wish to thank my juniors Mrs. Monima, Mrs. Sridevi garu, Mr. Veeranna, and Ms. Paulami for their cooperation, help, and creating cheerful work atmosphere. I thank to my project students Ragavaiah, Lavanya, Swathi, Sunitha, Sreenivas(ugc) and Venkateswarulu to work with me and helping to complete my thesis work. I further thank to project students Arti, Dhanabal, Nagaraju for their pleasant presence.

I also thank all the non-teaching staff of the School of Chemistry and COSIST for their assistance on various occasions. It's my privilege to acknowledge Mr. Shetty and Mr. A. R. Shetty for timely supply of chemicals, Mr. Vara Prasad for all his art with glass blowing, Mr. Satyanarayana, and Mr. Bhaskar Rao for their excellent job with NMR spectra and LC-MS spectra, Mr. Ramana helping in XRD room, and Ms. Asia Parwez for her tireless effort for collecting IR spectra. I would like to thank office staff Durgesh, Jayaram, Sharma, Sai, lab assistant Venky(NMR) and Krishna Rao(security guard)for

helping me at various occasions. The assistance of Dr. Manjunath and Mr. Suresh (EPR) are gratefully appreciated. A special note of thanks to Dr. P. Raghavaiah for teaching me the fundamentals of X-ray crystallography and helping me to solve the various crystallography problems.

I would like to acknowledge Prof. P. Someswara Rao, Prof. S. Murthy, Prof. A.V. Prasada Rao, Prof. GNR and Dr. Vani Madam, and all my teachers during my Post graduation at Andhra University, Visakhapatnam, and also thankful to all my teachers in graduation and under graduation studies especially NVC sir who is creating interest to study in chemistry, at C. R. Reddy college, Eluru and their suggestions, advice and timely guidance regarding higher studies.

I take this opportunity to thank all my school teachers, especially for their wonderful teaching, encouragement, kindness, and affection.

I feel fortunate to have friends Kondalu, Yesu, DK who have been good friends over the years, for keeping me sane, giving me perspective and who have made the time more enjoyable.

I am lucky enough to have the support of many School of Chemistry friends and colleagues Ramesh garu, Dr. Krishna kishore anna, Satish babai, Naga Raju(maya), Mallesh, NagaRaju (MP lab), Chaitanya, M. Ramu, Dr. Phani Pavan, Anjaneyalu, Ram Suresh, Dr. Venu Srinivas, Sanjeev, Ravi, Vikram, Vijji, P. Kishore, Anand, Kalyan, Santhosh, Balu, Narayana, Chandrasekhar, Ajay, Nagarjuna(VB lab), Gupta, Hari, John (Srinivas), Karunakar, Ramu Yadav, Mallesh, Bhanu, Shesu, Rama Krishna, Venu, Suresh, Madhu, Ramaraju, Ramesh, Anish, Sekhar Reddy, Ganesh, Vignesh, Praveen, Dr. Arindam, Dr. Arun Babu, Malakappa, Swami, Krishna Charry, Dr. Bijju, Dr. Bhargavi, Dr. Jagadish anna, Dr. Bipul, Ranjith, Naba, Palash, Suryanarayana, Rajesh, Ashok, Chandu, Dr. J. P. anna, Dr. Abijit, Dr. Rajesh, Balaswamy, Dr. Narahari anna, Tirupathi Reddy, Pavan, Yaseen, Dr. Bhuvan anna, Sajna, Ramesh, Gangadhar, Srinu, Nagarjuna reddy, Dr. Ramesh Reddy anna, Dr. Aravind, Sekhar Reddy, Satpal, Santosh, Mallikarjun, Guru Braham, Dr. Satish, Dr. Sivaranjan Reddy, Rajgopal Sr., Rajgopal Jr., Dr. Kishore anna, Dr. Ramkumar, Narayana, Rumpa, Vijendhra Reddy, Chary, Bharani, Shivaprasad, Srinivas Reddy, Ganesh, Srinivas(RB lab), Raveendra Babu, Vanaja, Naveen, Sandip, Tradib, Sasi, Basik, Pramithi exceptionally generous in helping me at various occasions.

I would like to acknowledge the NRS hostelmates chairman (phalgun), Sudhakar garu, Sanjeev, Anil, GK, for making the hostel life more memorable.

I specially thank my M.Sc. classmates Rajesh, Anji, Sudhakar, Maheendra garu, Srinivas, Suryakumari, Indirapriya, Suresh, Malayadri, Subbarao, Pardhasarthy, Nageswararao, Venkatarao, and AU seniors Ramu garu, Johnpaul, Asiri naidu, Charan, Harikrishna, Sunil, Phaneendra Sai, and AU juniors Rajesh, Phaneendra, Narisimha, Gopal, Raghavendra, Ravikiran, Ravibabu, Chiranjeevi, Anand, KLN Rao for the memorable moments which I have shared with them.

I would like to thank my B.Sc. and Intermediate friends Yesu, Srinu, Bandodu, srinu bondu, Subbarao, Parusuram. I should also thank my school friends Prasad, Vamsi, Satyanarayana, Maruthi Prasad, Sugasani, Narisimha Rao, Kasulu, kasu annaya. I also like to thank to my friends Srinu(bammardhi), Suryakumari, pandu, for their memorable presence in my life.

It is great pleasure to thank my Grandfather, grandmother, amamma and all of my family members for their support and affection throughout my life. I would take this opportunity to thank my sisters, brothers, brother-in-laws and their families for their love and support.

Most of all, I would like to thank my parents, for their absolute confidence in me. The knowledge that they will always be there to pick up the pieces is what allows me to repeatedly risk getting shattered. All my achievements are the outcome of my parent's encouragements and blessings.

Last but not least, I thank DST funded National Single Crystal X-ray Diffraction Facility, UGC / UPE for providing the basic requirements and CSIR for the financial support.

Ramababu Bolligarla...

University of Hyderabad

June, 2011

CONTENTS

	Page No.
Statement	i
Certificate	ii
Acknowledgements	iii
Synopsis	vii
Chapter 1:- Introduction	
1.1. Dithiolene Ligands and its Electronic Structure	1
1.2. Nomenclature	1
1.3. Classification of Dithiolenes	2
1.4. Metal 1,2–Dithiolene Complexes and its Classification	4
1.5. Properties and Applications of Metal 1,2–Dithiolene Complexes	6
1.5.1. Electrochemical Properties and Chemical Reactivity	7
1.5.2. Luminescence and Photochemical Properties	9
1.5.3. Photo-isomerization of Metal Dithiolenes	17
1.5.4. Solid-State Properties	18
1.5.5. Metal Dithiolene Complexes in Catalysis	32
1.6. Metal 1,2-Dithiolenes in Biology	33
1.7. Motivation of the Present Work	36
1.8. References	38
Chapter 2:- Self-Assembly of Alkali Metal Based Coordination Polymers of Metal Bis(Dithiolene) Complexes: Role of Coordinated Crystallizing Solvents and Counter Cations in Tuning the Structural Diversity and Dimensionality	
Abstract	47
2.1. Introduction	47
2.2. Experimental Details	49
2.3. Result and Discussion	
2.3.1. Synthesis and Spectroscopic Characterization	55
2.3.2. Electrochemical Studies	58

2.3.3. Description of Crystal Structures	59
2.4. Conclusion	90
2.5. References	91
Chapter 3:- New Square-Planar Metal-Bis(1,2-Dithiolene) Complexes Based on 2,1,3-Benzenethiadiazole-5,6-dithiolate ($\{btdt\}^{2-}$) ligand and Nickel Trans-disulfinate Complex: Synthesis, Crystallography and Properties	
Abstract	97
3.1. Introduction	97
3.2. Experimental Details	100
3.3. Results and Discussion	
3.3.1. Synthesis and Characterization	103
3.3.2. Electronic Absorption Spectroscopy	106
3.3.3. Electrochemical Studies	111
3.3.4. X-ray Crystallographic Studies	113
3.4. Conclusion	125
3.5. References	129
Chapter 4:-Acid-Base Behavior of a Simple and Nitrogen Rich Metal Bis(Dithiolene) System: Syntheses, Crystal Structures and Spectroscopy of $[Bu_4N]_2[M^{II}(ppdt)_2]$ ($M = Ni, Pt$; $\{Ppdt\}^{2-} = \text{Pyrido}[2,3-b]\text{pyrazine-2,3-dithiolate}$)	
Abstract	133
4.1. Introduction	133
4.2. Experimental Details	135
4.3. Results and Discussion	
4.3.1. Synthesis and Characterization	138
4.3.2. Electronic Absorption Spectra	138
4.3.3. Emission Spectra	144
4.3.4. Determination of Basicity Constants	146
4.3.5. Electrochemistry	147
4.3.6. X-ray Crystallographic Studies	148
4.4. Conclusions	152

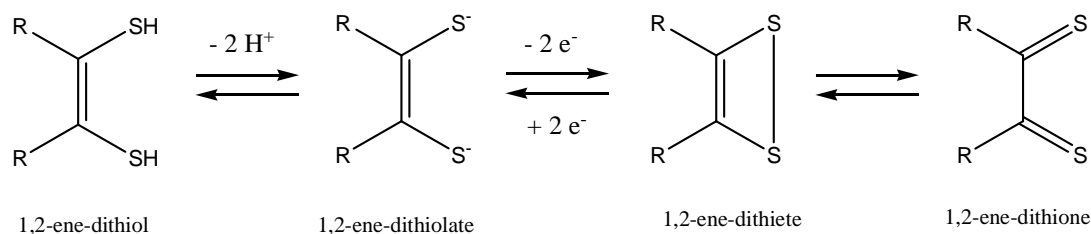
4.5. References	155
Chapter 5:- Nature of the Substituent Influences the Electronic and Electrochemical Properties of New Square-Planar Nickel-Bis(Quinoxaline-6,7-dithiolate) Complexes and Comparison of These Properties with Those of Existing [Bu₄N]₂[Ni(qdt)₂] (Qdt = Quinoxaline-2,3-dithiolate): Synthesis and Crystallographic study	
Abstract	157
5.1. Introduction	157
5.2. Experimental Details	159
5.3. Results and Discussion	
5.3.1. Synthesis and Characterization	167
5.3.2. Electronic Absorption Spectroscopy	169
5.3.3. Electrochemical Studies	174
5.3.4. X-ray Crystallographic Studies	176
5.4. Conclusion	192
5.5. References	193
Chapter 6:- Synthesis of New Intramolecular Charge Transfer A–D–A Tetrathiafulvalene-Fused Triads Exhibiting Large Solvent Sensitive Emission Behavior	
Abstract	197
6.1. Introduction	197
6.2. Experimental Details	199
6.3. Results and Discussion	
6.3.1. Synthesis and Spectroscopic Characterization	204
6.3.2. Electronic Spectra	206
6.3.3. Electrochemistry	209
6.3.4. X-ray Crystallographic Studies	211
6.4. Conclusion	217
6.5. References	218
Future Scope of the Present Thesis	223
List of Publications	227

Introduction and Motivation of the Present Work: A General Overview on Metal 1,2-Dithiolene Chemistry

1 Chapter

1.1. Dithiolene Ligands and its Electronic Structure

Dithiolene ligands are unsaturated bidentate ligands, in which the two donor atoms are sulfur. Dithiolene ligands can exist in three different forms (depending upon their oxidation states). They are the dianionic “ene-1,2-dithiolate”, the neutral “1,2-dithioketone or 1,2-dithione” and a monoanionic radical intermediate “1,2-ene-dithiete” between the dianionic and neutral forms as shown in Scheme 1.1. Dithiolene ligands are referred as non-innocent ligands. This is because when a dithiolene ligand is complexed to a metal center, the oxidation state of the ligand (and therefore the metal center) cannot be easily defined.



Scheme 1.1. The resonance forms of dithiolene ligand.

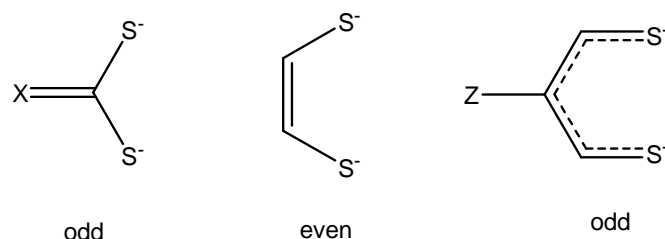
1.2. Nomenclature

In the naming of “dithiolene” there is considerable unpredictability, within in the literature, which is generally decided by the substituent(s) on dithiolene and the oxidation state of the concerned metal.¹ The term dithiolene was initially introduced by McCleverty and co-workers² and Balch *et al.*³ to give a general name for the ligand that does not specify a particular oxidation state. After that, this suggestion was generally accepted, and “dithiolene” is now universally accepted term. The general formula of 1,2-dithiolate dianion is $\text{R}_2\text{C}_2\text{S}_2^{2-}$. Nomenclature, such as, 1,2-ethenedithiolate or 1,2-benzenedithiolate as base terminology is useful as a reliable naming practice for the free ligands. However, the term dithiolate does not specify that dithiolenes are different from saturated 1,2-

dithiolate ligands and does not group structures that have related electronic configurations and bonding tendencies. This 1,2-dithiolene can also be described by different nomenclatures such as 1,2-alkenedithiol or 1,2-dithiete or 1,2-dithione depending on the oxidation states. This concept can be expressed by the Scheme 1.1.

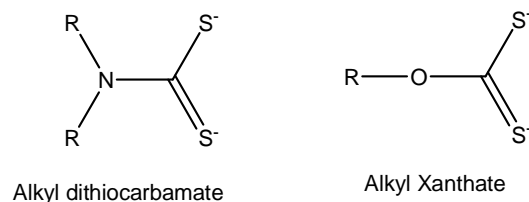
1.3. Classification of Dithiolenes

The unsaturated dithiolato ligands have been divided into groups of having odd and even numbers of π -orbitals, respectively.

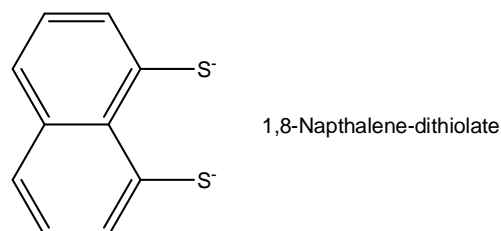


This classification results in the recognition three unique classes: 1,2-dithiolates (even), 1,1'-dithiolate (odd) and 1,3-dithiolates (odd).

1,1'-dithiolates

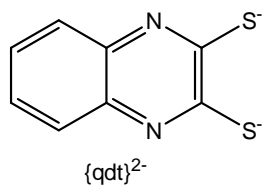


1,3-dithiolates

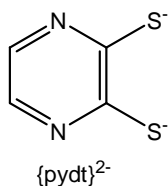


1,2-dithiolates

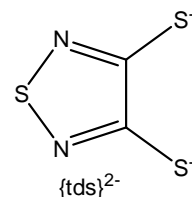
There is a considerable interest in the 1,2-dithiolate ligands and more number of 1,2-dithiolate ligands are reported in the literature.^{1a} Due to the broad range of 1,2-dithiolene in the literature, these can be further classified into following categories.

Arene-1,2-dithiolates

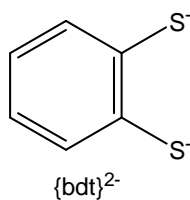
Quinoxaline-2,3-dithiolate



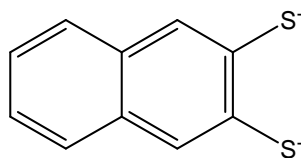
Pyrazine-2,3-dithiolate



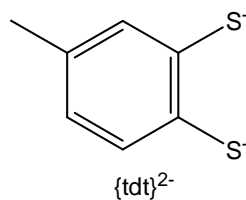
2,1,3-Thiadiazole-4,5-dithiolate



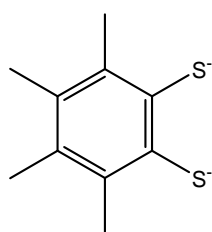
Benzene-1,2-dithiolate



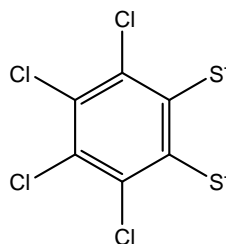
Naphthalene-2,3-dithiolate



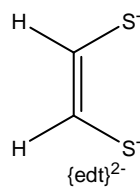
Toluene-3,4-dithiolate



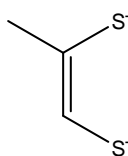
Toluene-3,4-dithiolate



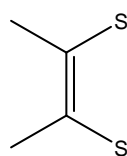
Toluene-3,4-dithiolate

Alkene-1,2-dithiolates

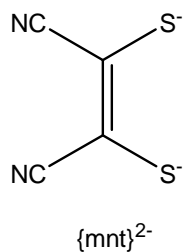
Ethene-1,2-dithiolate



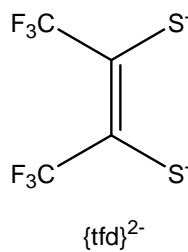
Propene-1,2-dithiolate



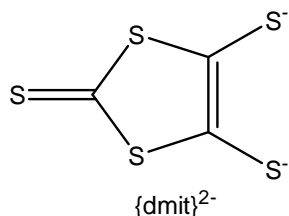
But-2-ene-2,3-dithiolate

Inorganic-1,2-dithiolates

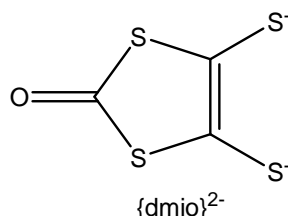
1,2-Malonitrile-1,2-dithiolate



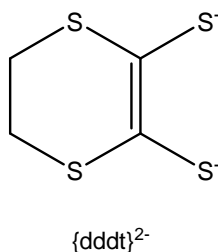
1,2-Bis(trifluoromethyl)ethylenedithiolate



1,3-Dithiole-2-thione-4,5-dithiolate



1,3-Dithiole-2-one-4,5-dithiolate

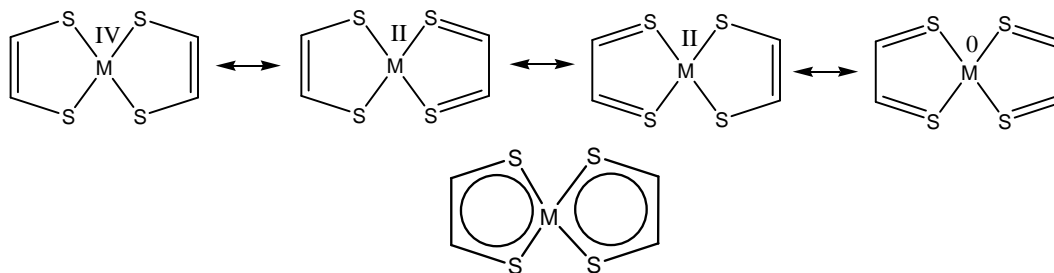


5,6-Dihydro-1,4-dithiine-2,3-dithiolate

1.4. Metal 1,2–dithiolene Complexes and its classification

Metal dithiolene complexes are known to exhibit a non-innocent character originating from these quasi-aromaticity and strong π –electron donor ability due to the involvement of sulfur atoms. Consequently, the rational development of 1,2–dithiolene based transition metal complexes are of current interest. However, the work had been done before 1960s to determine the metal quantification in the quantitative analysis. The modern era of dithiolene research was started in the early of 1960s with contributions from three research groups, namely, Schrauzer and co-workers,⁴ Gray and co-workers⁵ and Davison-Holm and co-workers.⁶ First they established that the square-planar nature, redox activity, and broad scope of the highly colored bis(dithiolene) complexes of late transition metals, such as Fe, Co, Rh, Ir, Ni, Pd, Pt, Cu, Au and Zn. Later on, this area became further interested in the synthesis and structural characterization of tris and tetrakis(dithiolene) complexes, whereby, their geometries were established by Eisenberg and Ibers.⁷ In the last three decades, remarkable progress in the research of this area arose because of their immense contributions in the areas of materials science, enzymology, analytical science and reactivity, which broadened the impact and importance of dithiolene chemistry. Metal dithiolene complexes are often exist in numerous oxidation states. This is due to the more delocalized nature of dithiolene ligands. The oxidized dithiolene complexes have relatively more 1,2-dithioketone character. In reduced complexes, the ligand assumes

more ene-1,2-dithiolate character. These descriptions are evaluated by examination of differences in C–C and C–S bond distances.



Scheme 1.2. Various bonding description of $M(\text{dithiolene})_2$ complexes.

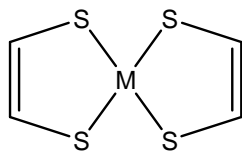
Many characteristics of dithiolene compounds can be rationalized in terms of the structure and bonding of the bidentate S-chelate of the dithiolene ligand. Distinct from saturated 1,2-dithiolate ligands, dithiolene ligands form relatively rigid and roughly planar five membered rings with considerable electronic flexibility in the relevant complexes. The Scheme 1.2 represents various bonding descriptions of a representative complex, in which the formal oxidation states of the metal and ligand vary. Such electronic versatility may make it difficult to establish, by examination, a bonding description of a dithiolene complex. However, bond distances, such as the S–C lengths, have been used as indicator of the electronic configuration of a dithiolene complex.^{2d} The long S–C distances of ~ 1.77 Å are characteristic of ligand bonding in the dithiolate form; and the short S–C distances, as low as ~ 1.64 Å, are more characteristic of dithione bonding. The dithiolene ligand π orbitals interact with the $d\pi$ orbitals of metal to give frontier orbitals of mixed–ligand and –metal character. Both bis- and tris-dithiolene complexes exhibit a certain degree of aromaticity.

Classification

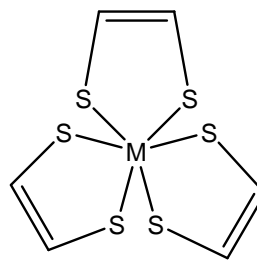
Although various dithiolene complexes have been developed so far, to our knowledge, they are classified into three main categories:

(a) Homoleptic dithiolene complexes: In this case, the coordinating ligand is 1,2-dithiolene.⁸ These are further classified into metal bis(1,2-dithiolene) with square-planar ($M = 8\text{--}10$ metals) or tetrahedral geometries ($M = 10\text{--}11$ metals), and metal tris(dithiolene) complexes with trigonal prismatic geometries ($M = 5\text{--}7$ metals) or octahedral geometries

(M = 4, 7–9 metals). New tetrakis(dithiolene) complexes (M = Ce, U) were recently prepared by Fourmigue's and Duval's groups.⁹

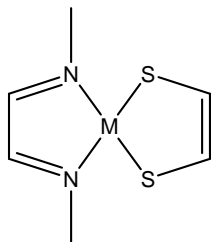


Metal bis(dithiolene)

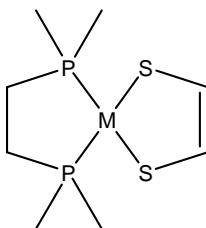


Metal tris(dithiolene)

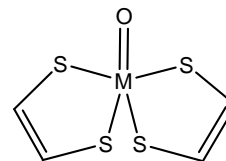
(b) Heteroleptic dithiolene complexes: It has a dithiolene and other inorganic ligands. The typical examples are the square-planar luminescent [(N \wedge N)M(dithiolene)] (M = Pt, N \wedge N = diimine),¹⁰ [(P \wedge P)M(dithiolene)] (M = Pt, P \wedge P = diphosphine)¹¹ and [oxo-M(dithiolene)₂] (M = Mo, W) complexes.¹²



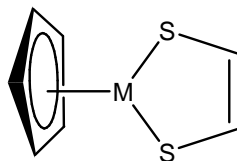
Metal(dithiolene)(diimine)



Metal(dithiolene)(diphosphine)

Metal-oxo(dithiolene)₂

(c) Organometallic dithiolene complexes: This incorporates the dithiolene ligand and some organic ligands for metal–carbon bond. Examples include [(ppy)Au(dithiolene)] (ppy = 2-phenylpyridyl)¹³ and [(cod)Pt(dithiolene)] (cod = 1,5-cyclooctadiene)¹⁴ complexes.



Metal(dithiolene)(cyclopentadienyl)

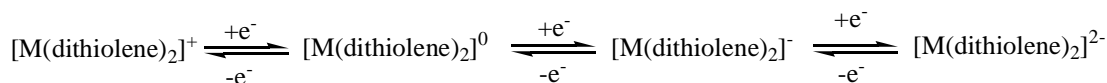
1.5. Properties and Applications of Metal 1,2–Dithiolene Complexes

Metal bis(1,2-dithiolene) complexes have been extensively studied since last five decades due to novel properties and application in diverse areas of research, such as, those of

conducting and magnetic materials, non-linear optics, dyes, catalysis and bioinorganic chemistry among others. These properties and applications arise due to their combination functional properties, *vivid* redox behavior, and diversity of molecular geometries, magnetic moments and specific intermolecular interactions.

1.5.1. Electrochemical Properties and Chemical Reactivity

The electrochemical properties of metal-dithiolene complexes are very interesting because of their unique redox properties and noninnocent behavior. The extensive π -electron delocalization in metal bis-dithiolene complexes makes it possible for the existence of variable charge levels and also difficult to assign oxidation states of the metal and ligands. Interestingly, square planar bis(dithiolene) complexes undergo one-, two- and even three-reversible one electron redox processes and these can be explained by the following equation.

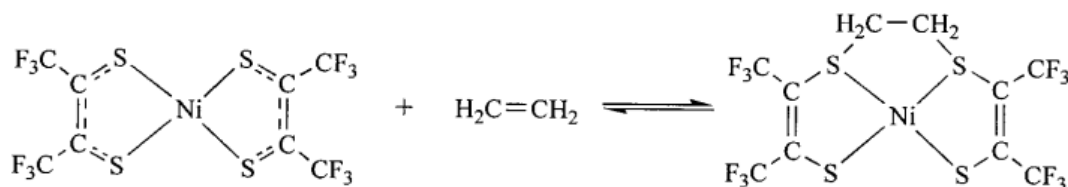


Based on chemical, electrochemical, structural, and spectroscopic studies,^{2a,f} the electron density in the metal orbitals does not change significantly as the charge level on the bis(dithiolene) complex is changed. Thus, the accessibility of a range of charge levels of dithiolene complex is possibly more related to the accessibility of a number of formal oxidation states of the dithiolene ligands. A large number of bis(dithiolene) complexes has been reported for the metals, such as, Ni, Pd, Pt, Cu, Au. The ease of oxidation of $[M(S_2C_2R_2)]^{Z-}$ for a particular metal decreases in the order $R = H > \text{alkyl} > \text{aryl} > CF_3 > CN$. This series parallels the electron donating-withdrawing ability of the substituent group R. For the transition metals $Fe < Co < Ni < Cu$, oxidative stability increases in this order for the dianion ($Z = 2$). This indicates that the participation of metal orbitals in the frontier orbitals of the dianionic species. Similarly, for $[M(\text{bdt})_2]^{Z-}$ (bdt = benzene-1,2-dithiolate) the redox potentials are dependent on the substituents on the aromatic ring. The potential 0/-1 couple increases as the substituent group becomes more electron-withdrawing. Square-planar bis(dithiolene) complexes are subjected to theoretical investigations.^{2e,15} As from the density functional theory (DFT), the HOMO (highest occupied molecular orbital) for $[Ni(S_2C_2H_2)]$ is primarily ligand based orbital consisting of four $3p_z$ orbitals of sulfur, perpendicular to molecular xy plane, and four $2p_z$ orbitals of carbons with opposite phases. The lowest unoccupied molecular orbital (LUMO) is a

mixture of ligand–metal orbitals, but still mostly the ligand character.^{15c} In general, electrochemical data supports the molecular orbital descriptions derived from quantum mechanical calculations. Because of rich redox chemistry of bis(dithiolene) chemistry and the redox active nature of the dithiolene ligands, these show much reactivity related to the redox properties and is often centered on the dithiolene ligands. Recently, Wang and Stiefel have reported^{16a} the separation of simple olefins mediated by the metal bis(dithiolene) complex anions. They proposed that, it is reversible olefin binding, controlled electrochemically and the whole reversible process is generally described as follows: when the olefin bound adduct (metal complex) is reduced, the reductant dissociates and forms an olefin and the metal-dithiolene anion. When this anion is oxidized, the oxidant binds the olefin again and so on.

Reactivity with Olefins

Nowadays, in chemical and petrochemical industry, olefins are the major volume feed stock. In most of the metal-mediated reactions, the alkene coordinates to the metal in at least one step of the reaction sequence, description of such systems easily poisoned by impurities in crude alkenes, which often bind more strongly to the metal than the alkene. These metal-based systems are most probably poisoned by C₂H₂, CO, and H₂S. In this context, Wang and Stiefel^{16a} argued that the metal complexes bind alkenes through chelated ligands, instead of, at the metal center. Thus the concerned system should be more resistant to deactivation by contaminants. They reported that neutral nickel bis(dithiolene) complexes form adducts with linear alkenes, such as ethylene or 1-hexene, where the alkene binds through the ligand S-atoms, even in the presence of H₂S or CO (Scheme 1.3).

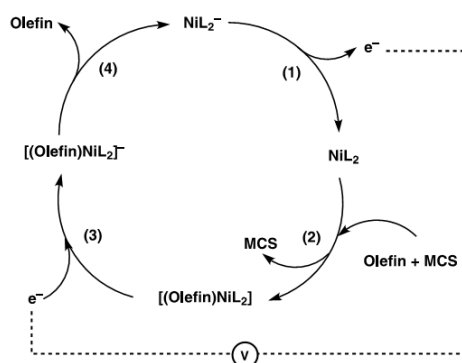


Scheme 1.3. Equilibrium reaction of metal(dithiolene) and with its olefin adduct.

This unusual tolerance toward poisoning led the authors to propose an olefin purification scheme in which the dithiolene-bound alkene is released by electrochemical reduction and it is regenerated by oxidation. Interestingly, the olefin binding and releasing

are controlled electrochemically in this case. Reversible olefin complexation to dithiolene complexes thus offers a novel approach in separating and purifying olefins.¹⁶

As shown Scheme 1.4, the mono-anionic complex $[\text{NiL}_2]^-$ (L, ligand) is oxidized electrochemically, forming the neutral species $[\text{NiL}_2]$. A multicomponent stream (MCS) containing an olefin(s) is introduced where upon the olefin reacts with $[\text{NiL}_2]$, forming the adduct $[(\text{olefin})\text{NiL}_2]$, while other (gaseous) components (such as alkanes, CO, C_2H_2 , and so on.) pass unreacted. The olefin adduct is electrochemically reduced. The reduced olefin adduct $[(\text{olefin})\text{NiL}_2]^-$ releases olefin (which is recovered) as $[\text{NiL}_2]^-$ is regenerated, completing the cycle. A similar scheme involves electrochemical reduction of the neutral species $[\text{NiL}_2]$ that is in equilibrium with the olefin adduct $[(\text{olefin})\text{NiL}_2]$, which drives the release of the olefin from the adduct as the complexation equilibrium (Scheme 1.3) shifts to replenish the neutral species.



Scheme 1.4. Schematic representation for electrochemically driven olefin separation using nickel dithiolene complexes.

1.5.2. Luminescence and Photochemical Properties

1.5.2.1. Square Planar Metal-Bis(dithiolene) Complexes

Excited States and Luminescence

Research of square planar metal bis(dithiolene) complexes has been focused on the electronic structure, spectroscopy, redox properties and conductivity to a large extent.¹⁷ The ground state properties of these compounds and orbital nature of the low energy excited states^{5,18} have been greatly determined by UV-Vis absorption spectroscopy. Molecular orbital nature of these complexes is further determined by several computational studies.^{2e} Square planar metal bis(dithiolene) complexes are highly colored and possess delocalized π -electron system to varying extents in the ground state. For

example, The deep red colored solutions of $[\text{Pt}(\text{mnt})_2]^{2-}$ are due to the absorption bands at 475-550 nm region, which are assigned as a $d(\text{Pt})\text{-}\pi^*(\text{mnt})$ MLCT transition.^{18b} In addition, very weak $d\text{-}d$ transitions are also observed at longer wavelengths (639 and 694 nm), and further bands occur at 336-228 nm region due to the mnt-localized $\pi\text{-}\pi^*$ transitions and ligand-metal charge transfer transitions. The relative ordering of energy of these orbitals depends upon the specific dithiolene, metal ion and its metal oxidation state. Because of the large extent of delocalization in bonding of these systems, it is difficult to assign the low-energy bands as arising from “pure” $d\text{-}d$, MLCT, LMCT, or $\pi\text{-}\pi^*$ excited state orbitals.

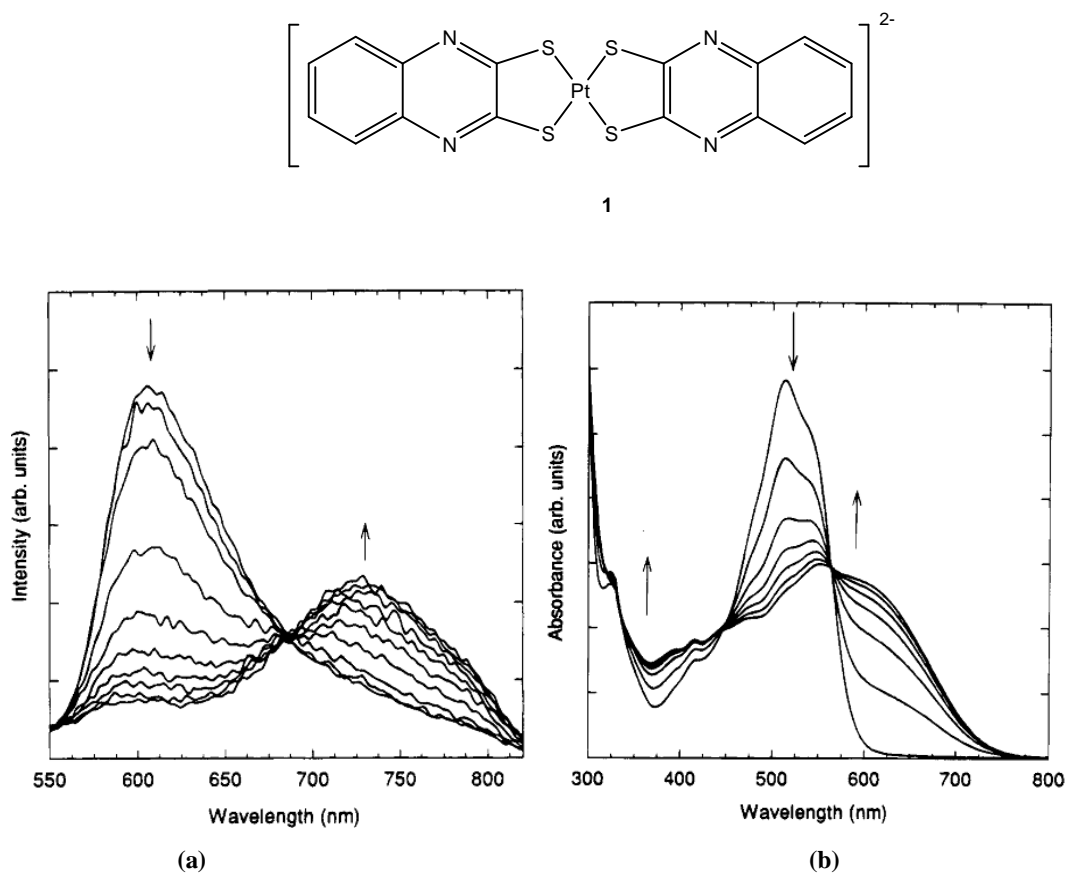


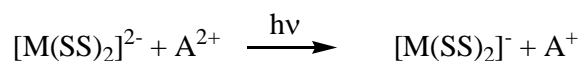
Figure 1.1. Changes in (a) absorption and (b) emission spectra of $(\text{Bu}_4\text{N})_2[\text{Pt}(\text{qdt})_2]$ upon addition of 10 μl aliquots of $4.25 \times 10^{-2} \text{ M}$ acetic acid in MeOH.

Photoluminescence properties from metal bis(dithiolene) complexes are rarely observed at ambient conditions. A weak emission ($\phi = 10^{-5}$) has been observed for the complex $[\text{Pt}(\text{mnt})_2]^{2-}$ at 775 nm at room temperature. Similarly, the compound $[\text{Pt}(\text{qdt})_2]^{2-}$ (**1**) also shows a weak emission at significantly higher energy compared to previous compound

at λ_{\max} at 606 nm.¹⁹ Absorption and emission spectra of this compound are largely dependent on the pH of the solution. This is due to the protonation of one of qdt-nitrogen atom leading to large shifts in absorption and emission spectra as shown in Figure 1.1. The shift in emission maximum from 606 nm to 728 nm in neutral solutions upon addition of acid may have sensor application. Luminescence of this compound in frozen glass solvent at 77k shows much stronger than RT.

Ion-Pair Charge-Transfer Photo Chemistry

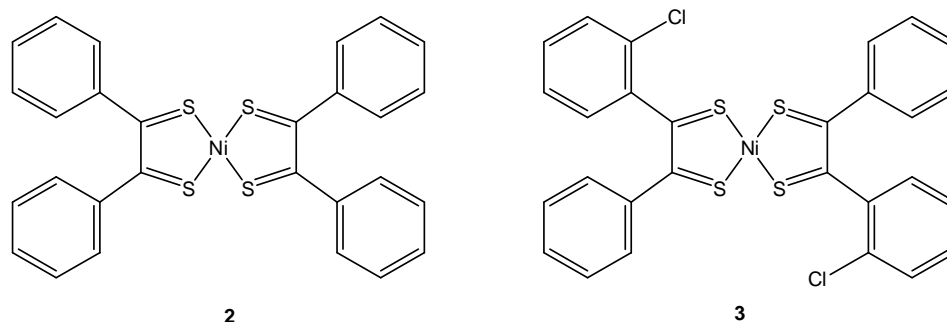
In the context of photochemistry of metal bis(dithiolene) complexes, the IPCT complexes have drawn considerable attention. Bis(1,2-dithiolene) complexes, especially those, that are dianionic, are good electron donors in the excited state. Kish and his co-workers²⁰ have investigated the IPCT complexes quite well of the type $A[M(SS)]$, where $A = MV^{2+}$ = organic acceptors such as dialkylated bipyridinium cations such as viologens, where $M = Ni, Pd$, and Pt including tetrahedral complexes of Cu and Zn , and SS corresponds to a number of different dithiolenes like mnt , $dmit$, and $dmid$ etc. The IPCT bands appearing for some ion-pair complexes, that include metal bis(1,2-dithiolene) complexes as donors, correspond to photo-induced charge transfer transition from donor to acceptor as outlined in equation.



The IPCT band energy and intensity depend on the metal ion and acceptor as well as the solvent and the absorption maxima are highly dependent on the nature of the dithiolene ranging from 450 to 730 nm for the $A[M(mnt)_2]$ complexes, and from 620 to 950 nm for $A[M(dmit)_2]$ complexes. For example, the metal-bis(1,2-dithiolene) complexes of the type $[MV^{2+}][Ni(SS)_2]^{2-}$ for which the IPCT band energies decrease with increasing electron donating ability of the dithiolene along the $[Ni(SS)_2]^{2-}$ series, where $SS = dmid < dmit < mnt < dto$ ($dto = 1,2$ -dithiooxalte).²¹ These ion-pair charge transfer transitions are also observed in the solid-state diffuse reflectance spectra. Surprisingly, the IPCT band do not appear for the corresponding monoanionic metal dithiolene complexes, although IPCT has been observed for the monoanionic complex $Ir(CO)_2(mnt)^-$ with methylviologen.

Photoproduction of Hydrogen

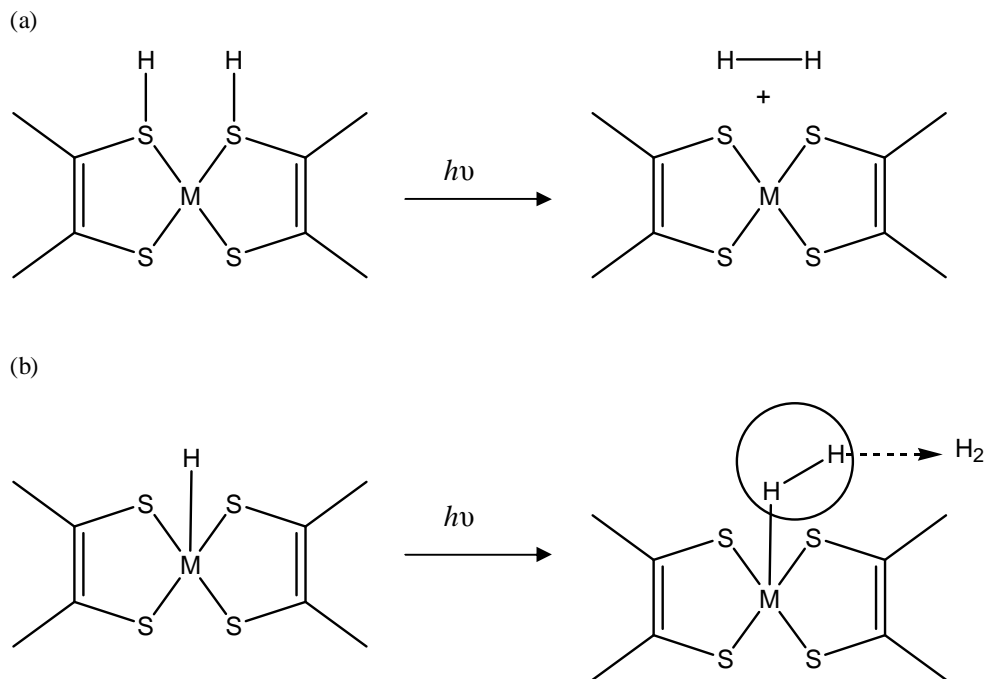
One of the most important aspect of photo chemistry research involving metal bis(dithiolene) complexes is the photochemical production of hydrogen. The first communication has been reported in 1980 by Kisch and co-workers, in which hydrogen was produced from water by using metal bis(dithiolene) complexes as photocatalysts.²² A neutral complex of following compound $\text{Ni}(\text{S}_2\text{C}_2\text{Ph}_2)$ (**2**) (Scheme 1.5) was used as photocatalyst for the production of hydrogen in the above communication.



Scheme 1.5

Another work has been published in 1983²³ on the photo production of hydrogen using square-planar bis (dithiolene) complexes of Ni, Pd, and Pt. However the actual mechanisms for the catalytic activity of square-planar bis(dithiolene) complexes has not been well understood. Theoretical studies by Alvarez and Hoffmann addressed two possible mechanisms for the hydrogen elimination as shown in Scheme 1.6. Concerted elimination of H_2 from protonated sulfur atoms in the complex was proposed to be thermally forbidden but photochemically allowed. Another proposed mechanism is protonation of metal hydride complex.

Subsequently, Katakis and co-workers²⁴ reported an another complex, bis(2-chlorodithiobenzil)nickel(II) (**3**) (Scheme 1.5) as a photocatalyst used for the production of hydrogen from water. However, further mechanistic, photochemical, and photophysical studies need to be done to clarify the chemistry behind the photoproduction of hydrogen and whether bis(dithiolene) complexes play a photochemical role or serving simply as precursor for the generation of colloidal metal sulfide semiconductor particles.



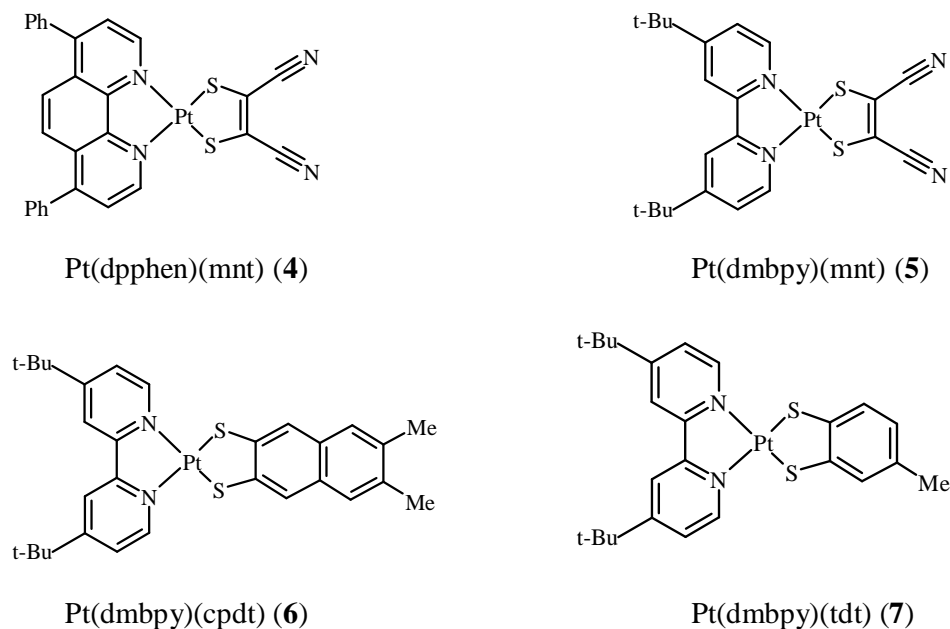
Scheme 1.6. Two possible pathways, for the photo production of hydrogen by using metal bis(dithiolene) complex.

1.5.2.2. Square-Planar Mixed-Ligand Dithiolene-Diimine and Related Complexes

Excited States and Luminescence

The combination of dithiolene and diimine chelating ligands in square-planar d^8 complexes gives rise to a unique CT excited state. This class of complexes has been the subject of rich and increasing amount of research in recent years. In this context, Eisenberg and his coworkers have focused on studying the excited state properties of mixed-ligand Pt(II) diimine dithiolate complexes.²⁵ They have synthesized an extensive series of [Pt(diimine)(1,2-dithiolate)] complexes, whose luminescent properties were extensively investigated. Some examples of Pt(diimine)(dithiolate) complexes which exhibits the luminescence in solution state are outlined below (**4–7**) (Scheme 1.7) . The Pt(diimine)(dithiolate) complexes exhibit the intense solvatochromic absorption band in the 450–700 nm region of the emission spectrum that shifts to higher energy with increasing solvent polarity. The solvatochromic transition was assigned as a charge transfer (CT) from HOMO which is a mixed orbitals of metal and dithiolate components to a lowest unoccupied orbital (LUMO) localized on the diimine ligand. This assignment can be due to the mixed-metal/ligand-to-ligand charge transfer (MMLL/CT) and ligand-ligand charge-transfer (LLCT) transitions.²⁶ Moreover, the [Pt(II)(diimine)(dithiolate)]

compounds have been investigated for their use in solar cells²⁷ as they possess a number of key features that make them of interest as sensitizers.

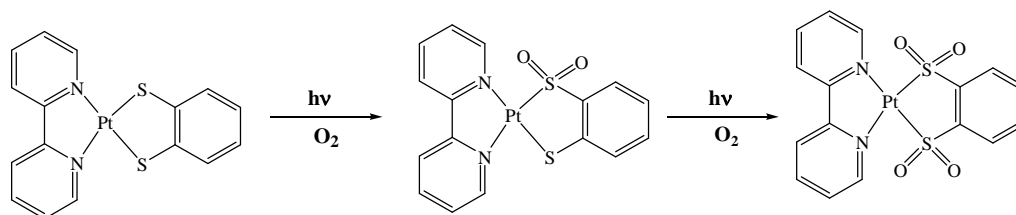


Scheme 1.7

These include an absorption band in the visible region with a relatively large molar extinction coefficient and in some cases, luminescent properties in fluid solution. Substituents on the diimine ligand affect the LUMO energy while substituents on the dithiolate ligand affect the HOMO energy and, therefore, the photophysical and electrochemical properties of the molecule. Tuning of these Pt dye compounds by manipulation both the HOMO and the LUMO energy levels has been shown by several groups.²⁸ This tuning is relevant in these systems, since the electrochemical and photophysical properties of the dye greatly affect the overall performance of the solar cell.

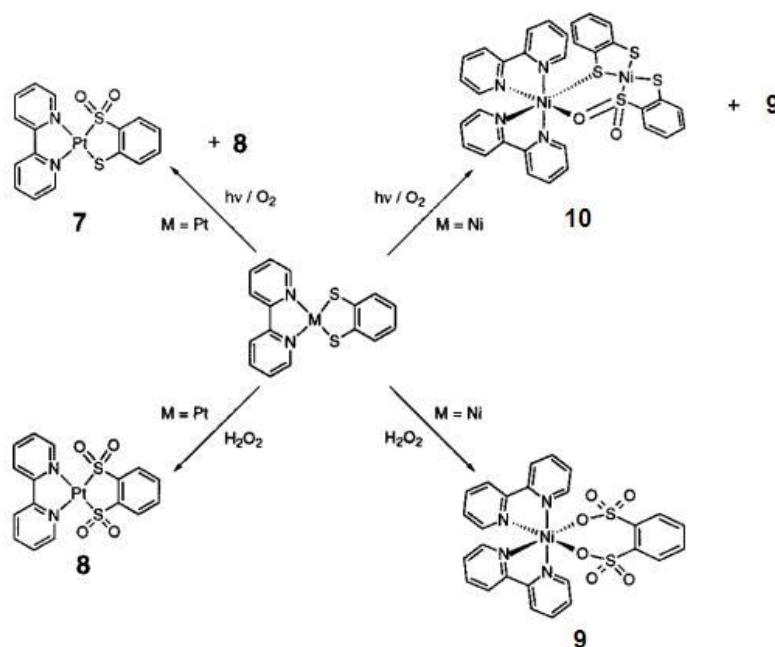
Photooxidation Chemistry

Conic and Gray²⁹ reported sulfur oxygenated products of dithiolene- α -diimine [Pt(bpy)(bdt)] complex and identifying both mono sulfinates and disulfinates products by photochemical oxidation as shown Scheme 1.8. Irradiation of oxygenated acetonitrile solution with $\lambda_{\text{ex}} > 450$ nm led to oxidation of dithiolene ligand in [Pt(bpy)(bdt)] and conversion of the complex to the monosulfinated and then disulfinated complexes as shown Scheme 1.8. But Cocker and Bachman³⁰ reported that the nickel complex



Scheme 1.8. Photooxidation of [Pt(bpy)(bdt)] complex.

[Ni(bpy)(bdt)] yields octahedral sulfonate complex by photo chemical oxidation; cocrystals of both monosulfinate [(bpy)₂Ni(bdtO₂)Ni(bdt)] and disulfinate [(bpy)₂Ni(bdtO₄)Ni(bdt)] bimetallic complexes were observed in solution, which indicates ligand disproportionation chemistry (Scheme 1.9). In order to investigate the role of the central metal ion, they have further explored photo reactivity of [Pt(bpy)(bdt)].³¹ Photooxidation of [Pt(bpy)(bdt)] in DMF afforded the monosulfinate complex [Pt(bpy)(bdtO₂)] along with minor amounts of the disulfinate complex [Pt(bpy)(bdtO₄)], whereas chemical oxidation of this compound results only disulfinate complex (Scheme 1.9). The authors suggest that the anomalous behavior complexes can be attributed to greater flexibility in the coordination chemistry.



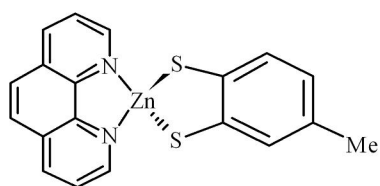
Scheme 1.9. Photo and chemical oxidations of [M(bpy)(bdt)] complexes.

However, metal-sulfonates, based on bis(dithiolene) complexes are still rare in the literature. To the best of our knowledge, only few reports are shown in literature.^{30,32} Robertson reported trans-di-sulfinate complex of [Ni(bdt)]⁻¹, in which sulfur atoms were

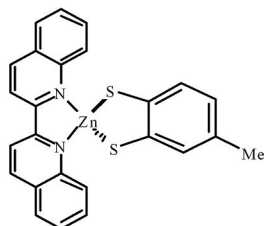
oxidized by receiving of oxygen atoms from counter cation.^{32a} Another report of an interesting S-bonded sulfinates based on Fe-bis(benzene-1,2-dithiolene) complex, which relates to the an inactive form of the Fe-containing nitrile hydratase (Fe-NHase) containing Cys-sulfinic (Cys-SO₂) and Cys-sulfenic (Cys-SO) groups.^{32b} Findings the photochemical oxidation products, based on the dithiolene complexes, are still rare and interesting is due to their relevance to the deactivated species of [Ni Fe] hydrogenase³³ and CO-dehydrogenase.³⁴

1.5.2.3. Tetrahedral d^{10} Complexes

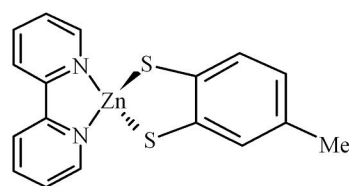
Few numbers of the tetrahedral mixed-ligand diimine dithiolate complexes of Zn(II) exhibit the absorption bands in the 465–590 nm regions. This absorption band assumes the LLCT transitions³⁵ and attributed to the transition from HOMO (that is localized on the dithiolene) to a LUMO (that is localized on the diimine). Some of the tetrahedral Zn(diimine)(dithiolate) complexes are described below (**11**–**13**).



Zn(phen)(tdt) (**11**)



Zn(biq)(tdt) (**12**)

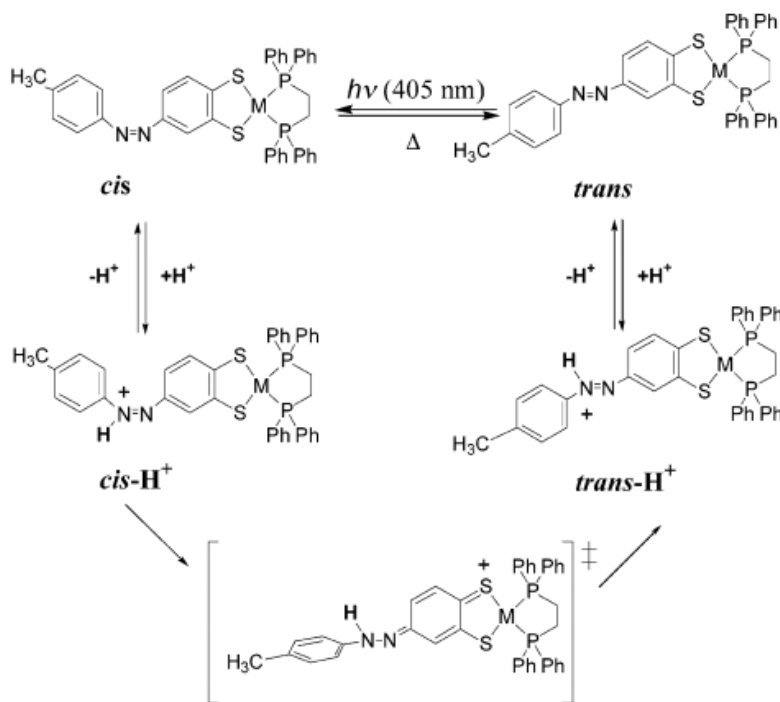


Zn(bpy)(tdt) (**13**)

Nevertheless, the d^8 complexes such as [M(dithiolate)(diimine)] (M= Ni(II), Pd(II), Pt(II)) exist in square planar geometry; in contrast, the Zn(diimine)(dithiolate) complexes are in tetrahedral geometry. Significantly, the photoluminescence studies have been reported for Zn(bpy)(tdt) in the solid state and in CH₂Cl₂/ethanol solvent glass at 77 K by Benedix *et al.*³⁶ The compounds [Zn(phen)(tdt)] and [Zn(bpy)(tdt)] show the room temperature solid state emission, reported by Bartecki *et al.*³⁷ But the photophysical properties of [Zn(diimine)(dithiolate)] complexes are still limited to our knowledge. More work to be needed to examine and characterize the unsymmetrical [M(diimine)(1,2-dithiolate)] complexes, including their photophysical properties.

1.5.3. Photo-isomerization of Metal Dithiolenes

Photoisomerization of azobenzenes is the subject of one of the most research interest in the area of photo-mode high-density information storage and photo-switching devices.³⁸ Transition metal complexes of azo-conjugated systems can provide new advanced molecular functions, based on the combinations of photo-isomerization of the azo group and changes in the intrinsic properties including optical, redox, and magnetic properties, originating from *d*-electrons. In this regard, Nishihara and his co-workers³⁹ introduced the versatile synthetic method of azo-conjugated metalladithiolenes with various central metals and substituent groups as shown in Scheme 1.10. They investigated the azo-conjugated metalladithiolenes including their photo and proton response. Novel proton coupled *cis-trans* isomerization, originating from the strong electronic interactions between the metalladithiolene and azo moiety, was also described. They examined the curious proton response and proton catalyzed *cis-trans* isomerization. A novel proton response of the azo group is occurred due to the strong electron-donating effect of the metalladithiolene moiety. This is responsible for the novel proton catalyzed *cis-trans* isomerization. Remarkably, isomerization behaviors of a wide range of azo-conjugated metalladithiolenes can be controlled by altering the central metal atoms or varying the substituents on the dithiolene part.



Scheme 1.10. Photo and proton responses of azo-conjugated metalladithiolenes.³⁹

1.5.4. Solid-State Properties

Since last two decades, inorganic molecule- based compounds show remarkable physical properties. These properties can be electrical, magnetic or optical. In this context, metal 1,2-dithiolene complexes exhibit the unusual solid-state properties, such as magnetic,⁴⁰ conducting⁴¹ and nonlinear optics⁴² (NLO) properties. The electronic structure of dithiolene complex is of crucial importance in determining the electron in the derived compounds exhibiting interesting physical properties. The electronically delocalized core comprising the central metal, four sulphur atoms and the C=C units, accounts for a rich electrochemical behavior that often yields one or more reversible redox processes. The redox properties of these complexes are strongly dependent on the ligand and its large contribution to the frontier orbitals. The possible oxidation states of these complexes range from dianionic to cationic states and partial oxidation situations often occur, especially, in the solid state. Also different spin states such as $S = 0, 1/2, 1$ or $3/2$, can be easily obtained, upon variation of both the transition metal M and oxidation state making these complexes suitable units for magnetic materials. Moreover, the dithiolene complexes exhibit multiple oxidation states due to this stable ion-radical species that are available at various redox potentials. Depending on the partial oxidation of these by electrochemical oxidation, it results in various nonintegral oxidation state (NIOS). Furthermore these complexes also show a diversity of geometry, ranging from the more general case of purely square planar coordination, favorable to solid state extended π - π interactions, to dimeric, trimeric⁴³ or even polymeric⁴⁴ arrangements. All these features have made dithiolene complexes suitable building blocks for the preparation of electrical and magnetic materials.

1.5.4.1. Electrical Properties (Conducting and Super Conducting Properties)

The first typical example of partially oxidized metal-like conductor KCP (kalium tetracyanoplatinat), $K_2[Pt(CN)_4X_{0.3}] \cdot nH_2O$; $X = Cl, Br$ was known to be prepared as early as 1842 by Knop and his co-workers⁴⁵. In these highly conducting salts, the square planar platinum complexes are stacked to form one dimensional platinum chains with a very short Pt...Pt distances of 2.8–3.0 Å in which, the one-dimensional metallic state is constructed by the partially filled energy band associated with the overlap of $5dz^2$ orbitals of the central platinum atoms along the stack without any contribution by the ligand to the conduction band. Over past few decades, large number of 1,2-dithiolene based conductor

and superconductor materials have been developed. Although the first dithiolene ligands were synthesized in the early 1960,⁴⁶ electrical properties of the dithiolene complexes were reported only in 1969.⁴⁷ These complexes exhibit low conductivity values in the range of 10^{-3} – 10^{-5} S cm⁻¹ at room temperature. Then much effort has been devoted to design new analogues in order to improve the transition metal based conducting properties. In this context, the first observation of metallic behavior in crystalline metal-dithiolene was reported for $\text{Li}_{0.75}[\text{Pt}(\text{mnt})_2] \cdot 2\text{H}_2\text{O}$ by Underhill *et al.* in 1981.⁴⁸ In this complexes the Pt...Pt distance 3.639 Å and this indicates that there is no $5d_{z^2}$ orbitals overlapping. This compound produces the uniform columnar structure. Therefore, the conduction band in molecular conductor originates from ligand π -orbitals or mixed metal(*d*)–ligand(π) orbitals, in which sulfur atoms play an important role as shown in Figure 1.2. From this, new aspect of molecular conductors, based on metal dithiolene complexes, has been developed. In order to improve the conductivity of molecular conductors, it needs the extension of delocalization and intermolecular interactions. Based on this argument, the first conducting $[\text{M}(\text{dmit})_2]^-$ salt, $(\text{Bu}_4\text{N})_2[\text{Ni}(\text{dmit})_2] \cdot 2\text{CH}_3\text{CN}$ was reported in 1983.⁴⁹ In this system, the degree of π -electron delocalization core is extended by sulfur atoms containing hetero rings and the $\text{M}(\text{dmit})_2$ molecule, which resembles to the organic donor BEDT-TTF. In the solid-state structure of this $\text{Ni}(\text{dmit})_2$, molecules are planar and stacked with short S...S interactions. Interestingly, the systematic variation of the nature of the alkyl cation in dmit-based compounds, with non-integral oxidation state, was carried out.

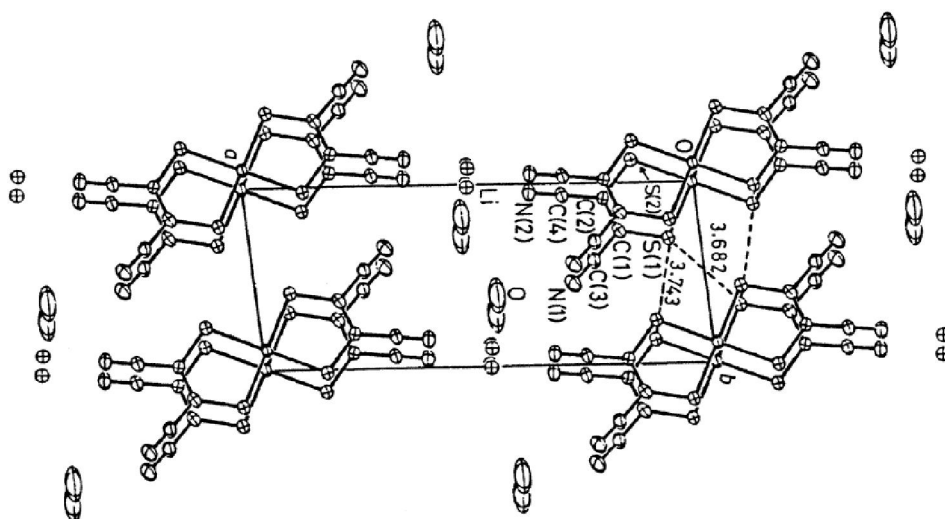


Figure 1.2. Crystal structure of $(\text{H}_3\text{O})_{0.33}\text{Li}_{0.8}[\text{Pt}(\text{mnt})_2] \cdot 1.67\text{H}_2\text{O}$.

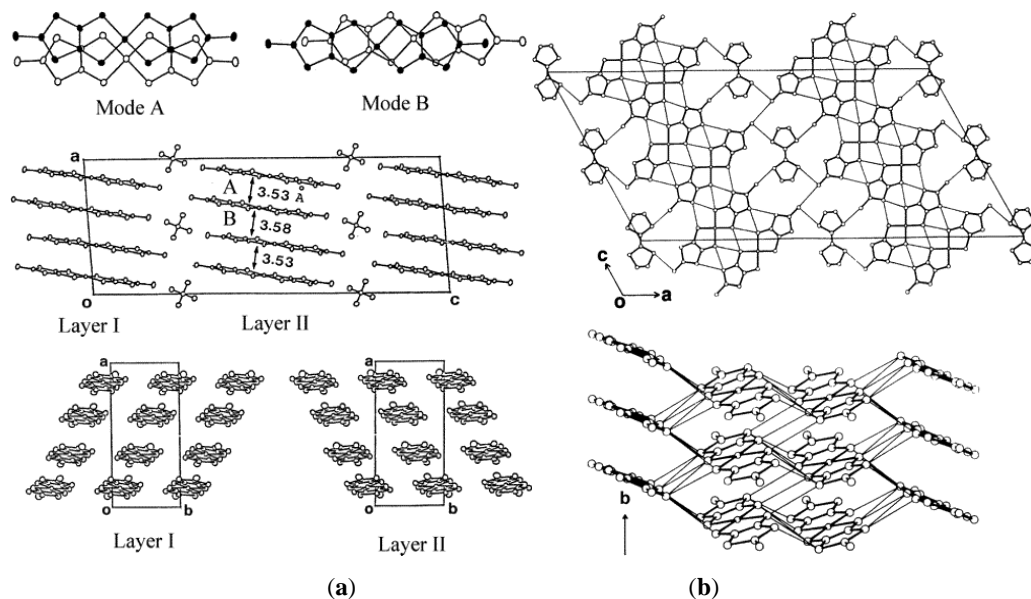
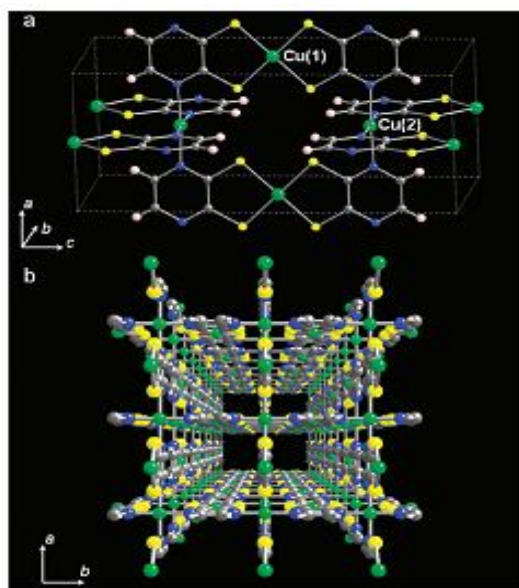


Figure 1.3. (a) Crystal structure of $(\text{Me}_4\text{N})[\text{Ni}(\text{dmit})_2]_2$, and (b) the crystal structure of $(\text{TTF})[\text{Ni}(\text{dmit})_2]_2$.

It was soon observed that a slight, even minute, modification of the cation may result in important, or even drastic, changes in the conducting behavior. To demonstrate, whether the cations play role for conductivity or not, in 1986 the $[\text{Bu}_4\text{N}]^+$ cation was replaced by TTF and the compound $(\text{TTF})[\text{Ni}(\text{dmit})_2]_2$ (Figure 1.3) was reported to undergo the superconducting transition at 1.62 K under 7 kbar.⁵⁰ This was the first report on transition metal dithiolene complex based superconductor. Metal dithiolene complexes show very interesting conducting behavior, which is mainly due to the involvement of sulfur-rich dithiolene ligands, owing to the intermolecular $\text{S}\cdots\text{S}$ interactions of the ligands. The superconductivity in the system, where the electron conduction originates from only the $\text{M}(\text{dmit})_2$ molecule, was first found in $(\text{Me}_4\text{N})[\text{Ni}(\text{dmit})_2]_2$ (Figure 1.3) at 5 K under 7 kbar.⁵¹ This clearly indicates that the improvement of the conducting properties connected with the morphology of the counter cation. For example, the comparison of conductivity of $(\text{Me}_4\text{N})_{0.5}[\text{Ni}(\text{dmit})_2]$ and $(\text{HMe}_3\text{N})_{0.5}[\text{Ni}(\text{dmit})_2]$ with non-integral oxidation states, for which the only chemical variation consists of substituting just one hydrogen atom for one methyl group. Few of the superconducting $[\text{M}(\text{dmit})_2]^-$ salts are described in Table 1.1.⁵² In addition to metal complexes of mnt and dmit ligands, $\text{M}(\text{dddt})_2$ complexes have been studied because the dddt complexes are closely related to TTF like molecules and especially BEDT–TTF. Moreover square-planar metal complexes, based on dddt ligand, share with BEDT–TTF and capacity for its existence as cationic radicals (not only as neutral species and anionic radicals) like most other dithiolene complexes.⁵³

Table 1.1. Molecular Superconductors Based Metal Dithiolene Complexes⁵²

compound	T_c/K	$P/kbar$
(TTF)[Ni(dmit) ₂] ₂	1.62	7
α -(EDT-TTF)[Ni(dmit) ₂]	1.3	-
(Me ₄ N)[Ni(dmit) ₂] ₂	5	7
α' -(TTF)[Pd(dmit) ₂] ₂	5.93	24
α -(TTF)[Pd(dmit) ₂] ₂	1.7	22
β -(Me ₄ N)[Pd(dmit) ₂] ₂	6.2	6.5
(Et ₂ Me ₂ N)[Pd(dmit) ₂] ₂	4.2	4
β' -(Et ₂ Me ₂ P)[Pd(dmit) ₂] ₂	4	6.9
β' -(Me ₄ Sb)[Pd(dmit) ₂] ₂	3	10
β' -(Me ₄ As)[Pd(dmit) ₂] ₂	4	7(ap)

**Figure 1.4.** (a) Crystal structure in Cu[Cu(pdt)₂]. (b) Perspective view of the crystal structure of Cu[Cu(pdt)₂]. Color code: green, Cu; yellow, S; gray, C; blue, N; pink, H.

Recently, porous coordination polymers (metal-organic frameworks) have been synthesized based on bis(dithiolene) complexes [Cu(pdt)₂][−] (Figure 1.4) and [Ni(pdt)₂][−] (Figure 1.5) as building blocks.⁵⁴ These polymers Cu[Cu(pdt)₂] and Cu[Ni(pdt)₂] show relatively high conductivity at room temperature with high porosity. In addition, conductivity of Cu[Ni(pdt)₂] has been enhanced through partial oxidation of the its

framework as shown in Figure 1.5. The increase in conductivity is due to oxidative doping and the resulting framework is a p-type semiconductor.^{54b} Metal-organic frameworks of these dithiolene based compounds exhibit relatively high electrical conductivity, doping and redox behavior with permanent porosity. Because of such solid-state properties, these compounds can create a potentially versatile platform for generating hybrid, ordered nanoscale electronics. Given the wide range of metal dithiolene chemistry known, these properties suggest that these and related metal organic frameworks may find applications as new electronic and photoactive microporous materials.

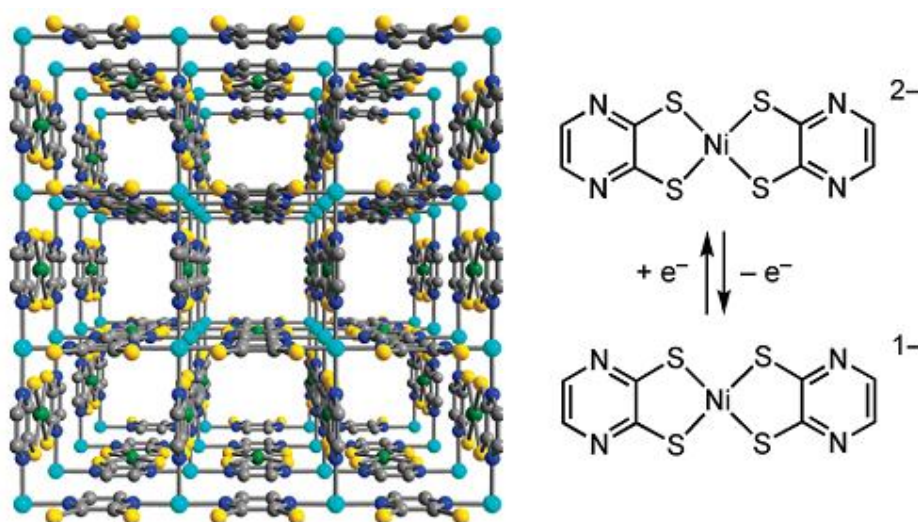


Figure 1.5. Left: Portion of the structure of the metal-organic framework $\text{Cu}[\text{Ni}(\text{pdt})_2]$, with light blue, green, yellow, blue, and gray spheres representing Cu, Ni, S, N, and C atoms, respectively; H atoms are omitted for clarity. Right: Redox behavior associated with the $[\text{Ni}(\text{pdt})_2]^{2-}$ units within the framework.

1.5.4.2. Magnetic Properties

Molecular magnetic materials are potential candidates to develop magnetic, electromagnetic and magnetic-optic devices. In this point of view, the metal bis(dithiolene) complexes are attractive. The planar metal bis(1,2-dithiolene) complexes have been widely investigated, because these complexes exhibit the conductivity / superconductivity including the magnetic properties at the same time.⁵⁵ Moreover, the rational development of new magnetic metal complexes involving both conducting π -electrons and local d spins is of further interest, since the novel electrical conducting and magnetic properties might be produced. Anti-ferromagnetism is the most common phenomena observed magnetic behavior for the most of the metal bis(dithiolene)

complexes. In spite the large number of dithiolene complexes, very few exhibit unusual and remarkable magnetic behaviors. These are undergo spin-Peierls (SP) like transitions, spin-ladder (SL) behavior, exhibiting ferromagnetic interaction and bulk ferromagnets.⁵⁶ Mostly, metal bis(1,2-dithiolene) complexes only show these interesting magnetic behavior.

Spin-Peierls Transition

Spin-Peierls transition⁵⁷ is magneto-elastic transition that occurs in quasi one-dimensional antiferromagnetic materials. For the occurrence of a spin-Peierls transition, several preconditions are necessary: first of all, a crystal must contain (quasi) one-dimensional antiferromagnetic spin chains of half-integer spin, i.e. the exchange coupling between neighboring spin along one crystal direction has to be much larger than those, which are perpendicular to this direction. Secondly, a finite magneto-elastic coupling is necessary, i.e. the exchange interaction depends on the distance between neighboring sites. It consists of an $S=1/2$ antiferromagnetic spin chain with a spin-lattice coupling. The dimerization of the lattice takes place at a finite temperature T_{SP} (**a**→**b**). The lattice dimerization alternatively enhances $[J(1+\delta)]$ or reduces $[J(1-\delta)]$ the antiferromagnetic interactions, and brings about singlet pair formations on the enhanced exchange links (form **b**) as shown in Figure 1.6. The Spin-Peierls transition has been theoretically predicted only for organic radicals⁵⁸ long before. Interestingly, the first experimentally characterized spin-Peierls system based on the 1,2-dithiolene system, $(TTF)[M(tfd)_2]$ $M = Cu$ and Au , was reported.

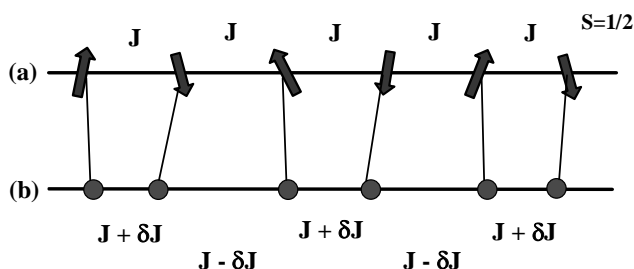


Figure 1.6. (a) An $S=1/2$ spin chain with a uniform antiferromagnetic interaction J . (b) The lattice dimerized state below the spin Peierls transition temperature (T_{SP}).

These undergo the spin-Peierls transition at 12K for Cu and 2K for Au.⁵⁹ The spin-Peierls transition was also observed in the case of $(Per)_2[Pt(mnt)_2]$.⁶⁰ In the ion-pair complexes, $[RbzPy][Ni(mnt)_2]$ ($R = Br, Cl, \text{ and } NO_2$), the $[Ni(mnt)_2]^{1-}$ anion favors one-dimensional

columnar molecular arrangements (Figure 1.7). Paramagnetic-diamagnetic phase transitions in this system involve spin-Peierls-like transition.⁶¹ The relevant arrangement is shown in Figure 1.7. Another ion-pair complex $[\text{FBzPy}][\text{Ni}(\text{mnt})_2]$, where $[\text{FBzPy}]^+ = 1$ -(4A-fluorobenzyl) pyridinium forms a discrete stacking column, that shows a peculiar magnetic transition from paramagnetic to diamagnetic around 90 K.

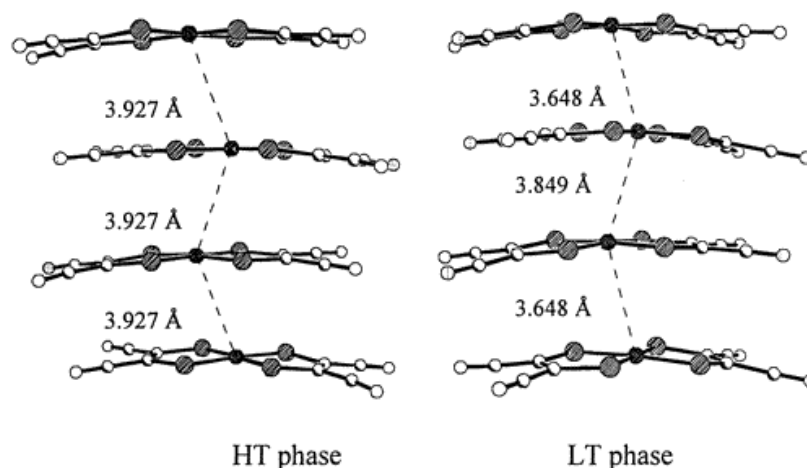


Figure 1.7. Side view of 1-D anion chain for $[\text{BrBzPy}][\text{Ni}(\text{mnt})_2]$ in the high-temperature (HT) and low-temperature phases.

Spin-Ladder System

The spin ladder system is an $S=1/2$ antiferromagnetic square lattice with finite width and infinite length (Figure 1.8). The ground state of this system depends on the lattice width, namely, the number of legs in the ladder. If the number of the legs is *even*, the ground state becomes non-magnetic with a finite energy gap to the excited states. For example, even-leg ladders of $S = 1/2$ Heisenberg antiferromagnetic spins are in a resonating valence bond state⁶² at low-temperature and have a finite spin-gap.⁶³

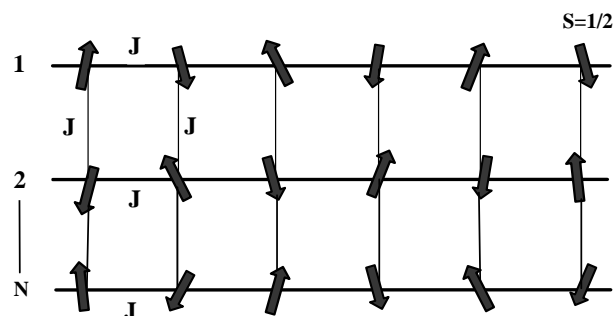


Figure 1.8. (a) The N -leg spin ladder structure and (b) a schematic ground state of the 2-leg spin ladder system.

It's *odd* number of legs display properties similar to those of single chains. Interestingly, some of the $[M(\text{dithiolene})_2]^-$ systems have a tendency to form stacks with side-by-side S...S interactions, resulting the ladder like structure with $S = 1/2$.

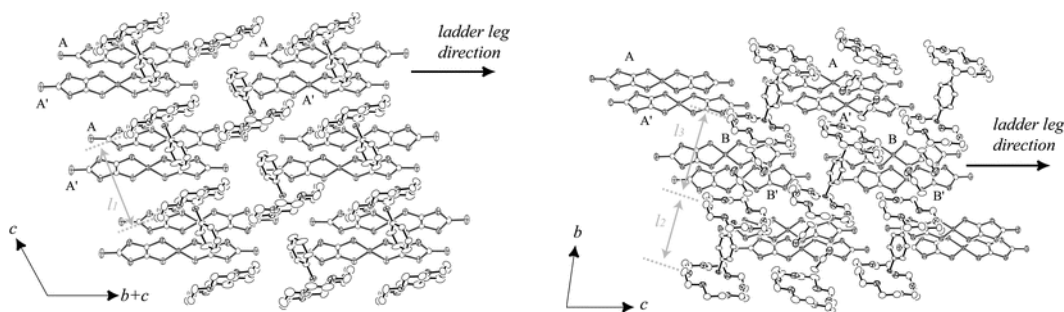


Figure 1.9. Crystal structure of the salts $[\text{Ph}(\text{NH}_3)](18\text{-crown-6})[\text{Ni}(\text{dmit})_2]$ (left) and $[p\text{-Ph}(\text{NH}_3)_2](18\text{-crown-6})_2[\text{Ni}(\text{dmit})_2]_2(\text{CH}_3\text{CN})_2$ (right). The molecular arrangement of $[\text{Ni}(\text{dmit})_2]^-$ forming dimer chain structures (red) is overlaid with spool arrays (black).

For example, very recently, Nakamura and co-workers have reported the formation of $[\text{Ni}(\text{dmit})_2]^-$ molecular spin ladder induced by $[\text{Ph}(\text{NH}_3)](18\text{-crown-6})_n$ and $[p\text{-Ph}(\text{NH}_3)_2](18\text{-crown-6})_2$ supramolecular cations (Figure 1.9).⁶⁴ A pair of $[\text{Ni}(\text{dmit})_2]^{1-}$ complex anions form a dimer surrounded between two adjacent 18-crown-6 moieties of a spool, and the 1D array of $\{[\text{Ni}(\text{dmit})_2]^- \}_2$ gives dimer chain structures which exhibit the spin-ladder magnetic behavior (Figure 1.9).

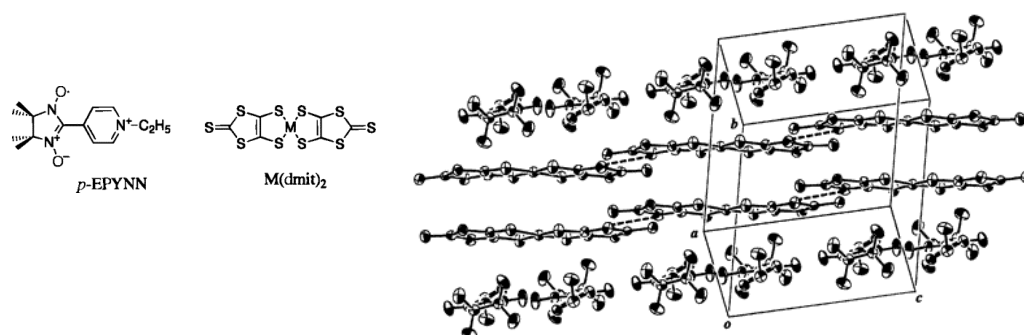


Figure 1.10. The structure of $p\text{-EPYNN}[\text{Ni}(\text{dmit})_2]$, showing one-dimensional chain of $p\text{-EPYNN}$ and one-dimensional ladder chain of $\text{Ni}(\text{dmit})_2$.

Imai and co-workers⁶⁵ reported $[\text{Ni}(\text{dmit})_2]^{1-}$ based two-leg ladder kind of structure, in which the $[\text{Ni}(\text{dmit})_2]^{1-}$ anion ladder is sandwiched between the $p\text{-EPYNN}$ ($p\text{-N}$ -

ethylpyridinium α -nitronyl nitroxide) chains, resulting in the Ni(dmit)₂ ladder-chain formation.⁶⁵ In the compound *p*-EPYNN[Ni(dmit)₂], the spin-ladder chain of the Ni(dmit)₂ radical anion coexists with the ferromagnetic one-dimensional chain of the *p*-EPYNN radical as shown in Figure 1.10.

1.5.4.3. Optical Materials

1.5.4.3.1. Near-Infrared (NIR) Absorbing Dyes

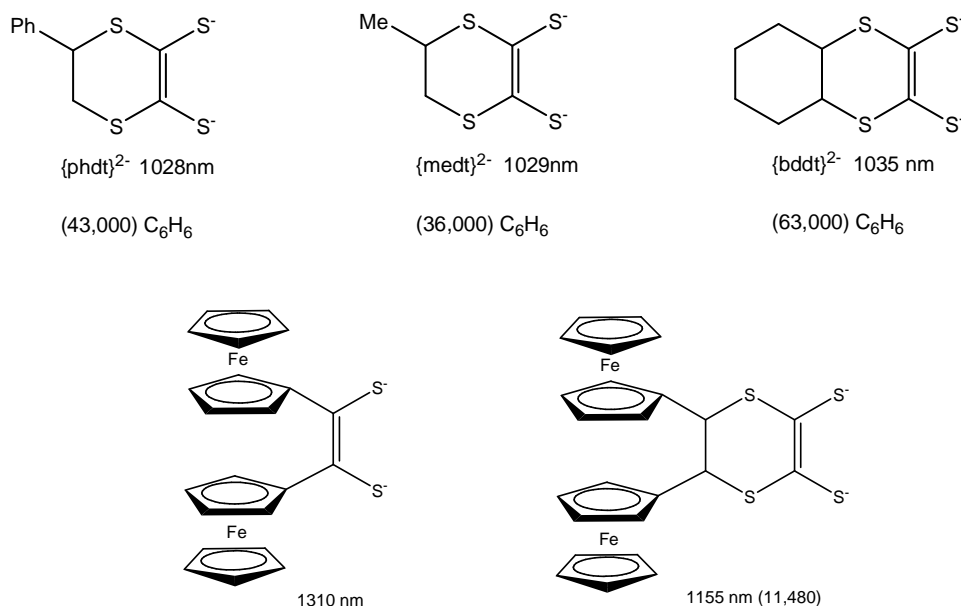
The near-infrared region is from about 800 nm to 2500 nm. Dyes for applications in the NIR region require small differences in the energy between HOMO and LUMO. The donor-acceptor concept was established by König⁶⁶ and Ismailsky⁶⁷ and further developed by Dilthey and Wizinger⁶⁸ and incorporated into the perturbation molecular orbital theory (PMO) model by Dewar.⁶⁹ According to this concept, long-wavelength absorption is expected if π -systems are substituted with donor (D) and acceptor (A) groups. Very strong donor and acceptor groups can be applied in a double arrangement according to building principle (**D — π — A — π — D**) and can cause long-wavelength absorption.

The literature provides extremely limited data about the near-IR dyes. The first near-infrared (NIR) absorbing organic compounds (some of phenylenediamine derivatives) were synthesized at the beginning of this century. The uses of NIR dyes has been realized comparably recently, because they serve as excellent indicators of the progress of novel technologies, especially the development of NIR semiconductor lasers, optical data storage field (DRAW (Direct Reading After Writing) or WORM (Write Once Read Many)). The optical data storage field (DRAW (Direct Reading After Writing) was first developed by Philips in 1978. The DRAW disk in the heat-mode system using organic NIR dyes is currently available. The other NIR-dyes devices are thermal writing displays, infrared photography, laser printer etc. The NIR dyes have also important medicinal applications. In the context of medicinal applications, Auler and Banzer (1942) reported that hemato-porphyrin could be absorbed into cancerous tissues.⁷⁰

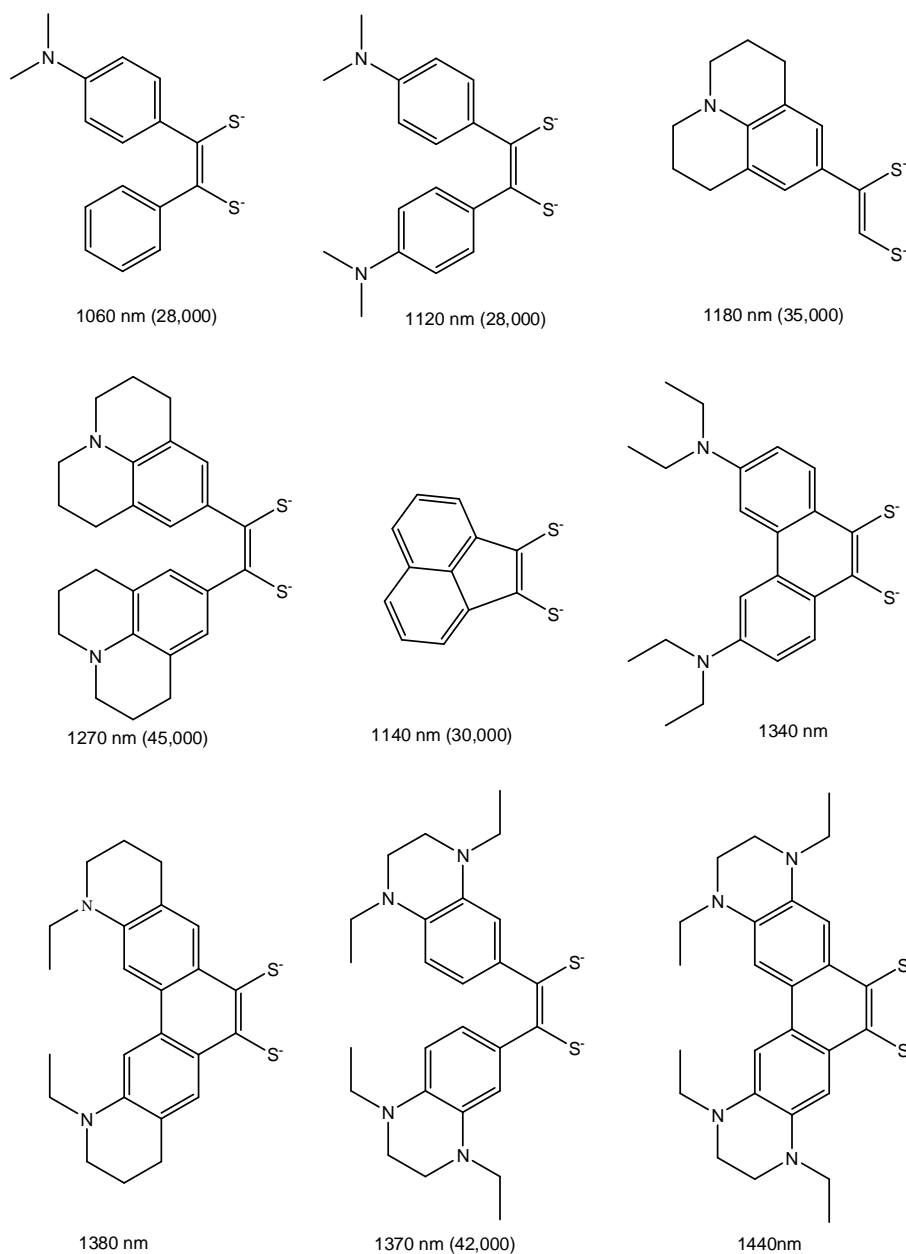
Metal bis(dithiolene) complexes have been used as good candidates for Near-IR dyes, because (1) metal bis(dithiolene) complexes show intense electronic absorption in the NIR region, especially Ni-dithiolene complexes. (2) Metal dithiolene complexes have their ability to exist in several clearly defined oxidation states which are fully connected through reversible redox steps. (3) Another characteristic property of dithiolene is their high thermal and photochemical stability. The absorption spectra of neutral

[Ni(dithiolene)₂] have been discussed and the longest wavelength of these complexes has been assigned to $b_{1u}-b_{2g}$ ($\pi-\pi^*$) transition. The highest occupied MO (b_{1u}) is virtually a pure ligand orbital and the lowest empty MO (b_{2g}) has some Ni (metal) character as well as ligand character.⁷¹ This absorption band can be smoothly tuned over desired wavelength region by simple and subtle changes on to the dithiolene ligands. Most of the dithiolene complexes used for the NIR dyes are derived from Ni because of the higher delocalization within these complexes compared to the Pd and Pt analogues. A detailed review by Muller-Westerhoff *et al.*⁷² is available on this NIR absorption topic and a number of Ni-based dithiolene complexes with absorption at wavelength > 700 nm have been described.^{72a,73} Some of the dithiolene ligands, involved in dithiolene complexes, exhibit such strong absorption as shown in Schemes 1.11 and 1.12. Many researchers aimed at increasing the intensity absorption maximum at low energy. Based on this research, it led to conclusion that the dithiolene complex should contain

- (1) Coplanarity of ligand π -system and dithiolene;
- (2) Presence of an extended π -system;
- (3) Presence of electron donating substituents;
- (4) Fixing of the substituents into rigid coplanarity with the ligand;
- (5) Attachment of sterically bulky substituents to increase solubility;
- (6) Variation of the central metal to obtain different shifts and to tune the relaxation time.



Scheme 1.11

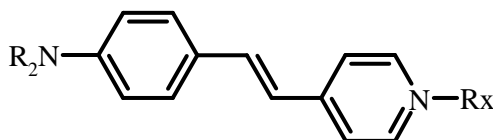
**Scheme 1.12**

Although the dithiolenes metal complexes show an absorption band in the NIR region, they are not useful as colorants in the recording layer of the optical DRAW disk,⁷⁴ due to their low reflectivity of the GaAlAs diode lasers. But the dithiolenes Ni complex has been applied to the optical DRAW disk as an inhibitor of laser induced fading.⁷⁵ The metal dithiolenes complexes have also attracted much interest as Q-switching NIR dyes applications.

1.5.4.3.2. Nonlinear Optical Materials

Second-Order NLO

The basic requirements for NLO active molecules, that possess large β values, contain an electron donor group (D) connected with an electron acceptor group (A) by a π -conjugated polarizable bridge.⁷⁶ The nonlinear optical properties of such dipolar, polarizable (D- π -A) molecules are characterized by low energy, D \rightarrow A intermolecular charge transfer (ICT) excitations. However, much number of papers have appeared on organic molecule-based compound exhibiting NLO properties, especially for SHG, but only few are reported for inorganic molecule-based materials. In this context, metal dithiolene complexes have attracted interest for NLO properties owing to their highly delocalized electron configuration and the possibility of the transfer of electron density between metal and ligand which induces an intense near-IR absorption transition.⁷⁷ Unfortunately, symmetrical homoleptic bis(dithiolene) complexes do not exhibit any second harmonic generation (SHG), because the SHG materials require the lack of a center of symmetry. Symmetrical homoleptic dithiolene complexes, involved in SHG, are synthesized as counterions with push-pull active molecules such as hemicyanine dye (HCD)⁷⁸ as shown in Scheme 1.13. Replacement of iodide ion in (HCD)I by dmit-based complex dianion results in the compounds of general formula $\{(HCD)[M(dmit)_2]\}$ ($M = Cd, Ni, Zn$).⁷⁹ Interestingly, LB films of these Zn-dmit compounds have been shown to improve SHG compared to the (HCD)I. This may be due to the fact that Zn complexes act as spacer avoiding aggregation and/or dispersion of the active chromophore (HCD) and allowing an ordered segregation of HCD in the films.

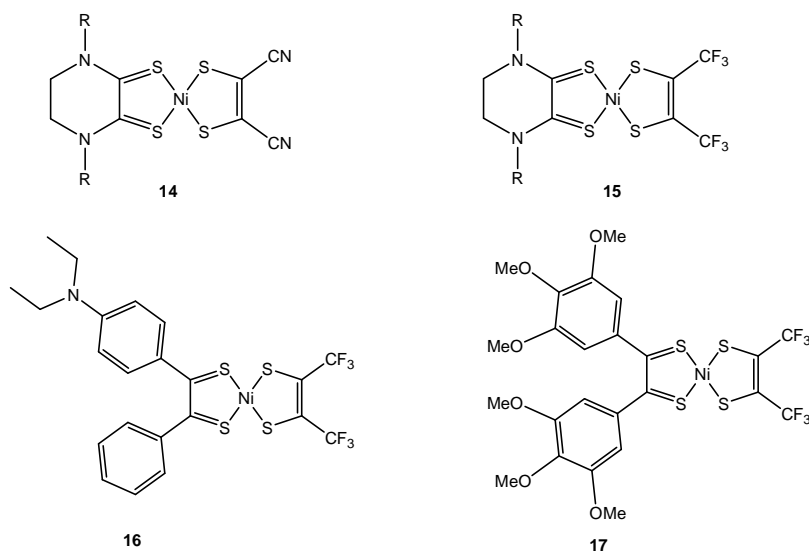


R = Me, Et, Bu, etc.

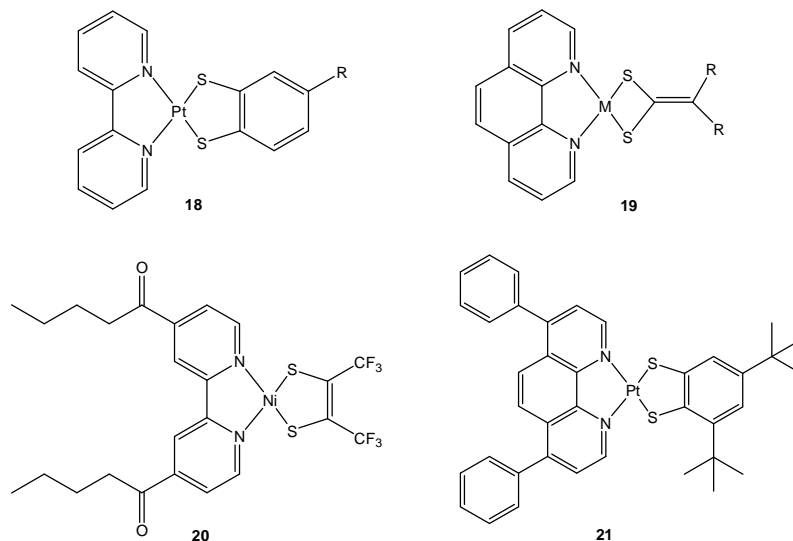
Scheme 1.13

Interestingly, unsymmetrical homoleptic bis(dithiolene) and heteroleptic dithiolene complexes are better candidates for SHG, due to their nonzero dipole momentums. Some of the unsymmetrical bis(dithiolene) complexes (**14–17**) and heteroleptic dithiolene complexes (**18–21**), which exhibit second order NLO properties are shown in Schemes

1.14 and 1.15, respectively. In those, most promising and extensively studied compounds are heteroleptic Ni(diimine)(dithiolate) complexes as shown Scheme 1.15.^{25,42,80} In order to increase hyperpolarizability of the complexes, the best candidate system should be Pt, with electron donating substituents on the dithiolate ligands (to increase the donor strength), whereas electron withdrawing substituents should be placed on diimine as for as Pt atom is concerned. These compounds exhibit β_0 values within the range from 0 to -16×10^{-30} esu, depending upon the substituents.



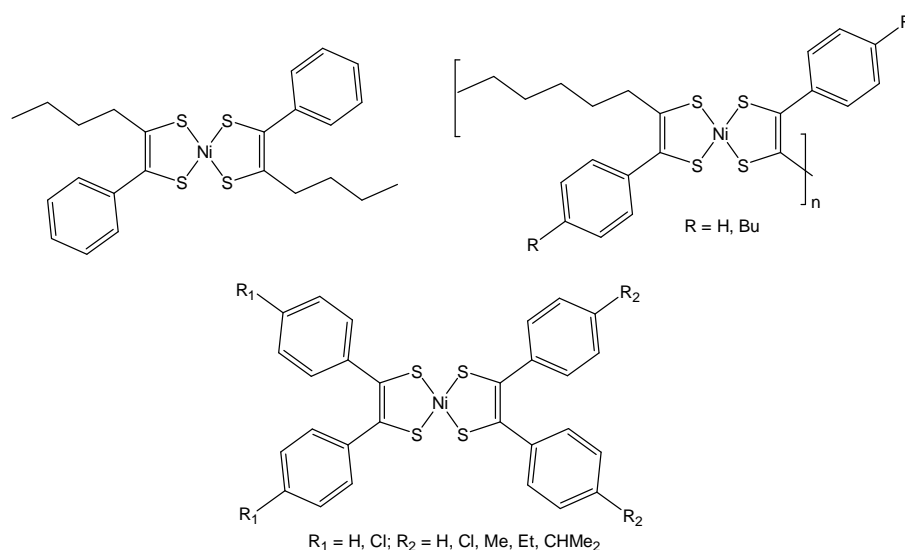
Scheme 1.14



Scheme 1.15

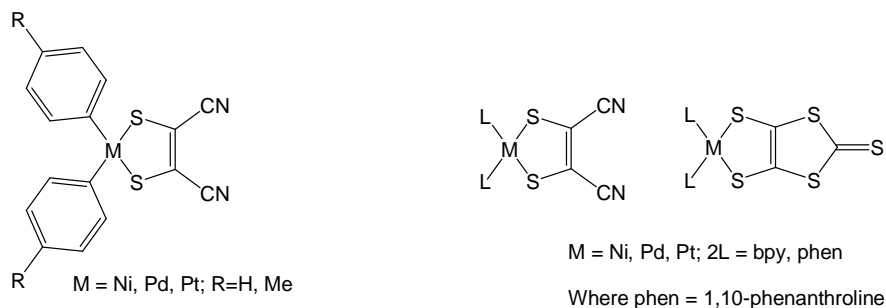
Third Order NLO

The application of third order NLO effects are in various fields such as optical-phase configuration (to restore distorted images), all-optical-switching and computing.⁸¹ Recently, more and more symmetrical bis(dithiolene) complexes with third-order optical nonlinearity or optical limiting effects have been explored because third order NLO effects do not require any symmetry restriction.⁸² Some of the metal bis(dithiolene) complexes exhibiting third order NLO are shown in Scheme 1.16. Third order NLO properties of dmit-based and mnt-based metal complexes with sandwiched organometallic cations $[\text{CpFe}(\eta\text{-C}_6\text{H}_6)]^+$ have also been reported.⁸³



Scheme 1.16

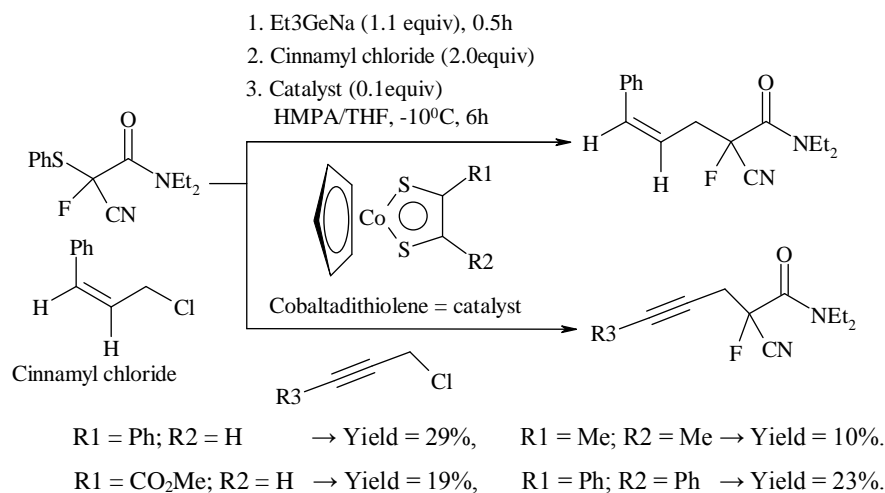
Heteroleptic dithiolene complexes also have been studied for their third-order NLO properties that involve the dmit and mnt ligands as shown in Scheme 1.17,⁸⁴ in which, only the dmit based compounds exhibit a large third-order optical nonlinearity, due to their large planar conjugated system compared to the mnt analogues.



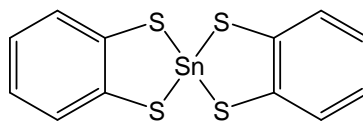
Scheme 1.17

1.5.5. Metal Dithiolene Complexes in Catalysis

The recent research on studying metal dithiolene complexes is a growing field in the sense of catalysis. The metal dithiolene complexes are useful for organic transformations. However, there are very few reports on organic transformations that use a metal bis(dithiolene) complex as a catalyst. Yokoyama and co-workers⁸⁵ described that, the cobaltadithiolene is effective catalyst for synthesis of γ,δ -unsaturated cyanofluoroamide and the reaction is shown in Scheme 1.18. This synthetic reaction proceeded smoothly under mild reaction conditions and only the cyanofluoroamide product was obtained. Interestingly, without cobaltadithiolene complex, no target product was obtained. Another compound tin-bis(1,2-benzenedithiolene) (**22**, Scheme 1.19) has been used as effective catalyst for the reduction of azides to amines, which is reported by Bosch et al.⁸⁶ They observed that a series of primary, secondary, tertiary, aromatic, and heteroaromatic azides can be reduced in excellent yields under very mild conditions in the presence of NaBH_4 . Thus, borohydride ion was a reasonable choice for the reduction of azides to amines, but it is not sufficiently active against azides and favorably the use of tin-bis(1,2-benzenedithiolene) as a catalyst has solved the problem.



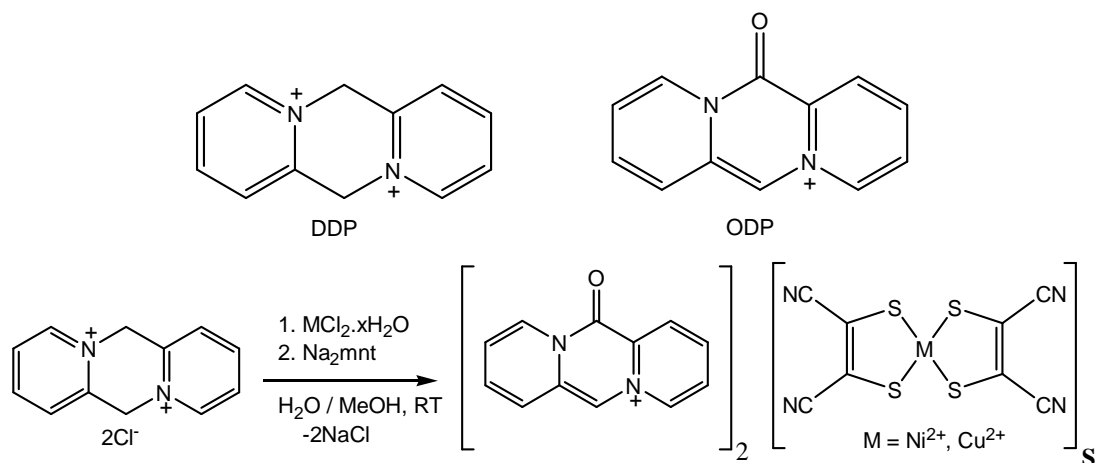
Scheme 1.18. Synthesis of γ,δ -unsaturated cyanofluoroamide with cobaltadithiolene complex as catalyst.



Tin-bis(1,2-benzenedithiolene)

Scheme 1.19

Das and madhu have described an easy oxidation of a condensed heterocyclic system (which incorporate pyridinium cations) in a metal bis(dithiolene) complex matrix.⁸⁷ They have used the metal bis(dithiolene) complex $[M(mnt)_2]^{2-}$ ($M = Ni, Cu$) for the oxidation of DDP ion to ODP ion as shown in Schemes 1.20.



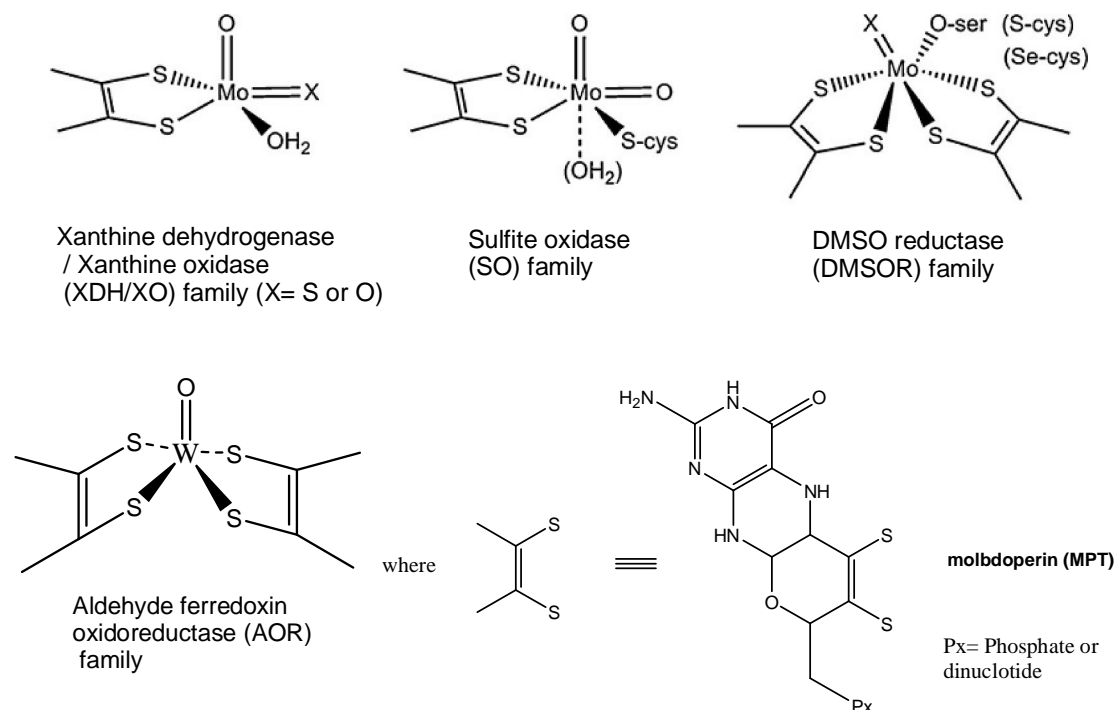
Scheme 1.20

Also some more examples illustrate that, metal dithiolene complexes are not only useful for organic synthesis, but they are also well known for photocatalysis, thermal and electrochemical catalysis.⁸⁸ Both square planar $M[S_2C_2R_1R_2]_2$ and trigonal prismatic $M[S_2C_2R_1R_2]_3$ dithiolenes can be used as photocatalysts, that have been studied in the water splitting reactions for the production of hydrogen. In this case, the dithiolene complex absorbs the light energy, transfers it to water and it also acts as a thermal catalyst in the formation of hydrogen and oxygen.

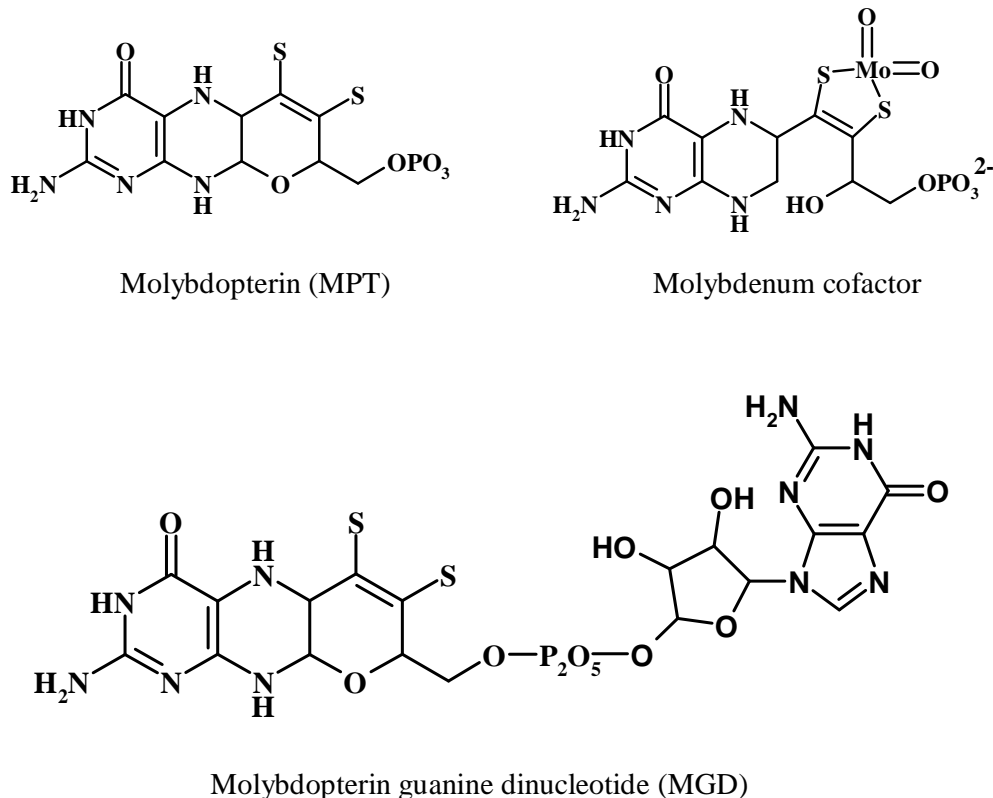
1.6. Metal Dithiolenes in Biology

In contrast to their long history of dithiolene complexes and the studies of their properties towards material science with respect to photonics and electronic conductors, only since last three decades receive considerable interest to those scientists studying biological systems. This is because dithiolene-chelate is involved / present in the active site of certain metalloenzymes, especially Mo- and W- containing enzymes. Depending upon the active-site of the structure dithiolene-containing molybdenum and tungsten enzymes are classified into four families as shown in Scheme 1.20.⁸⁹

Dithiolenes play an important role in natural systems. Thus, a dithiolene group is present an integral component of molybdopterin (MPT), the moiety that binds the molybdenum (or tungsten) at the catalytic centre of enzymes that transfer an oxygen atom to or from the substrate. A wide range of reactions are present in virtually all living systems catalyze by these enzymes, and many of these enzymes are structurally characterized. Each catalytic centre shown to involve a single metal atom bound to one or two MPT groups, plus other donor atoms. Spectroscopic information indicates that the oxygen atom transfer reaction takes place at the metal centre, the oxidation state of which changes from M(VI) to M(IV) (or vice-versa). This chemistry has been replicated by low molecular weight analogues of these centers. However, challenges remain in understanding the coordination chemistry of these centers, not the least of these is the role of the pterin and pyran ring that, together with the dithiolene, form MPT. Whether other roles for dithiolene complexes will be found in Nature remains to be seen. However, the present knowledge should encourage further investigations of dithiolene complexes as catalysts, especially when the process involves a redox change.



Scheme 1.20. The four families of dithiolene-containing molybdenum and tungsten enzymes based on structure of the catalytic reaction centers.



Scheme 1.21. Schematic representations of some of 1,2-dithiolene containing molybdenum and tungsten cofactors in relevant metalloenzymes.

More significantly, the complexes $[\text{Mo}_2(\text{bdt})_2]^{2-}$ and $[\text{Mo}_2(\text{mnt})_2]^{2-}$ ($\text{M} = \text{Mo}$ or W) constitute reasonable structural models for the active site of DMSO-reductase and *Pyrococcus furiosus* AOR, and also serve as functional models for oxotransferase enzymes.⁹⁰ The Mo containing enzyme is called molybdopterin and the crystal structure of one molybdenum-pterin cofactor enzyme, shows coordination of two pterin units to one molybdenum center.⁹¹ Some schematic representations of the 1,2-dithiolene containing molybdenum and tungsten enzymes are depicted in Scheme 1.21.

Rajagopalan and his co-workers⁹² have proposed a structure for the molybdenum cofactor from the various spectroscopic measurements. The proposed structure for the molybdenum cofactor depicts it as a complex of molybdopterin and Mo, with the metal linked to the dithiolene sulfurs. They have suggested that, the molybdopterin is not a unique molecule, since it is found in several forms that differ in the phosphate terminus of the side chain.

1.7. Motivation of the present work

From the above description we have seen that, since last five decades, metal-dithiolene complexes have proved to be an interesting subclass of inorganic coordination compounds that have generated continued interest in structure, bonding and reactivity. The findings show that the dithiolene complexes have useful reactivity and sensing properties and they are present in active sites of many biological essential metallo-enzymes and they display remarkable solid state properties, such as, super conductivity, magnetic, and optical properties. Because of their rich properties, the literature on metal-dithiolene complexes is so vast. However, the coordination polymers, based dithiolene complexes, are still rare in the literature. Metal coordination polymers are particularly interesting in materials chemistry and they display significant solid state properties in the fields of conducting, magnetic, optical (nonlinear) and gas-storage materials. To accomplish these materials, the use of crystal engineering tools becomes crucial to achieve the adequate packing of the molecules that may lead to the desired properties. Very recently, two electro conductive coordination polymers $\text{Cu}[\text{Cu}(\text{pdt})_2]$ and $\text{Cu}[\text{Ni}(\text{pdt})_2]$ have been reported, and these show relatively high electrical conductivity at room temperature with high porosity based on pyrazine bis(dithiolate) building blocks.⁵⁴ In addition, the conductivity of $\text{Cu}[\text{Ni}(\text{pdt})_2]$ has been enhanced through partial oxidation of its framework. The increase in conductivity is due to oxidative doping and the resulting framework is a p-type semiconductor.^{54b} Metal-organic frameworks of these dithiolene based compounds exhibit relatively high electrical conductivity, doping and reox behavior with permanent porosity. This inspired us to choose metal bis(dithiolene) complexes as building blocks for the construction of metal-coordination polymers. Moreover, Rovira and co-workers have reported the alkali coordination polymers of dithiolene complexes by using N-containing dithiolate ligands as building blocks.

Also N-containing based meta-dithiolene complexes are present in active sites of many metallo-enzymes. In this context, particularly qdt (quinoxaline-2,3-dithiolate) ligand and its molybdenum-oxo complexes have been investigated for modeling the active sites of molybdenum hydroxylase enzymes.⁹³ These studies have explored the changes in the redox properties⁹⁴ and the electronic absorption spectra of relevant metal dithiolene complexes upon reversible protonation of the coordinated qdt ligand.⁹⁵ The electronic spectral studies and redox properties would be greater interest in this area of heterocyclic based dithiolene chemistry. The photo-physical (luminescence) properties of platinum

complexes of qdt-type ligand have been studied extensively by Eisenberg's group.⁹⁶ Additionally, qdt-type ligands are useful in the area of analytical chemistry to analyze the metal quantification in ppm levels due to their absorption in visible region with large molar extension coefficient values.⁹⁷ These facts motivated us to design and synthesize new type of qdt-based ligands and to synthesize its metal bis(dithiolene) complexes, so that we can compare the chemistry of this new qdt-system with that of existing qdt compounds. Furthermore, H. B. Gray *et al.* studied that the effect of different substituents on the electronic structure of the $\{MS_4\}$ group in a systematic manner.⁹⁸ This situation encouraged us to design and synthesize, new quinoxaline-dithiolate systems followed by the physical properties. Currently, the generation of field-effect transistors (FET) is further interest in charger carrying semiconductor materials. Recently, qdt-based systems have been used in the development of field-effect transistors by introducing the fused qdt-based systems to the TTF-skeleton.⁹⁹ Based on this, only limited reports have been observed in the literature. This would be a good area of synthesizing new TTF-fused derivatives with new hetrocyclic based ligands in greater extent.

In addition, one or both nitrogen atoms of the $\{qdt\}^{2-}$ ligand in their complexes could be protonated and again deprotonated, meaning that it can show acid-base behavior, as observed in the Ni(II)-,¹⁰⁰ Pt(II)-⁹⁶ and Mo(IV)-qdt complexes.^{93b} This is also an important study, because understanding proton transfer reactions are essential for maintaining cellular life and they are part of the metabolic processes taking part in extra- and intra-cellular fluids.¹⁰¹ For example, the energy needed for maintaining the cell alive is produced by a cycle of reactions implying proton transfer(s).¹⁰¹ But in the literature, there is only one report (in the area of metal dithiolene systems) by Cummings and Eisenberg that described the detailed pH dependent absorption and emission studies of a Pt(II) quinoxaline-2,3-dithiolate ($\{qdt\}^{2-}$) complex $[Bu_4N]_2[Pt(qdt)_2]$.^{96b} Because of this significance of the reversible protonation and deprotonation behavior, we decided to choose another dithiolate ligand containing more number of nitrogen atoms to perform acid-base studies.

1.8. References

- 1 (a) Karlin, K. D.; Stiefel, E. I. *Prog. Inorg. Chem.* John Wiley, New York, **2004**, Volume 52. (b) Locke, J.; McCleverty, J. A.; Wharton, E. J.; Winscom, C. J. *Chem. Commun.* **1966**, 677.
- 2 (a) McCleverty, J. A. *Prog. Inorg. Chem.* **1968**, 10, 49. (b) Müller–Westerhoff, U. T.; Vance, B. in *Comprehensive Coordination Chemistry*, Vol. 2, Wilkinson, G.; Gillard, R. D.; McCleverty, J. A. Eds. Pergamon Press, Oxford, **1987**, p 595. (c) Farrugia, L. J. *J. Appl. Crystallogr.* **1997**, 32, 565. (d) Cowie, M.; Bennett, M. J. *Inorg. Chem.* **1976**, 15, 1595; (e) Alvarez, S.; Vicente, R.; Hoffmann, R. J. *Am. Chem. Soc.* **1985**, 107, 6253. (f) Burns R. P.; McAuliffe, *Adv. Inorg. Chem. Radiochem.* **1979**, 22, 303.
- 3 Balch, A. L.; Dance, I. G.; Holm, R. H. *J. Am. Chem. Soc.* **1968**, 90, 1139.
- 4 (a) Schrauzer, G. N.; Mayweg, V. P. *J. Am Chem. Soc.* **1962**, 84, 3221. (b) Smith, A.E.; Schrauzer, G. N.; Mayweg, V. P.; Heinrich, W. *J. Am Chem. Soc.* **1965**, 87, 5798.
- 5 (a) Baker-Hawkes, M. J.; Billig, E.; Gray, H. B. *J. Am. Chem. Soc.* **1966**, 88, 4870. (b) Shupack, S. I.; Billig, E.; Clark, R. J. H.; Williams, R.; Gray, H. B. *J. Am. Chem. Soc.* **1964**, 86, 4594.
- 6 Davison, A.; Edelstein, N.; Holm, R. H.; Maki, A. H. *J. Am Chem. Soc.* **1963**, 85, 2029.
- 7 (a) Eisenberg, R.; Ibers, J. A.; Clark, R. J. H.; Gray, H. B. *J. Am Chem. Soc.* **1964**, 86, 113. (b) Eisenberg, R.; Ibers, J. A. *Inorg. Chem.* **1965**, 4, 605.
- 8 (a) Beswick, C. L.; Schulman J. M.; Stiefel, E. I. *Prog. Inorg. Chem.* **2003**, 52, 55. (b) Sproules S.; Wieghardt, K. *Prog. Inorg. Chem.* **2003**, 52, 55.
- 9 (a) Roger, M.; Arliguie, T.; Thuery, P.; Fourmigué M.; Ephri-tikhine, M. *Inorg. Chem.* **2005**, 44, 594. (b) Weis, E. M.; Barnes C. L.; Duval, P. B. *Inorg. Chem.* **2006**, 45, 10126.
- 10 (a) Paw, W.; Cummings, S. D.; Mansour, M. A.; Connick, W. B.; Geiger D. K.; Eisenberg, R. *Coord. Chem. Rev.* **1998**, 171, 125. (b) Hissler, M.; McGarrah, J. E.; Connick, W. B.; Geiger, D. K.; Cummings S. D.; Eisenberg, R. *Coord. Chem. Rev.* **2000**, 208, 115.

- 11 (a) Bevilacqua, J. M.; Zuleta J. A.; Eisenberg, R. *Inorg. Chem.* **1994**, 33, 258. (b) Lee, S.-K.; Shin, K.-S.; Noh, D.-Y.; Jeannin, O.; Barrière, F.; Bergamini J.-F.; Fourmigué, M. *Chem.–Asian J.* **2010**, 5, 169.
- 12 (a) Burgmayer, S. J. N. *Prog. Inorg. Chem.* **2003**, 52, 491. (b) McMaster, J.; Tunney J. M.; Garner, C. D. *Prog. Inorg. Chem.* **2003**, 52, 539. (c) Holm, R. H. *Coord. Chem. Rev.* **1990**, 100, 183.
- 13 Kubo, K.; Nakao, A.; Ishii, Y.; Yamamoto, T.; Tamura, M.; Kato, R.; Yakushi K.; Matsubayashi, G. *Inorg. Chem.* **2008**, 47, 5495.
- 14 Bevilacqua, J. M.; Zuleta J. A.; Eisenberg, R. *Inorg. Chem.*, **1993**, 32, 3689.
- 15 (a) Schiødt, N. C.; Sommer-Larsen, P.; Bjørnholm, T.; Nielsen, M. F.; Larsen, J.; Bechgaard, K. *Inorg. Chem.* **1995**, 34, 3688. (b) Huyyett, J. E.; Choudhury, S. B.; Eichhorn, D. M.; Bryngelson, P. A.; Maroney, M. J.; Hoffman, B. M. *Inorg. Chem.* **1998**, 37, 1361. (c) Aragoni, M. C.; Arca, M.; Demartin, F.; Devillanova, F. A.; Garau, A.; Isaia, F.; Lelj, F.; Lippolis, V.; Verani, G. *J. Am. Chem. Soc.* **1999**, 121, 7098.
- 16 (a) Wang, K.; Stiefel, E. I. *Science* **2001**, 291, 106. (b) Harrison, D. J.; Nguyen, N.; Lough, A. J.; Fekl, U. *J. Am. Chem. Soc.* **2006**, 128, 11026.
- 17 Clemenson, P. I.; *Coord. Chem. Rev.* **1990**, 106, 171.
- 18 (a) Chandhramouli, G. V. R.; Manoharan, P. T. *Inorg. Chem.* **1986**, 25, 4680. (b) Lalitha, S.; Chandhramouli, G. V. R.; Manoharan, P.T. *Inorg. Chem.* **1988**, 27, 1492. (c) Vogler A.; Kunkely, H. *J. Chem Soc., Chem. Commun.* **1986**, 1616.
- 19 Cummings, S. D.; Eisenberg, R. *Inorg. Chem.* **1995**, 34, 2007.
- 20 (a) Kisch, H. *Coord. Chem. Rev.* **1997**, 159, 385. (b) Nunn, I.; Eisen, B.; Benedix, R.; Kisch, H. *Inorg. Chem.* **1994**, 33, 5079. (c) Handrosch, C.; Dinnebier, R.; Bondarenko, G.; Bothe, E.; Heinemann, F.; Kisch, H. *Eur. J. Inorg. Chem.* **1999**, 1259. (d) Schmauch, G.; Knoch, F.; Kisch, H.; *Chem. Ber.* **1994**, 127, 287. (e) Dümmler, W.; Kisch, H. *New J. Chem.* **1991**, 15, 649. (f) Kisch, H.; Eisen, B.; Dinnebier, R.; Shankland, K.; David, W. I. F.; Knoch, F.; *Chem. -Eur. J.* **2001**, 7, 738. (g) Kisch, H.; Dümmler, W.; Chiorboli, C.; Scandola, F.; Salbeck, J.; Daub, J. J. *Phys. Chem.* **1992**, 96, 10323.

- 21 Benedix, R.; Hofbauer, M.; Mobius, M.; Knoch, F. *Inorg. Chem. Acta.* **1997**, 262, 177.
- 22 Henning, R.; Schlamann, W.; Kisch, H. *Angew. Chem. Int. Ed. Engl.* **1980**, 19, 645.
- 23 Battaglia, R.; Henning, R.; Dinh-Ngoc, B.; Schlamann, W.; Kisch, H. *J. Mol. Catal.* **1983**, 21, 239.
- 24 (a) Hontzopoulos, E.; Vrachnouastra, E.; Konstantatos, J.; Katakis, D. *J. Photochem.* **1985**, 30, 117. (b) Hontzopoulos, E.; Konstantatos, J.; Vrachnouastra, E.; Katakis, D.; *J. Mol. Cat.* **1985**, 31, 327.
- 25 Cummings, S. D.; Eisenberg, R. *J. Am. Chem. Soc.* **1996**, 118, 1949.
- 26 (a) Miller, T. R.; Dance, G. *J. Am. Chem. Soc.* **1973**, 95, 6970. (b) Vogler, A.; Kunkely, H.; Hlavatsch, J.; Merz, A. *Inorg. Chem.* **1984**, 23, 506.
- 27 (a) Islam, A.; Sugihara, H.; Hara, K.; Singh, L. P.; Katoh, R.; Yanagida, M.; Takahashi, Y.; Murata, S.; Arakawa, H.; Fujihashi, G. *Inorg. Chem.* **2001**, 40, 5371. (b) Geary, E. A. M.; Hirata, N.; Clifford, J.; Durrant, J. R.; Parsons, S.; Dawson, A.; Yellowlees, L. J.; Robertson, N. *Dalton Trans.* **2003**, 3757.
- 28 (a) Islam, A.; Sugihara, H.; Hara, K.; Singh, L. P.; Katoh, R.; Yanagida, M.; Takahashi, Y.; Murata, S.; Arakawa, H.; Fujihashi, G. *Inorg. Chem.* **2001**, 40, 371. (b) Paw, W.; Cummings, S. D.; Mansour, M. A.; Connick, W. B.; Geiger, D. K.; Eisenberg, R. *Coord. Chem. Rev.* **1998**, 171, 125.
- 29 Connick, W. B.; Gray, H. B. *J. Am. Chem. Soc.* **1997**, 119, 11620–11627.
- 30 Cocker, T. M.; Bachman, R. E. *Chem. Commun.* **1999**, 875–876.
- 31 Cocker, T. M.; Bachman, R. E. *Inorg. Chem.* **2001**, 40, 1550–1556.
- 32 a) Robertson, N.; Parsons, S.; Awaga, K.; Fujita, W. *CrystEngComm* **2000**, 2, 121–124. b) Lee, C.-M.; Hsieh, C.-H.; Dutta, A.; Lee, G.-H.; Liaw, W.-F. *J. Am. Chem. Soc.* **2003**, 125, 11492–11493.
- 33 a) van der Zwaan, J. W.; Coremans, J. M. C. C.; Bouwens, E. C.; Albracht, S. P. J. *Biochim. Biophys. Acta.* **1990**, 1041, 101. b) Coremans, J. M. C. C.; van der Waan, J. W.; Albracht, S. P. J. *Biochim. Biophys. Acta.* **1992**, 1119, 157.
- 34 Shin, W.; Lindahl, P. A. *Biochim. Biophys. Acta.* **1993**, 1161, 317.
- 35 Koester, V. J. *Chem. Phys. Lett.* **1975**, 32, 575.

- 36 Benedix, R.; Hennig, H.; Kunkely, H.; Vogler, A. *Chem. Phys. Lett.* **1990**, 175, 483.
- 37 Bartecki, A.; Cieslakgolanka, M.; Pawlowska, M.; Lukowiak, E.; Strek, W.; Bolshakow, A. *Pol. J. Chem.* **1993**, 67, 1555.
- 38 (a) Liu, Z. F.; Hashimoto, K.; Fujishima, A. *Nature* **1990**, 347, 658. (b) Ikeda, T.; Tsutsumi, O. *Science* **1995**, 268, 1873. (c) Kawata, S.; Kawata, Y. *Chem. Rev.* **2000**, 100, 1777. (d) Ichimura, K. *Chem. Rev.* **2000**, 100, 1847.
- 39 (a) Nihei, M.; Kurihara, M.; Mizutani, J.; Nishihara, H., 125, 2964. (b) Nihei, M.; Kurihara, M.; Mizutani, J.; Nishihara, H. *Chem. Lett.* **2001**, 852.
- 40 (a) Coomber, A. T.; Beljonne, D.; Friend, R. H.; Brédas, J. L.; Charlton, A.; Robertson, N.; Underhill, A. E.; Kurmoo, M.; Day, P. *Nature* **1996**, 380, 144. (b) Ren, X. M.; Nishihara, S.; Akutagawa, T.; Noro, S.; Nakamura, T. *Inorg. Chem.* **2006**, 45, 2229. (c) Robertson, N.; Cronin, L. *Coord. Chem. Rev.* **2002**, 227, 93.
- 41 Kato, R. *Chem. Rev.* **2004**, 104, 5319.
- 42 Chen, C. -T.; Liao, S. -Y.; Lin, K. -J.; Lai, L. -L. *Adv. Mater.* **1998**, 3, 334.
- 43 Gama, V.; Henriques, R.T.; Almeida, M.; Veiros, L.; Calhorda, M. J.; Meetsma, A.; de Boer, J. L. *Inorg. Chem.* **1993**, 32, 3705.
- 44 Gama, V.; Henriques, R.T.; Bonfait, G.; Almeida, M.; Meetsma, A.; Van Smaalen, S.; de Boer, J. L. *J. Am. Chem. Soc.* **1992**, 114, 1986.
- 45 (a) Knop, W.; Schnedermann, G. *J. Prakt. Chem.* **1846**, 37, 461. (b) Knop, W. *Justus Liebig's Ann. Chem.* **1842**, 43, 111.
- 46 (a) Bähr, G.; Schleitzer, G.; *Chem. Ber.* **1957**, 90, 438. (b) Krespan, C. G.; Mckusick, B. C.; Carirns, T. L. *J. Am. Chem. Soc.* **1960**, 82, 1515. (c) Schroth, W.; Peschel, J. *Chimia.* **1964**, 18, 171.
- 47 Rosa E. J.; Schrauzer, G. N. *J. Phys. Chem.* **1969**, 73, 3132.
- 48 (a) Underhill, A. E.; Ahmad, M. M. *J. Chem. Soc., Chem. Commun.* **1981**, 67. (b) Kobayashi, A.; Sasaki, Y.; Kobayashi, H.; Underhill, A. E.; Ahmad, M. M. *J. Chem. Soc., Chem. Commun.* **1982**, 390.
- 49 Valade, L.; Bousseau, M.; Gleizes, A.; Cassoux, P. *J. Chem. Soc., Chem. Commun.* **1983**, 110.

- 50 Brossard, L.; Ribault, M.; Bousseau, M.; Valade, L.; Cassoux, P. *C. R. Acad. Sci., Ser. II* **1986**, 302, 205.
- 51 Kobayashi, A.; Kim, H.; Sasaki, Y.; Kato, R.; Kobayashi, H.; Moriyama, S.; Nishio, Y.; Kajita, K.; Sasaki, W. *Chem. Lett.* **1987**, 1819.
- 52 (a) Brossard, L.; Ribault, M.; Bousseau, M.; Valade, L.; Cassoux, P. *C. R. Acad. Sci., Ser. II* **1986**, 302, 205. (b) Kobayashi, A.; Kim, H.; Sasaki, Y.; Kato, R.; Kobayashi, H.; Moriyama, S.; Nishio, Y.; Kajita, K.; Sasaki, W. *Chem. Lett.* **1987**, 1819. (c) Tajima, H.; Inokuchi, M.; Kobayashi, A.; Ohta, T.; Kato, R.; Kobayashi, H.; Kuroda, H. *Chem. Lett.* **1993**, 1235. (d) Brossard, L.; Hurdequint, H.; Ribault, M.; Valade, L.; Legros, L.-P.; Cassoux, P. *Synth. Met.* **1988**, 27, B157. (e) Brossard, L.; Ribault, M.; Valade, L.; Cassoux, P. *J. Phys. (Paris)* **1989**, 50, 1521. (f) Kobayashi, A.; Kobayashi, H.; Miyamoto, A.; Kato, R.; Clark, R. A.; Underhill, A. E. *Chem. Lett.* **1991**, 2163. (f) Kobayashi, H.; Bun, K.; Naito, T.; Kato, R.; Kobayashi, A. *Chem. Lett.* **1992**, 1909. (g) Kato, R.; Kashimura, Y.; Aonuma, S.; Hanasaki, N.; Tajima, H. *Solid State Commun.* **1998**, 105, 561.
- 53 (a) Veldhuizen, Y. S. J.; Veldman, N.; Spek, A. L.; Haasnoot, J. G.; Reedijk, J. *Recl. Trav. Chim. Pays-Bas*, **1995**, 114, 337. (b) Veldhuizen, Y. S. J.; Veldman, N.; Spek, A. L.; Cassoux, P.; Carlier, R.; Mulder, M. J. J.; Haasnoot, J. G.; Reedijk, J. *J. Chem. Soc., Dalton Trans.* **1998**, 2989.
- 54 (a) Kobayashi, Y.; Jacobs B.; Allendorf, M. D.; Long, J. R.; *Chem. Mater.* **2010**, 22, 4120. (b) Takaishi, S.; Hosoda, M.; Kajiwarra, T.; Miyasaka, H.; Yamashita, M.; Nakanishi, Y.; Kitagawa, Y.; Yamaguchi, K.; Kobayashi, A.; Kitagawa, H. *Inorg. Chem.* **2009**, 48, 9048.
- 55 (a) Cassoux, P. *Science*, **1996**, 272, 1277. (b) Kobayashi, H.; Tomita, H.; Naito, T.; Kobayashi, A.; Sakai, F.; Watanabe, T.; Cassoux, P. *J. Am. Chem. Soc.* **1996**, 118, 368. (c) Ueda, K.; Kamata, Y.; Iwamatsu, M.; Sugimoto, T.; Fujita, H. *J. Mater. Chem.* **1999**, 9, 2979.
- 56 (a) Ren, X. M.; Meng, Q. J.; Song, Y.; Lu, C. S.; Hu, C. J.; Chen, X. Y. *Inorg. Chem.* **2002**, 41, 5686. (b) Xie, J. L.; Ren, X. M.; He, C.; Song, Y.; Meng, Q. J.; Kremer, R. K.; Yao, Y. G. *Chem. Phys. Lett.* **2003**, 369, 41. (c) Xie, J. L.; Ren, X. M.; Gao, S.; Zhang, W. W.; Li, Y. Z.; Lu, C. S.; Ni, C. L.; Liu, W. L.; Meng, Q. J.;

- Yao, Y. G. *Eur. J. Inorg. Chem.* **2003**, 2393. (d) Xie, J. L.; Ren, X. M.; Song, Y.; Zou, Y.; Meng, Q. J. *J. Chem. Soc., Dalton Trans.* **2002**, 2868.
- 57 Miller, J. S. *Extended Linear Chain Compounds*; Plenum Press: New York, **1983**.
- 58 (a) Bray, J. W.; Hart, H. R., Jr.; Interrante, L. V.; Jacobs, I. S.; Kasper, J. S.; Watkins, G. D.; Wee, S. H. *Phys. Rev. Lett.* **1975**, 35, 744. (b) Huizinga, S.; Kommandeur, J.; Sawatzky, G. A.; Thole, B. T.; Kopinga, K.; de Jongh, W. J. M.; Roos, J. *Phys. Rev. B* **1979**, 19, 4723. (c) Mukai, K.; Wada, N.; Jamali, J. B.; Achiwa, N.; Narumi, Y.; Kindo, K.; Kobayashi, T.; Amaya, K. *Chem. Phys. Lett.* **1996**, 257, 538. (d) Nakazawa, Y.; Sato, A.; Seki, M.; Saito, K.; Hiraki, K.; Takahashi, T.; Kanoda, K.; Sorai, M. *Phys. Rev. B* **2003**, 68, 085112.
- 59 (a) Bray, J. W.; Hart, H. R.; Interrante, L. V.; Jacobs, I. S.; Kasper, J. S.; Watkins, G. D.; Wee, S. H.; Bonner, J. C. *Phys. Rev. Lett.* **1975**, 35, 744. (b) Jacobs, I. S.; Bray, J. W.; Hart, H. R.; Interrante, L. V.; Kasper, J. S.; Watkins, G. D.; Prober, D. E.; Bonner, J. C. *Phys. Rev. Lett.* **1975**, 35, 744.
- 60 (a) Almeida, M.; Henriques, R. T. In *Handbook of Organic Conductive Molecules and Polymers*, Nalwa, H. S. Ed., John Wiley & Sons, Inc., New York, **1997**, p. 87. (b) Bourbonnais, C.; Henriques, R. T.; Wzietek, P.; Kongeter, D.; Voiron, J.; Jérôme, D. *Phys. Rev. B* **1991**, 44, 641.
- 61 (a) Xie, J.; Ren, X.; Song, Y.; Zhang, W.; Liu, W.; He, C.; Meng, Q. *Chem. Commun.* **2002**, 2346. (b) Ren, X.; Meng, Q.; Song, Y.; Lu, C.; Hu, C. *Inorg. Chem.* **2002**, 41, 5686.
- 62 Anderson, P. W. *Science* **1987**, 235, 1196.
- 63 (a) Dagotto, E.; Rice, T. M.; *Science* **1996**, 271, 618. (b) Scalapino, D. J.; *Nature* **1995**, 377, 12. (c) Hiroi, Z.; Takano, M.; *Nature* **1995**, 337, 41.
- 64 Nishihara, S.; Akutagawa, T.; Hasegawa, T.; Nakamura, T. *Chem. Commun.* **2002**, 408.
- 65 (a) Imai, H.; Otsuka, T.; Naito, T.; Awaga, K.; Inabe, T. *J. Am. Chem. Soc.* **1999**, 121, 8098. (b) Otsuka, T.; Awaga, K.; Imai, H.; Inabe, T. *Synth. Met.* **1999**, 103, 2292.
- 66 König, W. *J. Prakt. Chem.* **1925**, 112, 1.
- 67 Ismailsky, W.; Dissertation, Universität Dresden, **1913**.

- 68 (a) Dilthey, W.; Wizinger, R. *J. Prakt. Chem.* **1928**, *118*, 321. (b) Wizinger, R. *Chimia* **1961**, *15*, 89. (c) Griffiths, J. *Colors and Constitution of Organic Molecules*, Academic press, London, **1976**, ISBN, 0-12-303550-3, LCCC 76-016971.
- 69 Dewar, M. J. S.; Dougherty, R. C. *The PMO Theory of Organic Compounds*, Akademie Verlag, Berlin, **1977** (Abh. Akad. Wiss. DDR Nr.8).
- 70 Auler, H.; Banzer, G. Z. *Krebsforsch.* **1942**, *53*, 65.
- 71 (a) Schrauzer, G. N.; Mayweb, V. P. *J. Am. Chem. Soc.* **1965**, *87*, 1483; **1965**, *87*, 3585. (b) Schrauzer, G. N. *Acc. Chem. Res.* **1969**, *2*, 72. (c) Herman, Z. S.; Kirchner, R. F.; Loew, G. H.; Mueller-Westerhoff, U. T.; Nazzari, A.; Zerner, M. C. *Inorg. Chem.* **1982**, *21*, 46. (d) Lelj, F.; Rosa, A.; Ricciardi, G. P.; Caserin, M.; Christinziano, P. L.; Morelli, G. *Chem. Phys. Lett.* **1989**, *160*, 39.
- 72 U. T. Mueller-Westerhoff, B. Vance, D. I. Yoon, *Tetrahedron* **1991**, *47*, 909.
- 73 (a) Mueller-Westerhoff, U. T.; Vance, B.; Yoon, D. I. *Comp. Coordination. Chem Rev.* **1987**, *22*, 595. (b) Mueller-Westerhoff, U. T.; Yoon, D. I.; Plourde, K. *Mol. Cryst. Liq. Cryst.* **1990**, *183*, 291. (c) Wikes, S. B.; Butler, I. R.; Underhill, A. E.; Hursthouse, M. B.; Hibbs, D. E.; Abdul Malik, K. M. *J. Chem. Soc., Dalton Trans.* **1995**, 897. (d) Wang, F.; Qiu, Y. J.; Reynolds, J. R. *Macromolecules* **1991**, *24*, 4567. (e) Tabushi, I.; Yamamura, K.; Nonoguchi, H. *Chem. Lett.* **1999**, 1373. (f) Lee, H. J.; Noh, D. Y. *Polyhedron*, **2000**, *19*, 425. (g) Bigoli, F.; Deplano, P.; Devillanova, F. A.; Lippolis, V.; Lukes, P. J.; Mercuri, M. L.; Pellinghelli, M. A.; Trogu, E. F. *J. Chem. Soc., Chem. Commun.* **1995**, 371.
- 74 (a) Nakazumi, H. *J. Soc. Dyers Color.* **1988**, *104*, 121. (b) Shiozaki, H.; Nakazumi, H.; Kitao, T. *J. Soc. Dyers Color.* **1988**, *104*, 173. (c) Kuramoto, N. J. *J. Soc. Dyers Color.* **1990**, *106*, 181.
- 75 Namba, K. Jpn. Kokai Tokkyo Koho JP 60 73891, **1985**, *Eur. Pat. Appl. EP* 147083.
- 76 (a) Lehn, J.-M. *Supramolecular Chemistry: Concepts and Perspectives*, VCH: Weinheim, **1995**. (b) Steed, J. W.; Atwood, J. L. *Supramolecular Chemistry*, John Wiley: Chichester, **2000**.
- 77 Nalwa, N. S. *Appl. Organomet. Chem.* **1991**, *5*, 349.

78. Veldhuizen, Y. S. J.; Hassnoot, J. G.; Reedijk, J. *Synth. Met.* **1997**, 86, 1827.
79. (a) Zhai, J.; Huang, C. H.; Wei, T. X.; Gan, L. B.; Cao, H.; *Polyhedron*, **1999**, 18, 1513. (b) Li, H.; Zhou, D.; Huang, C.; Xu, J.; Li, T.; Zhao, X.; Xia, X. *J. Chem. Soc., Faraday Trans.* **1996**, 92, 2585. (c) Zhou, D.; Ashwell, G. J.; Huang, C. *Chem. Lett.* **1997**, 7.
- 80 (a) Chen, C.-T.; Liao, S. Y.; Lin, K. J.; Lin, T. Y. J.; Lia, L. L.; Chen, C. H.; *Nonlinear Optics*, **1999**, 22, 35. (b) Chen, C.-T.; Liao, S. Y.; Lin, K. J.; Chen, C. H.; Lin, T. Y. J. *Inorg. Chem.* **1999**, 38, 2734. (c) Cummings, S. D.; L.-T. Cheng Eisenberg, R. *Chem. Mater.* **1997**, 9, 440. (d) Base, K.; Tiernry, M. T.; Fort, A.; Muller, J.; Grinstaff, M. W. *Inorg. Chem.* **1999**, 38, 287. (e) Wenseleers, W.; Goovaerts, E.; Dhindsa, A. S.; Underhill, *Chem. Phys. Lett.* **1996**, 254, 410.
- 81 Special and Issue *Chem. Rev.* **1994**, 94, 1.
- 82 (a) Winter, C. S.; Hill, C. A. S.; Underhill, A. E. *Appl. Phys. Lett.* **1991**, 58, 107. (b) Zuo, J.-L.; Yao, T.-M.; You, F.; You, X.-Z.; Fun, H. K.; Yip, B. C. *J. Mater. Chem.* **1996**, 6, 1633. (c) Bai, J.-F.; Zuo, J.-L.; Tan, W.-L.; Ji, W.; Shen, Z.; Fun, H.-K.; Chinnakali, K.; Razak, I. A.; You, X.-Z.; Che, C.-M. *J. Mater. Chem.* **1999**, 9, 2419. (d) Ushijima, H.; Kawasaki, T.; Kamata, T.; Kodzasa, T.; Matsuda, H.; Fukaya, T.; Fujii, Y.; Mizukami, F.; *Mol. Cryst. Liq. Cryst.* **1996**, 286, 597.
- 83 Yang, C. L.; Qin, J. G.; Si, J. H.; Wang, Y. G.; Ye, P. X.; Li, Y. L. *Synth. Met.* **1999**, 102, 1578.
- 84 (a) Si, J.; Yang, Q.; Wang, Y.; Ye, P.; Wang, S.; Qin, J.; Liu, D. *Opt. Commun.* **1996**, 132, 311. (b) Yang, C.; Yang, Q.; Si, J.; Wang, S.; Ye, P.; Qin, J. *Poc. SPIE-Int. Soc. Opt. Eng.* **1998**, 3556, 102.
- 85 Yokoyama, Y.; Suzuki, S.; Furihata, H.; Takahi, S.; Nomura, M.; Kajitani, M. *Synthesis*, **2004**, 701.
- 86 Bosch, I.; Costa, A. M.; Martin, M.; Urpi, F.; Vilarrasa, J. *Org. Lett.* **2000**, 2, 397.
- 87 Madhu, V.; Das, S. K.; *Inorg. Chem.* **2006**, 45, 10037.
- 88 Samios, J.; Katakis, D.; Dellis, D.; Lyris, E; Mitsopoulou, C.-A. *J. Chem. Soc., Faraday T rans.* **1998**, 94, 3169.

- 89 (a) Hille, R. *Chem. Rev.* **1996**, 96, 2757. (b) Johnson, M. K.; Rees, D. C.; Adams, M. W. W. *Chem. Rev.* **1996**, 96, 2817. (c) Kisker, C.; Schindelin, H.; Rees, D. C. *Annu. Rev. Biochem.* **1997**, 66, 233.
- 90 Ueyama, N.; Oku, H.; Kondo, M.; Okamura, T.; Yoshinaya, N.; Nakamura, A. *Inorg. Chem.* **1996**, 35, 643.
- 91 Boyington, J. C.; Gladyshev, V. N.; Khangulov, S. V.; Stadtman, T. C.; Sun, P. D. *Science*, **1997**, 275, 1305.
- 92 (a) Kramer, S. P.; Johnson, J. L.; Ribeiro, A. A.; Millington, D. S.; Rajagopalan, K. V. *J. Biol. Chem.* **1987**, 262, 16357. (b) Pilato, R. S.; Stiefel, E. I. in *Bioinorganic catalysis*, Reedijk, J., Bouwman, E., Eds.; Marcel Dekker, New York, **1999**. (c) Rajagopalan, K. V. *Adv. Enzymol. Relat. Areas Mol. Biol.* **1991**, 64, 215–290. (d) Johnson, J. L.; Rajagopalan, K. V. *Proc. Natl. Acad. Sci. U. S. A.* **1982**, 79, 6856.
- 93 (a) Boyde, S.; Garner, C. D.; Enemark, J. H.; Bruck, M. A.; Kristofzski, J. G. *J. Chem. Soc., Dalton. Trans.* **1987**, 2267. (b) Boyde, S.; Garner, C. D.; Enemark, J. H.; Ortega, R. B. *J. Chem. Soc., Dalton. Trans.* **1987**, 297. (c) Boyde, S.; Garner, C. D.; Enemark, J. H.; Ortega, R. B. *Polyhedron* **1986**, 5, 377.
- 94 Theriot, L. J.; Ganguli, K. K.; Kavarnos, S.; Bernal, I. *J. Inorg. Nucl. Chem.* **1969**, 31, 3133.
- 95 Rignedoli, A.; Peyronel, G.; Malavasi, W. *J. Inorg. Nucl. Chem.* **1976**, 38, 1963.
- 96 a) Cummings, S. D.; Eisenberg, R. *Inorg. Chem.* **1995**, 34, 2007–2014; b) Cummings, S. D.; Eisenberg, R. *Inorg. Chem.* **1995**, 34, 3396–3403.
- 97 Bruke, R. W.; Deardorff, E. R. *Talanta* **1970**, 17, 255–264.
- 98 Baker-Hawkes, M. J.; Billig, E.; Gray, H. B. *J. Am. Chem. Soc.* **1966**, 88, 4870–4875.
- 99 Naraso, J. Nishida, D. Kumaki, S. Tokito, Y. Yamashita, *J. Am. Chem. Soc.* **2006**, 128, 9598–9599. b) Naraso, J. Nishida, S. Ando, J. Yamaguchi, K. Itaka, H. Koinuma, H. Tada, S. Tokito, Y. Yamashita, *J. Am. Chem. Soc.* **2005**, 127, 10142–10143.
- 100 Mukhopadhyay, S.; Ray, D. *J. Chem. Soc., Dalton Trans.* **1993**, 1159.
- 101 Bünzli, J. –C. G.; Chauvin, A. –S.; Imbert, D. *Module 4: Proton Tranfer Reactions.*

Self-Assembly of Alkali Metal Based Coordination Polymers of Metal Bis(Dithiolene) Complexes: Role of Coordinated Crystallizing Solvents and Counter Cations in Tuning the Structural Diversity and Dimensionality

2 Chapter

Abstract:– Self assembly of coordination networks based on metal bis(dithiolene) complexes $[M(btdt)_2]^{1-}$ ($M = Cu(III)$ and $Au(III)$; $btdt = 2,1,3$ -benzenethiadiazole-5,6-dithiolate) are influenced by the coordinating solvents through the coordination with sodium metal ion. In order to investigate the effect of coordinating solvent on the dimensionality of the coordination networks, we have synthesized ten coordination polymers $\{[Na(CH_3OH)_4][Cu(btdt)_2]\}_n$ (**1**), $\{[Na(THF)_4][Cu(btdt)_2]\}_n$ (**2**), $\{[Na(CH_3COCH_3)_2][Cu(btdt)_2]\}_n$ (**3**), $\{[Na(DMF)_2][Cu(btdt)_2]\}_n$ (**4**), $\{[Na(CH_3CN)_2][Cu(btdt)_2]\}_n$ (**5**), $\{[Na(CH_3OH)_4][Au(btdt)_2]\}_n$ (**6**), $\{[Na(THF)_2][Na(THF)(OH_2)][Au_2(btdt)_4]\}_n$ (**7**), $\{[Na(CH_3COCH_3)_2][Au(btdt)_2]\}_n$ (**8**), $\{[Na(DMF)_2][Au(btdt)_2]\}_n$ (**9**) and $\{[Na(CH_3CN)_2][Au(btdt)_2]\}_n$ (**10**) by varying the coordinating solvents in respective recrystallization process. In addition to this, a discrete compound $[Na_2(H_2O)_6(\mu-H_2O)_2][Au(btdt)_2]_2$ (**11**) has been synthesized by the recrystallization of the gold compound in MeOH in open air. In the self-assembly process, the dimensionality of the networks of coordination polymers **1–10** has greatly been influenced by the hybridization of central carbon atom attached to the coordinating solvent atom ('N' or 'O') of the recrystallizing solvents. To study the counter cation effect on the structural diversity and dimensionality, we have synthesized two potassium-based coordination polymers $\{[K(CH_3COCH_3)_3][Cu(btdt)_2]\}_n$ (**12**) and $\{[K(CH_3CN)_2][Cu(btdt)_2]\}_n$ (**13**). All these compounds have been structurally characterized unambiguously by single crystal X-ray crystallography. Interestingly, copper compounds **1–5** show two quasi-reversible reduction responses at -0.13 V and -1.10 V vs Ag/AgCl in DMF solutions.

2.1. Introduction

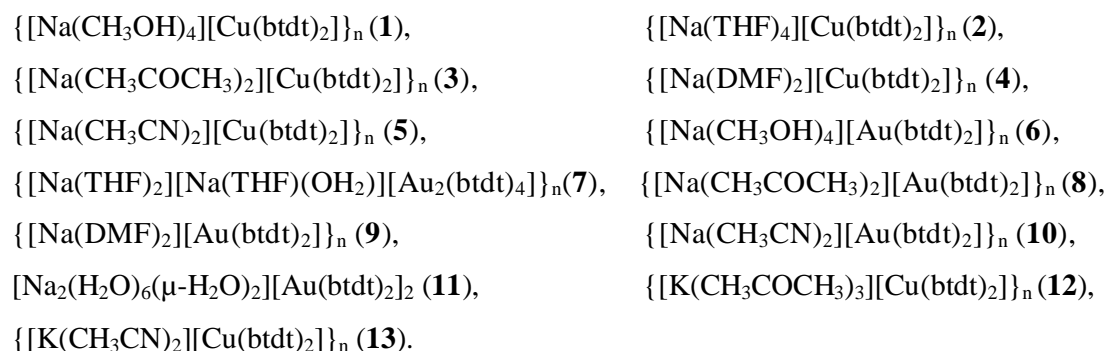
The design and syntheses of coordination polymers or metal-organic frameworks (MOFs), that involves attentive selection of organic ligands with suitable functional groups and metal ions, have attracted considerable attention for producing solid-functional materials, which have the potential to be used as gas storage, nonlinear optical, conducting and magnetic materials.¹⁻² Controlling the self-assembly of coordination polymers in terms of their dimensionality (1D, 2D and 3D) is a challenging task. This is because the properties of these coordination polymers can be tuned by the structural diversity and dimensionality of polymeric materials. Thus, by precise prediction of diversity and dimensionality of self-assembled-coordination networks, we can control the properties of solid-functional materials.³ In the self-assembly process of a coordination polymer, generally, the structural diversity and dimensionality are greatly effected by the choice of the ligands,⁴ metal / ligand ratios,⁵

solvents⁶ and counterions.⁷ Among these factors, influence of solvents and counterions are particularly interesting because, simply, the variations in solvents and counterions, results in a variety of self assembled structures.⁶⁻⁷ Generally, a solvent can influence the structure assemblies of coordination architecture either by playing role as reaction medium or in the re-crystallization process. In the course of crystallization, the solvents can control the crystal structure of coordination networks by its lattice formation without involving in the final product or its incorporation as guests into the structures without coordination to the complexing moiety or its involvement in the coordination to metal ion by coordinate covalent bond.⁶ In the latter case (its coordination to a metal ion), solvents can directly influence the dimensionality of self-assembled network, due to difference in their shape, size and polarity. Effects of solvents on the dimensionality of self-assembled coordination networks are demonstrated in previous reports.⁶ However, the role of a coordinating solvent on the structure assemblies of coordination networks has still not been well understood.

On the other hand, square-planar metal-dithiolene complexes have been used as building blocks for the construction of polymeric compounds to obtain promising materials, such as, conducting, magnetic and non linear optical materials.⁸ However, the investigation of influence of solvents on the coordination networks, based on a square-planar metal bis(dithiolene) complex, is hardly explored. In the present chapter, we have demonstrated a systematic study of the solvent effects on the formation of crystalline coordination networks of diverse dimensionalities (from 1D to 3D) by employing different coordinating solvents such as, MeOH, THF, CH₃COCH₃, DMF and CH₃CN through their coordination with the sodium cation. We have demonstrated that the geometry of the central carbon of crystallizing coordinating solvents plays an important role in directing the dimensionality of coordination polymers. We have also described that, during recrystallization process, sp³ hybridized central carbon containing solvents, such as, MeOH and THF solvents lead to 1D coordination polymers, sp² hybridized central carbon containing solvents, such as, DMF and acetone solvents lead to 2D coordination polymers and sp hybridized central carbon containing solvents, such as, acetonitrile solvent leads to 3D coordination polymers.

We have reported here, five new coordination polymers **1–5** based on [Cu^{III}(btdt)₂]¹⁻ and five new coordination polymers **6–10** and one discrete compound **11** based on

$[\text{Au}^{\text{III}}(\text{btdt})_2]^{1-}$ (btdt = 2,1,3-benzenethiadiazole-5,6-dithiolate) systems by varying the coordinating solvents, by coupling with Na^+ ion, where the dimensionality would be controlled by the nature of the hybridization of the sodium coordinating solvent. In order to investigate the counterion effect, we have synthesized two coordination polymers **12** and **13**, by using the potassium(I) as a counter cation. All these compounds have been structurally characterized unambiguously by single crystal X-ray crystallography including with their spectral characterizations (IR, NMR and UV-Vis), and elemental analysis. We have also described electrochemical properties of compounds **1–5** in solution state.



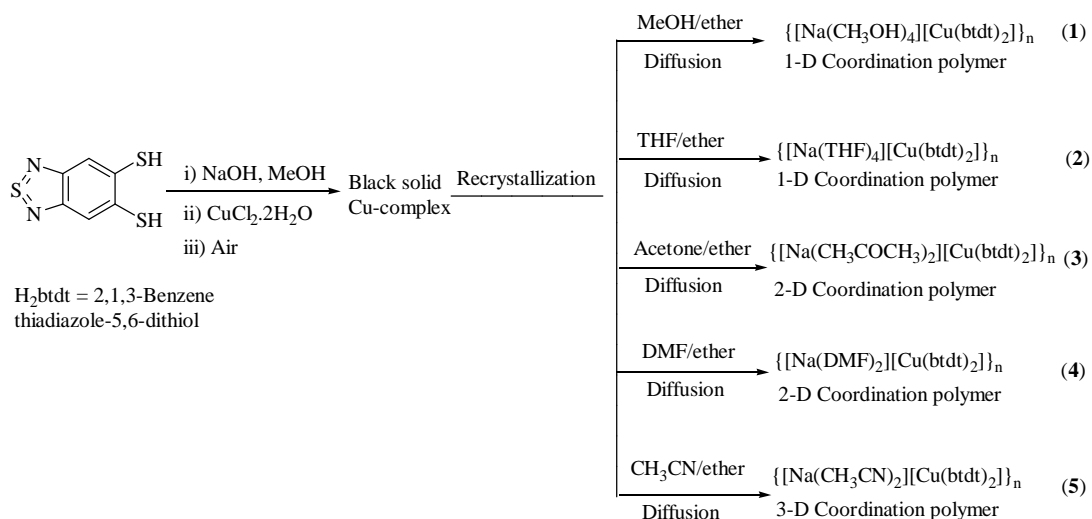
2.2. Experimental Details

2.2.1. General

FLASH EA series 1112 CHNS analyzer performed elemental analyses. Infrared spectra were recorded as KBr pellets on a JASCO-5300 FT-IR spectrophotometer at 298K. Electronic absorption spectra of solutions were recorded on a Cary 100 Bio UV-Vis spectrophotometer. Diffuse reflectance spectra of solid compounds were recorded on a UV-3600 Shimadzu UV-Vis-NIR spectrophotometer. NMR spectra were recorded in Bruker 400 MHz spectrometer. The chemical shifts (δ) are reported in ppm. A Cypress model CS-1090/CS-1087 electro analytical system was used for cyclic voltammetric experiments. The electrochemical experiments were performed in DMF containing $[\text{Bu}_4\text{N}][\text{ClO}_4]$ as a supporting electrolyte, using a conventional cell consisting of two platinum wires as working and counter electrodes, and a Ag/AgCl electrode as a reference. The potentials reported here are uncorrected for junction contributions.

2.2.2. Materials

All the reagents for the syntheses were commercially available and used as received. 2,1,3-Benzenethiadiazole-5,6-dithiol (H_2btdt) ligand was synthesized according to literature procedure.⁹ Syntheses of metal complexes were performed under N_2 using standard inert-atmosphere techniques. Solvents were dried by standard procedures.



Scheme 2.1. Synthesis of coordination polymers **1–5**.

2.2.3. Synthesis and Characterization

Synthesis of Copper Complexes 1-5

The $btdt$ dianion is generated, *in situ*, by treatment of H_2btdt (0.070 g, 0.35 mmol) with excess amount of NaOH (0.040 g, 1.0 mmol) in MeOH (7.0 mL). To the resulting clear red solution, solid $CuCl_2 \cdot 2H_2O$ (0.030 g, 0.176 mmol) was added and the reaction mixture was stirred for 30 min in presence of open atmosphere. The resulting dark black micro crystalline solid was separated by filtration and air dried. Yield: 0.040 g. IR (KBr, cm^{-1}): 3396w, 1630m, 1477s, 1419s, 1242s, 1078s, 825s, 640m, 522m. 1H NMR (400 MHz, δ ppm) ($DMSO-d_6$): 7.63(s, 4H). Coordination polymers **1–5** have been prepared from the different solvent recrystallizations of this black colored solid.



Black colored crystals of compound **1** were obtained from the vapor diffusion of diethyl ether into a solution of the black solid compound dissolved in MeOH solvent. Anal. Calcd.

for $C_{16}H_{20}N_4O_4S_6NaCu$: C, 31.44; H, 3.30; N, 9.17. Found: C, 31.62; H, 3.19; N, 9.05. IR (KBr, cm^{-1}): 3398w, 1633m, 1475s, 1419s, 1244s, 1078s, 823s, 640m, 522m. 1H NMR (400 MHz, δ ppm) (DMSO- d_6): 7.64(s, 4H).

$\{[Na(THF)_4][Cu(btdt)_2]\}_n$ (2)

Black colored crystals of compound **2** were obtained from the vapor diffusion of diethyl ether into a solution of the black solid compound dissolved in THF solvent. Anal. Calcd. for $C_{28}H_{36}N_4O_4S_6NaCu$: C, 43.59; H, 4.70; N, 7.26. Found: C, 43.28; H, 4.51; N, 7.68. IR (KBr, cm^{-1}): 1626m, 1471s, 1419s, 1242s, 1076s, 852m, 825s, 626m, 520m. 1H NMR (400 MHz, δ ppm) (DMSO- d_6): 7.64(s, 4H).

$\{[Na(CH_3COCH_3)_2][Cu(btdt)_2]\}_n$ (3)

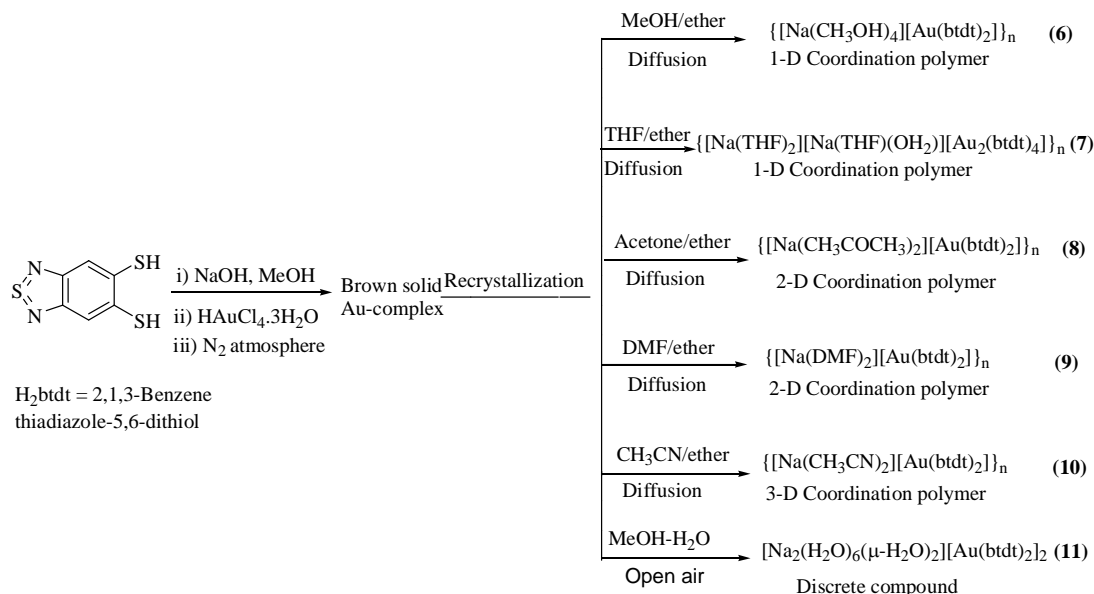
Black colored crystals of compound **3** were obtained from the vapor diffusion of diethyl ether into a solution of the black solid compound dissolved in acetone solvent. Anal. Calcd. for $C_{18}H_{16}N_4O_2S_6NaCu$: C, 36.08; H, 2.69; N, 9.35. Found: C, 35.79; H, 2.81; N, 9.58. IR (KBr, cm^{-1}): 1697m, 1633m, 1477s, 1419s, 1242s, 1078s, 825s, 640m, 522m. 1H NMR (400 MHz, δ ppm) (DMSO- d_6): 7.64(s, 4H).

$\{[Na(DMF)_2][Cu(btdt)_2]\}_n$ (4)

Black colored crystals of compound **4** were obtained from the vapor diffusion of diethyl ether into a solution of the black solid compound dissolved in DMF solvent. Anal. Calcd. for $C_{18}H_{18}N_6O_2S_6NaCu$: C, 34.36; H, 2.88; N, 13.35. Found: C, 34.51; H, 3.02; N, 13.14. IR (KBr, cm^{-1}): 1658s, 1631m, 1477s, 1419s, 1242s, 1079s, 824s, 640m, 522m. 1H NMR (400 MHz, δ ppm) (DMSO- d_6): 7.64(s, 4H).

$\{[Na(CH_3CN)_2][Cu(btdt)_2]\}_n$ (5)

Black colored crystals of compound **5** were obtained from the vapor diffusion of diethyl ether into a solution of the black solid compound dissolved in acetonitrile solvent. Anal. Calcd. for $C_{16}H_{10}N_6S_6NaCu$: C, 34.00; H, 1.78; N, 14.87. Found: C, 33.61; H, 1.91; N, 15.08. IR (KBr, cm^{-1}): 2254m, 1633m, 1477s, 1419s, 1242s, 1078s, 823s, 640m, 522m. 1H NMR (400 MHz, δ ppm) (DMSO- d_6): 7.64(s, 4H).



Scheme 2.2. Synthesis of gold compounds **6–11**.

Syntheses of Gold Complexes **6–11**

The btdt dianion is generated, *in situ*, by treatment with H_2btdt (0.165 g, 0.825 mmol) with excess amount of NaOH (0.15 g, 3.75 mmol) in MeOH (10 mL). To the resulting clear red solution, solid $\text{H[AuCl}_4\text{]}\cdot 3\text{H}_2\text{O}$ (0.175 g, 0.444 mmol) was added and the reaction mixture was stirred for 30 min under nitrogen atmosphere. The resulting brown solid was separated by filtration and air dried. Yield: 0.250 g. IR (KBr, cm^{-1}): 3435br, 1628s, 1602m, 1475s, 1419s, 1238s, 1074s, 827s, 706m, 636m, 522m. ^1H NMR (400 MHz, δ ppm) ($\text{DMSO-}d_6$): 7.81(s, 4H). Coordination polymers **6–10** and a discrete compound **11** have been prepared from the various solvent recrystallization of the above mentioned brown-colored solid.

$\{[\text{Na}(\text{CH}_3\text{OH})_4][\text{Au}(\text{btdt})_2]\}_n$ (**6**)

The red colored crystals of compound **6** was obtained from the vapor diffusion of ether into a solution of the brown solid compound dissolved in dry MeOH. Anal. calcd. for $\text{C}_{16}\text{H}_{20}\text{N}_4\text{O}_4\text{S}_6\text{NaAu}$: C, 25.81; H, 2.71; N, 7.52%. Found: C, 25.45; H, 2.93; N, 7.40%. IR spectrum (KBr, cm^{-1}): 3427br, 1633s, 1602m, 1475s, 1421s, 1238s, 1074s 827s, 706m, 634m, 522m. ^1H NMR (400 MHz, δ ppm) ($\text{DMSO-}d_6$): 7.81(s, 4H).

$\{[\text{Na}(\text{THF})_2][\text{Na}(\text{THF})(\text{OH}_2)][\text{Au}_2(\text{btdt})_4]\}_n$ (7)

Red colored crystals of compound **7** were obtained from the vapor diffusion of ether into a solution of the brown colored solid compound dissolved in THF solvent. Anal. calcd. for $\text{C}_{36}\text{H}_{30}\text{N}_8\text{O}_4\text{S}_{12}\text{Na}_2\text{Au}_2$: C, 29.55; H, 2.07; N, 7.66%. Found: C, 30.10; H, 2.38; N, 7.89%. IR (KBr, cm^{-1}): 3474s, 1630m, 1477s, 1423s, 1242s, 1074s, 831s, 524m. ^1H NMR (400 MHz, δ ppm) ($\text{DMSO}-d_6$): 7.81(s, 4H).

 $\{[\text{Na}(\text{CH}_3\text{COCH}_3)_2][\text{Au}(\text{btdt})_2]\}_n$ (8)

Red colored crystals of compound **8** were obtained from the vapor diffusion of diethyl ether into a solution of the brown colored solid compound dissolved in acetone solvent. Anal. Calcd. for $\text{C}_{18}\text{H}_{16}\text{N}_4\text{O}_2\text{S}_6\text{NaAu}$ (**8**): C, 29.51; H, 2.20; N, 7.65%. Found: C, 28.94; H, 2.38; N, 7.90%. IR (KBr, cm^{-1}): 1699s, 1628m, 1473s, 1421s, 1242s, 1074s, 821s, 634m, 522m. ^1H NMR (400 MHz, δ ppm) ($\text{DMSO}-d_6$): 7.81(s, 4H).

 $\{[\text{Na}(\text{DMF})_2][\text{Au}(\text{btdt})_2]\}_n$ (9)

The red colored crystals of compound **9** was obtained from the vapor diffusion ether into a solution of the brown solid compound dissolved in DMF. Anal. calcd. for $\text{C}_{18}\text{H}_{18}\text{N}_6\text{O}_2\text{S}_6\text{NaAu}$: C, 28.35; H, 2.38; N, 11.02%. Found: C, 28.20; H, 2.16; N, 11.24%. IR spectrum (KBr, cm^{-1}): 2918w, 2868w, 1657s, 1477s, 1419s, 1242s, 1080s, 823s, 640s, 526m. ^1H NMR (400 MHz, δ ppm) ($\text{DMSO}-d_6$): 7.81(s, 4H).

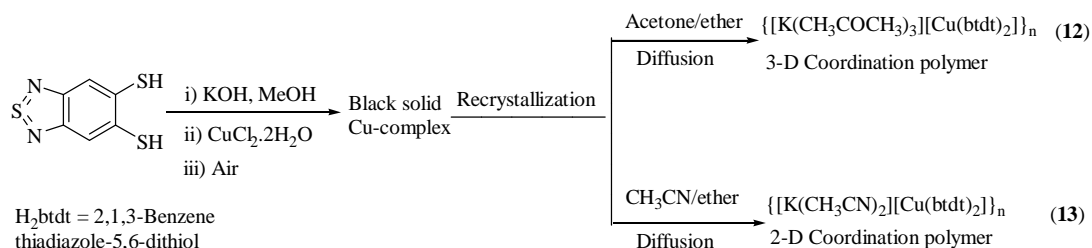
 $\{[\text{Na}(\text{CH}_3\text{CN})_2][\text{Au}(\text{btdt})_2]\}_n$ (10)

The red colored crystals of compound $\{[\text{Na}(\text{CH}_3\text{CN})_2][\text{Au}(\text{btdt})_2]\}_n$ (**10**) was obtained from the vapor diffusion ether into a solution of the brown solid compound dissolved in CH_3CN . Anal. calcd. for $\text{C}_{16}\text{H}_{10}\text{N}_6\text{S}_6\text{NaAu}$ (**10**): C, 27.51; H, 1.44; N, 12.29%. Found: C, 27.78; H, 1.30; N, 12.08%. IR spectrum (KBr, cm^{-1}): 2255m, 1630m, 1476s, 1421s, 1241s, 1077s, 826s, 640m, 525m. ^1H NMR (400 MHz, δ ppm) ($\text{DMSO}-d_6$): 7.81(s, 4H).

 $[\text{Na}_2(\text{H}_2\text{O})_6(\mu\text{-H}_2\text{O})_2][\text{Au}(\text{btdt})_2]_2$ (11)

The dark brown colored crystals of compound $[\text{Na}_2(\text{H}_2\text{O})_6(\mu\text{-H}_2\text{O})_2][\text{Au}(\text{btdt})_2]_2$ (**11**) was obtained from the slow evaporation of solution of the brown solid compound dissolved in commercial MeOH in open air conditions. Anal. calcd. for $\text{C}_{12}\text{H}_{12}\text{N}_4\text{O}_4\text{S}_6\text{NaAu}$: C, 20.93;

H, 1.76; N, 8.14%. Found: C, 21.22; H, 1.67; N, 8.07%. IR spectrum (KBr, cm^{-1}): 3466br, 3369br, 1637s, 1477s, 1425s, 1242s, 1078s 833s, 706m, 528m.



Scheme 2.3. Synthesis of potassium-based coordination polymers **12–13**.

Synthesis of Potassium-Based Coordination Polymers **12–13**

The btdt dianion is generated, *in situ*, by treatment of H_2btdt (0.200 g, 1.0 mmol) with excess amount of KOH (0.2 g, 3.57 mmol) in MeOH (10.0 mL). To the resulting clear red solution, solid $\text{CuCl}_2 \cdot 2\text{H}_2\text{O}$ (0.085 g, 0.5 mmol) was added and the reaction mixture was stirred for 30 min in presence of open atmosphere. The resulting dark black micro crystalline solid was separated by filtration and air dried. Yield: 0.180 g. IR (KBr, cm^{-1}): 3417, 2964, 1597, 1478, 1422, 1384, 1361, 1262, 1242, 1080, 853, 799, 701, 618, 525, 475. ^1H NMR (400 MHz, δ ppm) ($\text{DMSO}-d_6$): 7.63(s, 4H). K-based coordination polymers **12–13** have been prepared from the acetone and acetonitrile solvents recrystallization of this black colored solid, respectively.

$\{[\text{K}(\text{CH}_3\text{COCH}_3)_3][\text{Cu}(\text{btdt})_2]\}_n$ (12)

Black colored crystals of compound **12** were obtained from the vapor diffusion of diethyl ether into a solution of the black solid compound dissolved in acetone solvent. Anal. calcd. for $\text{C}_{21}\text{H}_{22}\text{N}_4\text{O}_3\text{S}_6\text{KCu}$: C, 37.45; H, 3.29; N, 8.32%. Found: C, 37.25; H, 3.52; N, 8.19%. IR (KBr, cm^{-1}): 3414, 2963, 1594, 1479, 1420, 1363, 1261, 1242, 1079, 1022, 800, 701, 524, 467. ^1H NMR (400 MHz, δ ppm) ($\text{DMSO}-d_6$): 7.63(s, 4H).

$\{[\text{K}(\text{CH}_3\text{CN})_2][\text{Cu}(\text{btdt})_2]\}_n$ (13)

Black colored crystals of compound **13** were obtained from the vapor diffusion of diethyl ether into a solution of the black solid compound dissolved in acetonitrile solvent. Anal. calcd. for $\text{C}_{16}\text{H}_{10}\text{N}_6\text{S}_6\text{KCu}$: C, 33.06; H, 1.73, N, 14.46%. Found: C, 33.47; H, 1.99; N,

14.12%. IR (KBr, cm^{-1}): 3405, 2963, 2925, 2833, 1585, 1479, 1419, 1363, 1261, 1242, 1097, 1078, 1022, 862, 844, 825, 800, 524. ^1H NMR (400 MHz, δ ppm) ($\text{DMSO}-d_6$): 7.63(s, 4H).

2.2.4. Single Crystal Structure Determination

Single crystals suitable for facile structural determination for the compounds (**1–3**, **5–10** and **13**), were measured on a three circle Bruker SMART APEX CCD area detector system under $\text{Mo-K}\alpha$ ($\lambda = 0.71073 \text{ \AA}$) graphite monochromatic X-ray beam. The frames were recorded with an ω scan width of 0.3° , each for 8 s, crystal-detector distance 60 mm, collimator 0.5 mm. Data reduction performed by using SAINTPLUS.¹⁰ Empirical absorption corrections using equivalent reflections performed program SADABS.¹⁰ Crystal data for compounds **4** and **11–12** were collected on Oxford, Gemini diffractometer equipped with EOS CCD detector at 100 K. Monochromatic $\text{Mo K}\alpha$ radiations (0.71073 \AA) was used for the measurements. Absorption corrections using multi ψ -scans were applied. The Structures were solved by direct methods and least-square refinement on F^2 for all the compounds **1–13** by using SHELXS-97.¹¹ All non-hydrogen atoms was refined anisotropically. The hydrogen atoms were included in the structure factor calculation by using a riding model. The crystallographic parameters, data collection and structure refinement of the compounds **1–13** are summarized in Tables 2.1–2.5. Selected bond lengths and angles for the compounds **1–13** are listed in Tables 2.6–2.18.

2.3. Results and Discussion

2.3.1. Synthesis and Spectroscopic Characterization

The synthetic route for the compounds **1–5** are shown in Scheme 2.1. Copper coordination polymers **1–5** were obtained from different solvent recrystallization of black colored solid which was obtained from the reaction of one mole equivalent of $\text{CuCl}_2 \cdot 2\text{H}_2\text{O}$ with two mole equivalents of H_2btdt in MeOH treated with excess amount of NaOH in presence of open atmosphere. Recrystallization from the MeOH/ether and THF/ether diffusion lead to the formation of 1D coordination polymers, acetone/ether and DMF/ether diffusion leads to formation of 2D coordination polymers and acetonitrile / ether diffusion leads to the formation of 3D coordination polymer. In all these polymeric compounds **1–5**, Na^+ ion is

the counter cation. In the same way, we have synthesized gold compounds **6–11**, by using $\text{HAuCl}_4 \cdot 3\text{H}_2\text{O}$ instead of $\text{CuCl}_2 \cdot 2\text{H}_2\text{O}$, in the reaction procedure, as shown in Scheme 2.2. The K-based coordination polymers **12** and **13** have been prepared by using same reaction procedure using for the synthesis of Na-based coordination polymers **1–5**, but the KOH is used for the de-protonation (Scheme 2.3) instead of using NaOH in the Scheme 2.1. The black colored solid compound obtained from the reaction Scheme 2.3 was used for the synthesis of coordination polymers **12–13**. Recrystallizations from acetone and acetonitrile / ether diffusions lead to the formation of 3-D and 2-D coordination polymers, respectively. All the Compounds **1–13** have been characterized by single crystal X-ray crystallography and further characterized by IR, ^1H NMR, UV-Visible spectroscopy and including their elemental analysis (experimental section).

Spectroscopy

IR Spectroscopy

From the IR spectra (Figure 2.1), we have observed three bands at 1697, 1657 and 2255 cm^{-1} , that are due to the coordinated solvent molecules such as acetone ($\nu_{\text{C=O}}$) in complexes **3** and **8**, DMF ($\nu_{\text{C=O}}$) in complexes **4** and **9**, and CH_3CN ($\nu_{\text{C}\equiv\text{N}}$) in complexes **5** and **10**, respectively. A discrete gold compound **11** shows a broad IR bands at 3466 and 3369 cm^{-1} , are due to the O–H stretching frequency, conforming the presence of water molecules present in the compound.

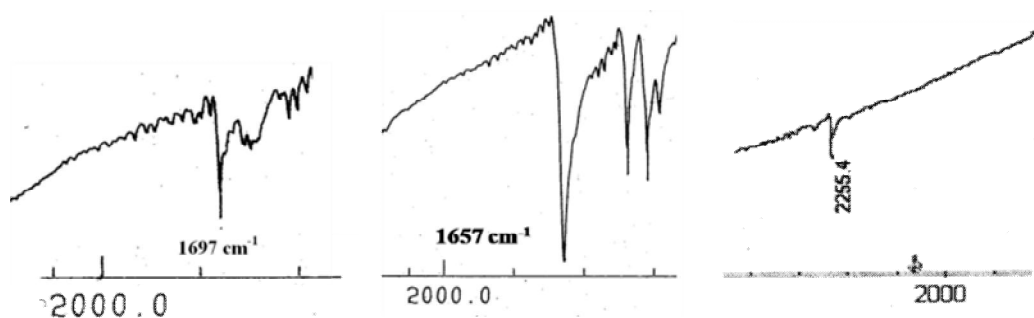


Figure 2.1. IR spectra of (a) compound **3** ($\nu_{\text{C=O}}$); (b) compound **4** ($\nu_{\text{C=O}}$) and (c) compound **5** ($\nu_{\text{C}\equiv\text{N}}$) in the frequency regions of respective coordinating solvents.

^1H NMR Spectroscopy

^1H NMR spectra of Cu-coordination polymers **1–5** show single narrow peak at 7.63 ppm in $\text{DMSO-}d_6$ corresponding to the four benzene protons from the btdt ligands. As representative example, the ^1H NMR spectrum of compound **3** in $\text{DMSO-}d_6$ solution is shown in Figure 2.2. According to the nature and position of the signal, copper compounds in the present study are diamagnetic square planar $\text{Cu(III) } d^8$ coordination complexes, as expected.^{8c} As in the case of Au-coordination polymers **6–10**, also we have observed single narrow peak at 7.81 ppm in $\text{DMSO-}d_6$ related to the four benzene protons from the btdt ligands.

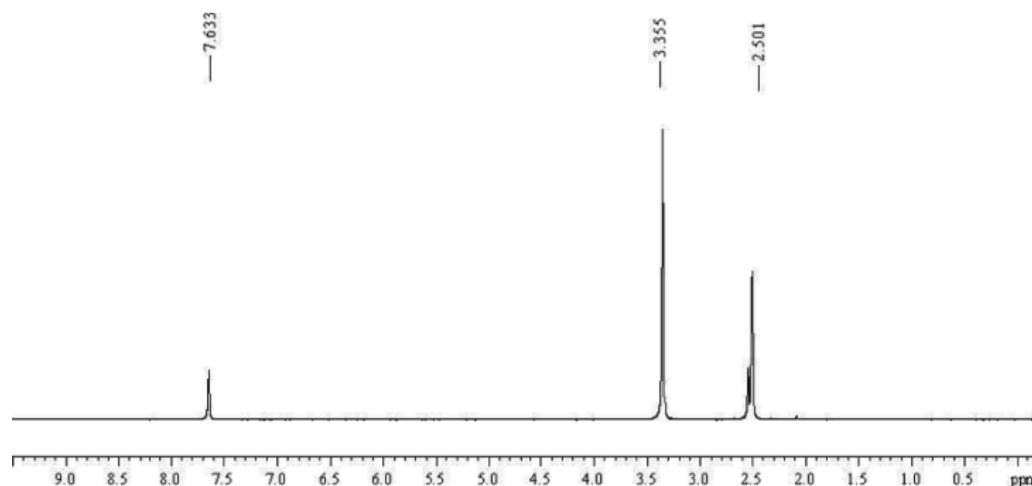


Figure 2.2. ^1H NMR spectrum of compound **3** in $\text{DMSO-}d_6$ solution.

ESR Spectroscopy

None of these copper compounds exhibit any ESR signals confirming again that these complexes are Cu(III) complexes.

UV-Visible Absorption Spectroscopy

Copper coordination polymers **1–5** show strong absorption band at 425–435 nm in the visible region in the solutions of their corresponding recrystallizing solvents as shown in Figure 2.3(a). In addition to this common feature, there is a weak absorption band observed at higher concentrations in the region of 540–600 nm, for the copper complexes **1–5**, as shown in inset of Figure 2.3(a). The appearance of this weak feature at relatively higher concentrations can be explained by the intermolecular interactions that may occur

at higher concentrations.¹² The weak band feature at around 540–600 nm can also be due to $d-d$ transition for a Cu(III) (d^8) system. In the solid state, copper coordination polymers **1**, **3** and **4** show band at ~ 435 nm, in its diffuse reflectance spectra, as shown in Figure 2.3(b); this band position is consistent with that of the solution state of all copper complexes. The similar spectral feature has been observed for the gold compounds **6–11**. We have also observed the similar spectral feature has been observed for the K-coordination polymers **12–13**. The diffuse reflectance of spectra of compounds **12–13** show absorption bands at 420–450 nm regions as shown in Figure 2.3(c).

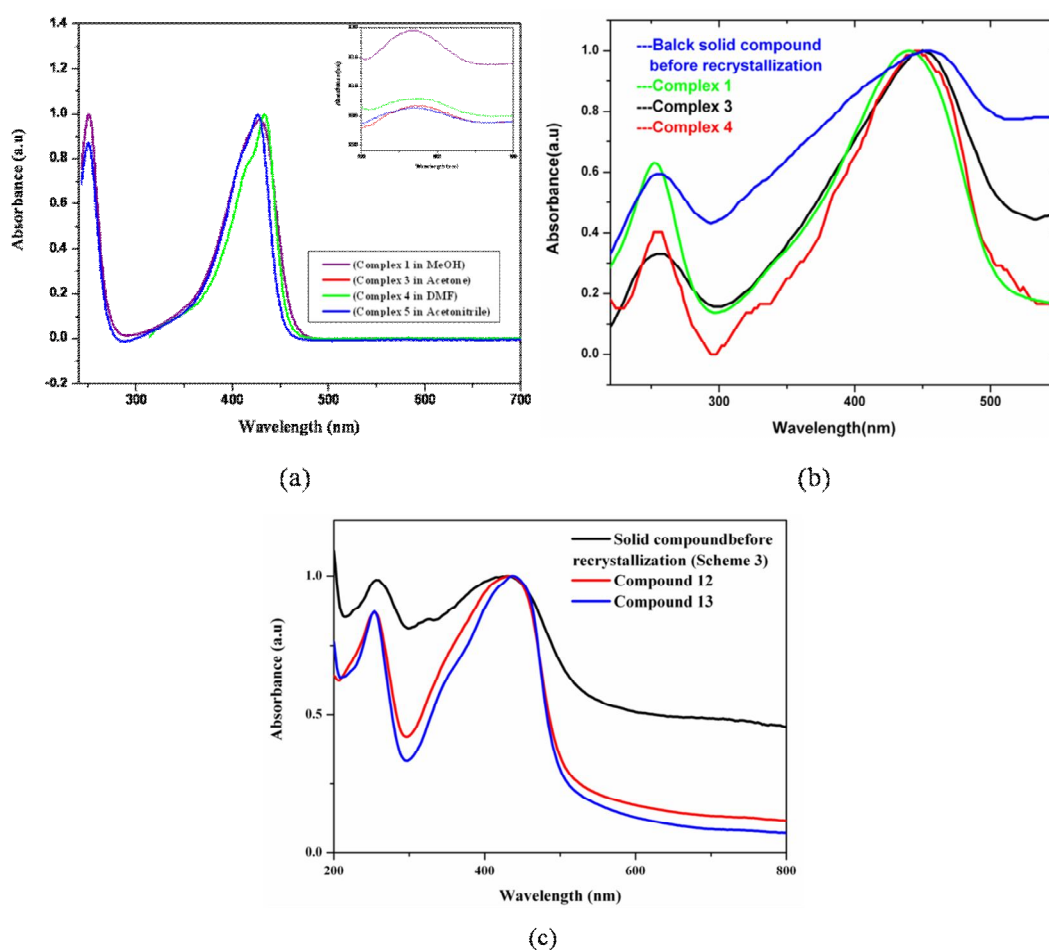


Figure 2.3. (a) Normalised electronic absorption spectra of compounds **1–5** in their respective recrystallizing solvents; (b) The solid state (diffuse reflectance) spectra (normalised) of compounds **1**, **3** and **4** and black solid compound (Scheme 1); (c) The solid state (diffuse reflectance) spectra (normalised) of compounds **12** and **13** and black solid compound (Scheme 3).

2.3.2. Electrochemical Studies

In cyclic voltammetric studies of Cu-compounds **1–5**, a common Cu(III)/Cu(II) redox

couple appears as quasi-reversible wave at $E_{1/2} = -0.13$ V vs Ag/AgCl ($\Delta E = 90$ mV) in DMF solutions as shown in Figure 2.4 for compound **3**. Interestingly, this is a very low reduction potential for a Cu(III)-coordination complex and even it is less than that of reported Cu(III) compound of pds ligand [$E_{1/2} = -0.54$ V (quasi-reversible)], reported by Rovira and co-workers,^{8c} showing that the present system $[\text{Cu}^{\text{III}}(\text{btdt})_2]^{1-}$ is more easily reduced compared with $[\text{Cu}^{\text{III}}(\text{pds})_2]^{1-}$. In other words, the corresponding Cu(II)-complex $[\text{Cu}^{\text{II}}(\text{btdt})_2]^{2-}$ (which we could not isolate) would be very susceptible to oxidation. This is supported by the fact that Cu(III)-compounds **1–5** have been prepared by simple and rapid air oxidation. We could not isolate the Cu(II) compounds of btdt ligand because reaction of $\text{CuCl}_2 \cdot 2\text{H}_2\text{O}$ with Na_2btdt results in the formation of immediate precipitate as a Cu(III) black-coloured solid (Scheme 1). The second reductive response that appears at $E_{1/2} = -1.10$ V ($\Delta E = 120$ mV, quasi-reversible), can be assigned to the red-ox couple $[\text{Cu}^{\text{II}}(\text{btdt})_2]^{2-}/[\text{Cu}^{\text{I}}(\text{btdt})_2]^{3-}$.

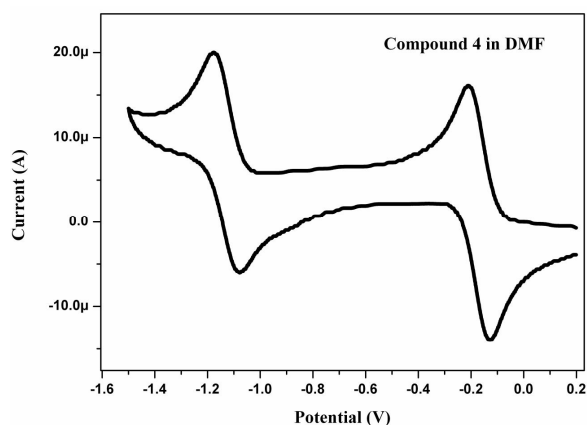


Figure 2.4. Cyclic voltammetry of complex **4** in DMF with a scan rate 50 mV s^{-1} ($n\text{Bu}_4\text{NClO}_4$ as supporting electrolyte).

2.3.3. Description of Crystal Structures

2.3.3.1. 1D Coordination Polymers

Recrystallization from MeOH Solvent

Both crystal structures of the complexes $\{[\text{Na}(\text{CH}_3\text{OH})_4][\text{Cu}(\text{btdt})_2]\}_n$ (**1**) and $\{[\text{Na}(\text{CH}_3\text{OH})_4][\text{Au}(\text{btdt})_2]\}_n$ (**6**) were grown from MeOH solvent, which are isomorphous and crystallize in triclinic space group $P\bar{1}$. The asymmetric unit in the crystal structures of

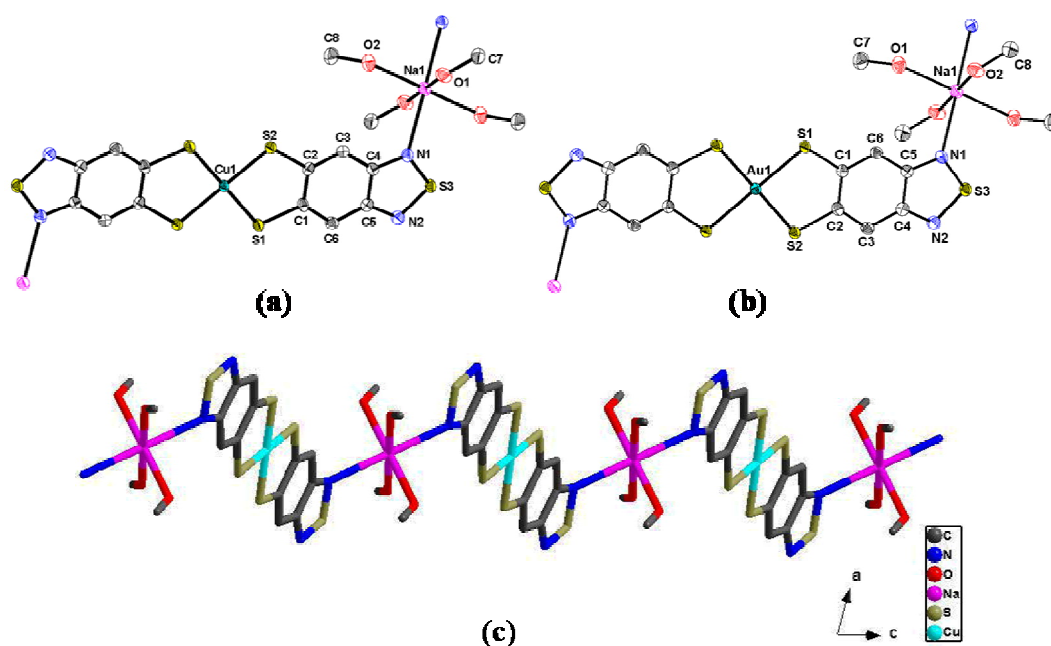


Figure 2.5. Thermal ellipsoid plots of: (a) compound **1** (70% probability); (b) compound **6** (70% probability); (c) extended network observed in the crystal structure of compound **1**. Hydrogen atoms omitted for clarity

complexes **1** and **6** [represented as labeled atoms] contain one {btdt}²⁻ ligand and two CH₃OH molecules in general positions, and one-half Cu and Na atoms, both metals being located at symmetry centers as shown in Figures 2.5(a) and 2.5(b), respectively. The structures of complexes **1** and **6** show square planar geometry around the M(III) (M = Cu, Au) ion, with the average Cu–S and Au–S bond distances 2.174 ± 0.002 Å and 2.309 ± 0.000 Å, respectively and there is no deviation between the two btdt ligands. The whole dithiolene complex (anionic fragment) maintains almost planarity with respect to {MS₄} plane as shown in Figure 2.6(a), unlike the case of [Cu(pds)₂]¹⁻, where pyrazine rings were shown to be twisted with respect to the {CuS₄} plane.^{8c} However, there is a very small deviation in planarity of dithiolene chelating rings with bending angle (η) of 0.92° between the SMS and SCCS planes present in the {Cu1S1S2C1C2} chelating rings. In the crystal structures of complexes **1** and **6**, two nitrogen atoms of dithiolene complex are coordinated to two different Na⁺ counter ions (Mode 1, Scheme 2.4, vide infra). When we consider the geometry around Na⁺ ion, it is found to be in almost octahedral environment, and each Na⁺ ion is coordinated by two nitrogen atoms from two different [M(btdt)₂]¹⁻ anions that are parallel to each other and the remaining four coordination sites are occupied by four different MeOH molecules. This way, complexes **1** and **6**, in their crystal

structures, are extended to one-dimensional coordination polymers as shown Figure 2.5(c). The Na–N1 bond distance is 2.520 Å in both complexes **1** and **6**, which are in good agreement with relevant literature reports.¹³ The Na–O_(solvent) coordination bond distances lie in the range of 2.336 to 2.352 Å.

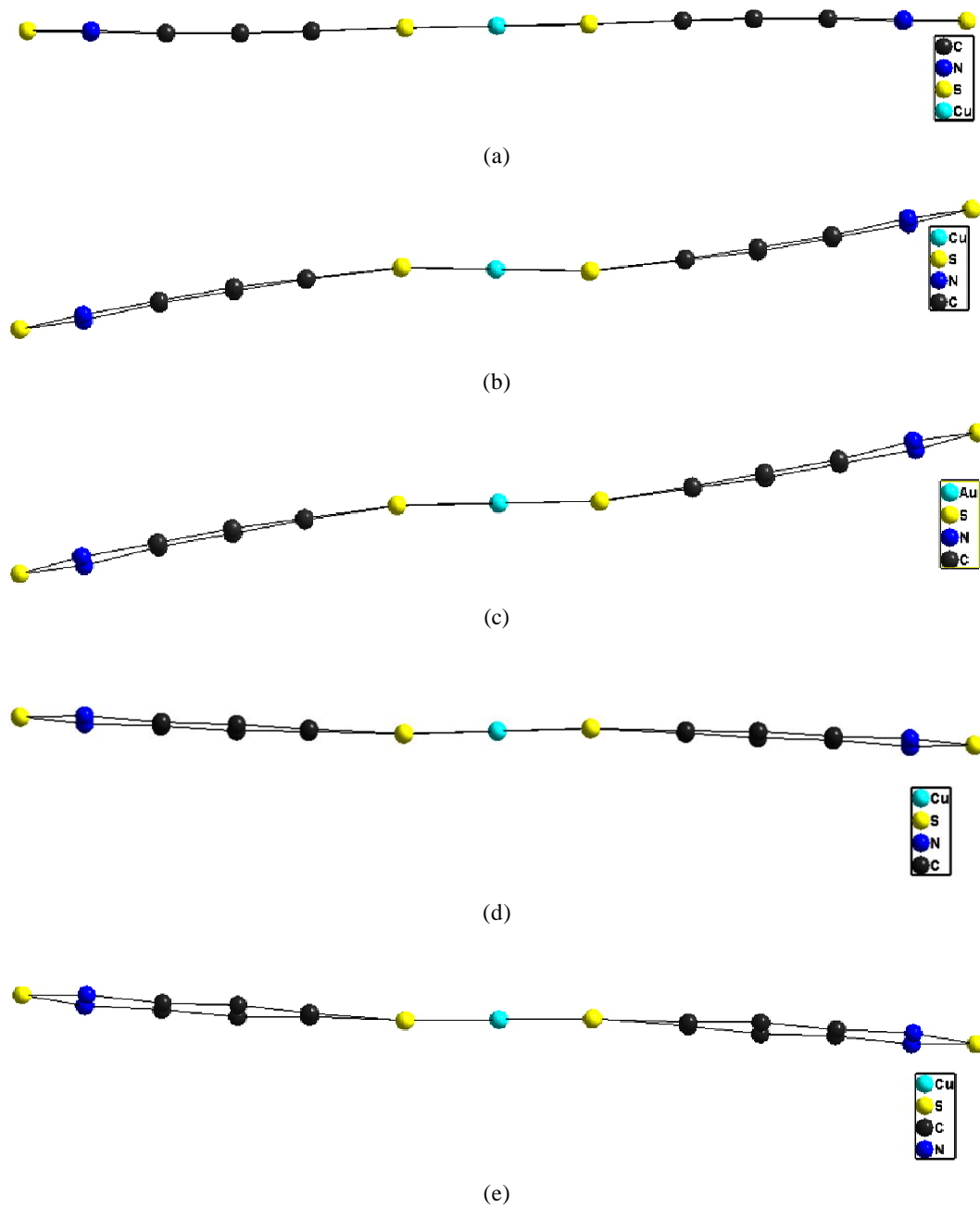


Figure 2.6. (a) Anionic complex units through side view of: (a) compound **1**; (b) compound **3**; (c) compound **8**; (d) compound **4** and (e) compound **5**.

Recrystallization from THF solvent

The crystals of the Cu-complex $\{[\text{Na}(\text{THF})_4][\text{Cu}(\text{btdt})_2]\}_n$ (**2**) were grown from THF solvent, crystallizes in monoclinic space group $C2/c$. The asymmetric unit in the crystal structure of complex **2** [represented as labeled atoms, Figure 2.7(a)] contains one $\{\text{btdt}\}^{2-}$ ligand and two THF molecules in general positions, and one-half Cu and Na atoms, both metals being located at symmetry centers as shown in Figure 2.7(a). In the crystal structure the carbon atom C1 suffer a significant disorder problem. The structure of the complex **2** shows square planar geometry around the Cu(III) ion between the two SMS plane with 0.0° dihedral angle and the coordination bond angles range from $87.95(13)^\circ$ to $92.05(13)^\circ$. The average Cu–S distance is $2.152 \pm 0.001 \text{ \AA}$. But there is a more deviation in the planar nature of the dithiolene ligand (chelate) present in the anionic units of complex **2**. The bending deviation (η) between the SMS plane and SCCS plane is characterized by the angle of 14.77° present in the $\{\text{Cu1S1S2C1C2}\}$ chelate (Figure 2.8(a)). In the crystal structure of the complex **2**, two nitrogen atoms of dithiolene complex are coordinated to two different Na^+ counter ions (Mode 1, Scheme 2.4, vide infra). When we consider the geometry around Na^+ ion, it is found to be in almost octahedral environment, and each Na^+ ion is coordinated by two nitrogen atoms from two different $[\text{Cu}(\text{btdt})_2]^{1-}$ anions that are parallel to each other and the remaining four coordination sites are occupied by four different THF molecules. In this manner, complex **2**, in its crystal structure, is extended to one-dimensional coordination polymer as shown Figure 2.7(b). The Na–N1 bond distance is 2.512 \AA in the complex **2**, which are in good agreement with relevant literature reports.¹³ The Na–O_(solvent) coordination bond distances lie in the range of 2.282 – 2.430 \AA .

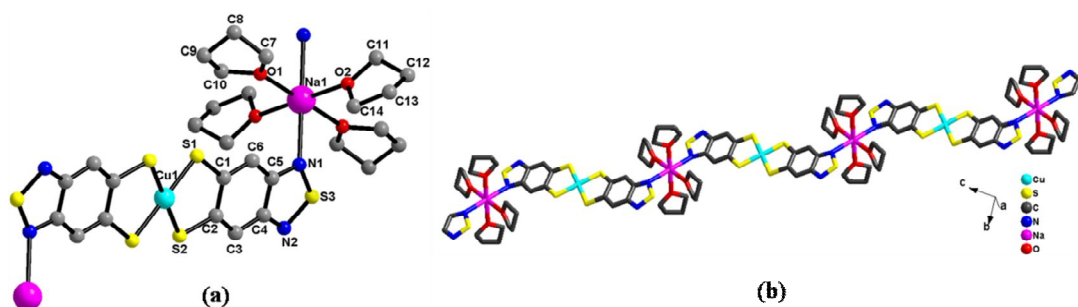
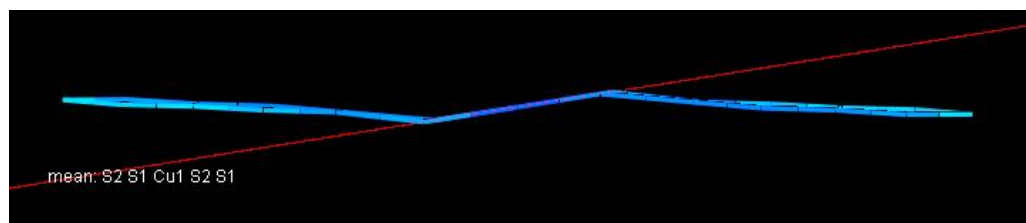
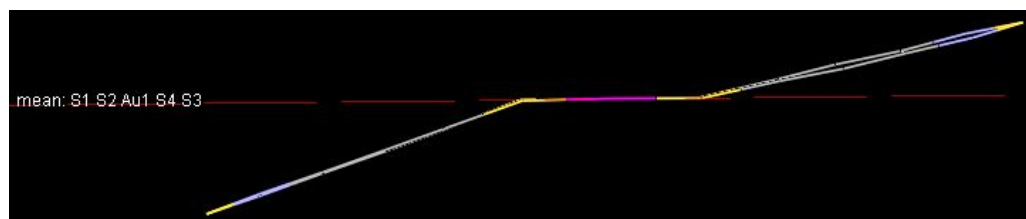


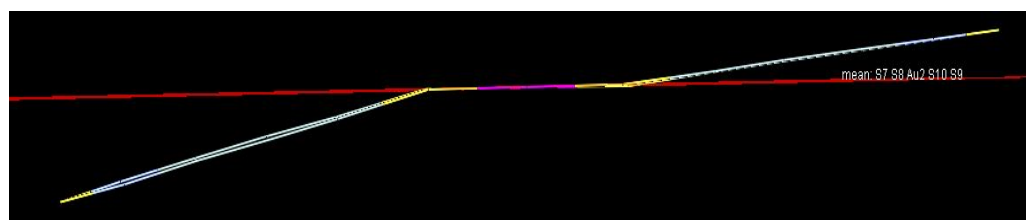
Figure 2.7. (a) Crystal structure of the compound **2** (ball and stick representation); and (b) its extended network in the crystal structure. Hydrogen atoms omitted for clarity (wire frame representation).



(a)



(b)



(c)

Figure 2.8. Anionic complex units through side view of: (a) compound **7** (btdt planes deviated from the Au1S4 plane); (b) compound **7** (btdt planes deviated from the Au2S4 plane).

The crystals of the complex $\{[\text{Na}(\text{THF})_2][\text{Na}(\text{THF})(\text{OH}_2)][\text{Au}_2(\text{btdt})_4]\}_n$ (**7**) were grown from THF solvent, crystallizes in monoclinic space group $P2(1)/c$. The asymmetric unit of compound **7** reveals that it consists of two molecules of $[\text{Au}(\text{btdt})_2]^-$ anions and two Na^+ cations; among sodium cations, one is coordinated with two THF solvent molecules, another is coordinated with one THF and one water molecule as shown in Figure 2.9 as thermal ellipsoidal plot. In contrast to copper complex **2**, the structure of complex **7** shows slight deviation from square planar geometry around the Au(III) ion, with the average Au–S distance is 2.305 ± 0.007 Å. The dihedral angles between the two SMS planes are 1.19° and 0.52° present both complexic units Au1S1S2S3S4 and Au2S7S8S9S10, respectively. In addition to these dihedral angles between the SMS planes, both the complex units are shown by large deviations in the planar nature of the dithiolene-chelates. The bending deviations (η) between the $\{\text{S1Au1S2}\}$ and $\{\text{S1C1C2S2}\}$ planes, and $\{\text{S3Au1S4}\}$ and $\{\text{S3C7C12S4}\}$ planes, are characterized by the angles of 19.49° and 12.83° present in $\{\text{Au1S1S2C1C2}\}$ and $\{\text{Au1S3S4C7C12}\}$ dithiolate-chelates

respectively are shown in Figure 2.8(b). In other complexic-unit, the $\{\text{Au}_2\text{S}_7\text{S}_8\text{C}_{13}\text{C}_{18}\}$ and $\{\text{Au}_2\text{S}_9\text{S}_{10}\text{C}_{19}\text{C}_{24}\}$ dithiolate chelates have the bending deviations (η) of 11.87° and 5.65° [between $\{\text{S}_7\text{Au}_2\text{S}_8\}$ and $\{\text{S}_7\text{C}_{13}\text{C}_{18}\text{S}_8\}$ planes, $\{\text{S}_9\text{Au}_2\text{S}_{10}\}$ and $\{\text{S}_9\text{C}_{19}\text{C}_{24}\text{S}_{10}\}$ planes respectively, as shown in Figure 2.8(c)].

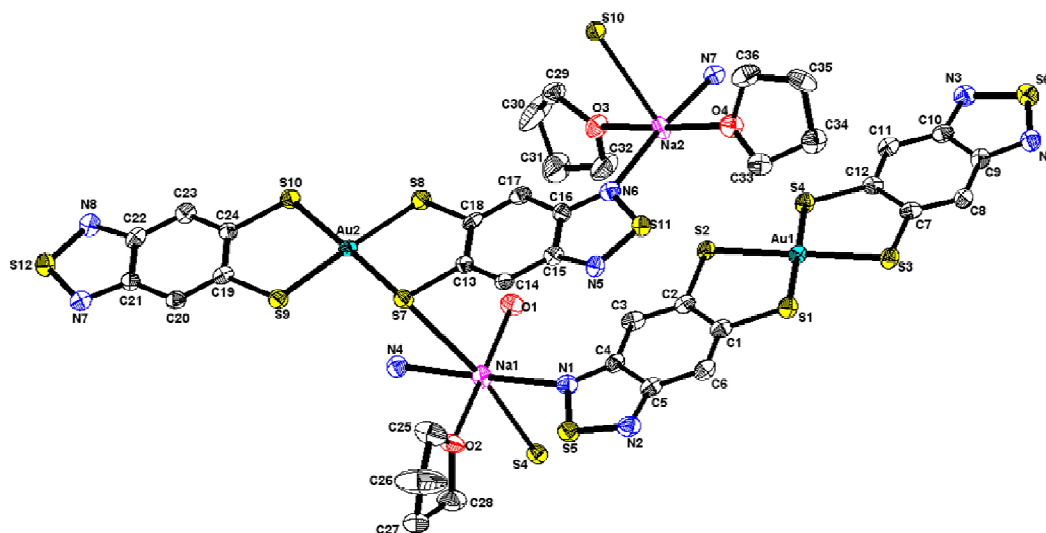
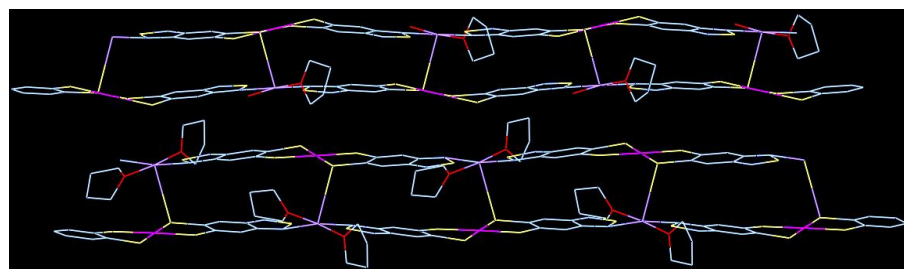
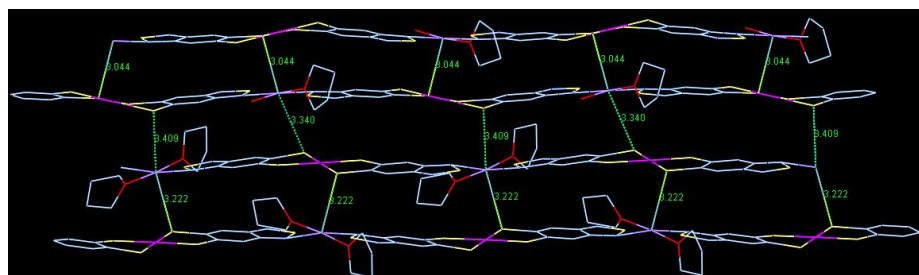


Figure 2.9. Thermal ellipsoidal plot of compound **7** (40% probability, hydrogen atoms are omitted for clarity)

In the crystal structure of compound **7**, two nitrogen atoms and one sulfur atom of dithiolene complex are coordinated to three Na^+ counter ions. Two types of Na^+ counter ions are present and geometry around the each Na^+ ion is slightly distorted square pyramidal. The coordination environment around the one of the Na^+ ions (Na1) is defined by two nitrogen atoms from two different $[\text{Au}(\text{btdt})_2]^{1-}$ anions that are parallel to each other, one sulfur atom of another different dithiolene $[\text{Au}(\text{btdt})_2]^{1-}$ complex and rest of the coordination sites are occupied with one THF and one water molecule, resulting a one-dimensional ladder type of coordination polymer in the crystal structure as shown Figure 2.10(a) (upper ladder). The Na1-N1 , Na1-N4 and Na1-S4 bond distances are $2.486(0)$ Å, $2.501(1)$ Å and $3.044(3)$ Å respectively, which are in the range of relevant literature values.¹³ The second Na^+ counter ion (Na2) is coordinated by two nitrogen atoms from two different $[\text{Au}(\text{btdt})_2]^{1-}$ anions that are parallel to each other, one sulfur atom of another different dithiolene $[\text{Au}(\text{btdt})_2]^{1-}$ complex, but rest of the coordination sites

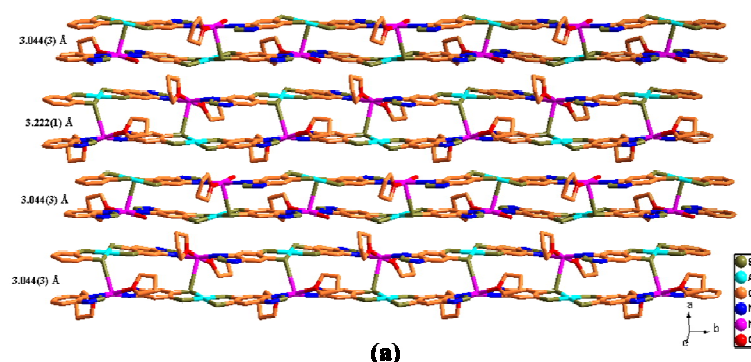


(a)

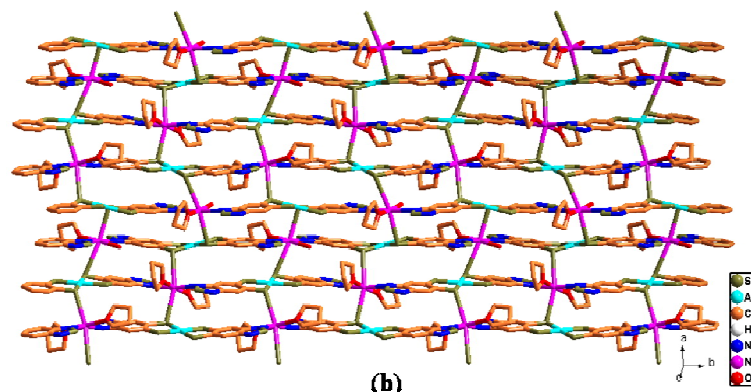


(b)

Figure 2.10. Molecular packing diagrams of compound **7** (a) two types of one dimensional ladders constructed through two types of sodium coordination's; (b) Two dimensional network was connected through Na...S short contacts between the one dimensional ladders.



(a)



(b)

Figure 2.11. Two dimensional layered structure of compound **7**.

are occupied with two THF solvent molecules resulting in an extended one-dimensional ladder type coordination polymer as shown in Figure 2.10(a) (lower ladder). Upper ladder involves Na(1) coordination environment which is separated by Na(1)–S(4) coordination bond with a distance of 3.044(3) Å [Figure 2.10(b) (upper ladder)], whereas, the lower ladder involves Na(2) coordination environment which is separated by Na(2)–S(10) coordination bond with a distance of 3.222(1) Å [Figure 2.10(b) (lower ladder)]. These two ladders are connected with two types of Na...S contacts (Na(1)···S(7) and Na(1)···S(2) with bond distances 3.340(3) Å and 3.409(1) Å respectively) resulting in a two dimensional layered structure as shown in Figures 2.10(b) and 2.11.

Influence of steric hindrance of coordinating solvents in the compound 7

From the crystal structure of $[\{\text{Na}(\text{THF})_2\}\{\text{Na}(\text{THF})(\text{OH}_2)\}\{\text{Au}_2(\text{btdt})_4\}]_n$ (**7**), Na(1) octa-coordination is accustomed with Na(1)···S(7) having contact distance of 3.340(3) Å and Na(2) octa-coordination completed with Na(1)···S(2) with contact distance of 3.409(1) Å. As shown in the Figure 2.12, Na(2)–S(10) and Na(2)–S(2) coordination bonds are longer than Na(1)–S(4) and Na(1)–S(7) coordination bonds respectively. This is due to more steric hindrance created by two THF solvent molecules around Na(2) cation, whereas, only one THF and a water molecule are present around Na(1) cation. As a result, tendency to allow sulfur atoms is less in Na(2) cation compared to Na(1) cation.

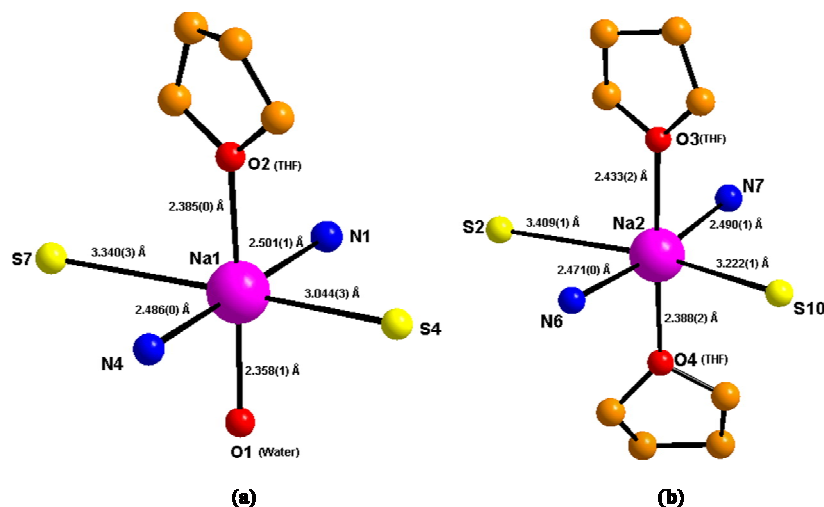


Figure 2.12. The coordination environment around the two sodium ions containing the crystal structure of the complex $[\{\text{Na}(\text{THF})_2\}\{\text{Na}(\text{THF})(\text{OH}_2)\}\{\text{Au}_2(\text{btdt})_4\}]_n$ (**7**), (a) Na(1) octahedral coordination environment; (b) Na(2) octacoordination environment.

2.3.3.2. 2D coordination polymers

Recrystallization from Acetone Solvent

Crystal structure of the complex $\{[\text{Na}(\text{CH}_3\text{COCH}_3)_2][\text{Cu}(\text{btdt})_2]\}_n$ (**3**) crystallizes in monoclinic space group $P2/c$, whereas the complex $\{[\text{Na}(\text{CH}_3\text{COCH}_3)_2][\text{Au}(\text{btdt})_2]\}_n$ (**8**) crystallizes in triclinic space group $P-1$. The asymmetric unit in the crystal structures of the both complexes **3** and **8** (represented as labeled atoms) contain one btdt^{2-} ligand and one CH_3COCH_3 molecule in general positions, and one-half M (Cu, Au) and Na atoms, both metals being located at symmetry centers are shown in Figures 2.13(a) and 2.13(b), respectively as thermal ellipsoidal plots. The structures of the both complexes show a square planar geometry around the M(III) ion with the average Cu–S and Au–S bond distances $2.168 \pm 0.002 \text{ \AA}$ and $2.306 \pm 0.000 \text{ \AA}$ in complexes **3** and **8**, respectively. However, there are deviations in the planar rings of dithiolene chelates (anionic fragment) with respect to {SMS} (M = Cu, Au) plane as shown in Figures 2.6(b) and 2.6(c), respectively.

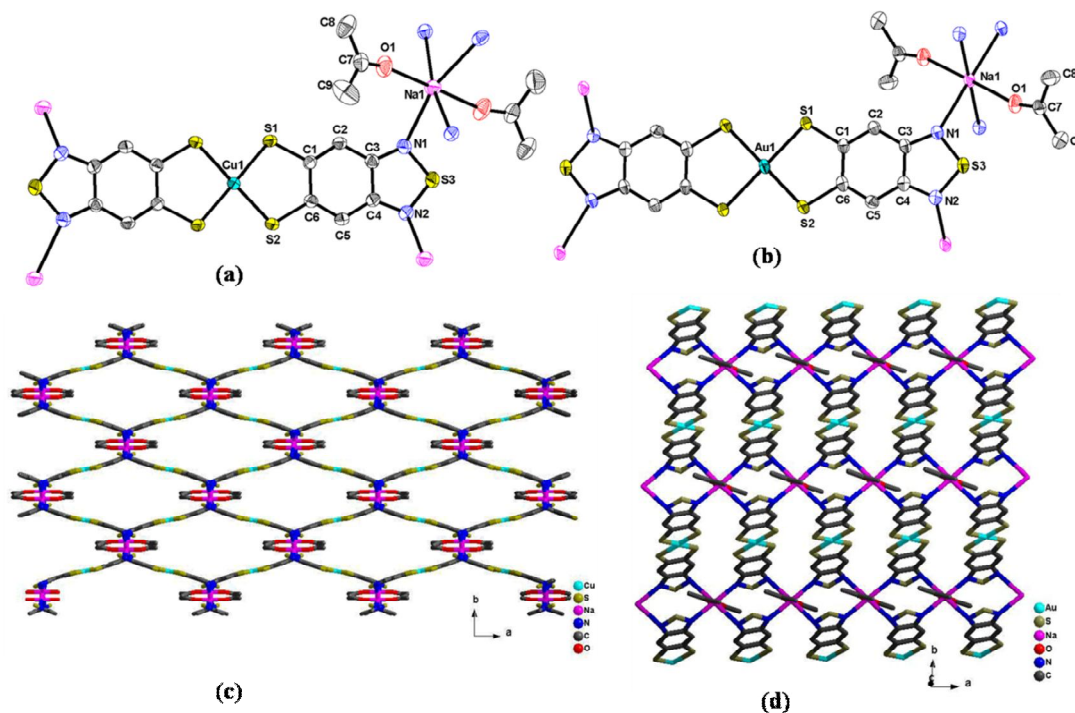


Figure 2.13. Thermal ellipsoid plots of: (a) compound **3** (40% probability); (b) compound **8** (40% probability); Extended networks observed in the crystal structures of compounds (c) **3** and (d) **8**. Hydrogen atoms omitted for clarity.

The bending deviations (η) between the {S1Cu1S2} and {S1C1C6S2} planes, and {S1Au1S2} and {S1C1C6S2} planes, are characterized by the angles of 7.98° and 7.22° present in {Cu1S1S2C1C6} and {Au1S1S2C1C6} dithiolate–chelates, in complexes **3** and **8**, respectively. In the crystal structures of both the complexes **3** and **8**, all four nitrogen donor atoms of each $[M(\text{btdt})_2]^{1-}$ anion are coordinated to four different Na^+ counterions (Mode 3, Scheme 2.4). Each Na^+ ion present in the crystal structures **3** and **8**, extends its coordination ability to the four nitrogen donor atoms of four different $[M(\text{btdt})_2]^{1-}$ anions and hence resulting in the formation of 2D coordination polymeric networks as shown in Figures 2.13(c) and 2.13(d), respectively. The remaining two coordination sites are occupied by two oxygen atoms of two different acetone (solvent) molecules. Interestingly, octahedral geometry around the sodium ion is highly distorted in crystal structure of complex **3**, whereas in the crystal structure of complex **8**, it is closed to octahedral. In complex **3**, the coordination bond angle between $\text{N1—Na—N2}'$ is 159.1° and it shows deviation from octahedral geometry (180°) and the bond angle between the atoms $\text{N1—Na—N1}'$ is 120.2° , highly distorted from octahedral geometry (90°). On the other hand, in crystal structure of the complex **8**, all the coordination bond angles between $\text{N1—Na—N1}'$, $\text{N2}'\text{—Na—N2}'$ and $\text{O1—Na—O1}'$ are 180° . This difference in geometry around the sodium ion in complexes **3** and **8**, results in two different types of 2D coordination networks in their crystal structures as shown in Figures 2.13(c) and 2.13(d), respectively.

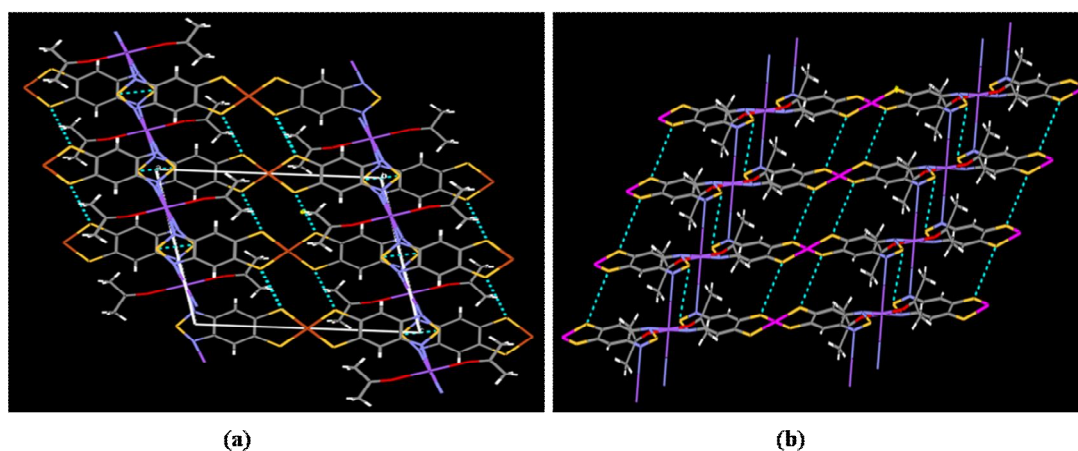


Figure 2.14. S...S non-covalent interactions between the dithiolate anions in the crystal structure of (a) compound **3** and (b) compound **8**.

In complex **3**, Na–N2 bond distance (2.978 Å) is longer than the bond distance Na–N1 (2.56 Å), which are in good agreement with related literature values.¹³ But in the crystal structure of complex **8**, Na–N2 and Na–N1 bond distances are of 2.918 and 2.482 Å, respectively, which are the slightly shorter than the corresponding bond distances in complex **3**. The Na–O1_(solvent) coordination bond distances from acetone molecules in complexes **3** and **8**, are 2.288 and 2.275 Å, respectively. Fascinatingly, both complexes **3** and **8** are further characterized by interesting S··S contacts as shown in Figures 2.14(a) and 2.14(b), respectively. The S··S contacts are 3.547 Å and 3.574 Å in complex **3** and 3.553 Å and 3.583 Å in complex **8**, which are less than the sum of their van-der waals radii.¹⁴

Recrystallization from DMF Solvent

Both crystal structures of the complexes $\{[\text{Na}(\text{DMF})_2][\text{Cu}(\text{btdt})_2]\}_n$ (**4**) and $\{[\text{Na}(\text{DMF})_2][\text{Au}(\text{btdt})_2]\}_n$ (**9**) were grown from DMF solvent, which are isomorphous and crystallize in triclinic space group *P*-1. The asymmetric unit in the crystal structures of the complexes **4** and **9** [represented as labeled atoms, in Figures 2.15(a) and 2.15(b)] contain one {btdt}²⁻ ligand and one DMF (solvent) molecule in general positions, and one-half Cu and Na atoms, both metals being located at symmetry centers as shown in Figures 2.15(a) 2.15(b), respectively. The structures of the complexes **4** and **9** show square planar geometry around the M(III) ion. However, small distortion (3.90° bending angle) are observed in the planarity of the dithiolene chelates (CSSC plane), with respect to the {SMS} plane in the both complexes **4** and **9** [Figure 2.6(d)]. The average Cu–S and Au–S bond distances are 2.178 ± 0.006 Å and 2.308 ± 0.003 Å in complexes **4** and **9**, respectively. Interestingly, in the crystal structures of the complexes **4** and **9**, sodium ion is coordinated *via* two S atoms from two different dithiolene complexes. The Na–S bond distances are 3.188 Å and 3.202 Å in complexes **4** and **9**, respectively, which are in good agreement with relevant literature values.¹⁵ The sodium ion is further coordinated by two N atoms from two different $[\text{M}(\text{btdt})_2]^{1-}$ anions with bond distances 2.484 Å and 2.488 Å in complexes **4** and **9**, respectively and remaining two coordination sites of the octahedral geometry (because all the coordination bond angle between N1—Na—N1', S2—Na—S2' and O1—Na—O1' are 180°) around sodium ion occupied by two O atoms from two different DMF molecules. For each dithiolene complex unit $[\text{M}(\text{btdt})_2]^{1-}$, two nitrogen atoms and two sulfur atoms are coordinated to four different Na⁺ counterions (Mode 2,

(69)

Scheme 4). Extended 2D coordinated networks of complexes **4** and **9** in their crystal structures are shown Figure 2.15(c).

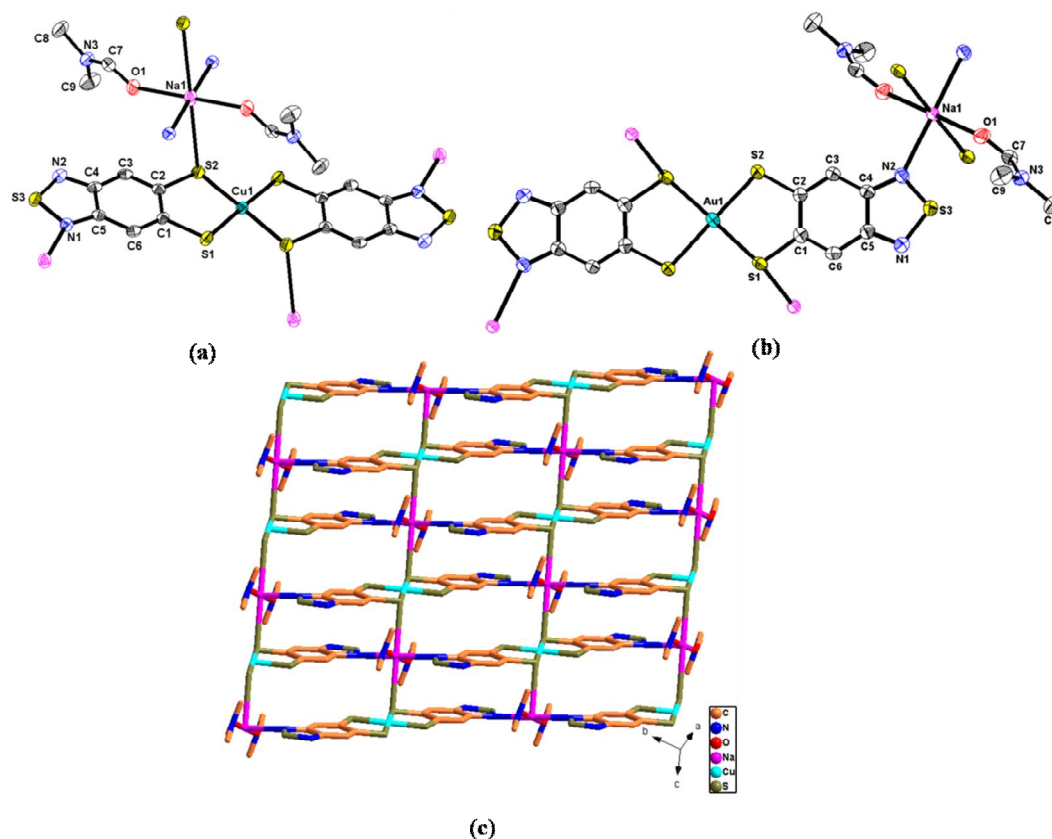


Figure 2.15. Thermal ellipsoid plots of: (a) compound **4** (70% probability); (b) compound **9** (60% probability); (c) extended network in the crystal structure of the compound **4**. Hydrogen atoms omitted for clarity.

2.3.3.3. 3D Coordination Polymers

Recrystallization from Acetonitrile Solvent

Both crystal structures of the complexes $\{[\text{Na}(\text{CH}_3\text{CN})_2][\text{Cu}(\text{btdt})_2]\}_n$ (**5**) and $\{[\text{Na}(\text{CH}_3\text{CN})_2][\text{Au}(\text{btdt})_2]\}_n$ (**10**) were grown from acetonitrile solvent, which are isomorphous and crystallize in monoclinic space group $P2_1/c$. The asymmetric unit in the crystal structures of complexes **5** and **10** [represented as labeled atoms, in Figures 2.16(a), and 2.16(b)] contain one {btdt}²⁻ ligand and one acetonitrile (solvent) molecule in general positions, and one-half M (= Cu, Au) and Na atoms, that are located at symmetry centers as shown in Figures 2.16(a) and 2.16(b), respectively.

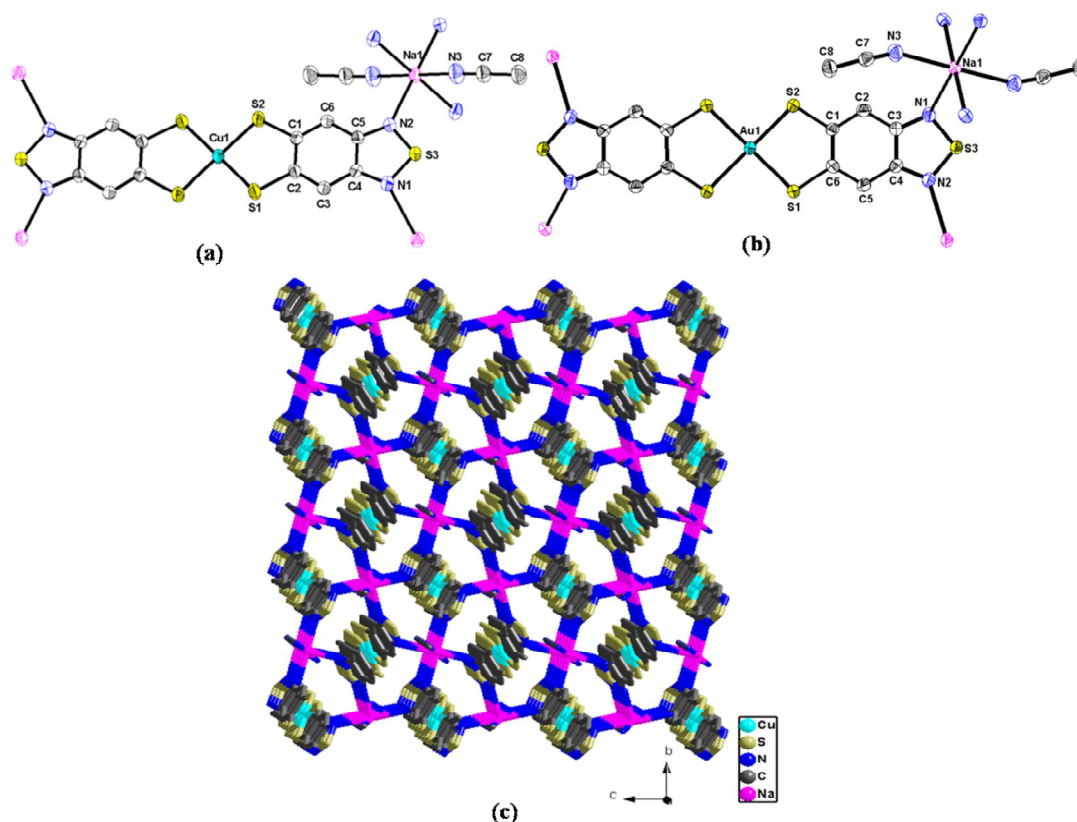
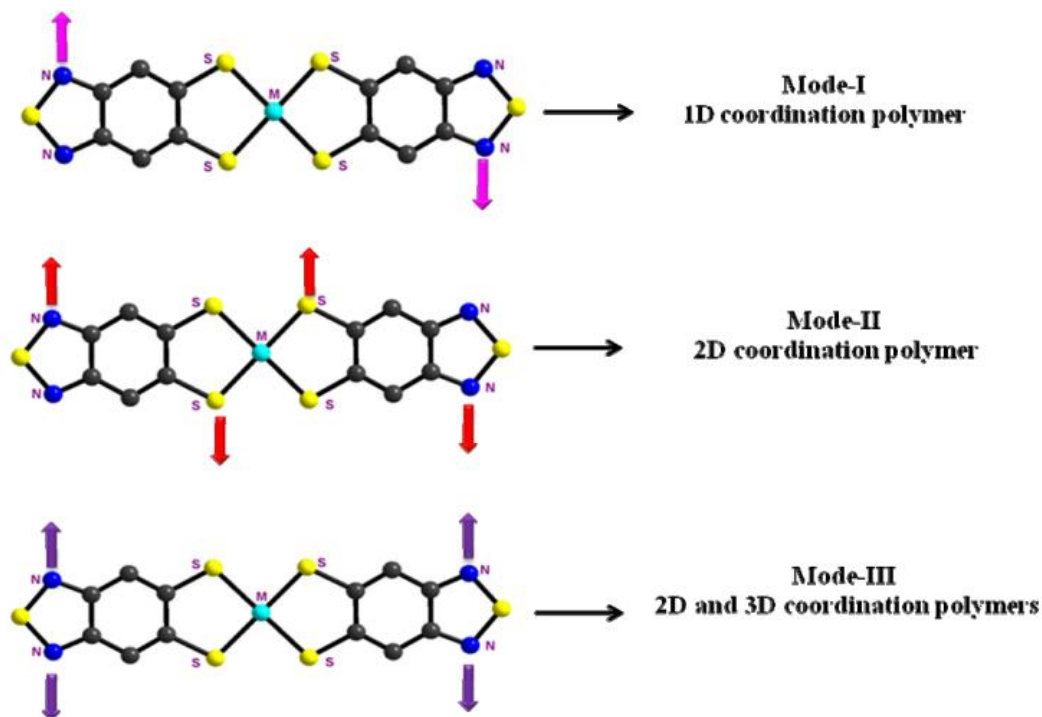


Figure 2.16. Thermal ellipsoid plots of: (a) compound **5** (40% probability); (b) compound **5** (60% probability); (c) extended network in the crystal structure of the compound **5**. Hydrogen atoms omitted for clarity.

The structures of complexes **5** and **10** show square planar geometry around the M(III) ion and with a small bending deviation (3.66°) in the planarity of the dithiolene chelating rings (CSSC plane) with respect to the {SMS} plane in complexes **5** and **10** as shown in Figure 2.6(e). The average Cu–S and Au–S bond distances are $2.175 \pm 0.003 \text{ \AA}$ and $2.304 \pm 0.001 \text{ \AA}$ in complexes **5** and **10**, respectively. In the crystal structure, all the four nitrogen atoms of dithiolene complex $[\text{M}(\text{btdt})_2]^{1-}$ are coordinated to four different Na^+ counter ions (Mode 3, scheme 2.4). Geometry around the sodium ion in these complexes, is almost octahedral (the entire coordination bond angles between N1—Na—N1' , N2—Na—N2' and N3—Na—N3' are 180°). In the crystal structures, each sodium ion is coordinated to six nitrogen atoms, in which four nitrogen atoms are from four different dithiolene complex $[\text{M}(\text{btdt})_2]^{1-}$ anions and the remaining two nitrogen atoms are from two different acetonitrile (solvent) molecules. Na—N1 , Na—N2 and $\text{Na—N3}_{(\text{solvent})}$ bond distances are 2.584 , 2.489 and 2.472 \AA , and 2.542 , 2.456 and 2.455 \AA in complexes **5** and

10, respectively. The crystal structure of complexes **5** and **10** show an interesting and rare kind of $(5,^3_4)^{16}$ Catalan 3-D coordination network as shown in Figure 2.16(c).



Scheme 2.4. Observed coordination modes of counter ion with $[M(btdt)_2]^{-1}$ in the coordination polymers **1**–**10**.

2.3.3.4. Discrete structure

$[Na_2(H_2O)_6(\mu-H_2O)_2][Au(btdt)_2]_2$ (**11**)

Single crystals of the compound $[Na_2(H_2O)_6(\mu-H_2O)_2][Au(btdt)_2]_2$ (**11**) were grown from commercial MeOH (water containing) solvent by slow evaporation in open atmosphere, that crystallizes in orthorhombic space group *Pccn*. The asymmetric unit in the crystal structure of compound **11** consists of one $[Au(btdt)_2]^{-}$ anion and one Na^{+} cation surrounded by four water molecules. Thus, the molecular structure of compound **11** contains $[Na_2(H_2O)_6(\mu-H_2O)_2]$ dimer, in which both sodium ions are bridged by two water molecules and each sodium center is penta-coordinated with 3 terminal and 2 bridged aqua- ligands, as shown in Figures 2.17(a). It is worth mentioning that $\{[Na_2(H_2O)_6(\mu-H_2O)_2]\}$ dimer was observed in few systems as a counter cation,¹⁷ but there is no report of its presence in metal dithiolene systems. The structure of the complex **11** shows square-

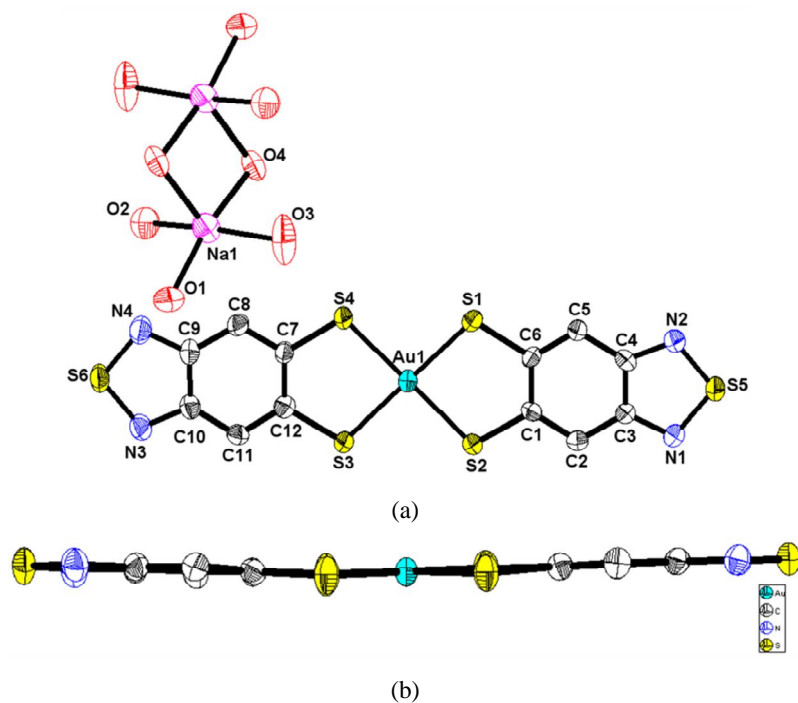


Figure 2.17. Thermal ellipsoid plots of: (a) compound **11**; (b) Anionic complex units through side view of compound **11**.

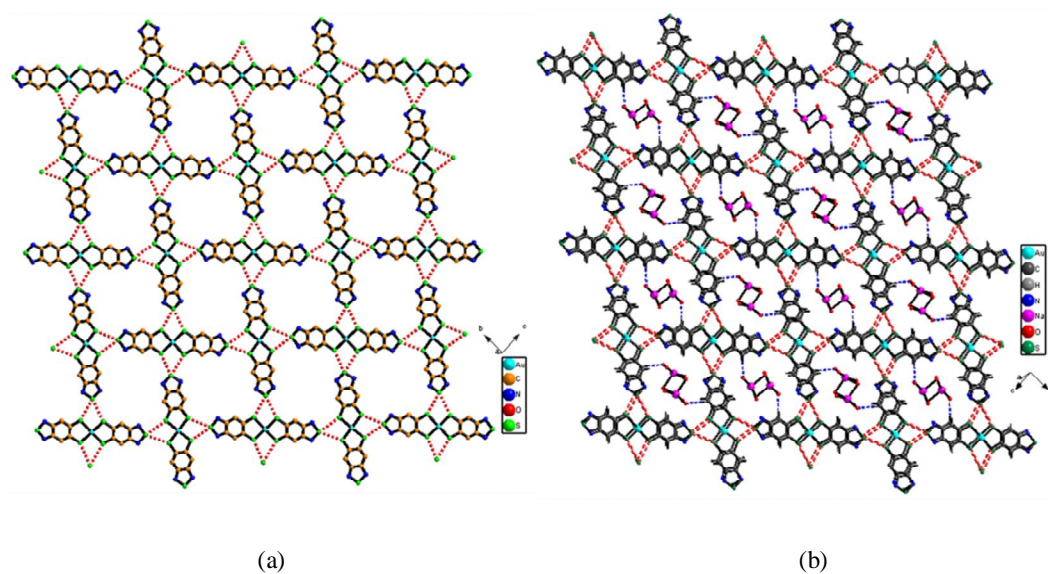


Figure 2.18. (a) Two dimensional supramolecular layered network characterized by S...S non-covalent interactions (Hydrogen atoms omitted for clarity).; (b) 2D supramolecular network formed by the combination of S...S and S...N non-covalent interactions and C-H...O hydrogen bonding interaction.

planar geometry around the Au(III) metal ion with dihedral angle of 2.17° between the two SMS planes. In addition to dihedral angle, there are deviations in the planar nature of the dithiolene ligands (chelates) present in the anionic units of complex **11**. The bending

deviations (η) between the {S1Au1S2} and {S1C1C6S2} planes, and {S3Au1S4} and {S3C7C12S4} planes are characterized by the angles of 3.01° and 4.79° present in {Au1S1S2C1C6} and {Au1S3S4C7C12} dithiolate–chelated rings, respectively are shown in Figure 2.17(b). Interestingly all the sulfur atoms present in the dithiolene complex are involved in the S...S non covalent interactions and resulting in 2-dimensional layered network as shown in Figure 2.18(a), which is further connected through S...N interaction results in 2D double layered network. The S...S contact distance are in the range from 3.495 Å to 3.541 Å and S...N contact distance is 3.254 Å, which are less than the sum of their van-der waals radii.¹⁴ The Na₂O₈ cationic dimers were connected through C–H...O hydrogen bonding interactions inside the channels of above 2-dimensional double layered network resulting supramolecular network as shown in Figure 2.18(b).

2.3.3.5. Potassium Based Coordination Polymers

Recrystallization from Acetone Solvent

Crystal structure of the complex $\{[K(CH_3COCH_3)_3][Cu(btdt)_2]\}_n$ (**12**) crystallizes in monoclinic space group *C2/c*. The asymmetric unit in the crystal structures of the complex **12** (represented as labeled atoms) contains one {btdt}²⁻ ligand and one CH₃COCH₃ molecule in general positions, and one-half of acetone, one Cu and K atoms are being located at symmetry centers as shown in Figure 2.19(a) as thermal ellipsoidal plot. The structure of the complex shows square planar geometry around the Cu(III) ion because the coordination angles are in the range of $87.87(3)^\circ$ – $92.13(3)^\circ$ which are slightly deviated from 90.0° and other coordination angles are 180.0° , which are not deviated. The Cu–S bond distances are in the range of 2.1526(19)–2.1653(17) Å. However, there is a deviation in the planar nature of the dithiolene ligand (chelate) present in the anionic units of complex **12**. The bending deviation (η) between the SMS plane and SCCS plane is characterized by an angle of 1.23° present in the {Cu1S1S2C1C6} chelate as shown in Figure 2.20(a). In the crystal structure of the complex **12**, two nitrogen and two sulfur donor atoms of each $[Cu(btdt)_2]^{1-}$ anion are coordinated to four different K⁺ counter ions. Each K⁺ ion present in the crystal structure **12**, extends its coordination ability to the two nitrogen and two sulfur donor atoms of four different $[Cu(btdt)_2]^{1-}$ anions and hence resulting in the formation of 3D coordination polymeric networks are shown in Figures 2.19(b) and 2.19(c). The remaining three coordination sites of hepta-coordinated geometry

of potassium ion are occupied by three oxygen atoms of three different acetone (solvent) molecules. In complex **12**, K–N bond distance is 2.845(5) Å and K–S bond distance is 3.498(2) Å. The Na–O1_(solvent) coordination bond distances from acetone molecules are in the range from 2.605(8) to 2.703(5) Å.

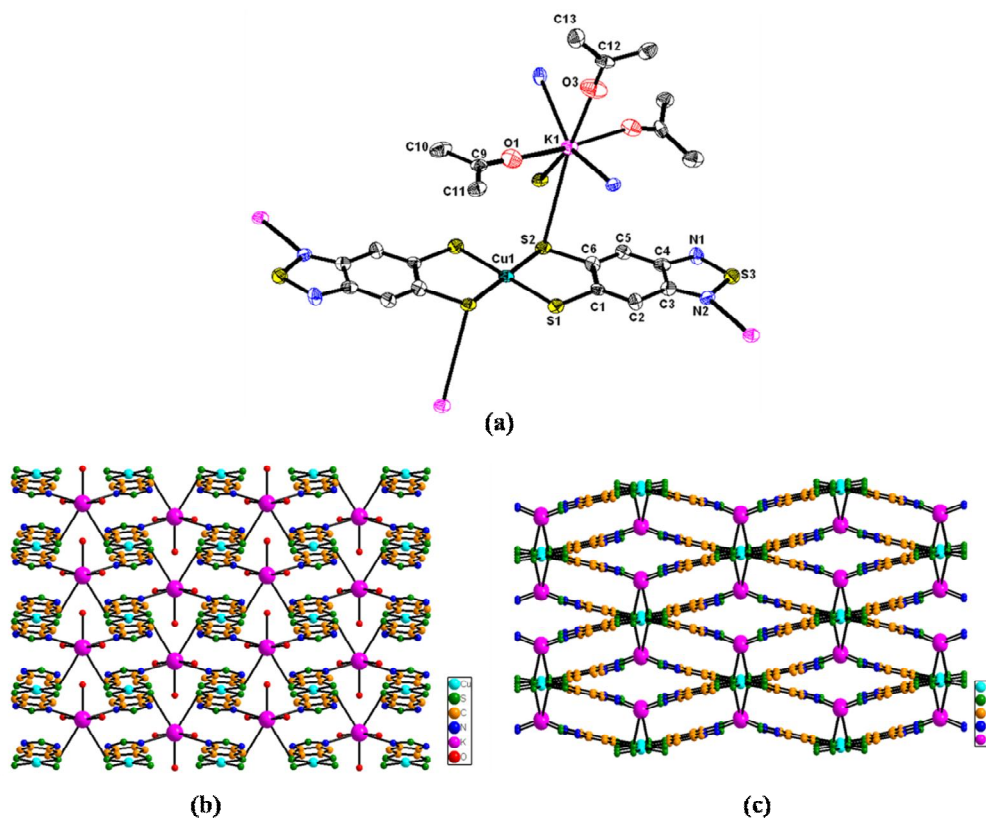


Figure 2.19. (a) Thermal ellipsoid plot of compound **12** (50% probability); Extended networks observed in the crystal structures of compound **12** when views down to crystallographic (b) *a* axis (Hydrogen atoms removed for clarity) and (c) *c* axis (Hydrogen atoms and coordinated acetone molecules are removed for clarity).

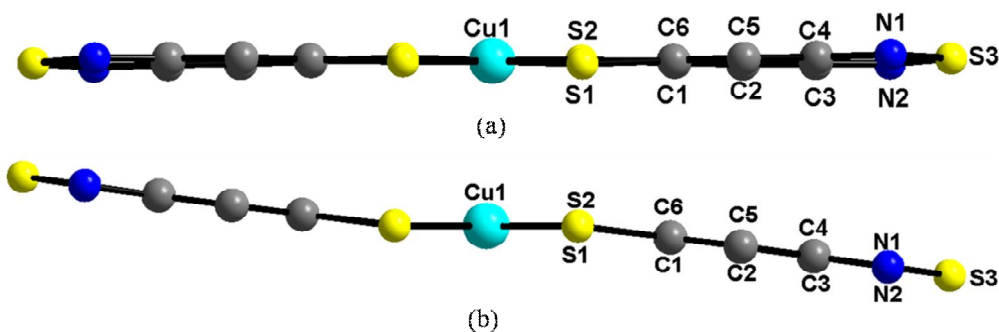


Figure 2.20. Anionic complex units through side view of: (a) compound **12**; (b) compound **13**.

Recrystallization from acetonitrile solvent

Single crystals of the complex $\{[K(CH_3CN)_2][Cu(btdt)_2]\}_n$ (**13**) were grown from acetonitrile, and crystallizes in triclinic space group $P-1$. The asymmetric unit in the crystal structure of complex **13** [represented as labeled atoms] contains one $btdt^{2-}$ ligand and one acetonitrile (solvent) molecule in general positions, and one-half Cu and K atoms, that are located at symmetry centers as shown in Figure 2.21(a). The structure of complex **13** shows square planar geometry around the Cu(III) ion because the coordination angles are in the range of $88.034(16)^\circ$ – $91.966(16)^\circ$ which are slightly deviated from 90.0° and other coordination angles are 180.0° , which are not deviated. The Cu–S bond distances are in the range of 2.1730(5)–2.1817(5) Å. However, there is a deviation in the planar nature of the dithiolene ligand (chelate) present in the anionic units of complex **13**. The bending deviation (η) between the SMS plane and SCCS plane is characterized by the angle of 6.91° present in the $\{Cu1S1S2C1C6\}$ chelate as shown in Figure 2.20(b). In the crystal structure of the complex **13**, two nitrogen and two sulfur donor atoms of each $[Cu(btdt)_2]^{1-}$ anion are coordinated to four different K^+ counter ions. Geometry around the potassium ion in this complex, is close to octahedral (the entire coordination bond angles between $S2-K-S2'$, $N2-K-N2'$ and $N3-K-N3'$ are 180°). In the crystal structure, each potassium ion is coordinated to four nitrogen atoms and sulfur atoms, in which two nitrogen and two sulfur atoms are from four different dithiolene complex $[Cu(btdt)_2]^{1-}$ anions and the remaining two nitrogen atoms are from two different acetonitrile (solvent) molecules. K–S2, K–N2 and K–N3_(solvent) bond distances are 3.3795(5), 2.7649(16) and 2.7873(17), in complex **13**, respectively. The extended crystal structure of complex **13** shows 2-D coordination network, as shown in Figure 2.21(b).

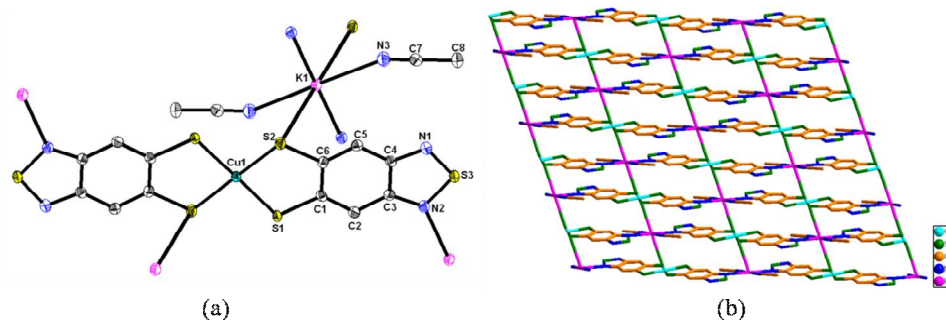


Figure 2.21. (a) Thermal ellipsoid plot of compound **13** (50% probability); (b) Extended network observed in the crystal structures of compound **13** when views down to crystallographic *a* axis (Hydrogen atoms have been omitted clarity).

Table 2.1. Crystal Data and Structural Refinement for Compounds 1–2

	1	2
Empirical formula	C ₁₆ H ₂₀ N ₄ O ₄ S ₆ NaCu	C ₂₈ H ₃₆ N ₄ O ₄ S ₆ NaCu
Formula weight	611.25,	771.50
T [K], λ [Å]	100(2), 0.71073	100(2), 0.71073
Crystal system	Triclinic	Monoclinic
Space group	<i>P</i> -1	<i>C</i> 2/c
<i>a</i> [Å]	7.4010(5)	22.428(13)
<i>b</i> [Å]	9.0175(6)	9.673(6)
<i>c</i> [Å]	10.1302(7)	17.730(10)
α [deg]	64.183(10)	90.000
β [deg]	76.489(10)	120.880(8)
γ [deg]	85.946(10)	90.000
<i>V</i> [Å ³]	591.3(7)	3301(3)
<i>Z</i> , <i>D</i> _{calc} [Mg m ⁻³]	1, 1.716	4, 1.552
μ [mm ⁻¹], <i>F</i> [000]	1.504, 312	1.095, 1600
Crystal size [mm ³]	0.24 x 0.16 x 0.08	0.24 x 0.14 x 0.06
θ range for data collection [deg]	2.29 to 25.89	2.12 to 25.24
Reflections collected / unique	6071/2277	13058/2965
R(int)	0.0174	0.1055
Data / restraints / parameters	2277 / 0 / 158	2965/0/202
Goodness-of-fit on <i>F</i> ²	1.120	1.193
<i>R</i> ₁ / <i>wR</i> ₂ [<i>I</i> > 2 σ (<i>I</i>)]	0.0225/0.0567	0.1381/0.3392
<i>R</i> ₁ / <i>wR</i> ₂ (all data)	0.0229/0.0570	0.1469/0.3446
Largest diff. Peak/hole [e Å ⁻³]	0.284/-0.389	1.942/-1.372

Table 2.2. Crystal Data and Structural Refinement for Compounds 3–5

	3	4	5
Empirical formula	C ₁₈ H ₁₆ N ₄ O ₂ S ₆ NaCu	C ₁₈ H ₁₈ N ₆ O ₂ S ₆ NaCu	C ₁₆ H ₁₀ N ₆ S ₆ NaCu
Formula weight	599.24	629.27	565.19
T [K], λ [Å]	298(2), 0.71073	100(2), 0.71073	298(2), 0.71073
Crystal system	Monoclinic	Triclinic	Monoclinic
Space group	<i>P</i> 2/c	<i>P</i> -1	<i>P</i> 2 ₁ /c
<i>a</i> [Å]	12.549(4)	8.5323(17)	12.981(3)
<i>b</i> [Å]	7.391(2)	8.5509(17)	10.299(2)
<i>c</i> [Å]	13.095(4)	9.1258(18)	8.4568(17)
α [deg]	90.000	105.69(3)	90.000
β [deg]	102.817(4)	95.52(3)	101.53(3)
γ [deg]	90.000	99.88(3)	90.000
<i>V</i> [Å ³]	1184.3(6)	624.3(2)	1107.7(4)
<i>Z</i> , <i>D</i> _{calc} [Mg m ⁻³]	2, 1.680	1, 1.674	2, 1.695
μ [mm ⁻¹], <i>F</i> [000]	1.494, 608	1.424, 320	1.588, 568
Crystal size [mm ³]	0.48 x 0.24 x 0.12	0.46 x 0.20 x 0.10	0.26 x 0.16 x 0.12
θ range for data collection [deg]	1.66 to 25.04	3.64 to 24.71	1.60 to 25.01
Reflections collected / unique	10777/2073	4169/2104	10246/1947
R(int)	0.0242	0.0212	0.0229
Data / restraints / parameters	2073/0/149	2104 / 0 / 167	1947/0/140
Goodness-of-fit on <i>F</i> ²	1.062	1.103	1.062
<i>R</i> ₁ / <i>wR</i> ₂ [<i>I</i> > 2 σ (<i>I</i>)]	0.0280/0.0738	0.0246/0.0651	0.0288/0.0729
<i>R</i> ₁ / <i>wR</i> ₂ (all data)	0.0311/0.0756	0.0282/0.0663	0.0350/0.0775
Largest diff. Peak/hole [e Å ⁻³]	0.325/-0.269	0.309/-0.329	0.416/-0.238

Table 2.3. Crystal Data and Structural Refinement for Compounds **6–7**

	6	7
Empirical formula	C ₁₆ H ₂₀ N ₄ O ₄ S ₆ NaAu	C ₃₆ H ₃₀ N ₈ O ₄ S ₁₂ Na ₂ Au ₂
Formula weight	744.68	1463.31
T [K], λ [Å]	100(2), 0.71073	100(2), 0.71073
Crystal system	Triclinic	Monoclinic
Space group	<i>P</i> -1	<i>P</i> 2(1)/c
<i>a</i> [Å]	7.4087(5)	14.7196(8)
<i>b</i> [Å]	9.1583(6)	16.9437(10)
<i>c</i> [Å]	10.1717(7)	20.3793(9)
α [deg]	63.777(10)	90.000
β [deg]	76.735(10)	113.843(3)
γ [deg]	86.033(10)	90.000
<i>V</i> [Å ³]	602.2(7)	4648.9(4)
<i>Z</i> , <i>D</i> _{calc} [Mg m ⁻³]	1, 2.053	4, 2.091
μ [mm ⁻¹], <i>F</i> [000]	6.678, 362	6.912, 2824
Crystal size [mm ³]	0.46 x 0.18 x 0.08	0.18 x 0.08 x 0.06
θ range for data collection [deg]	2.29 to 26.03	1.51 to 25.99
Reflections collected / unique	6241/2361	47565/9115
R(int)	0.0186	0.0489
Data / restraints / parameters	2361/ 0 / 158	9155/0/577
Goodness-of-fit on <i>F</i> ²	1.125	1.151
R ₁ /wR ₂ [<i>I</i> > 2 σ (<i>I</i>)]	0.0155/0.0401	0.0396/0.0787
R ₁ /wR ₂ (all data)	0.0155/0.0401	0.0448/0.0806
Largest diff. Peak/hole [e Å ⁻³]	0.877/-1.350	1.493/-0.643

Table 2.4. Crystal Data and Structural Refinement for Compounds **8–10**

	8	9	10
Empirical formula	C ₁₈ H ₁₆ N ₄ O ₂ S ₆ NaAu	C ₁₈ H ₁₈ N ₆ O ₂ S ₆ NaAu	C ₁₆ H ₁₀ N ₆ S ₆ NaAu
Formula weight	732.66	762.70	698.62
T [K], λ [Å]	100(2), 0.71073	100(2), 0.71073	100(2), 0.71073
Crystal system	Triclinic	Triclinic	Monoclinic
Space group	<i>P</i> -1	<i>P</i> -1	<i>P</i> 2(1)/c
<i>a</i> [Å]	6.4374(5)	8.4687(7)	12.9803(14)
<i>b</i> [Å]	7.6809(5)	8.6531(7)	10.1794(11)
<i>c</i> [Å]	11.9468(8)	9.2081(7)	8.4481(9)
α [deg]	85.773(4)	106.467(10)	90.000
β [deg]	81.274(4)	95.289(10)	102.981(2)
γ [deg]	85.366(4)	98.941(10)	90.000
<i>V</i> [Å ³]	580.8(7)	632.59(9)	1087.7(2)
<i>Z</i> , <i>D</i> _{calc} [Mg m ⁻³]	1, 2.095	1, 2.002	2, 2.133
μ [mm ⁻¹], <i>F</i> [000]	6.916, 354	6.356, 370	7.376, 668
Crystal size [mm ³]	0.18 x 0.12 x 0.08	0.44 x 0.22 x 0.10	0.20x0.16x0.20
θ range for data collection [deg]	1.73 to 25.99	2.33 to 26.02	1.61 to 26.36
Reflections collected / unique	5933/2246	6479/2493	11244/2224
R(int)	0.0186	0.0155	0.0318
Data / restraints / parameters	2246/0/150	2463 / 0 / 159	2224/0/140
Goodness-of-fit on <i>F</i> ²	1.068	1.073	1.069
R ₁ /wR ₂ [<i>I</i> > 2 σ (<i>I</i>)]	0.0156/0.0388	0.0172/0.0434	0.0218/0.460
R ₁ /wR ₂ (all data)	0.0156/0.0388	0.0172/0.0434	0.218/0.471
Largest diff. Peak/hole [e Å ⁻³]	1.078/-0.891	1.008/-1.114	0.905/-0.635

Table 2.5. Crystal Data and Structural Refinement for Compounds **11–13**

	11	12	13
Empirical formula	C ₁₂ H ₄ N ₄ O ₄ S ₆ NaAu	C ₂₁ H ₂₂ N ₄ O ₃ S ₆ KCu	C ₁₆ H ₁₀ N ₆ S ₆ KCu
Formula weight	680.51	673.43	581.30
T [K]	298(2)	100(2)	100(2)
λ [Å]	0.71073	0.71073	0.71073 Å
Crystal system	Orthorhombic	Monoclinic	Triclinic
Space group	Pccn	C2/c	P-1
<i>a</i> [Å]	13.3285(20)	18.244(4)	7.6325(7)
<i>b</i> [Å]	18.0188(12)	10.794(2)	7.9361(7)
<i>c</i> [Å]	17.3305(12)	15.035(3)	9.1797(8)
α [deg]	90.000	90.000	81.6030(10)
β [deg]	90.000	113.94(3)	78.3720(10)
γ [deg]	90.000	90.000	80.3500(10)
<i>V</i> [Å ³]	4162(7)	2723.9(9)	533.28(8)
<i>Z</i>	8	4	1
<i>D</i> _{calc} [Mg m ⁻³]	2.172	1.642	1.810
μ [mm ⁻¹]	7.718	1.447	1.825
F(000)	2576	1376	292
Crystal size [mm ³]	0.42 x 0.32 x 0.20	0.32 x 0.14 x 0.04	0.58 x 0.20 x 0.10
θ range for data collection [deg]	2.97 to 28.28	2.95 to 25.00	2.28 to 26.01
Reflections collected / unique	15074/5165	4877/2392	5546/2092
R(int)	0.0339	0.0525	0.0169
Data / restraints / parameters	5165/0/253	2392 / 0 / 169	2092/0/140
Goodness-of-fit on F ²	0.990	1.407	1.068
R ₁ /wR ₂ [I > 2 σ (I)]	0.0320/0.0743	0.0808/0.2381	0.0238/0.0606
R ₁ /wR ₂ (all data)	0.0757/0.0818	0.1017/0.3170	0.0244/0.0609
Largest diff. Peak/hole [e Å ⁻³]	1.197/-0.646	2.652/-2.938	0.340/-0.354

Table 2.6. Selected Bond lengths and Bond Angles for Compound **1**

Cu(1)-S(2)	2.1727(4)	Cu(1)-S(2)#1	2.1727(4)
Cu(1)-S(1)	2.1761(4)	Cu(1)-S(1)#1	2.1761(4)
N(1)-S(3)	1.6206(15)	N(1)-Na(1)	2.5202(14)
N(2)-S(3)	1.6251(15)	Na(1)-O(2)#2	2.3356(13)
Na(1)-O(2)	2.3356(13)	Na(1)-O(1)#2	2.3518(14)
Na(1)-O(1)	2.3518(14)	Na(1)-N(1)#2	2.5202(14)
S(2)-Cu(1)-S(2)#1	180.0	S(2)-Cu(1)-S(1)	92.113(15)
S(2)#1-Cu(1)-S(1)	87.886(15)	S(2)-Cu(1)-S(1)#1	87.887(16)
S(2)#1-Cu(1)-S(1)#1	92.113(15)	S(1)-Cu(1)-S(1)#1	180.000(1)
C(4)-N(1)-S(3)	106.86(12)	C(4)-N(1)-Na(1)	127.01(11)
S(3)-N(1)-Na(1)	113.93(7)	C(5)-N(2)-S(3)	106.76(12)
O(2)#2-Na(1)-O(2)	180.00(4)	O(2)#2-Na(1)-O(1)#2	81.12(5)
O(2)-Na(1)-O(1)#2	98.88(5)	O(2)#2-Na(1)-O(1)	98.88(5)
O(2)-Na(1)-O(1)	81.12(5)	O(1)#2-Na(1)-O(1)	179.999(2)
O(2)#2-Na(1)-N(1)	84.32(5)	O(2)-Na(1)-N(1)	95.68(5)
O(1)#2-Na(1)-N(1)	86.27(5)	O(1)-Na(1)-N(1)	93.73(5)
O(2)#2-Na(1)-N(1)#2	95.68(5)	O(2)-Na(1)-N(1)#2	84.32(5)
O(1)#2-Na(1)-N(1)#2	93.73(5)	O(1)-Na(1)-N(1)#2	86.27(5)
N(1)-Na(1)-N(1)#2	180.0	C(7)-O(1)-Na(1)	121.56(11)
C(8)-O(2)-Na(1)	140.09(12)	C(1)-S(1)-Cu(1)	105.17(6)
C(2)-S(2)-Cu(1)	105.15(6)	N(1)-S(3)-N(2)	100.20(8)

Symmetry transformations used to generate equivalent atoms: #1 -x+1,-y,-z+2; #2 -x+1,-y+2,-z+1.

Table 2.7. Selected Bond lengths and Bond Angles for Compound 2

Cu(1)-S(1)	2.150(3)	Cu(1)-S(1)#1	2.150(3)
Cu(1)-S(2)	2.153(3)	Cu(1)-S(2)#1	2.153(3)
N(1)-Na(1)	2.518(10)	Na(1)-O(2)#2	2.282(8)
Na(1)-O(2)	2.282(8)	Na(1)-O(1)	2.430(9)
Na(1)-O(1)#2	2.430(9)	S(1)-Cu(1)-S(1)#1	180.0
S(1)-Cu(1)-S(2)	92.05(13)	S(1)#1-Cu(1)-S(2)	87.95(13)
S(1)-Cu(1)-S(2)#1	87.95(13)	S(1)#1-Cu(1)-S(2)#1	92.05(13)
S(2)-Cu(1)-S(2)#1	179.999(1)	C(1)-S(1)-Cu(1)	104.1(4)
C(2)-S(2)-Cu(1)	104.5(4)	C(5)-N(1)-Na(1)	123.0(8)
S(3)-N(1)-Na(1)	119.4(6)	C(4)-N(2)-S(3)	107.2(10)
O(2)#2-Na(1)-O(2)	179.999(1)	O(2)#2-Na(1)-O(1)	93.3(3)
O(2)-Na(1)-O(1)	86.7(3)	O(2)#2-Na(1)-O(1)#2	86.7(3)
O(2)-Na(1)-O(1)#2	93.3(3)	O(1)-Na(1)-O(1)#2	179.999(1)
O(2)#2-Na(1)-N(1)#2	94.9(3)	O(2)-Na(1)-N(1)#2	85.1(3)
O(1)-Na(1)-N(1)#2	81.1(3)	O(1)#2-Na(1)-N(1)#2	98.9(3)
O(2)#2-Na(1)-N(1)	85.1(3)	O(2)-Na(1)-N(1)	94.9(3)
O(1)-Na(1)-N(1)	98.9(3)	O(1)#2-Na(1)-N(1)	81.1(3)
N(1)#2-Na(1)-N(1)	179.999(1)	C(7)-O(1)-Na(1)	132.9(8)
C(10)-O(1)-Na(1)	120.7(8)	C(11)-O(2)-Na(1)	132.6(8)
C(14)-O(2)-Na(1)	117.2(8)		

Symmetry transformations used to generate equivalent atoms: #1 -x+1/2,-y+3/2,-z+1; #2 -x,-y+1,-z.

Table 2.8. Selected Bond lengths and Bond Angles for Compound 3

Cu(1)-S(1)	2.1668(8)	Cu(1)-S(1)#1	2.1668(8)
Cu(1)-S(2)#1	2.1707(7)	Cu(1)-S(2)	2.1707(7)
Na(1)-O(1)	2.2877(19)	Na(1)-O(1)#2	2.2877(19)
Na(1)-N(1)	2.560(2)	Na(1)-N(1)#2	2.560(2)
Na(1)-N(2)#3	2.978(3)	Na(1)-N(2)#4	2.978(3)
N(2)-C(4)	1.341(3)	N(2)-Na(1)#4	2.978(3)
S(1)-Cu(1)-S(1)#1	179.999(1)	S(1)-Cu(1)-S(2)#1	88.17(3)
S(1)#1-Cu(1)-S(2)#1	91.83(3)	S(1)-Cu(1)-S(2)	91.83(3)
S(1)#1-Cu(1)-S(2)	88.17(3)	S(2)#1-Cu(1)-S(2)	179.998(1)
C(6)-S(2)-Cu(1)	105.01(8)	O(1)-Na(1)-O(1)#2	179.29(14)
O(1)-Na(1)-N(1)	96.36(7)	O(1)#2-Na(1)-N(1)	84.00(8)
O(1)-Na(1)-N(1)#2	84.00(8)	O(1)#2-Na(1)-N(1)#2	96.36(7)
N(1)-Na(1)-N(1)#2	120.27(12)	O(1)-Na(1)-N(2)#3	90.06(7)
O(1)#2-Na(1)-N(2)#3	89.40(8)	N(1)-Na(1)-N(2)#3	159.10(8)
N(1)#2-Na(1)-N(2)#3	80.10(7)	O(1)-Na(1)-N(2)#4	89.40(8)
O(1)#2-Na(1)-N(2)#4	90.06(7)	N(1)-Na(1)-N(2)#4	80.10(7)
N(1)#2-Na(1)-N(2)#4	159.10(8)	N(2)#3-Na(1)-N(2)#4	80.10(9)
C(4)-N(2)-S(3)	107.14(16)	C(4)-N(2)-Na(1)#4	107.91(15)
S(3)-N(2)-Na(1)#4	116.48(11)	C(6)-C(5)-C(4)	118.5(2)
C(3)-N(1)-Na(1)	132.05(15)	S(3)-N(1)-Na(1)	113.96(10)
C(7)-O(1)-Na(1)	163.2(2)		

Symmetry transformations used to generate equivalent atoms: #1 -x+1,-y+1,-z+1; #2 -x+2,y,-z+1/2; #3 x,-y+2,z-1/2; #4 -x+2,-y+2,-z+1.

Table 2.9. Selected Bond lengths and Bond Angles for Compound 4

Cu(1)-S(2)	2.1727(10)	Cu(1)-S(2)#1	2.1727(10)
Cu(1)-S(1)	2.1844(7)	Cu(1)-S(1)#1	2.1844(7)
S(2)-Na(1)	3.1878(10)	N(1)-Na(1)#2	2.4838(19)
Na(1)-O(1)#3	2.3043(17)	Na(1)-O(1)	2.3044(17)
Na(1)-N(1)#4	2.4838(19)	Na(1)-N(1)#5	2.4838(19)
Na(1)-S(2)#3	3.1878(10)	S(2)-Cu(1)-S(2)#1	180.0
S(2)-Cu(1)-S(1)	92.21(4)	S(2)#1-Cu(1)-S(1)	87.79(4)
S(2)-Cu(1)-S(1)#1	87.79(4)	S(2)#1-Cu(1)-S(1)#1	92.21(4)
S(1)-Cu(1)-S(1)#1	179.999(1)	C(1)-S(1)-Cu(1)	105.00(8)
C(2)-S(2)-Cu(1)	104.85(8)	C(2)-S(2)-Na(1)	89.28(7)
Cu(1)-S(2)-Na(1)	115.38(3)	C(5)-N(1)-Na(1)#2	138.35(14)
S(3)-N(1)-Na(1)#2	114.39(9)	O(1)#3-Na(1)-O(1)	180.0
O(1)#3-Na(1)-N(1)#4	96.57(6)	O(1)-Na(1)-N(1)#4	83.43(6)
O(1)#3-Na(1)-N(1)#5	83.43(6)	O(1)-Na(1)-N(1)#5	96.57(6)
N(1)#4-Na(1)-N(1)#5	180.0	O(1)#3-Na(1)-S(2)#3	90.59(5)
O(1)-Na(1)-S(2)#3	89.41(5)	N(1)#4-Na(1)-S(2)#3	89.60(5)
N(1)#5-Na(1)-S(2)#3	90.40(5)	O(1)#3-Na(1)-S(2)	89.41(5)
O(1)-Na(1)-S(2)	90.59(5)	N(1)#4-Na(1)-S(2)	90.40(5)
N(1)#5-Na(1)-S(2)	89.60(5)	S(2)#3-Na(1)-S(2)	180.000(8)
C(7)-O(1)-Na(1)	142.92(15)		

Symmetry transformations used to generate equivalent atoms: #1 -x+1,-y,-z; #2 x,y+1,z; #3 -x+1,-y,-z+1; #4 x,y-1,z; #5 -x+1,-y+1,-z+1.

Table 2.10. Selected Bond lengths and Bond Angles for Compound 5

Cu(1)-S(1)#1	2.1722(8)	Cu(1)-S(1)	2.1722(8)
Cu(1)-S(2)#1	2.1783(8)	Cu(1)-S(2)	2.1783(8)
Na(1)-N(3)#2	2.472(3)	Na(1)-N(3)	2.472(3)
Na(1)-N(2)	2.489(2)	Na(1)-N(2)#2	2.489(2)
Na(1)-N(1)#3	2.584(2)	Na(1)-N(1)#4	2.584(2)
N(1)-Na(1)#5	2.584(2)	S(1)#1-Cu(1)-S(1)	180.0
S(1)#1-Cu(1)-S(2)#1	87.91(3)	S(1)-Cu(1)-S(2)#1	92.09(3)
S(1)#1-Cu(1)-S(2)	92.09(3)	S(1)-Cu(1)-S(2)	87.91(3)
S(2)#1-Cu(1)-S(2)	180.0	C(1)-S(2)-Cu(1)	104.91(9)
C(2)#1-S(1)-Cu(1)	105.19(9)	N(3)#2-Na(1)-N(3)	180.0
N(3)#2-Na(1)-N(2)	94.90(9)	N(3)-Na(1)-N(2)	85.10(9)
N(3)#2-Na(1)-N(2)#2	85.10(9)	N(3)-Na(1)-N(2)#2	94.90(9)
N(2)-Na(1)-N(2)#2	180.00(2)	N(3)#2-Na(1)-N(1)#3	87.99(9)
N(3)-Na(1)-N(1)#3	92.01(9)	N(2)-Na(1)-N(1)#3	93.66(7)
N(2)#2-Na(1)-N(1)#3	86.34(7)	N(3)#2-Na(1)-N(1)#4	92.02(9)
N(3)-Na(1)-N(1)#4	87.99(9)	N(2)-Na(1)-N(1)#4	86.34(7)
N(2)#2-Na(1)-N(1)#4	93.66(7)	N(1)#3-Na(1)-N(1)#4	180.00(2)
C(5)-N(2)-Na(1)	131.87(17)	S(3)-N(2)-Na(1)	119.53(10)
C(7)-N(3)-Na(1)	153.1(3)	C(4)-N(1)-Na(1)#5	130.83(16)
S(3)-N(1)-Na(1)#5	106.06(10)		

Symmetry transformations used to generate equivalent atoms: #1 -x+1,-y+1,-z+2; #2 -x+2,-y+2,-z+2; #3 -x+2,y+1/2,-z+3/2; #4 x,-y+3/2,z+1/2; #5 -x+2,y-1/2,-z+3/2.

Table 2.11. Selected Bond lengths and Bond Angles for Compound **6**

Au(1)-S(2)#1	2.3085(6)	Au(1)-S(2)	2.3085(6)
Au(1)-S(1)#1	2.3085(6)	Au(1)-S(1)	2.3085(6)
N(1)-Na(1)	2.518(2)	O(1)-Na(1)	2.3479(18)
O(2)-Na(1)	2.3511(19)	Na(1)-O(1)#2	2.3479(18)
Na(1)-O(2)#2	2.3511(19)	Na(1)-N(1)#2	2.518(2)
S(2)#1-Au(1)-S(2)	180.0	S(2)#1-Au(1)-S(1)#1	90.01(2)
S(2)-Au(1)-S(1)#1	89.99(2)	S(2)#1-Au(1)-S(1)	89.99(2)
S(2)-Au(1)-S(1)	90.01(2)	S(1)#1-Au(1)-S(1)	179.999(1)
C(1)-S(1)-Au(1)	103.82(8)	C(2)-S(2)-Au(1)	103.88(8)
C(5)-N(1)-S(3)	106.59(16)	C(5)-N(1)-Na(1)	127.01(15)
S(3)-N(1)-Na(1)	114.02(10)	C(7)-O(1)-Na(1)	140.13(17)
C(8)-O(2)-Na(1)	122.17(15)	O(1)-Na(1)-O(1)#2	180.00(10)
O(1)-Na(1)-O(2)#2	98.25(7)	O(1)#2-Na(1)-O(2)#2	81.75(7)
O(1)-Na(1)-O(2)	81.75(7)	O(1)#2-Na(1)-O(2)	98.25(7)
O(2)#2-Na(1)-O(2)	180.0	O(1)-Na(1)-N(1)	95.58(6)
O(1)#2-Na(1)-N(1)	84.42(6)	O(2)#2-Na(1)-N(1)	85.82(7)
O(2)-Na(1)-N(1)	94.18(7)	O(1)-Na(1)-N(1)#2	84.41(6)
O(1)#2-Na(1)-N(1)#2	95.59(6)	O(2)#2-Na(1)-N(1)#2	94.18(7)
O(2)-Na(1)-N(1)#2	85.82(7)	N(1)-Na(1)-N(1)#2	180.0

Symmetry transformations used to generate equivalent atoms: #1 -x+2,-y,-z+1; #2 -x+2,-y+2,-z.

Table 2.13. Selected Bond lengths and Bond Angles for Compound **8**

Au(1)-S(2)	2.3063(7)	Au(1)-S(2)#1	2.3063(7)
Au(1)-S(1)	2.3072(6)	Au(1)-S(1)#1	2.3072(6)
Na(1)-O(1)#2	2.2756(19)	Na(1)-O(1)	2.2756(19)
Na(1)-N(1)	2.482(2)	Na(1)-N(1)#2	2.482(2)
Na(1)-N(2)#3	2.918(2)	Na(1)-N(2)#4	2.918(2)
N(2)-Na(1)#5	2.918(2)	S(2)-Au(1)-S(2)#1	180.00(3)
S(2)-Au(1)-S(1)	89.79(2)	S(2)#1-Au(1)-S(1)	90.21(2)
S(2)-Au(1)-S(1)#1	90.21(2)	S(2)#1-Au(1)-S(1)#1	89.79(2)
S(1)-Au(1)-S(1)#1	180.0	C(1)-S(1)-Au(1)	103.75(9)
C(6)-S(2)-Au(1)	103.54(9)	O(1)#2-Na(1)-O(1)	180.0
O(1)#2-Na(1)-N(1)	96.49(7)	O(1)-Na(1)-N(1)	83.51(7)
O(1)#2-Na(1)-N(1)#2	83.51(7)	O(1)-Na(1)-N(1)#2	96.49(7)
N(1)-Na(1)-N(1)#2	180.0	O(1)#2-Na(1)-N(2)#3	93.38(7)
O(1)-Na(1)-N(2)#3	86.62(7)	N(1)-Na(1)-N(2)#3	99.59(7)
N(1)#2-Na(1)-N(2)#3	80.41(7)	O(1)#2-Na(1)-N(2)#4	86.62(7)
O(1)-Na(1)-N(2)#4	93.38(7)	N(1)-Na(1)-N(2)#4	80.41(7)
N(1)#2-Na(1)-N(2)#4	99.59(7)	N(2)#3-Na(1)-N(2)#4	180.0
C(7)-O(1)-Na(1)	162.16(19)	C(4)-N(2)-Na(1)#5	101.73(15)
S(3)-N(2)-Na(1)#5	114.49(10)	C(3)-N(1)-Na(1)	135.57(17)
S(3)-N(1)-Na(1)	113.21(11)		

Symmetry transformations used to generate equivalent atoms: #1 -x+1,-y+1,-z+2; #2 -x,-y,-z+1; #3 x-1,y,z; #4 -x+1,-y,-z+1; #5 x+1,y,z.

Table 2.12. Selected Bond lengths and Bond Angles for Compound 7

Au(1)-S(4)	2.2983(15)	Au(1)-S(2)	2.3033(15)
Au(1)-S(1)	2.3101(15)	Au(1)-S(3)	2.3123(15)
S(4)-Na(1)#1	3.044(3)	Na(1)-O(1)	2.358(5)
Na(1)-O(2)	2.385(5)	Na(1)-N(4)#2	2.486(6)
Na(1)-N(1)	2.501(6)	Na(1)-S(4)#3	3.044(3)
Na(1)-S(7)	3.340(3)	N(4)-Na(1)#4	2.486(6)
Au(2)-S(9)	2.2978(16)	Au(2)-S(7)	2.2987(15)
Au(2)-S(10)	2.3045(15)	Au(2)-S(8)	2.3174(16)
S(10)-Na(2)#5	3.222(3)	Na(2)-O(4)	2.388(5)
Na(2)-O(3)	2.433(5)	Na(2)-N(6)	2.471(5)
Na(2)-N(7)#4	2.490(6)	Na(2)-S(10)#6	3.222(3)
N(7)-Na(2)#2	2.490(6)	S(4)-Au(1)-S(2)	88.81(5)
S(4)-Au(1)-S(1)	178.04(6)	S(2)-Au(1)-S(1)	89.57(5)
S(4)-Au(1)-S(3)	90.16(5)	S(2)-Au(1)-S(3)	178.89(6)
S(1)-Au(1)-S(3)	91.45(5)	C(1)-S(1)-Au(1)	102.2(2)
C(2)-S(2)-Au(1)	102.4(2)	C(7)-S(3)-Au(1)	103.1(2)
C(12)-S(4)-Au(1)	102.9(2)	C(12)-S(4)-Na(1)#1	102.88(19)
Au(1)-S(4)-Na(1)#1	91.23(7)	O(1)-Na(1)-O(2)	174.55(19)
O(1)-Na(1)-N(4)#2	85.08(18)	O(2)-Na(1)-N(4)#2	97.28(18)
O(1)-Na(1)-N(1)	94.04(18)	O(2)-Na(1)-N(1)	83.54(18)
N(4)#2-Na(1)-N(1)	178.9(2)	O(1)-Na(1)-S(4)#3	89.73(13)
O(2)-Na(1)-S(4)#3	94.79(13)	N(4)#2-Na(1)-S(4)#3	97.98(14)
N(1)-Na(1)-S(4)#3	82.71(13)	O(1)-Na(1)-S(7)	93.14(13)
O(2)-Na(1)-S(7)	82.85(12)	N(4)#2-Na(1)-S(7)	73.77(13)
N(1)-Na(1)-S(7)	105.60(14)	S(4)#3-Na(1)-S(7)	170.97(9)
C(28)-O(2)-Na(1)	127.7(4)	C(25)-O(2)-Na(1)	124.5(4)
C(4)-N(1)-Na(1)	137.3(4)	S(5)-N(1)-Na(1)	115.7(3)
C(5)-N(2)-S(5)	106.7(4)	C(9)-N(4)-Na(1)#4	135.2(4)
S(6)-N(4)-Na(1)#4	118.2(3)	S(9)-Au(2)-S(7)	87.86(5)
S(9)-Au(2)-S(10)	90.32(5)	S(7)-Au(2)-S(10)	178.11(6)
S(9)-Au(2)-S(8)	177.51(5)	S(7)-Au(2)-S(8)	89.65(5)
S(10)-Au(2)-S(8)	92.17(5)	C(13)-S(7)-Au(2)	103.7(2)
C(13)-S(7)-Na(1)	76.37(19)	Au(2)-S(7)-Na(1)	111.34(7)
C(18)-S(8)-Au(2)	103.5(2)	C(19)-S(9)-Au(2)	104.3(2)
C(24)-S(10)-Au(2)	103.2(2)	C(24)-S(10)-Na(2)#5	110.60(19)
Au(2)-S(10)-Na(2)#5	108.53(7)	O(4)-Na(2)-O(3)	173.80(19)
O(4)-Na(2)-N(6)	90.86(18)	O(3)-Na(2)-N(6)	94.89(18)
O(4)-Na(2)-N(7)#4	92.20(18)	O(3)-Na(2)-N(7)#4	81.78(17)
N(6)-Na(2)-N(7)#4	171.3(2)	O(4)-Na(2)-S(10)#6	94.61(14)
O(3)-Na(2)-S(10)#6	87.76(13)	N(6)-Na(2)-S(10)#6	89.62(13)
N(7)#4-Na(2)-S(10)#6	98.20(14)	C(32)-O(3)-Na(2)	114.5(4)
C(29)-O(3)-Na(2)	136.5(4)	C(36)-O(4)-Na(2)	118.2(4)
C(33)-O(4)-Na(2)	136.1(4)	C(16)-N(6)-Na(2)	133.3(4)
S(11)-N(6)-Na(2)	119.3(3)	C(21)-N(7)-Na(2)#2	136.0(4)
S(12)-N(7)-Na(2)#2	114.5(3)		

Symmetry transformations used to generate equivalent atoms: #1 -x+1,y-1/2,-z+3/2; #2 x,y+1,z; #3 -x+1,y+1/2,-z+3/2; #4 x,y-1,z; #5 -x,y+1/2,-z+3/2; #6 -x,y-1/2,-z+3/2.

Table 2.14. Selected Bond lengths and Bond Angles for Compound **9**

Au(1)-S(1)#1	2.3051(7)	Au(1)-S(1)	2.3051(7)
Au(1)-S(2)	2.3107(7)	Au(1)-S(2)#1	2.3107(7)
N(2)-Na(1)	2.488(2)	Na(1)-O(1)#2	2.316(2)
Na(1)-O(1)	2.316(2)	Na(1)-N(2)#2	2.488(2)
Na(1)-S(1)#3	3.2020(8)	S(1)#1-Au(1)-S(1)	179.999(2)
S(1)#1-Au(1)-S(2)	89.94(2)	S(1)-Au(1)-S(2)	90.06(2)
S(1)#1-Au(1)-S(2)#1	90.06(2)	S(1)-Au(1)-S(2)#1	89.94(2)
S(2)-Au(1)-S(2)#1	180.0	C(4)-N(2)-Na(1)	137.23(18)
S(3)-N(2)-Na(1)	115.70(12)	O(1)#2-Na(1)-O(1)	180.0
O(1)#2-Na(1)-N(2)#2	83.55(7)	O(1)-Na(1)-N(2)#2	96.45(7)
O(1)#2-Na(1)-N(2)	96.45(7)	O(1)-Na(1)-N(2)	83.55(7)
N(2)#2-Na(1)-N(2)	180.00(8)	O(1)#2-Na(1)-S(1)#3	87.99(6)
O(1)-Na(1)-S(1)#3	92.01(6)	N(2)#2-Na(1)-S(1)#3	92.31(5)
N(2)-Na(1)-S(1)#3	87.69(5)	O(1)#2-Na(1)-S(1)#4	92.01(6)
O(1)-Na(1)-S(1)#4	87.99(6)	N(2)#2-Na(1)-S(1)#4	87.69(5)
N(2)-Na(1)-S(1)#4	92.31(5)	S(1)#3-Na(1)-S(1)#4	179.999(12)
C(7)-O(1)-Na(1)	143.47(19)	C(1)-S(1)-Au(1)	103.61(9)
C(1)-S(1)-Na(1)#5	91.78(9)	Au(1)-S(1)-Na(1)#5	112.42(3)
C(2)-S(2)-Au(1)	103.75(9)		

Symmetry transformations used to generate equivalent atoms: #1 -x+1,-y+2,-z+2; #2 -x+1,-y,-z+1; #3 -x+1,-y+1,-z+1; #4 x,y-1,z; #5 x,y+1,z.

Table 2.15. Selected Bond lengths and Bond Angles for Compound **10**

Au(1)-S(2)#1	2.3033(9)	Au(1)-S(2)	2.3033(9)
Au(1)-S(1)#1	2.3052(9)	Au(1)-S(1)	2.3052(9)
N(2)-Na(1)#2	2.456(3)	N(1)-Na(1)	2.542(3)
Na(1)-N(3)	2.455(3)	Na(1)-N(3)#3	2.455(3)
Na(1)-N(2)#4	2.456(3)	Na(1)-N(2)#5	2.456(3)
Na(1)-N(1)#3	2.542(3)	Na(1)-S(3)#3	3.3616(8)
S(2)#1-Au(1)-S(2)	180.0	S(2)#1-Au(1)-S(1)#1	90.03(3)
S(2)-Au(1)-S(1)#1	89.97(3)	S(2)#1-Au(1)-S(1)	89.97(3)
S(2)-Au(1)-S(1)	90.03(3)	S(1)#1-Au(1)-S(1)	180.0
C(6)-S(1)-Au(1)	103.42(11)	C(1)-S(2)-Au(1)	103.49(11)
C(4)-N(2)-Na(1)#2	129.5(2)	S(3)-N(2)-Na(1)#2	121.63(14)
C(3)-N(1)-Na(1)	132.4(2)	S(3)-N(1)-Na(1)	105.46(13)
N(3)-Na(1)-N(3)#3	180.0	N(3)-Na(1)-N(2)#4	95.90(10)
N(3)#3-Na(1)-N(2)#4	84.10(10)	N(3)-Na(1)-N(2)#5	84.10(10)
N(3)#3-Na(1)-N(2)#5	95.90(10)	N(2)#4-Na(1)-N(2)#5	180.0
N(3)-Na(1)-N(1)#3	88.37(10)	N(3)#3-Na(1)-N(1)#3	91.63(10)
N(2)#4-Na(1)-N(1)#3	92.80(9)	N(2)#5-Na(1)-N(1)#3	87.20(9)
N(3)-Na(1)-N(1)	91.63(10)	N(3)#3-Na(1)-N(1)	88.37(10)
N(2)#4-Na(1)-N(1)	87.20(9)	N(2)#5-Na(1)-N(1)	92.79(9)
N(1)#3-Na(1)-N(1)	180.0	N(3)-Na(1)-S(3)#3	67.55(7)
N(3)#3-Na(1)-S(3)#3	112.45(7)	N(2)#4-Na(1)-S(3)#3	112.10(7)
N(2)#5-Na(1)-S(3)#3	67.90(7)	N(1)#3-Na(1)-S(3)#3	27.74(6)
N(1)-Na(1)-S(3)#3	152.26(6)	C(7)-N(3)-Na(1)	152.5(3)

Symmetry transformations used to generate equivalent atoms: #1 -x+1,-y+1,-z+2; #2 -x+2,y+1/2,-z+3/2; #3 -x+2,-y+1,-z+1; #4 x,-y+3/2,z-1/2; #5 -x+2,y-1/2,-z+3/2

Table 2.16. Selected Bond lengths and Bond Angles for Compound **11**

Au(1)-S(2)	2.3090(15)	Au(1)-S(4)	2.3100(14)
Au(1)-S(3)	2.3174(15)	Au(1)-S(1)	2.3176(15)
Na(1)-O(1)	2.282(5)	Na(1)-O(3)	2.335(6)
Na(1)-O(2)	2.384(6)	Na(1)-O(4)	2.415(5)
Na(1)-O(4)#1	2.422(5)	Na(1)-Na(1)#1	3.282(5)
O(4)-Na(1)#1	2.422(5)	S(2)-Au(1)-S(4)	177.85(6)
S(2)-Au(1)-S(3)	90.17(5)	S(4)-Au(1)-S(3)	89.62(5)
S(2)-Au(1)-S(1)	89.60(5)	S(4)-Au(1)-S(1)	90.60(5)
S(3)-Au(1)-S(1)	179.57(6)	O(1)-Na(1)-O(3)	90.9(2)
O(1)-Na(1)-O(2)	96.0(2)	O(3)-Na(1)-O(2)	162.0(2)
O(1)-Na(1)-O(4)	168.0(2)	O(3)-Na(1)-O(4)	88.2(2)
O(2)-Na(1)-O(4)	81.64(19)	O(1)-Na(1)-O(4)#1	97.20(18)
O(3)-Na(1)-O(4)#1	105.4(2)	O(2)-Na(1)-O(4)#1	90.31(19)
O(4)-Na(1)-O(4)#1	94.56(17)	O(1)-Na(1)-Na(1)#1	144.3(2)
O(3)-Na(1)-Na(1)#1	99.9(2)	O(2)-Na(1)-Na(1)#1	84.09(16)
O(4)-Na(1)-Na(1)#1	47.37(13)	O(4)#1-Na(1)-Na(1)#1	47.19(13)
Na(1)-O(4)-Na(1)#1	85.44(17)	C(6)-S(1)-Au(1)	103.91(18)
C(1)-S(2)-Au(1)	103.97(18)	C(12)-S(3)-Au(1)	103.65(18)
C(7)-S(4)-Au(1)	103.77(18)		

Symmetry transformations used to generate equivalent atoms: #1 -x+1,-y+1,-z+1.

Table 2.17. Selected Bond lengths and Bond Angles for Compound **12**

Cu(1)-S(1)	2.1526(19)	Cu(1)-S(1)#1	2.1526(19)
Cu(1)-S(2)#1	2.1653(17)	Cu(1)-S(2)	2.1653(17)
S(2)-K(1)	3.498(2)	N(2)-K(1)#2	2.845(5)
K(1)-O(3)	2.605(8)	K(1)-O(1)#3	2.703(5)
K(1)-O(1)	2.703(5)	K(1)-N(2)#4	2.845(5)
K(1)-N(2)#2	2.845(5)	K(1)-S(2)#3	3.498(2)
S(1)-Cu(1)-S(1)#1	180.0	S(1)-Cu(1)-S(2)#1	87.87(7)
S(1)#1-Cu(1)-S(2)#1	92.12(7)	S(1)-Cu(1)-S(2)	92.13(7)
S(1)#1-Cu(1)-S(2)	87.88(7)	S(2)#1-Cu(1)-S(2)	180.00(8)
C(1)-S(1)-Cu(1)	104.8(2)	C(6)-S(2)-Cu(1)	105.6(2)
C(6)-S(2)-K(1)	92.7(2)	Cu(1)-S(2)-K(1)	120.25(6)
C(3)-N(2)-K(1)#2	135.4(4)	S(3)-N(2)-K(1)#2	118.9(3)
O(3)-K(1)-O(1)#3	86.19(11)	O(3)-K(1)-O(1)	86.19(11)
O(1)#3-K(1)-O(1)	172.4(2)	O(3)-K(1)-N(2)#4	74.63(11)
O(1)#3-K(1)-N(2)#4	78.78(15)	O(1)-K(1)-N(2)#4	99.17(15)
O(3)-K(1)-N(2)#2	74.63(11)	O(1)#3-K(1)-N(2)#2	99.17(15)
O(1)-K(1)-N(2)#2	78.79(15)	N(2)#4-K(1)-N(2)#2	149.3(2)
O(3)-K(1)-S(2)#3	148.30(3)	O(1)#3-K(1)-S(2)#3	75.07(11)
O(1)-K(1)-S(2)#3	111.75(12)	N(2)#4-K(1)-S(2)#3	76.76(11)
N(2)#2-K(1)-S(2)#3	132.84(12)	O(3)-K(1)-S(2)	148.30(3)
O(1)#3-K(1)-S(2)	111.75(12)	O(1)-K(1)-S(2)	75.07(11)
N(2)#4-K(1)-S(2)	132.84(12)	N(2)#2-K(1)-S(2)	76.76(11)
S(2)#3-K(1)-S(2)	63.39(6)	C(9)-O(1)-K(1)	163.7(5)
C(12)-O(3)-K(1)	180.000(4)		

Symmetry transformations used to generate equivalent atoms: #1 -x,-y+1,-z+2; #2 -x+1/2,-y+3/2,-z+2; #3 -x,y,-z+3/2; #4 x-1/2,-y+3/2,z-1/2.

Table 2.18. Selected Bond lengths and Bond Angles for Compound **13**

Cu(1)-S(2)	2.1730(5)	Cu(1)-S(2)#1	2.1730(5)
Cu(1)-S(1)	2.1817(5)	Cu(1)-S(1)#1	2.1817(5)
S(2)-K(1)	3.3795(5)	N(2)-K(1)#2	2.7649(16)
K(1)-N(2)#3	2.7649(16)	K(1)-N(2)#4	2.7649(16)
K(1)-N(3)#5	2.7872(17)	K(1)-N(3)	2.7873(17)
K(1)-C(5)#5	3.2917(18)	K(1)-C(6)#5	3.2919(18)
K(1)-S(2)#5	3.3794(5)	S(2)-Cu(1)-S(2)#1	180.0
S(2)-Cu(1)-S(1)	91.966(16)	S(2)#1-Cu(1)-S(1)	88.034(16)
S(2)-Cu(1)-S(1)#1	88.034(16)	C(7)-N(3)-K(1)	148.32(16)
S(2)#1-Cu(1)-S(1)#1	91.966(16)	S(1)-Cu(1)-S(1)#1	180.0
C(6)-S(2)-Cu(1)	104.92(6)	C(6)-S(2)-K(1)	71.99(6)
Cu(1)-S(2)-K(1)	109.589(18)	C(1)-S(1)-Cu(1)	104.96(6)
C(3)-N(2)-K(1)#2	134.24(12)	S(3)-N(2)-K(1)#2	118.42(8)
N(2)#3-K(1)-N(2)#4	180.0	N(2)#3-K(1)-N(3)#5	103.12(5)
N(2)#4-K(1)-N(3)#5	76.88(5)	N(2)#3-K(1)-N(3)	76.88(5)
N(2)#4-K(1)-N(3)	103.12(5)	N(3)#5-K(1)-N(3)	180.0
N(2)#3-K(1)-C(5)#5	79.62(5)	N(2)#4-K(1)-C(5)#5	100.38(5)
N(3)#5-K(1)-C(5)#5	66.49(5)	N(3)-K(1)-C(5)#5	113.51(5)
N(2)#3-K(1)-C(6)#5	75.57(4)	N(2)#4-K(1)-C(6)#5	104.43(4)
N(3)#5-K(1)-C(6)#5	90.40(5)	N(3)-K(1)-C(6)#5	89.60(5)
C(5)#5-K(1)-C(6)#5	24.08(4)	N(2)#3-K(1)-S(2)#5	98.92(3)
N(2)#4-K(1)-S(2)#5	81.08(3)	N(3)#5-K(1)-S(2)#5	104.05(4)
N(3)-K(1)-S(2)#5	75.95(4)	C(5)#5-K(1)-S(2)#5	47.96(3)
C(6)#5-K(1)-S(2)#5	30.51(3)	N(2)#3-K(1)-S(2)	81.08(3)
N(2)#4-K(1)-S(2)	98.92(3)	N(3)#5-K(1)-S(2)	75.95(4)
N(3)-K(1)-S(2)	104.05(4)	C(5)#5-K(1)-S(2)	132.04(3)
C(6)#5-K(1)-S(2)	149.49(3)	S(2)#5-K(1)-S(2)	180.0

Symmetry transformations used to generate equivalent atoms: #1 -x+1, -y+2, -z-1; #2 x, y-1, z; #3 x, y+1, z; #4 -x+1, -y+1, -z; #5 -x+1, -y+2, -z.

2.3.3.6. Role of coordinating solvents in directing the dimensionality of sodium based coordination polymers 1–10

Since we obtained coordination polymers of diverse dimensions (one-dimension through three-dimension) in diverse solvents, an obvious question comes at the first place to our mind: does the coordinating solvent influence /direct the dimensionality of coordination networks in coordination polymers **1–10**? There are some reports on this topic.^{6a,b,f-j} A recent report^{6a} of solvent effects on dimensionality of the coordination networks says that DMF with the more steric hindrance is expected to reduce the possibility for the formation of 2D or 3D networks and thus forms 1D chain. On the other hand, the less steric hindrance for CH₃CN and CH₃OH are suggested to be responsible for the formation of 2D or 3D networks respectively. The authors also have mentioned that, besides solvent effect, the coordinated ligand Py₂S might play an important role on this diverse dimensionality. The present study deals with a binary system consisting of a square planar M(III)-dithiolene complex and an octahedral Na(I)-solvent complex, in which the M(III)-

dithiolene complex $[\text{Mu}^{\text{III}}(\text{btdt})_2]^{1-}$ [$\text{M} = \text{Cu}(\text{III}), \text{Au}(\text{III})$] acts as a “N” and “S” donor ligands towards sodium coordination. Careful analyses on the crystal structures of compounds **1–10** demonstrate that the coordination around sodium ion decides the fate of dimensionality. Sodium ion, when it is present in a solvent, is expected to be preferentially solvated due to its high positive charge density. If the same system contains other auxiliary ligands, for example, N or S donor containing ligands, as in the present case, some of these sodium coordinated solvent molecules would be replaced by these auxiliary ligands during the crystallization of the relevant system. As the nucleation starts from solution, dithiolene complex anion and the counterion Na^+ come closer to each other, and a coordinate covalent bond will be formed between the N or S atoms and Na^+ counterion, leaving some coordinated solvent molecules around sodium ion. In this course of action, the structural diversity and dimensionality of this system are expected, because the auxiliary ligand (ligand $\{\text{btdt}\}^{2-}$, in the present case), having more donor centers, can coordinate with more than one sodium ion. In such situation, the dimensionality would be influenced by the factors such as shape, size and polarity of the coordinating solvents.

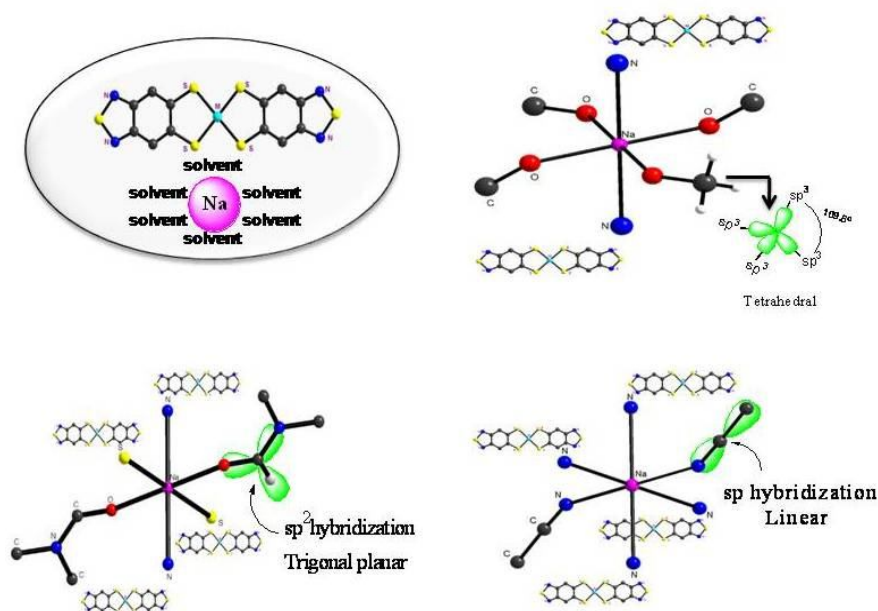


Figure 2.22. $[\text{Na}(\text{solvent})_n][\text{M}(\text{btdt})_2]$ [$\text{M} = \text{Cu}(\text{III}), \text{Au}(\text{III})$] complexes present in solution state (left above); crystallization from MeOH and THF (sp^3 hybridized orbitals of central carbon) directs the formation of 1D coordination polymer (right above); crystallizing in DMF and acetone (sp^2 hybridized orbitals of central carbon) influences the formation of 2D coordination polymer (left below); crystallization from CH_3CN (sp hybridized orbitals of central carbon) directs the formation of 3D coordination polymer (right below).

Thus we have investigated the solvent coordination to sodium ion more vigilantly. The following observations are noteworthy: during crystallization, the 1D coordination polymers **1** and **6** are obtained from MeOH, **2** and **7** are obtained from THF and the hybridization of central carbon atom attached to the sodium-coordinated solvent atom (O) is sp^3 (Figure 2.22); likewise, the sp^2 hybridized central carbon atom (of acetone and DMF solvents) attached to the coordinating atom (O) leads to the formation of 2D coordination polymers (**3** and **8** are crystallized from acetone and **4** and **9** are crystallized from DMF solvents). The 3D coordination polymers **5** and **10**, crystallized from CH_3CN , includes N as coordinating solvent atom, which is attached to sp hybridized central carbon atom. These three observations clearly reveal that the diverse hybridizations of the central carbon atoms of the solvents (MeOH, THF, acetone, DMF and CH_3CN in the present study), attached to the coordinating atoms, have a wonderful relationship with the dimensional-topologies of the compounds **1–10**. As shown in Figure 2.22, in the case of compounds **1–2** and **6–7**, the more bulkier sp^3 hybridized orbitals (tetrahedral) of the central carbon atom of methanol and THF solvents occupies more space around the alkali metal ion (sodium cation) and prevent further coordination of more dithiolene complex units (through N or S donor atoms), thereby it allows the extension only in 1-dimension rather than 2-dimensions or 3-dimensions. The less bulkier sp hybridized orbitals (linear shape) of the central carbon atom of CH_3CN occupy less space around sodium cation, thus allow more dithiolene complex units to coordinate sodium ion leading to 3-dimensional coordination polymers (compounds **5** and **10**). The recrystallization from acetone and DMF type of coordinating solvents, the planar shape of sp^2 hybridized orbitals of the central carbon atom attached to coordinating donor atom of acetone and DMF solvents, direct towards the formation of 2-dimensional networks (compounds **3** and **8** from acetone recrystallization, **4** and **9** from DMF recrystallization). However, even though, both acetone and DMF coordinating solvents direct towards the 2-dimensional coordination polymers (**3**, **4**, **8** and **9**), the structural diversity was observed among acetone recrystallized products and DMF recrystallized products, probably due to difference in the size of the relevant solvent molecules. Thus, the shape and space occupied by the hybridized orbitals of central carbon atom attached to the coordinating solvent atoms are the major factors in directing the dimensionality of coordination polymers of the present system, as described in Table 2.19.

Table 2.19. Role of coordinating solvent in directing the dimensionality of sodium based coordination polymers **1–10**

S. No	Recrystallizing solvent	Hybridization and geometry of central carbon	Dimensionality of coordination networks observed in compounds
1	MeOH	sp ³ , Tetrahedral	1D in 2 and 7
2	Acetone	sp ² , Trigonal planar	2D in 3 and 8
3	DMF	sp ² , Trigonal planar	2D in 4 and 9
4	Acetonitrile	sp, Linear	3D in 5 and 10

2.3.3.7. Influence of counter cations on the dimensionality of coordination polymers

From the above coordination polymers **1–10**, the dimensionality of a sodium coordination based polymer system, coupled with a metal(III) bis(dithiolene) complex (metal = copper and gold), has been shown to be regulated by the type of hybridization of the central carbon atom of the solvent coordinating to the sodium ion. From careful crystal structure analyses, it has been generalized a relation between dimensionality of coordination polymers (based on a square planar metal(III) bis(dithiolene) complex coupled with an octahedral sodium complex) and the type hybridization of the central carbon atom of the sodium coordinated solvent molecules. It has been stressed that the hybridization of the central carbon atoms of the solvents (MeOH, CH₃COCH₃, DMF and CH₃CN), attached to the coordinating atoms, plays an important role in directing the dimensional-topologies of the coordination polymers **1–10**. As a continuation of our systematic investigations of coordinating solvents and counter cations (i.e. K⁺ ion instead of Na⁺ ion) effect on the structural diversity and dimensionality of coordination networks, we have investigated two new potassium-coordination polymers (**12–13**) based on [Cu^{III}(btdt)₂]¹⁻. Interestingly, compounds **12** and **13** are 3-D and 2-D extended networks observed in the crystal structures which are obtained from recrystallization of acetone and acetonitrile coordinating solvents, respectively.

When we compare the crystal structures of the compounds **3** and **12** (both obtained from acetone recrystallization), in which coordinated acetone solvents coordinated to the Na⁺ and K⁺ ions, respectively, compound **3** is coordinated to sodium ion through the four

nitrogen atoms whereas compound **12** is coordinated to potassium ion through the two nitrogen and two sulfur atoms. In compound **3** the coordination number of Na^+ ion is six with two coordinated solvent molecules, whereas in compound **12**, the K^+ ions as coordination number seven with three coordinated acetone solvent molecules. This is probably due to the difference in the size of the counter ion (between sodium and potassium) influences the diversities in the crystal structures and also results in the variation in the dimensionality of extended networks. i.e. compound **3** is extended into 2-D, whereas compound **12** extended into 3-D coordinated networks in their solids.

The comparison of the crystal structures of compounds **5** and **13** (both obtained from acetone recrystallization), in which coordinated acetone nitrile solvents is coordinated to the Na^+ and K^+ ions, respectively, compound **5** is coordinated to sodium ion through the four nitrogen atoms of four different dithiolene units whereas in compound **13** coordinated to potassium ion through the two nitrogen and two sulfur atoms of four different dithiolene units. Due to the difference in coordination environment, compounds **5** and **13** are not isomorphs, even though both having the coordination number six, and the diversities in the crystal structures. Compound **5** is extending into 3-D, whereas compound **13** was extended into 2-D coordinated networks in their crystal structures.

2.4. Conclusion

In summary, We have demonstrated here, the synthesis of sodium metal based coordination polymers of diverse dimensionality (from 1D to 2D through 3D) based on a Metal(III) dithiolene complex anion $[\text{M}^{\text{III}}(\text{btdt})_2]^{1-}$ [$\text{M} = \text{Cu(III)}, \text{Au(III)}$] by changing the solvents of recrystallization. We have shown that dimensionality of a sodium coordination based polymer system, coupled with a Metal(III) (bis)dithiolene complex, can be regulated by the type of hybridization of the central carbon atom of the solvent coordinating to the sodium ion. In which, Cu(III) analogues offers us opportunity to perform electrochemical studies and to carry out spectroscopy. The electrochemistry of the copper (III) complexes is very interesting in the sense that these complexes get reduced more easily. This indicates that the present system (Cu(III) dithiolate) might act as oxidation catalyst for organic transformations / oxidation reactions of industrial importance. In order to attempting to generalize above concept (relation between the hybridization and dimensionality) by choosing an alkali metal ion (e.g., K^+ cations instead of Na^+ ions)

coupled with a transition metal(bis) dithiolene complex, additionally we have synthesized, two new potassium metal coordination polymers of diverse dimensionality based on a Metal(III) dithiolene complex anion $[\text{Cu}^{\text{III}}(\text{btdt})_2]^{1-}$ by changing the solvents of recrystallization. From the recrystallization the coordinating acetone and acetonitrile solvents are results in the formation of 3-D and 2-D extended networks in their crystal structures, respectively. We have also described the comparisons in the structures and dimensionalities with previously reported sodium coordination polymers. Interestingly, the potassium based polymeric compounds **12-13**, are not supports the above mentioned concept (i.e relation between the hybridization and dimensionality). This is probably due to difference in size of the counter cations (between sodium and potassium). So that the above concept is only limited to sodium based coordination polymers. We believe that in the sodium based coordination polymeric system, octahedral geometry of sodium ion playing a role in directing the dimensionality of coordination polymers compared to the K-based coordination polymers (because of its larger size, coordination number is varying). In order to get good conducting and magnetic coordination polymeric materials based on dithiolene complexes, we are now attempting to synthesizing by choosing an alkali metal ion (e.g., Na^+ , K^+ cations etc) coupled with a transition metal(bis) dithiolene complex (e.g., Ni(III)(bis) dithiolene complex) in synthesizing a new class of coordination polymers system. Finally it is worth mentioning that we have established a new class of dithiolene-based materials, where hybridization of central carbon atom of the coordinating solvent plays an important role in determining the dimensionality of the resulting coordination polymer. Thus this work is not only importance in terms of practical applications, but also it serves in understanding the basic principle of crystal engineering chemistry.

2.5. References

- 1 (a) Moulton, B.; Zaworotko, M. J. *Chem. Rev.* **2001**, *101*, 1629. (b) *Design and Construction of Coordination Polymers*, John Wiley & Sons, NewYork, **2009**. (c) Batten, S. R.; Robson, R. *Angew. Chem., Int. Ed.* **1998**, *37*, 1460. (d) Yagi, O. M.; O'Keeffe, M.; Ockwig, N. W.; Chae, H. K.; Eddaouji, M.; Kim, J. *Nature* **2003**, *423*, 705. (e) Biradha, K. *CrystEngComm* **2003**, *5*, 374. (f) Janiak, C.; *Dalton*

- Trans.* **2003**, 2781. (g) Fujita, M.; Umemoto, K.; Yoshizawa, M.; Fujita, N.; Kusukawa, T.; Biradha, K. *Chem. Commun.* **2001**, 509. (h) Blake, A. J.; Champness, N. R.; Hubberstey, P.; Li, W.-S.; Withersby, M. A.; Schröder, M. *Coord. Chem. Rev.* **1999**, 183, 117. (i) Swiegers G. F.; Malefetse, T. J. *Chem. Rev.* **2000**, 100, 3483. (j) Aakeröy, C. B.; Champness, N. R.; Janiak, C. *CrystEngComm* **2010**, 12, 22. (f) Miao, D.; Xianhe, B. *Prog. in Chem.* **2009**, 21, 2458. (g) James, S. L. *Chem. Soc. Rev.* **2003**, 32, 276. (h) Rabaça, S.; Almeida, M. *Coord. Chem. Rev.* **2010**, 254, 1493. (i) Perry IV, J. J.; Perman, J. A.; Zaworotko, M. J. *Chem. Soc. Rev.* **2009**, 38, 1400. (j) Adachi, K.; Kawata, S.; Kabir, Md. K.; Kumagai, H.; Inoue, K.; Kitagawa, S. *Chem. Lett.* **2001**, 30, 50.
- 2 (a) Matsuda, R.; Kitaura, R.; Kitagawa, S.; Kubota, Y.; Belosludov, R. V.; Kobayashi, T. C.; Sakamoto, H.; Chiba, T.; Takata, M.; Kawazoe, Y.; Mita, Y. *Nature* **2005**, 436, 238. (b) Rowsell, J. L. C.; Yaghi, O. M. *Angew. Chem., Int. Ed.* **2005**, 44, 4670. (c) Evans, O. R.; Lin, W. *Chem. Mater.* **2001**, 13, 2705. (d) Geng, Y.; Wang, X.-J.; Chen, B.; Xue, H.; Zhao, Y.-P.; Lee, S.; Tung, C.-H.; Wu, L.-Z. *Chem. –Eur. J.* **2009**, 15, 5124. (e) Okubo, T.; Tanaka, N.; Kim, K. H.; Yone, H.; Maekawa, M.; Kuroda-Sowa, T. *Inorg. Chem.* **2010**, 49, 3700. (f) Wang, X.-Y.; Wang, Z.-M.; Gao, S. *Chem. Commun.* **2008**, 281. (g) Todokoro, M.; Yasuzuka, S.; Nakamura, M.; Shinoda, T.; Tatenuma, T.; Mitsumi, M.; Ozawa, Y.; Toriumi, K.; Yoshino, H.; Shiomi, D.; Sato, K.; Takui, T.; Mori, T.; Murata, K. *Angew. Chem., Int. Ed.* **2006**, 45, 5144. (h) Coronado, E.; Galán-Mascarós, J. R.; Gómez-García, C. J.; Laukhin, V. *Nature* **2000**, 408, 447. (i) Lin, X.; Jia, J.; Hubberstey, P.; Schröder M.; Champness, N. R. *CrystEngComm* **2007**, 9, 438. (j) Liu, M.-L.; Shi, W.; Song, H.-B.; Cheng, P.; Liao, D.-Z.; Yan, S.-P. *CrystEngComm* **2009**, 11, 102. (k) Dincă, M.; Long, J. R. *Angew. Chem., Int. Ed.* **2008**, 47, 6766. (l) Burrows, A. D.; Frost, C. G.; Mahon, M. F.; Winsper, M.; Richardson, C.; Attafield, J. P.; Rodgers, J. A. *Dalton Trans.* **2008**, 6788. (m) Pardo, E.; Ruiz-García, R.; Cano, J.; Ottenwaelde, X.; Lescouëzec, R.; Journaux, Y.; Lloret, F.; Julve, M. *Dalton Trans.* **2008**, 2780. (n) Gu, Z.-G.; Xu, Y.-F.; Yin, X.-J.; Zhou, X.-H.; Zuo, J.-L.; You, X.-Z. *Dalton Trans.* **2008**, 5593. (o) Drabent, K.; Ciunik, Z.; Ozarowski, A. *Inorg. Chem.* **2008**, 47, 3358. (p) Collins, D. J.; Zhou, H.-C. *J. Mater. Chem.* **2007**, 17, 3154.

- 3 (a) Gavezzotti, A. *Theoretical Aspects and Computer Modeling of the Molecular Solid State*, John Wiley & Sons, Chichester, **1997**. (b) Desiraju, G. R. *Angew. Chem., Int. Ed. Engl.* **1995**, *34*, 2311. (c) Desiraju, G. R.; Gavezzotti, A. *Acta Crystallogr., Sect. B* **1989**, *45*, 473. (d) Williams, D. E. *Acta Crystallogr., Sect. A* **1996**, *52*, 326. (e) Robson, R. *J. Chem. Soc., Dalton Trans.* **2000**, 3735. (f) Prior, T. J.; Bradshaw, D.; Teat, S. J.; Rosseinsky, M. J. *Chem. Commun.* **2003**, 500. (g) Tabellion, F. M.; Seidel, S. R.; Arif, A. M.; Stang, P. J. *J. Am. Chem. Soc.* **2001**, *123*, 7740. (g) Bu, X.-H.; Chen, W.; Lu, S.-L.; Zhang, R.-H.; Liao, D.-Z.; Shionoya, M.; Brisse, F.; Ribas, J. *Angew. Chem., Int. Ed.* **2001**, *40*, 3201.
- 4 (a) Yoshizawa, M.; Nagao, M.; Umemoto, K.; Biradha, K.; Fujita, M.; Sakamoto, S.; Yamaguchi, K. *Chem. Commun.* **2003**, 1808. (b) Dong, G.; Ke-liang, P.; Chun-ying, D.; Cheng, H.; Qing-jin, M. *Inorg. Chem.* **2002**, *41*, 5978. (c) Wang, X.-L.; Chen, Y.-Q.; Liu, G.-C.; Lin, H.-Y.; Zheng, W.-Y.; Zhang, J.-X. *J. Organomet. Chem.* **2009**, *694*, 2263. (d) Li, J.-R.; Bu, X.-H.; Jiao, J.; Du, W.-P.; Xu, X.-H.; Zhang, R.-H. *Dalton Trans.* **2005**, 464. (e) Banfi, S.; Carlucci, L.; Caruso, E.; Ciani, G.; Proserpio, D. M. *J. Chem. Soc., Dalton Trans.* **2002**, 2714. (f) Shi, W.-J.; Ruan, C.-X.; Li, Z.; Li, M.; Li, D. *CrystEngComm* **2008**, *10*, 778. (g) Liu, P.-P.; Cheng, A.-L.; Yue, Q.; Liu, N.; Sun, W.-W.; Gao, E.-Q. *Cryst. Growth Des.* **2008**, *8*, 1668.
- 5 (a) Liu, Y.; Qi, Y.; Su, Y.-H.; Zhao, F.-H.; Che, Y.-X.; Zheng, J.-M. *CrystEngComm* **2010**, *12*, 3283. (b) Cui, F.-Y.; Huang, K.-L.; Xu, Y.-Q.; Han, Z.-G.; Liu, X.; Chi, Y.-N.; Hu, C.-W. *CrystEngComm* **2009**, *11*, 2757. (c) Liu, J.-Q.; Zhang, Y.-N.; Wang, Y.-Y.; Jin, J.-C.; Lermontova, E. Kh.; Shi, Q.-Z.; *Dalton Trans.* **2009**, 5365. (d) Feazell, R. P.; Carson, C. E.; Klausmeyer, K. K. *Inorg. Chem.* **2006**, *45*, 2635.
- 6 (a) Tzeng, B.-C.; Yeh, H.-T.; Chang, T.-Y.; Lee, G.-H.; *Cryst. Growth Des.* **2009**, *9*, 2552. (b) Chen, S.-C.; Zhang, Z.-H.; Huang, K.-L.; Chen, Q.; He, M.-Y.; Cui, A.-J.; Li, C.; Liu, Q.; Du, M. *Cryst. Growth Des.* **2008**, *8*, 3437. (c) Yang, J.; Li, G.-D.; Cao, J.-J.; Yue, Q.; Li, G.-H.; Chen, J.-S.; *Chem. –Eur. J.* **2007**, *13*, 3248. (d) Wang, C.-J.; Ma, H.-R.; Wang, Y.-Y.; Liu, P.; Zhou, L.-J.; Shi, Q.-Z.; Peng, S.-M. *Cryst. Growth Des.* **2007**, *7*, 1811. (e) Prasad, T. K.; Rajasekharan, M. V. *Cryst. Growth Des.* **2008**, *8*, 1346. (f) Pedireddi, V. R.; Varughese, S. *Inorg. Chem.*

- 2004**, *43*, 450. (g) Chen, B.; Fronczek, F. R.; Maverick, A. W. *Chem. Commun.* **2003**, 2166. (h) Lopez, S.; Keller, S. W. *Inorg. Chem.* **1999**, *38*, 1883. (i) Lee, S. Y.; Jung, J. H.; Vittal, J. J.; Lee, S. S. *Cryst. Growth Des.* **2010**, *10*, 1033. (j) Lin, X.-M.; Fang, H.-C.; Zhou, Z.-Y.; Chen, L.; Zhao, J.-W.; Zhu, S.-Z.; Cai, Y.-P. *CrystEngComm* **2009**, *11*, 847. (k) Hennigar, T. L.; MacQuarrie, D. C.; Losier, P.; Rogers, R. D.; Zaworotko, M. J. *Angew. Chem., Int. Ed.* **1997**, *36*, 972. (l) Withersby, M. A.; Blake, A. J.; Champness, N. R.; Cooke, P. A.; Hubberstey, P.; Li, W.-S.; Schröder, M. *Inorg. Chem.* **1999**, *38*, 2259.
- 7 Chatterton, N. P.; Goodgame, D. M. L.; Grachvogel, D. A.; Hussain, I.; White, A. J. P.; Williams, D. J. *Inorg. Chem.* **2001**, *40*, 312.
- 8 (a) Baudron, S. A.; Hosseini, M. W. *Inorg. Chem.* **2006**, *45*, 5260. (b) Ribas, X.; Dias, J. C.; Morgado, J.; Wurst, K.; Molins, E.; Ruiz, E.; Almeida, M.; Veciana, J.; Rovira, C. *Chem. Eur. J.* **2004**, *10*, 1691. (c) Ribas, X.; Dias, J.; Morgado, J.; Wurst, K.; Almeida, M.; Veciana, J.; Rovira, C. *CrystEngComm* **2002**, *4*, 564. (d) Ribas, X.; MasPOCH, D.; Dias, J.; Morgado, J.; Almeida, M.; Wurst, K.; Vaughan, G.; Veciana, J.; Rovira, C. *CrystEngComm* **2004**, *6*, 589. (e) Takaishi, S.; Hosoda, M.; Kajiwara, T.; Miyasaka, H.; Yamashita, M.; Nakanishi, Y.; Kitagawa, Y.; Yamaguchi, K.; Kobayashi, A.; Kitagawa, H. *Inorg. Chem.* **2009**, *48*, 9048. (f) X Ribas, X.; Dias, J. C.; Morgado, J.; Wurst, K.; Santos, I. C.; Almeida, M.; Vidal-Gancedo, J.; Veciana, J.; Rovira, C. *Inorg. Chem.* **2004**, *43*, 3631. (g) Dawe, L. N.; Miglio, J.; Turnbow, L.; Taliaferro, M. L.; Shum, W. W.; Bagnato, J. D.; Zakharov, L. N.; Rheingold, A. L.; Arif, A. M.; Fourmigué, M. Miller, J. S. *Inorg. Chem.* **2005**, *44*, 7530.
- 9 Brusso, J. L.; Clements, O. P.; Haddon, R. C.; Itkis, M. E.; Leitch, A. A.; Oakley, R. T.; Reed, R. W.; Richardson, J. F. *J. Am. Chem. Soc.* **2004**, *126*, 8256.
- 10 Bruker. *SADABS*, *SMART*, *SAINT* and *SHELXTL*, **2000** (Bruker AXS Inc., Madison, Wisconsin, USA).
- 11 Sheldrick, G. M. *Acta Crystallogr. Sect. A* **2008**, *64*, 112–122.
- 12 Madhu, V.; Das, S. K. *Inorg. Chem.* **2006**, *45*, 10037.
- 13 (a) Changtao, Q.; Bing, W.; Yin, X.; Yonghua, L. *J. Chem. Soc., Dalton. Trans.* **1994**, 2109. (b) Daniel, R.; James, E. C.; Walter, A. F.; Arnold, L. R.; Christopher,

- I.; Llia, A. G. *Polyhedron* **2001**, 20, 2491. (c) José, M. D.-V.; José, M. M.; Enrique, C. *Inorg. Chem. Acta*. **2004**, 357, 611. (d) Reglinski, J.; Garner, M.; Cassidy, I. D.; Slavin, P. A.; Spicer, M. D.; Armstrong, D. R. *J. Chem. Soc., Dalton Trans.* **1999**, 2119.
- 14 Bondi, A. *J. Phys. Chem.* **1964**, 68, 441.
- 15 (a) Rothenberger, A.; Shafaei-Fallah, M.; Shi, W. *Chem. Commun.* **2007**, 1499. (b) Chen, Z.; Sutton, L. R.; Moran, D.; Hirsch, A.; Thiel, W.; Schleyer, P. R. *J. Org. Chem.* **2003**, 68, 8808. (c) Cendrowski-Guillaume, S. M.; Gland, G. L.; Nierlich, M.; Ephritikhine, M. *Organometallics* **2000**, 19, 5654.
- 16 (a) Moulton, B.; Lu, J.; Zaworotko, M. J. *J. Am. Chem. Soc.* **2001**, 123, 9224. (b) Thakuria, R.; Sarma, B.; Nangia, A. *Cryst. Growth Des.* **2008**, 8, 1471. (c) Thakuria, R.; Sarma, B.; Nangia, A. *New J. Chem.* **2010**, 34, 623.
- 17 (a) Laborda, S.; Clérac, R.; Anson, C. E.; Powell, A. K. *Inorg. Chem.* **2004**, 43, 5931. (b) Patrick, B. O.; Stevens, C. L.; Storr, A.; Thompson, R. C. *Polyhedron* **2003**, 22, 3025.

New Square-Planar Metal-Bis(1,2-Dithiolene) Complexes Based on 2,1,3-Benzenethiadiazole-5,6-dithiolate ($\{\text{btdt}\}^{2-}$) ligand and Nickel Trans-disulfinate Complex: Synthesis, Crystallography and Properties

3 Chapter

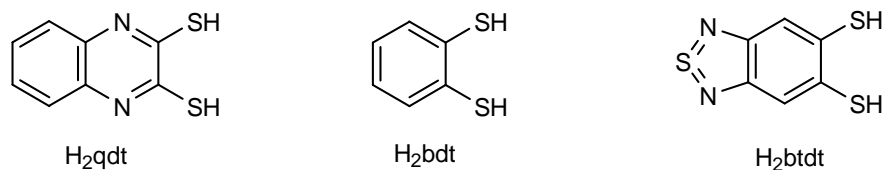
Abstract:- The syntheses, crystal structures and properties of four new coordination complexes $[\text{Bu}_4\text{N}][\text{M}^{\text{III}}(\text{btdt})_2]$ [$\text{M} = \text{Cu}$ (**1**), Au (**2**)] and $[\text{Bu}_4\text{N}]_2[\text{M}^{\text{II}}(\text{btdt})_2]$ [$\text{M} = \text{Pt}$ (**3**), Ni (**4**)] ($\{\text{btdt}\}^{2-} = 2,1,3$ -benzenethiadiazole-5,6-dithiolate) have been described. In addition to this, trans disulfinate complex $[\text{Bu}_4\text{N}]_2[\text{Ni}(\text{btdtO}_4)_2] \cdot \text{H}_2\text{O}$ (**5**) has been synthesized by the air oxidation of the compound **4** in MeOH solutions. Single crystal X-ray structural analyses of complexes **1–5** show that $\{\text{MS}_4\}$ chromophores lies in almost square-planar coordination environment in complexes **1** and **4**, whereas in complexes **2**, **3** and **5**, this chromophore has slightly distorted square-planar geometry around the central metal ion. Interactions in the solid-state for all these compounds have been studied by intermolecular contacts, such as, weak hydrogen bonding interactions and non-covalent interactions. Complexes **1–5** show broad absorption bands in the visible region, with that of **3** and **4** are being sensitive to solvent polarity. Blue-colored air-saturated solutions of $[\text{Bu}_4\text{N}]_2[\text{Ni}(\text{btdt})_2]$ (**4**) gradually turn red in the presence of visible light (room light). This transformation requires both oxygen (air) and light. Electrochemical properties of all these compounds have been described by cyclic voltammetric studies.

3.1. Introduction

Since 1960s, the interests are continuing in the design and synthesis of square planar metal-bis(dithiolene) complexes, because the redox active dithiolene ligands have ability to form highly electron delocalized systems.¹ Metal bis(dithiolene) complexes are important in terms of their potential applications in the areas of conducting-, magnetic-,² nonlinear optical-materials,³ and near-infrared (NIR) dyes.⁴ The scope of metal dithiolene complexes has extended to bioinorganic modeling studies because of the existence of metal-dithiolene moiety in the active sites of many metallo-enzymes.⁵ Families of arene-dithiolene complexes are highly stable with metals in their higher oxidation states. Quinoxaline based dithiolate-system ($\{\text{qdt}\}^{2-}$, Scheme 3.1) and its molybdenum-oxo complexes have been investigated for modeling the active sites of molybdenum hydroxylase enzymes.⁶ The changes in electronic absorption spectra and redox properties of relevant metal dithiolene complexes have been explored by the reversible protonation of the coordinated qdt-ligand.⁷ In addition, qdt-type ligands are useful in the area of analytical chemistry.⁸ The utility of qdt- complexes as ion-active substances of membrane electrodes has also been reported in literature.⁹ The photo-physical (luminescence)

properties of platinum complexes of qdt-type ligand have been studied extensively.¹⁰ On the other hand, benzene-1,2-dithiolato ligand ($\{\text{bdt}\}^{2-}$, Scheme 3.1) containing molybdenum and tungsten complexes have been reported in literature, that are described as structural analogues of the oxidized active sites in the xanthine oxidoreductase enzyme family.¹¹ Some of the metal(III) complexes of benzene-1,2-dithiolate ($\{\text{bdt}\}^{2-}$) and 1-toluene-3,4-dithiolate ($\{\text{tdt}\}^{2-}$) have been studied by Kameníček group.¹² The detailed physical properties of bis-(benzene-1,2-dithiolato)-gold(IV) $\{[\text{Au}(\text{bdt})_2]\}$ compound have been reported by the Bjørnholm group.¹³ This group has also studied the electronic structure of substituted aromatic dithiolene complexes of gold(III).¹⁴

Based on the importance of heterocyclic based dithiolene complexes, it has prompted us to choose a dithiolate ligand H_2btdt system ($\{\text{btdt}\}^{2-} = 2,1,3\text{-benzenethiadiazole-5,6-dithiolate}$, Scheme 3.1) for the synthesis of a new series of ‘discrete’ metal dithiolene complexes with various metal ions which are able to form square-planar complexes. In this context, we must mention that we have recently reported the sodium-associated ‘coordination polymers’ based on this ligand system (chapter 2).¹⁵ In this contribution, we wish to report synthesis, crystal structures and supramolecular features of the complexes $[\text{Bu}_4\text{N}][\text{M}^{\text{III}}(\text{btdt})_2]$ $[\text{M} = \text{Cu}$ (**1**), Au (**2**)] and $[\text{Bu}_4\text{N}]_2[\text{M}^{\text{II}}(\text{btdt})_2]$ $[\text{M} = \text{Pt}$ (**3**), Ni (**4**)]. The electronic absorption and electrochemical properties of these compounds have also been described.

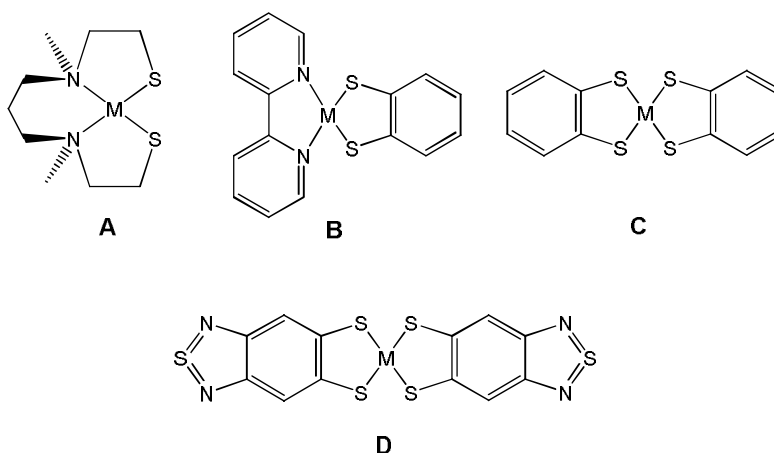


Scheme 3.1. Structural representation of some arene dithiols.

On the other hand, $[\text{Ni Fe}]$ hydrogenase¹⁶ and CO-dehydrogenase¹⁷ belong to the nickel-containing enzymes possessing a sulfur-rich (cysteinate) environment around nickel. These nickel-containing enzymes show an interesting and complicated air sensitivity, which includes reversible inhibition of activity and irreversible deactivation of the enzyme by dioxygen. The electrochemical and spectroscopic studies of enzymes support that the deactivated species might be the products of oxygen addition at sites other than the metal. Excluding metal center, the only possible site is the sulfur that may be

involved in oxidation.¹⁶ The possible sulfur oxygenates are (a) sulfinates, or metallosulfones $M-SO_2R$, and (b) sulfenates, or metallosulfoxides, $M-(S=O)R$. Darensbourg research group¹⁸ and others¹⁹ extensively studied, synthesis and mechanistic understanding about sulfinates and sulfenates of nickel-thiolate (type A, Scheme 3.2) complexes. Nickel-sulfinates are quite interesting because these are all S-bound and the oxygen atoms cannot be removed by any chemical agents. That's why S-bound Ni-sulfinates can be represented as an irreversibly oxygen-damaged deactivated species of nickel-containing enzymes. All these literatures show that production of Ni-sulfinates are from the reactions with H_2O_2 or gaseous O_2 .

Gray²⁰ and Bachman²¹ reported sulfur oxygenated products of dithiolene- α -diimine (type B, Scheme 3.2) complexes and identified both mono sulfinates and disulfinates depending on the oxidation conditions. Photochemical oxidation of dithiolene- α -diimine (type B, Scheme 3.2) results in mono-sulfinates and chemical oxidation with H_2O_2 results in di-sulfinates. However, metal-sulfinates based, on bis(dithiolene) complexes (type C, Scheme 3.2), are still rare in the literature. To the best of our knowledge, only few reports are shown in literature,^{21b,22} wherein, Robertson reported trans-di-sulfinate complex of $[Ni(bdt)]^{1-}$, in which sulfur atoms were oxidized by receiving of oxygen atoms from counter cation.^{22a} Another report of an interesting S-bonded sulfinates, based on Fe-bis(benzene-1,2-dithiolene) complex (type C, Scheme 3.2), relates to the an inactive form of the Fe-containing nitrile hydratase (Fe-NHase) containing Cys-sulfinic (Cys- SO_2) and Cys-sulfenic (Cys-SO) groups.^{22b}



Scheme 3.2. Structural representation of metal dithiolene complexes.

We have described here, trans-disulfinate nickel complex **5** by the simple and air oxidation of compound **4** (type D, Scheme 3.2) at room temperature. We have demonstrated here that, compound **5** has been characterized unambiguously by X-ray crystallography along with its spectral studies (IR, UV-Vis in solution and solid), electro chemistry and elemental analysis.

3.2. Experimental Details

3.2.1. General Methods

Micro analytical (C, H, N) data were obtained with a FLASH EA 1112 Series CHNS Analyzer. Infrared (IR) spectra were recorded on KBr pellets with a JASCO FT/IR-5300 spectrometer in the region of 400-4000 cm^{-1} . ^1H NMR spectra of compounds were recorded on Bruker DRX- 400 spectrometer using $\text{Si}(\text{CH}_3)_4$ [TMS] as an internal standard. Electronic absorption spectra were recorded on a Cary 100 Bio UV-Visible spectrophotometer. A Cypress model CS-1090/CS-1087 electro analytical system was used for cyclic voltammetric experiments. The electrochemical experiments were measured in MeOH containing $[\text{Bu}_4\text{N}][\text{ClO}_4]$ as a supporting electrolyte, using a conventional cell consisting of two platinum wires as working and counter electrodes, and a Ag/AgCl electrode as a reference. The potentials reported here are uncorrected for junction contributions.

3.2.2. Materials

All the chemicals for the synthesis were commercially available and used as received. 1,2-Diaminobenzene-bis(thiocyanate)²³ was prepared according to literature procedure. Syntheses of metal complexes were performed under N_2 using standard inert-atmosphere techniques. Solvents were dried by standard procedures.

3.2.3. Synthesis and Characterization

Synthesis of $[\text{Bu}_4\text{N}][\text{Cu}(\text{btdt})_2]$ (**1**)

The $\{\text{btdt}\}^{2-}$ ion is generated, *in situ*, by treatment of H_2btdt (0.070 g, 0.35 mmol) with excess amount of NaOH (0.040 g, 1.0 mmol) in MeOH (20.0 mL). To the resulting clear red solution, solid $\text{CuCl}_2 \cdot 2\text{H}_2\text{O}$ (0.030 g, 0.176 mmol) was added and the reaction

mixture was stirred for 30 min in presence of open atmosphere. The precipitates were then removed by filtration; to the filtrate obtained, tetrabutylammonium bromide solution (0.1 g in 40.0 mL deionised water) was added and stirred for 15 min. The resulting black precipitate was separated by filtration, washed with water followed by diethyl ether, and dried at room temperature. It was recrystallized from acetonitrile solution by vapor diffusion with diethyl ether. Yield: 0.050 g (40.4% based on Cu). IR (KBr, cm^{-1}): 2957, 2870, 1556, 1460, 1419, 1377, 1226, 1114, 1039, 976, 814, 528. ^1H NMR (400 MHz, δ ppm) ($\text{DMSO}-d_6$): 0.92(br, 12H), 1.29(br, 8H), 1.55(br, 8H), 3.15(br, 8H), 7.63(s, 4H). Anal. Calcd. for $\text{C}_{28}\text{H}_{40}\text{N}_5\text{S}_6\text{Cu}$: C 47.87 H 5.74, N 9.97%. Found: C 47.50, H 5.88, N 10.13%.

Synthesis of $[\text{Bu}_4\text{N}][\text{Au}(\text{btdt})_2]$ (2)

The *in situ* generation of $\{\text{btdt}\}^{2-}$ ion was performed by the treatment of H_2btdt (0.165 g, 0.825 mmol) with excess amount of NaOH (0.15 g, 3.75 mmol) in MeOH (40 mL). To the resulting clear red solution, solid $\text{HAuCl}_4 \cdot 3\text{H}_2\text{O}$ (0.175 g, 0.444 mmol) was added and the reaction mixture was stirred for 30 min under nitrogen atmosphere. The precipitates were then separated by filtration; to the filtrate obtained, tetrabutylammonium bromide solution (0.2 g in 40.0 mL deionised water) was added and stirred for 15 min. The resulting dark brown precipitate was separated by filtration, washed with water followed by diethyl ether, and dried at room temperature. It was recrystallized by the slow evaporation of the acetone solution. Yield: 0.222 g (59.6% based on Au). IR (KBr, cm^{-1}): 2957, 2868, 1628, 1469, 1423, 1381, 1240, 1072, 875, 814, 636. ^1H NMR (400 MHz, δ ppm) ($\text{DMSO}-d_6$): 0.92(br, 12H), 1.30(br, 8H), 1.55(br, 8H), 3.15(br, 8H), 7.81(s, 4H). Anal. Calcd. for $\text{C}_{28}\text{H}_{40}\text{N}_5\text{S}_6\text{Au}$: C 40.23, H 4.82, N 8.38%. Found: C 40.52, H 4.68, N 8.52%.

Synthesis of $[\text{Bu}_4\text{N}]_2[\text{Pt}(\text{btdt})_2]$ (3)

The $\{\text{btdt}\}^{2-}$ dianion was generated, *in situ*, by treatment of H_2btdt (0.058 g, 0.29 mmol) with excess amount of NaOH (0.040 g, 1.0 mmol) in MeOH (10.0 mL). To the resulting clear red solution, 10.0 mL aqueous solution of K_2PtCl_4 solution (0.060 g, 0.145 mmol) was added and the reaction mixture was stirred for 24 h resulting in dark purple solution. Dark red micro-crystals were precipitated by adding tetrabutylammonium bromide (0.150 g, 0.47 mmol); the micro crystals were filtered, washed with water followed by diethyl

ether, and dried at room temperature. It was recrystallized from acetonitrile solution by vapor diffusion with diethyl ether. Yield: 0.083 g (53.9% based on Pt). IR (KBr, cm^{-1}): 2959, 2872, 1641, 1579, 1483, 1425, 1381, 1236, 1170, 1062, 985, 860, 812, 736, 707, 667, 528. ^1H NMR (400 MHz, δ ppm) (CD_3CN): 0.92(br, 24H), 1.32(br, 16H), 1.57(br, 16H), 3.09(br, 16H), 7.81(s, 4H). Anal. Calcd. for $\text{C}_{44}\text{H}_{76}\text{N}_6\text{S}_6\text{Pt}$: C 49.09, H 7.12, N 7.81%. Found: C 48.62, H 7.31, N 8.13%.

Synthesis of $[\text{Bu}_4\text{N}]_2[\text{Ni}(\text{btdt})_2]$ (**4**)

The $\{\text{btdt}\}^{2-}$ ion is generated, *in situ*, by the treatment of H_2btdt (0.076 g, 0.38 mmol) with excess amount of NaOH (0.045 g, 1.125 mmol) in dry MeOH (8.0 mL) through purging with nitrogen gas. To the resulting clear red solution, solid $\text{NiCl}_2 \cdot 6\text{H}_2\text{O}$ (0.045 g, 0.189 mmol) was added and the reaction mixture was stirred for 30 min under nitrogen atmosphere. Dark black micro crystalline solid was precipitated by adding tetrabutylammonium bromide (0.2 g, 0.621 mmol) in degassed (N_2 gas bubbled) water (20 mL); the solid was filtered immediately, washed with water followed by diethyl ether, and dried at room temperature. Black colored blocks type crystals of compound $[\text{Bu}_4\text{N}]_2[\text{Ni}(\text{btdt})_2]$ (**4**), suitable for single crystal X-ray structure analysis, were grown from vapor diffusion of diethyl ether into acetonitrile solution. Yield: 0.140 g (79.0% based on nickel metal). IR (KBr, v/cm^{-1}): 2959, 2868, 1574, 1458, 1425, 1242, 1168, 1059, 827, 800, 738, 640, 520. ^1H NMR (400 MHz, δ ppm) (CD_3CN): 0.92(t, 24H), 1.30-1.35(m, 16H), 1.60(s, 16H), 3.13(t, 16H), 7.22(s, 4H). Anal. Calcd. for $\text{C}_{44}\text{H}_{76}\text{N}_6\text{S}_6\text{Ni}$: C, 56.21; H, 8.15; N, 8.94%. Found: C, 56.03; H, 7.96; N, 9.38%.

Synthesis of $[\text{Bu}_4\text{N}]_2[\text{Ni}(\text{btdtO}_4)_2] \cdot \text{H}_2\text{O}$ (**5**)

The btdt dianion is generated, *in situ*, by the treatment of H_2btdt (0.076 g, 0.38 mmol) with excess amount of NaOH (0.045 g, 1.125 mmol) in dry MeOH (8.0 mL). To the resulting clear red solution, solid $\text{NiCl}_2 \cdot 6\text{H}_2\text{O}$ (0.045 g, 0.189 mmol) was added and the reaction mixture was stirred for 30 min in open atmospheric conditions. Reddish brown micro crystalline solid was precipitated by adding tetrabutylammonium bromide (0.2 g, 0.621 mmol) in water (20 mL); the solid was filtered, washed with water followed by diethyl ether, and dried at room temperature. This compound was recrystallized in acetonitrile by diffusing with diethyl ether. Black colored block crystals of compound **4** and red colored

needle crystals of compound **5** were obtained as mixture in recrystallization. Compound **5** has been separated as red needle crystals different from the black colored block crystals of compound **4** by manually under microscope from the above mixture. Yield: 0.025g (13.0% based on nickel metal). IR (KBr, v/cm^{-1}): 3441, 2959, 2868, 1743, 1575, 1469, 1381, 1230, 1159, 1022, 862, 798, 524. ^1H NMR (400 MHz, δ ppm) (CD_3CN): 0.98(t, 24H), 1.32-1.38(m, 16H), 1.56-1.64(m, 16H), 3.09(t, 16H), 7.68(s, 2H), 7.79(s, 2H). Anal. Calcd. for $\text{C}_{44}\text{H}_{78}\text{N}_6\text{O}_5\text{S}_6\text{Ni}$: C, 51.70; H, 7.69; N, 8.22%. Found: C, 51.89; H, 7.83; N, 7.96%.

3.2.4. Single Crystal Structure Determination

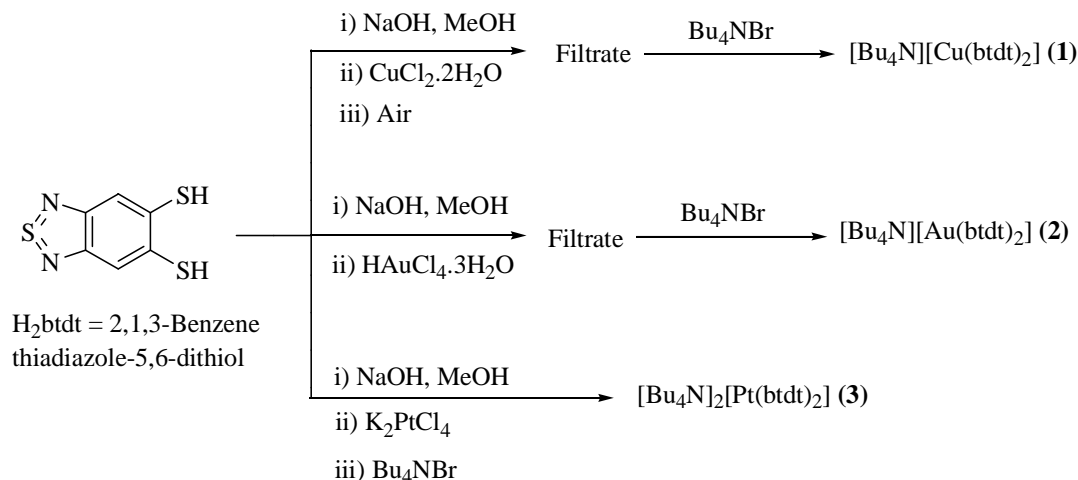
Single crystals suitable for facile structural determination for the compounds **1–5**, were measured on a three circle Bruker SMART APEX CCD area detector system under Mo- $\text{K}\alpha$ ($\lambda = 0.71073 \text{ \AA}$) graphite monochromatic X-ray beam. The frames were recorded with an ω scan width of 0.3° , each for 8 s, crystal-detector distance 60 mm, collimator 0.5 mm. Data reduction performed by using SAINTPLUS.²⁴ Empirical absorption corrections using equivalent reflections performed program SADABS.²⁴ The structures were solved by direct methods and least-square refinement on F^2 for all the compounds **1–5** by using SHELXS-97.²⁵ All non-hydrogen atoms were refined anisotropically. The hydrogen atoms were included in the structure factor calculation by using a riding model. The crystallographic parameters, data collection and structure refinement of the compounds **1–3** and **4–5** are summarized in Tables 3.1 and 3.2, respectively. Selected bond lengths and angles for the compounds **1–3** and **4–5** are listed in Tables 3.3 and 3.4, respectively.

3.3. Results and Discussion

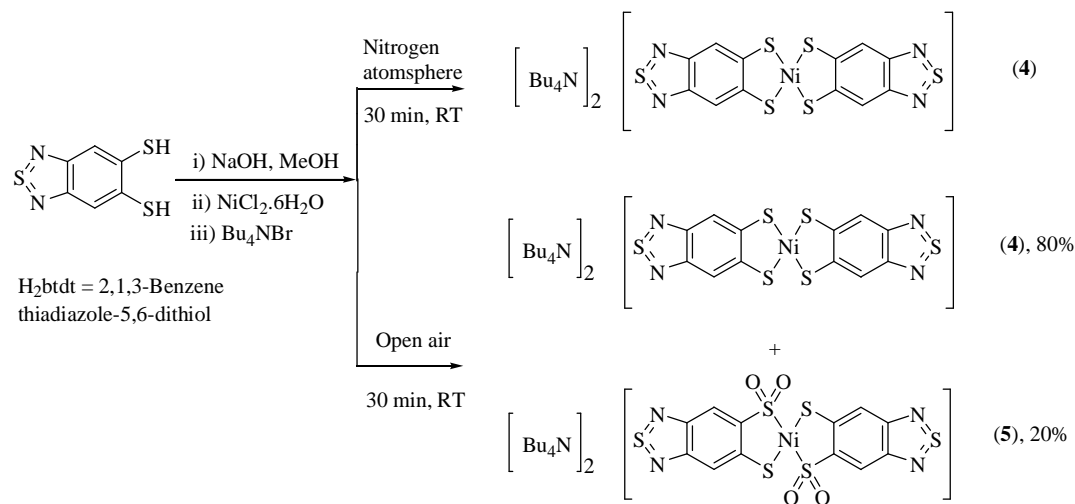
3.3.1. Synthesis and Characterization

The synthetic route for the complexes **1–3** are presented in Scheme 3.3. The square planar metal bis(dithiolene) complexes **1–3** were synthesized by the reactions of one mole equivalent of metal chlorides with two mole equivalents of Na_2btdt (*in situ* preparation by the de-protonation of H_2btdt in excess of NaOH treated MeOH). The synthesis of the copper(III) bis(dithiolate) complex **1** has been carried out in an aerial atmosphere so that Cu(II) can be oxidized to Cu(III), whereas the synthesis of other two complexes **2** and **3** are carried out in nitrogen atmosphere. These bis(dithiolate) complexes are isolated by the

addition of tetrabutylammonium bromide, affording respective microcrystalline forms of compounds **1–3** in reasonable yields.



Scheme 3.3. Schematic representation for the synthesis of metal bis(dithiolene) complexes **1–3**.



Scheme 3.4. Schematic representation for the synthesis of metal-dithiolene complexes **4** and **5**.

The synthetic approach for the compounds **4** and **5** is shown in Scheme 3.4. Compound **4** has been synthesized by the reaction of one mole equivalent of $\text{NiCl}_2 \cdot 6\text{H}_2\text{O}$ with two mole equivalents of H_2btdt in MeOH, treated with NaOH under nitrogen atmospheric conditions and then precipitated by adding tetrabutylammonium bromide, yielding the microcrystalline form of compound **4** in reasonable yield (Scheme 3.4). If the above reaction is carried out in an open atmospheric condition, compound **5** is obtained

along with compound **4**. Compound **5** can be separated as red needle crystals, which are different from the black colored block crystals of compound **4** by manually under microscope from the mixture of compounds after recrystallization. ^1H NMR and UV-Vis absorption spectra are consistent with the separated crystals of compound **5**.

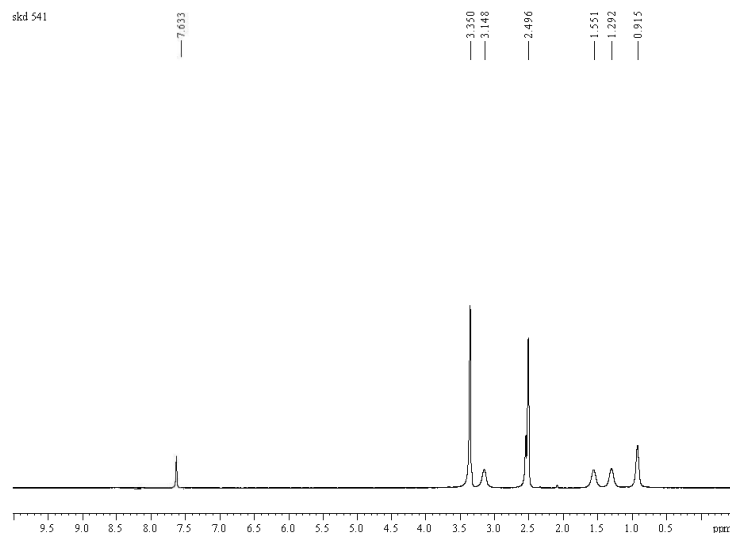


Figure 3.1. ^1H NMR spectrum of compound **1** in $\text{DMSO}-d_6$

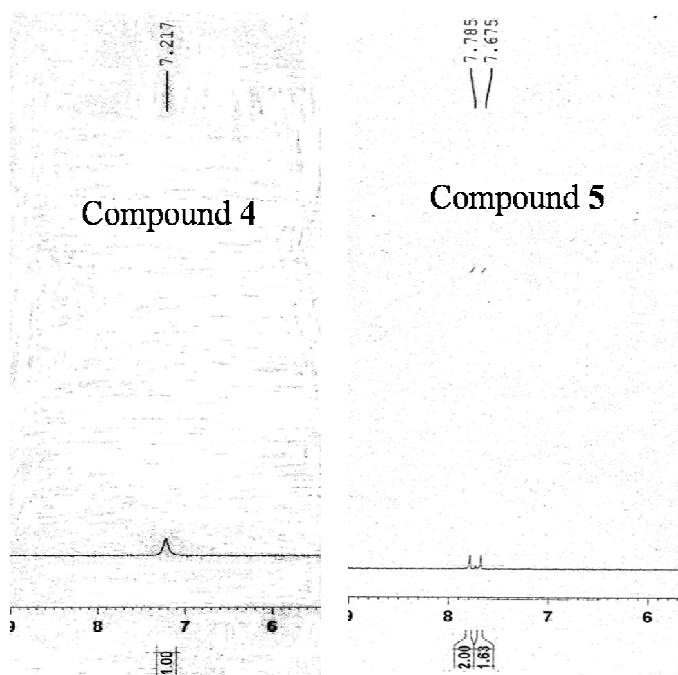


Figure 3.2. ^1H NMR spectra of compounds **4** and **5** in CD_3CN .

Infrared spectra of complexes **1–3** show two strong absorption bands at 2957, 2870 cm^{-1} , are characteristic of the alkane C–H stretching frequency, confirming the presence of Bu_4N^+ cations in the complexes **1–3** as a counter cation. ^1H NMR spectrum of complex **1** shows single narrow peak at δ 7.63 ppm in $\text{DMSO-}d_6$ corresponding to four benzene protons from the $\{\text{btdt}\}^{2-}$ ligands as shown in Figure 3.1. According to the nature and position of the signal, copper compound **1** is diamagnetic square planar Cu(III) d^8 coordination complex, as expected.²⁶ Copper compound **1** does not show any ESR signals, which further confirms that our present copper system is a Cu(III) complex. In the case of Au(III) complex **2** also, we have observed a single narrow ^1H NMR peak at δ 7.81 ppm in $\text{DMSO-}d_6$ related to the four benzene protons from the two $\{\text{btdt}\}^{2-}$ ligands. Complex **3** displays single narrow peak at δ 7.81 ppm in CD_3CN , which is related to the four benzene protons from the two $\{\text{btdt}\}^{2-}$ ligands. Proton NMR spectra of all three complexes **1–3** exhibit four peaks in aliphatic region corresponding to the tetrabutylammonium counter cation present in the respective complexes.

The infrared spectrum of complex **5** shows strong bands at 1159 and 1022 cm^{-1} (KBr), corresponding to the $\nu(\text{SO})$ stretching frequency of the S-bonded sulfinate group.^{18a,22b} Both the complexes **4** and **5** show IR bands at 2959 and 2868 cm^{-1} (KBr), corresponding to the $\nu(\text{alkane C–H})$ stretching frequencies of the tetrabutylammonium salts. ^1H NMR spectrum of complex **4** shows singlet proton at 7.22 ppm (Figure 3.2) in deuterated acetonitrile solution, but complex **5** shows two type's singlet protons at 7.68 and 7.79 ppm (Figure 3.2) and shifts to low magnetic field region. The electron withdrawing capability of sulfinate group reduces the electron density on aromatic protons observed at 7.68 and 7.79 ppm for the compound **5**.

3.3.2. Electronic Absorption Spectroscopy

Copper and gold complexes **1** and **2** show strong absorption bands at 420–430 nm in the visible region in acetonitrile as shown in Figure 3.3. In addition to this common feature, there is a weak absorption bands observed at higher concentrations in the region of 540–600 nm, for the complexes **1** and **2**, as shown in inset of Figure 3.3. The appearance of this weak feature at relatively higher concentrations can be explained by the intermolecular interactions that may occur at higher concentrations.²⁷ The weak feature at around 540–600 nm can also be due to $d-d$ transitions for a Cu(III) / Au(III) (d^8) system. This spectral

feature is similar to the Cu(III) and Au(III) coordination polymers, reported in our previous chapter 2.¹⁵ The electronic absorption spectrum for complex **3** in acetonitrile is shown in Figure 3.3. The complex **3** shows a broad band in low energy region compared to the copper and gold compounds. The broad feature observed in the visible region for the Pt-complex **3**, centered at ~483 nm, is due to the charge transfer (CT) transitions involving electronic excitation from a HOMO which is a mixture of dithiolate (π) and metal (d) orbital character to a LUMO which is a π^* orbital of the dithiolate, that are characteristics of metal(II) bis(dithiolene) complexes.^{10a,28}

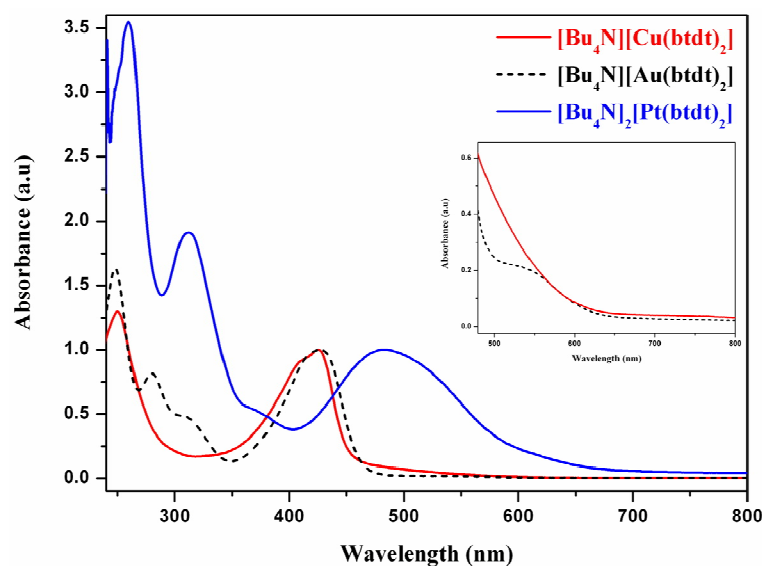


Figure 3.3. Electronic absorption spectra of compounds **1–3** in acetonitrile solutions.

The effect of solvent polarity on the absorption band in the visible region for the complex **3** is shown in Figure 3.4. However, the effect of solvent polarity has been studied previously in dianionic dithiolene complexes.²⁹ The CT band is sensitive to the solvent polarity, shifting significantly to low energy region in less polar solvents, which is further considerable charge-transfer character as shown in Figure 3.4. This negative solvatochromism (hypsochromic shift) indicates a polar ground state and non-polar excited state: with increasing polarity of solvents, polar ground state is more stabilized than non-polar excited state, thus increasing the energy gap between HOMO and LUMO of the CT band and shifts to high energy region. Absorption maxima (λ) of the complex **3** (λ , nm) in solutions of MeOH, acetonitrile, DMF, acetone, DCM and toluene are observed at 469, 483, 492, 497, 497 and 507 nm respectively. In polar aprotic solvents, the CT

bands in the visible region get slightly resolved into two maxima and absorption maxima shifts to higher energy region. In the case of non-polar aprotic solvent, the absorption maxima shift to low energy region. It is worth mentioning that, in MeOH (protic solvent), the band is not resolved but observed as broad band for the compound **3**.

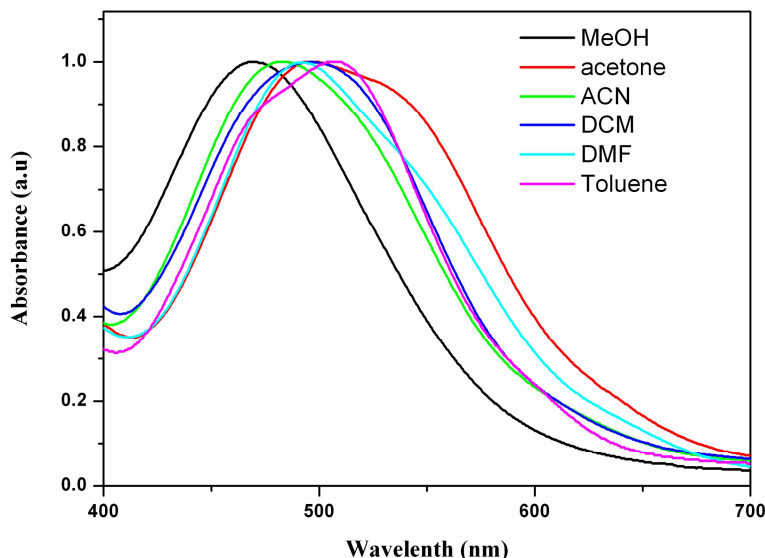


Figure 3.4. Electronic absorption spectra of complex $[\text{Bu}_4\text{N}]_2[\text{Pt}^{\text{II}}(\text{btdt})_2]$ (**3**) in different solvents.

UV-Visible absorption spectrum of complex **4** in MeOH is shown in Figure 3.5. The band observed at 360 nm is slightly sensitive to solvent. In solutions of toluene, this band slightly shifts to 378 nm. Blue solution of the complex **4** is due to the highly dominated broad band feature observed in the visible region at 586 nm. This band can be described as charge transfer (CT) transition, which involve electronic excitation from a HOMO which is a mixture of dithiolate (π) and metal (d) orbital character to a LUMO which is a π^* orbital of the dithiolate, that are characteristics of metal(II) bis(dithiolene) complexes.^{10a,28} This broad band is highly sensitive to the solvent polarity, shifting significantly to higher energy region in less polar solvents, which is further considerably charge-transfer character. This positive solvatochromism (bathochromic shift) indicates a non-polar ground state and polar excited state: with increasing the polarity of solvents polar excited state is more stabilized than non-polar excited state, thereby reducing the energy gap between HOMO and LUMO of the CT band and shifts to low energy region. Absorption maxima (λ , nm) in solutions of acetone (665), DMF (667), DMSO (644), acetonitrile (617), DCM (617), chloroform (613), and toluene (611) are shown in Figure 3.6.

However, in protic solvent, such as, CT band MeOH (585 nm) further shifts to higher, even it is more polar. In polar aprotic solvents, this CT band slightly separated into two resolved maxima and absorption maxima is in low energy region, which was observed in DMF and acetone solutions. Nevertheless, in polar protic solvent such as in MeOH solutions CT band not separated.

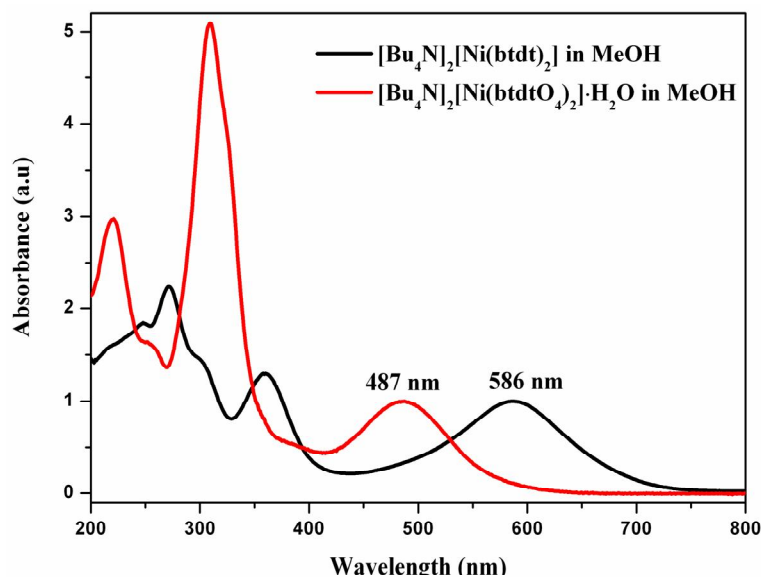


Figure 3.5. Electronic absorption spectra for the compounds **4** and **5** are in MeOH solutions.

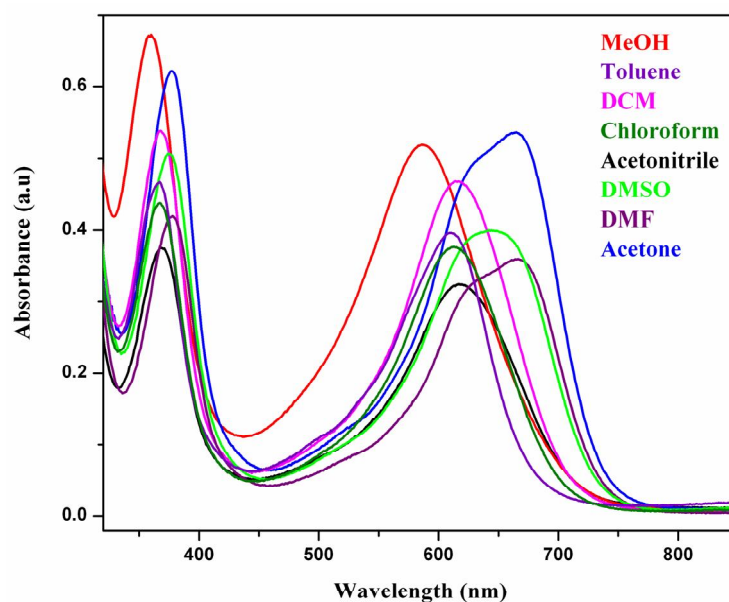


Figure 3.6. Electronic absorption spectra of complex $[\text{Bu}_4\text{N}]_2[\text{Ni}^{\text{II}}(\text{btdt})_2]$ (**4**) in different solvents.

Absorption spectrum of separated red needles of complex **5** in MeOH, is shown in Figure 3.5. Blue shift of the complex **5**, is due to the non planarity of $[\text{Ni}(\text{btdtO}_2)_2]^{2-}$ molecule, broad band is observed at 480 nm in comparison to the square-planar complex **4** (585 nm). Blue-colored air-saturated solutions of $[\text{Bu}_4\text{N}]_2[\text{Ni}(\text{btdt})_2]$ (**4**) gradually turn red in the presence of visible light (room light). This transformation requires both oxygen (air) and light. Methanolic solution of complex **4**, under oxygen atmosphere (1 atmospheric pressure) was stirred at room conditions for 1 week to result in the formation of complex **5**, which was confirmed by ^1H NMR and absorption spectroscopy. We have recorded the absorption spectra at different intervals of time as shown in Figure 3.7. As shown in Figure 3.7, the CT band at 586 nm gradually decreases with appearance of new absorption band at 485 nm in the blue region. At the same time, the band at 360 nm also gradually decreases with the appearance of new band at 310 nm. The appearance of new bands at 485 and 310 nm are due to the characteristics of the oxidized (sulfinate) compound **5** for corresponding compound **4**. These absorption spectral changes are maximum at the initial intervals / stages of the time as shown in Figure 3.7. The solid-state diffuse reflectance spectra (DRS) of compounds **4** and **5** match with the solution spectra as shown in Figure 3.8. In DRS, the CT band observed at 600-680 nm and absorption maxima split in two well resolved maxima, whereas sulfinate-compound **5** shows only broad band at 510 nm as shown in Figure 3.8.

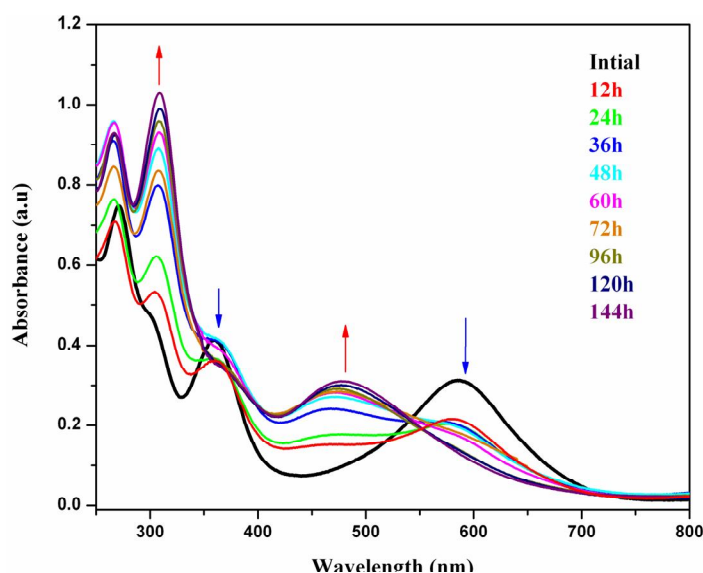


Figure 3.7. Absorption spectral changes for the methanolic solution of complex $[\text{Bu}_4\text{N}]_2[\text{Ni}^{\text{II}}(\text{btdt})_2]$ (**4**) in oxygen atmosphere at different intervals of time.

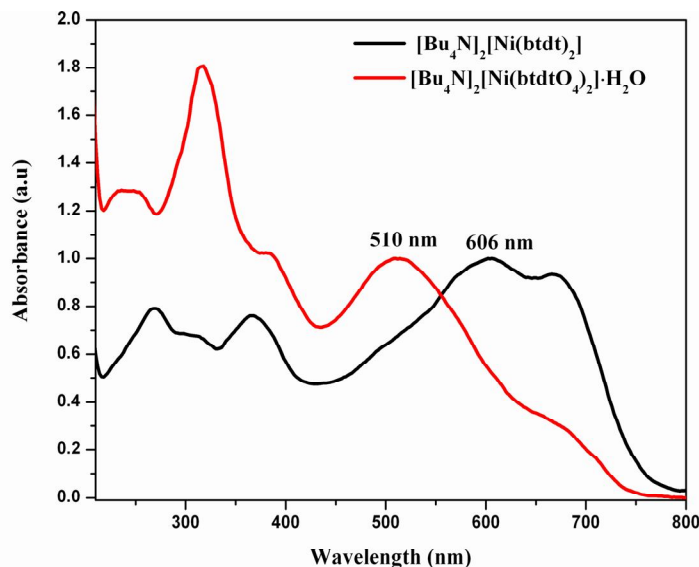


Figure 3.8. Solid-state diffuse reflectance spectra of compounds **4** and **5**.

3.3.3. Electrochemical Studies

The cyclic voltammetric studies of compound **1** shows a Cu(III)/Cu(II) redox couple appearing as a reversible wave at $E_{1/2} = -0.11$ V *vs* Ag/AgCl ($\Delta E = 74$ mV) in DMF solution as shown in Figure 3.9. Interestingly, this is a very low reduction potential for a Cu(III)-coordination complex and it is even less than that of similar reported Cu(III) compound of pds ligand (pds²⁻ = pyrazine-2,3-diselenote) [$E_{1/2} = -0.54$ V (quasi-reversible)], reported by Rovira and co-workers.²⁶ Thus the present system [Cu^{III}(btdt)₂]¹⁻ is more

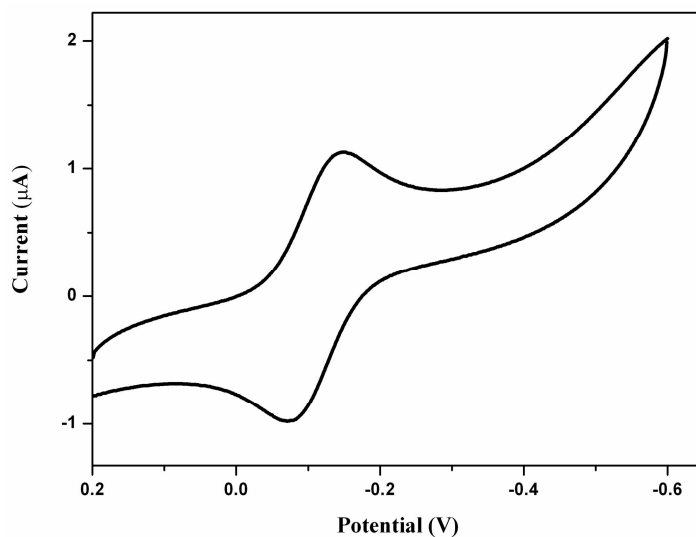


Figure 3.9. Cyclic voltammogram of compound **1** in TBAP/DMF at a scan rate 50 mV s⁻¹.

easily reduced than $[\text{Cu}^{\text{III}}(\text{pds})_2]^{1-}$. In other words, the corresponding Cu(II)-complex $[\text{Cu}^{\text{II}}(\text{btdt})_2]^{2-}$ (which we could not isolate) would be very susceptible to oxidation. This is supported by the fact that Cu(III)-compound **1** has been prepared by simple and rapid air oxidation. The same type of reduction potentials are observed in the case of previously described copper coordination polymers in Chapter 2.

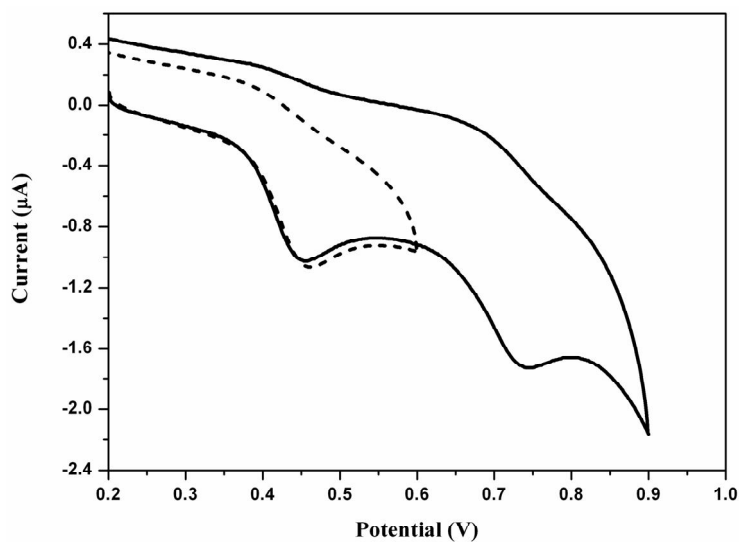


Figure 3.10. Cyclic voltammograms of compound $[\text{Bu}_4\text{N}]_2[\text{Pt}^{\text{II}}(\text{btdt})_2]$ (**3**) in TBAP/MeOH at a scan rate 50 mV s^{-1} (dotted line corresponding to the first oxidation).

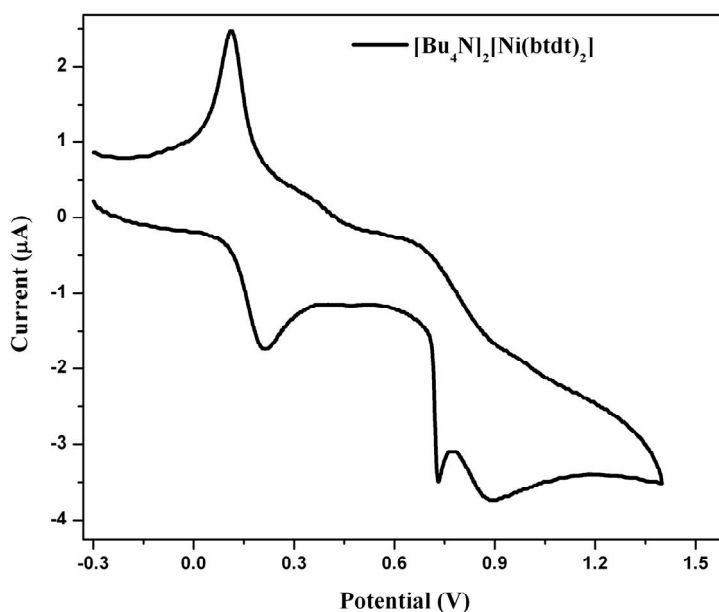


Figure 3.11. Cyclic voltammogram of compound **4** in TBAP/MeOH at a scan rate 50 mV s^{-1} .

The platinum complex **3** exhibits two irreversible oxidative responses at 0.45 V and 0.74 V *vs* Ag/AgCl in MeOH as shown in Figure 3.10. The first irreversible oxidation peak appears at +0.45 V of the Pt-complex **3** suggesting that the $[\text{Pt}(\text{btdt})_2]^{1-}$ is unstable in electrochemical cell. As shown in Figure 3.11, complex **4** undergoes quasi-reversible oxidation ($\Delta E = 0.10$ V) at $E_{1/2} = +0.16$ V *vs* Ag/AgCl, that corresponds to the $[\text{Ni}(\text{ppdt})_2]^{1-} / [\text{Ni}(\text{ppdt})_2]^{2-}$ redox couple, indicating that Ni(III) complex $[\text{Ni}(\text{ppdt})_2]^{1-}$ is fairly stable in the electrochemical scale. Interestingly, compound **4** is oxidized to Ni(III) oxidation state at very low oxidation potentials. However, complex **5** is inactive in electrochemical cell.

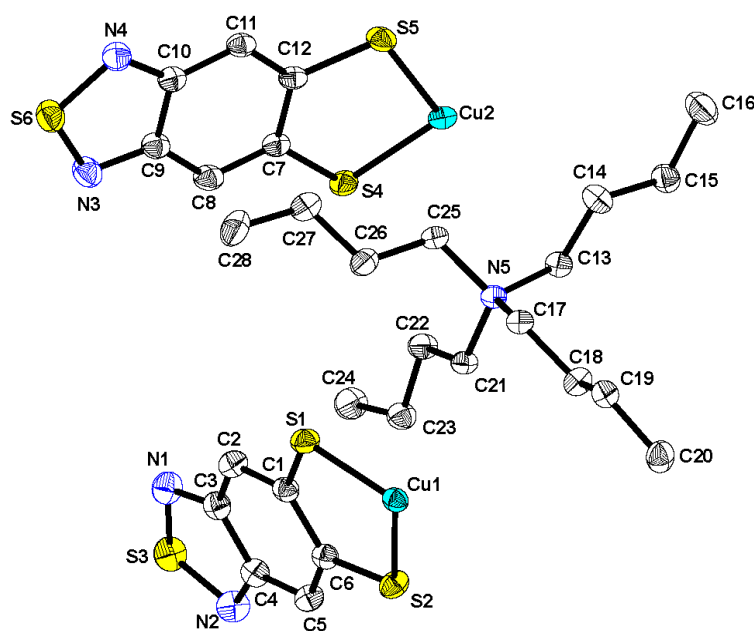


Figure 3.12. Thermal ellipsoidal plot of the asymmetric unit in compound **1** (20% probability).

3.3.4. X-ray Crystallographic Studies

Crystal Structure Description of $[\text{Bu}_4\text{N}][\text{Cu}(\text{btdt})_2]$ (**1**)

The crystals of complex **1**, suitable for single crystal X-ray structure determination, were obtained from acetonitrile solution by the vapor diffusion of diethyl ether. Crystallographic analysis revealed that complex **1** crystallizes in triclinic space group *P*-1. The relevant asymmetric unit contains two half molecules of $[\text{Cu}(\text{btdt})_2]^{1-}$ anion and one tetrabutylammonium cation, as shown in Figure 3.12. In the anion, the geometry around the copper (III) ion, which is coordinated by four sulfur atoms from two $\{\text{btdt}\}^{2-}$ ligands,

is almost square planar geometry, because the coordination angles are in the range of $87.80(3)^{\circ}$ – $92.20(3)^{\circ}$ which are slightly deviated from 90.0° and other coordination angles are 180.0° , which are not deviated. The Cu–S bond distances are in the range of $2.1595(8)$ – $2.1769(8)$ Å. However, there is a deviation in the planar nature of the dithiolene ligand (chelate) present in the both anionic units of complex **1**. The bending deviation (η) between the SMS plane and SCCS plane are characterized by the angles of 2.91° and 8.08° present in the $\{\text{Cu1S1S2C1C6}\}$ and $\{\text{Cu2S4S5C7C12}\}$ chelates respectively. In general, if $\eta < 6$, it is considered as highly planar nature of the dithiolate-chelate.¹ In the present study, in the case of chelate $\{\text{Cu2S4S5C7C12}\}$ in compound **1**, the bending angle (η) is

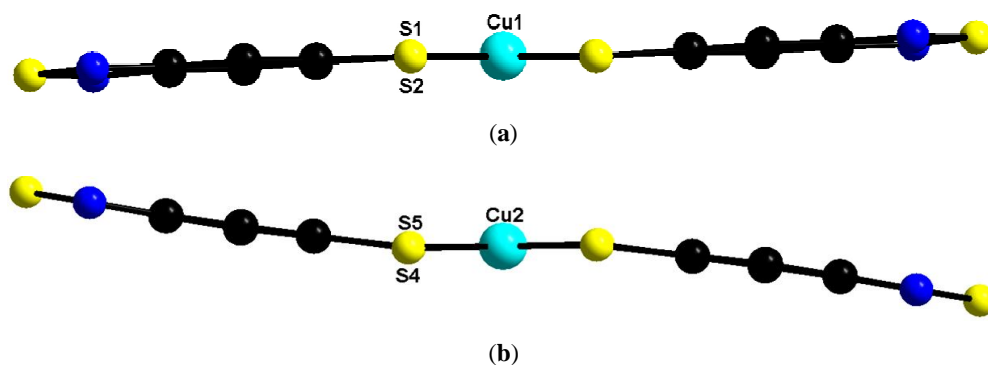


Figure 3.13. Anionic complex units through side view of: (a) complex **1** $\{\text{Cu1S4}\}$ plane; (b) complex **1** $\{\text{Cu2S4}\}$ plane.

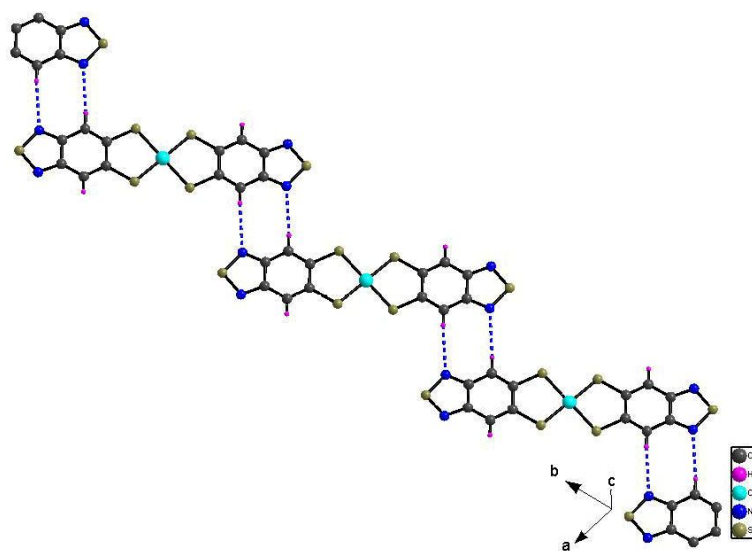


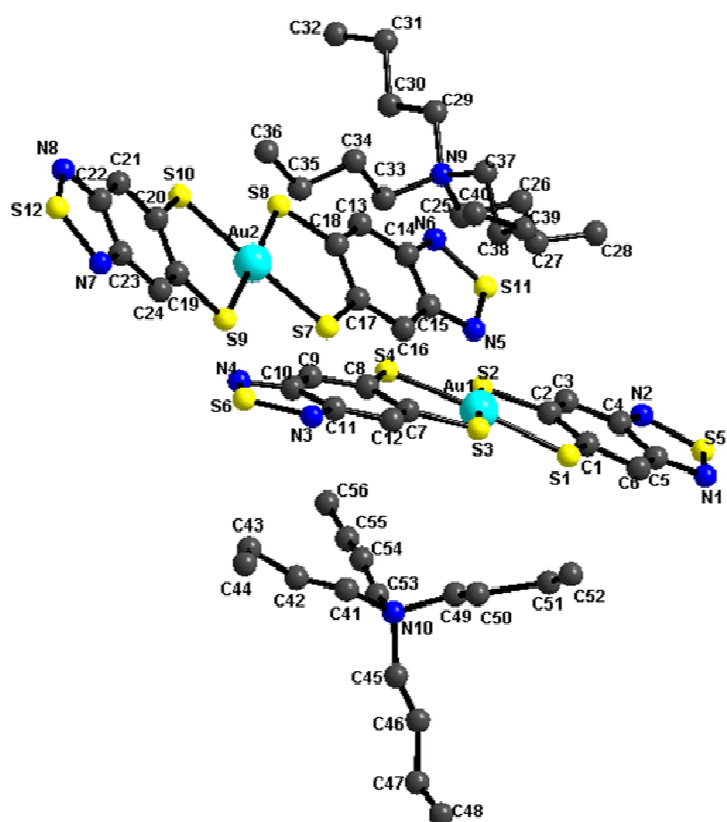
Figure 3.14. One dimensional supramolecular chain characterized by C–H...N weak interactions among the anions in the crystal structure of compound **1**.

8.08°, indicating the considerable deviation of the planar nature of the metal chelate system. These bending of the dithiolate–chelates present in the crystal structure of the complex **1** are shown in Figures 3.13(a) and 3.13(b) with respect to their SMS planes (the side view).

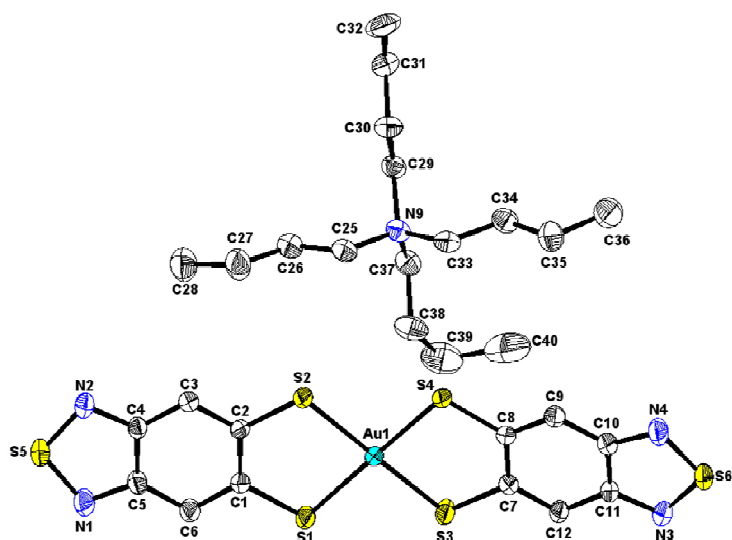
In the crystal structure of the compound **1**, the intermolecular interactions, such as, C–H···N hydrogen bonding contacts (H···N contact distance of 2.67 Å and CHN bond angle of 163.9°) among the anions [Cu(btdt)₂]^{1–} result in the formation of one dimensional supramolecular chain (stepwise) as shown in Figure 3.14. In addition to this, complex **1** is further characterized by C–H···N hydrogen bonding interactions between the [Cu(btdt)₂]^{1–} anion and [Bu₄N]⁺ cation with a H···N contact distance of 2.62 Å.

Crystal Structure Description of [Bu₄N][Au(btdt)₂] (**2**)

Single crystals of compound **2**, suitable for single crystal X-ray structure determination, were obtained by slow evaporation of acetone solution of compound **2**. Crystallographic analysis reveals that complex **2** crystallizes in monoclinic space group *P*2₁/*c*. The relevant asymmetric unit contains two molecules of [Bu₄N][Au(btdt)₂] as shown in Figure 3.15(a). Thermal ellipsoid diagram of compound **2** containing one of these units is shown in Figure 3.15(b). In the two anionic portions of compounds present in the asymmetric unit, the geometry around gold(III) ion, which is coordinated by four sulfur atoms from two {btdt}^{2–} ligands, is slightly distorted from square planar geometry with dihedral angles of 1.62° and 4.63° between the two SMS planes; this is unlike to [Bu₄N][Cu(btdt)₂] (**1**), in which the geometry is almost square planar with 0.0° dihedral angle. The coordination angles are in the range of 89.28(6)–91.16(6)° and 175.99(8)–177.28(7)° in the anionic portion of one of the asymmetric unit (Au1S1S2S3S4). In other complexic unit, the coordination angles are in the range of 89.61(6)–90.74(6)° and 178.38(7)–179.18(6)° ({Au2S7S8S9S10}). Here, in both complexic units, coordination angles have deviations from the 180.0°. The Au–S bond distances are in the range of 2.2965(16)–2.3101(16) Å in both the anionic units. The deviation in the planarity of dithiolene units are shown in Figures 3.16(a) and 3.16(b). In addition to this, there is a deviation in the planar nature of the dithiolate–chelate present in the both complexic units of compound **2**. The bending deviations (η) between the {S1Au1S2} and {S1C1C2S2} planes, and {S3Au1S4} and {S3C7C8S4} planes, are characterized by the angles of 3.92° and 7.76° present in



(a)



(b)

Figure 3.15. (a) Asymmetric unit in compound **2** (20% probability, ball and stick representation) [There are two molecules in the asymmetric unit, the carbon atoms (C42, C43, C45, C47, C49, C50, C51, C53, C54, C55) and nitrogen atom (N10) in one of the $[\text{Bu}_4\text{N}]^+$ cations suffer a significant disorder problem]. Hydrogen atoms omitted for clarity; (b) Thermal ellipsoidal plot of one of the unit found in the asymmetric unit in compound **2** (20% probability). Hydrogen atoms are omitted for clarity.

{Au1S1S2C1C2} and {Au1S3S4C7C8} dithiolate-chelates respectively. In other complexic-unit, the {Au2S7S8C17C18} and {Au2S9S10C19C20} dithiolate chelates have the bending deviations (η) of 3.33° and 12.64° (between {S7Au2S8} and {S7C17C18S8} planes, {S9Au2S10} and {S9C19C20S10} planes respectively). Hence the bending deviations (η) are more in compound **2** than those in compound **1**. In other words, compound **2** is less planar than compound **1** as far as dithiolate-chelates are concerned. The deviation from planarity in the case of compound **2** is not only supported by dihedral angles and bending variations, but also by its c_1 -M- c_2 angles (where c_1 and c_2 are midpoints between the two S atoms of each dithiolene ligand). In the crystal structure of compound **2**, these angles 178.72° and 178.97° , which are some extent of deviations from 180.0° , found in the compound **1**.

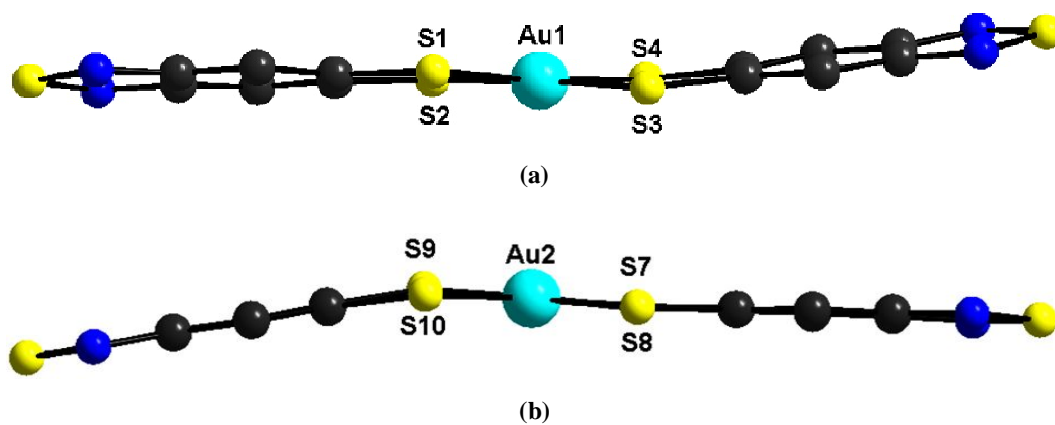


Figure 3.16. Anionic complex units through side view of: (a) complex **2** {Au1S4} plane; (b) complex **2** {Au2S4} plane.

Compound **2** is further characterized by non-covalent interactions, such as, weak S \cdots N and S \cdots S supramolecular contacts among the [Au(btdt) $_2$] $^{1-}$ ions [Figure 3.17(a)]. The S \cdots N contact distances are in the range 3.131–3.190 Å and S \cdots S contact distance is 3.534 Å, which are less than the sum of van-der waals radii (1.55 Å for nitrogen and 1.80 Å for sulfur).³⁰ The resulting two dimensional network is shown in Figure 3.17(b). The distortions are more in the complex **2** compared to those in complex **1** may be due to the presence of S \cdots N and S \cdots S non-covalent intermolecular interactions.

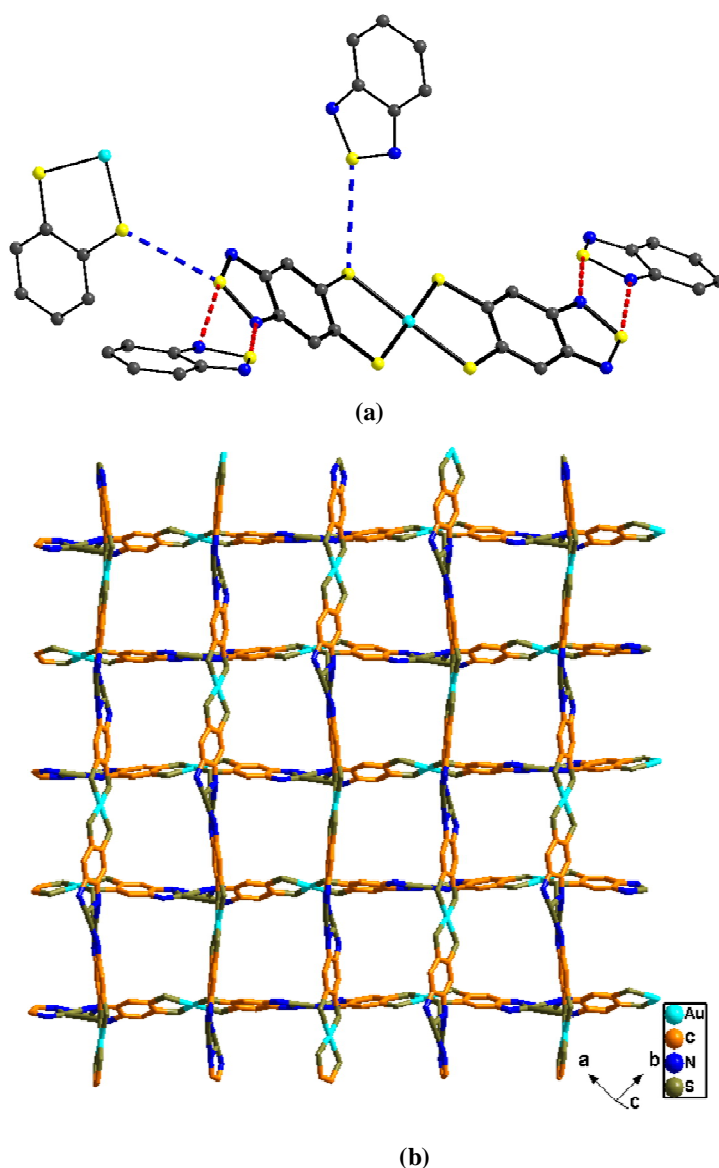


Figure 3.17. (a) S...N and S...S interactions around one $[\text{Au}(\text{btdt})_2]^{1-}$ ion with surrounding anions in the crystal structure of compound **2**; and (b) the resulting two-dimensional supramolecular network characterized by S...N and S...S interactions among the anions in the crystal structure of compound **2**.

Crystal Structure Description of $[\text{Bu}_4\text{N}]_2[\text{Pt}(\text{btdt})_2]$ (**3**)

The crystals of compound **3**, suitable for single crystal X-ray structure determination, were obtained from acetonitrile solution by the vapor diffusion of diethyl ether. Single crystal X-ray analysis shows that complex **3** crystallizes in monoclinic space group $C2/c$. The relevant asymmetric unit contain half molecule of $[\text{Bu}_4\text{N}]_2[\text{Pt}(\text{btdt})_2]$ as shown in Figure 3.18(a). In this complex, the geometry around the Pt(II) ion, which is coordinated by four sulfur atoms from two $\{\text{btdt}\}^{2-}$ ligands, is slightly distorted from square planar geometry

with dihedral angle (λ) of 3.90° between the two SMS planes. The coordination angles are in the range of $88.52(6)$ – $91.83(8)^\circ$ and $177.26(6)$ – $177.27(6)^\circ$ and deviates from 90.0° and 180.0° respectively. The deviation in the planarity of the complex has been shown Figure 3.18(b). The Pt–S bond distances are in the range of $2.2785(19)$ – $2.2830(17)$ Å in complex **3**. In this complex also, there is a deviation in the planar nature of the dithiolate-chelate present in the complexic unit of complex **3**. The bending deviation (η) between the {S1Pt1S2} and {S1C1C6S2} planes has been observed with an angle of 2.09° present in {Pt1S1S2C1C6} dithiolate-chelate system. This complex also shows small deviation of c_1 –M– c_2 angle (179.82°).

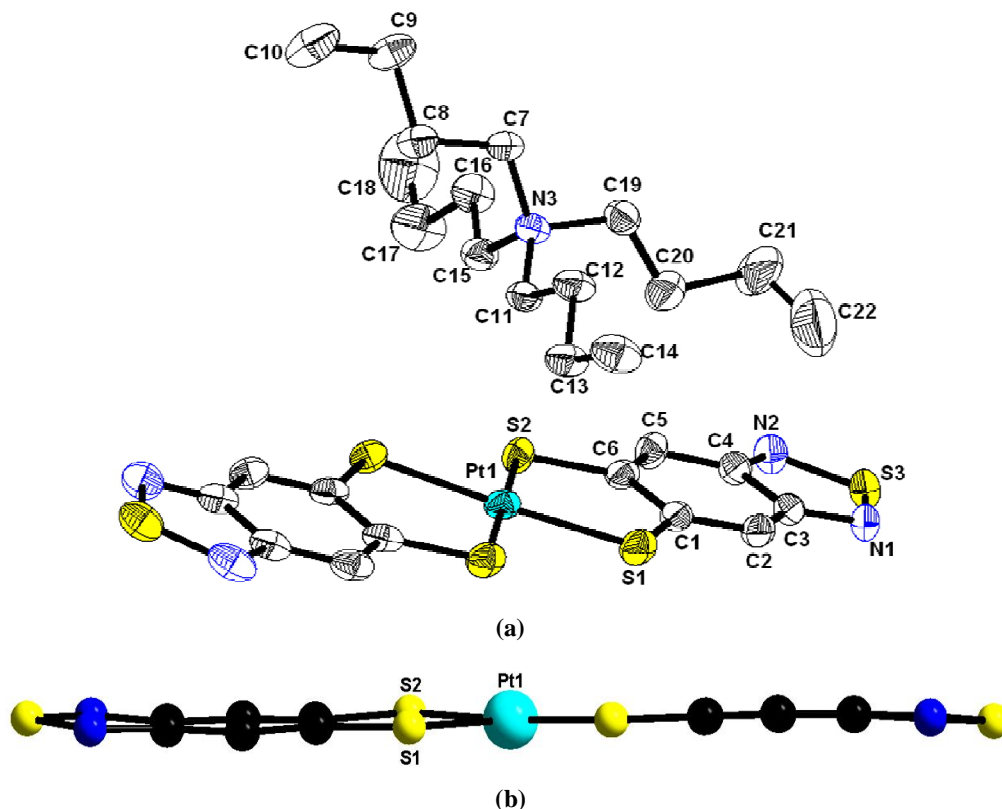


Figure 3.18. (a) Thermal ellipsoidal plot of the asymmetric unit of compound $[\text{Bu}_4\text{N}]_2[\text{Pt}(\text{btdt})_2]$ (**3**), that contains one tetrabutylammoniumcation and half molecule of $[\text{Pt}(\text{btdt})_2]^{2-}$ ion. Hydrogen atoms are not shown for clarity (20% probability). (b) Anionic complex unit through side view of complex **3** {Pt1S4} plane.

Complex **3** has been characterized by non-covalent interactions, such as $\text{S}\cdots\text{N}$ supramolecular interactions among $[\text{Pt}(\text{btdt})_2]^{2-}$ anions. The $\text{S}\cdots\text{N}$ contact is 3.127 Å, which is less than the sum of van-der waals radii (1.55 Å for nitrogen and 1.80 Å for

sulfur).³⁰ The resulting one dimensional supramolecular chain as shown in Figure 3.19(a). In addition to this non covalent interaction, complex **3** is further characterized by C–H...N and C–H...S hydrogen bonding interactions between the $[\text{Pt}(\text{btdt})_2]^{2-}$ anion and $[\text{Bu}_4\text{N}]^+$ cation with H...N and H...S bond distances are 2.59 Å and 2.81 Å respectively. The relevant hydrogen bonding parameters are listed in the Table 3.5. The effective combination of S...N non covalent interaction and C–H...N and C–H...S hydrogen bonding interactions, results in a three dimensional supramolecular network as shown in Figure 3.19(b).

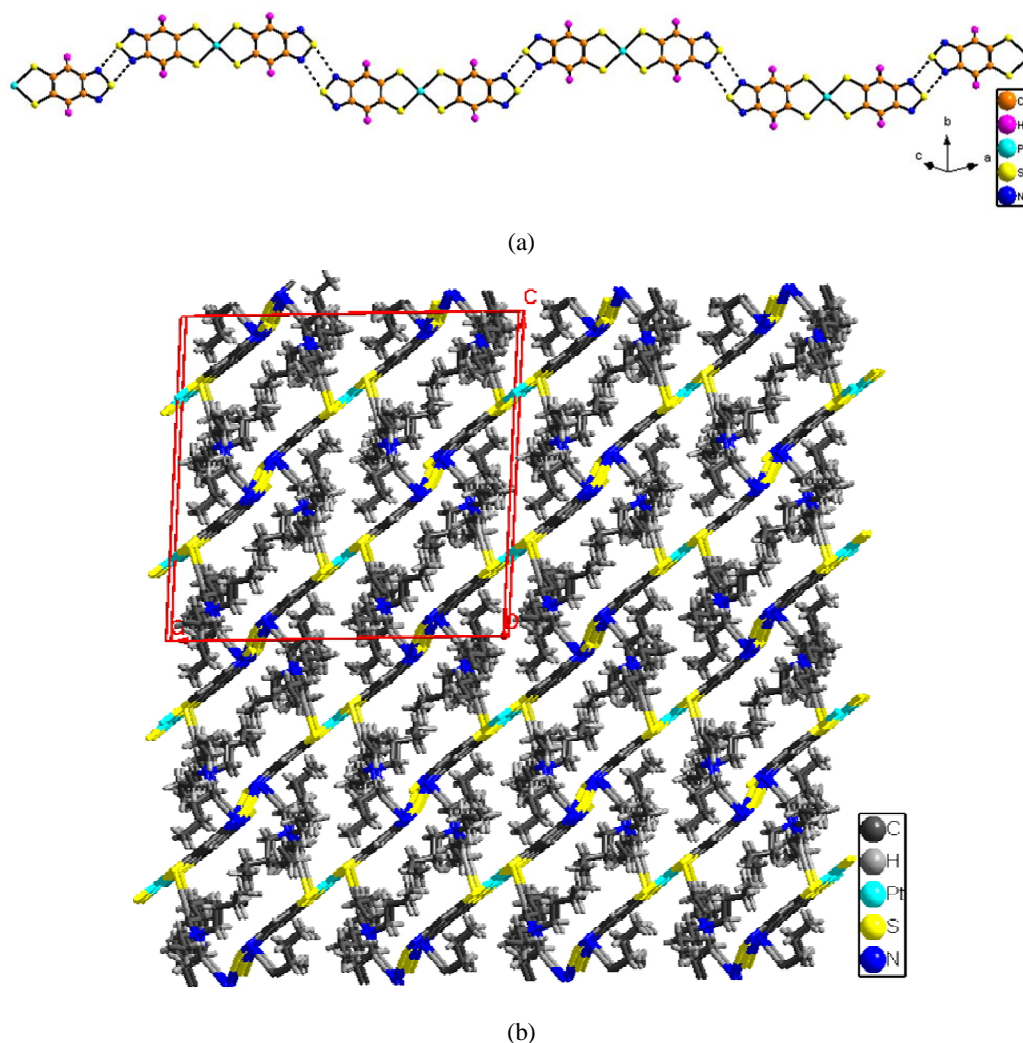
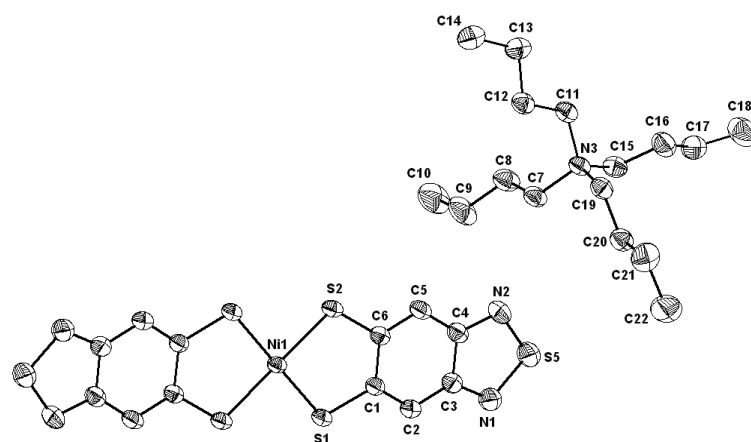
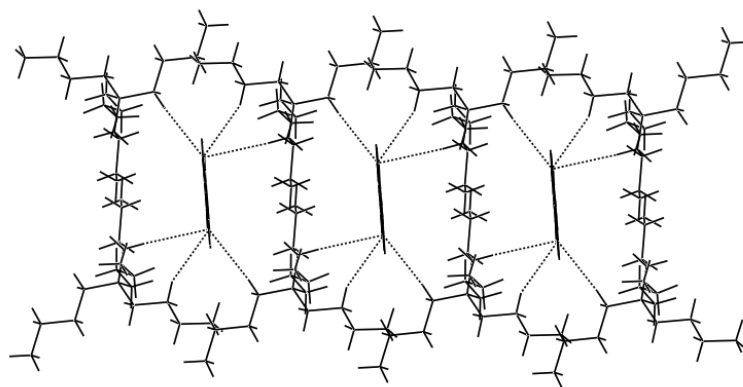


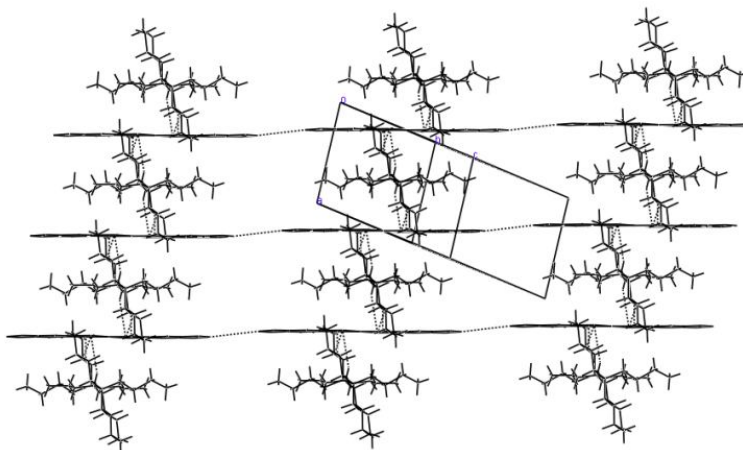
Figure 3.19. (a) The S...N interactions among the $[\text{Au}(\text{btdt})_2]^{1-}$ ions, resulting in one-dimensional supramolecular chain, observed in Complex **3**. (b) Three-dimensional supramolecular network as a result of combination of S...N non-covalent interactions and C–H...N and C–H...S interaction between the cation and anions in the crystal structure of complex **3** ($2 \times 2 \times 2$ cells).



(a)



(b)



(c)

Figure 3.20. (a) Thermal ellipsoidal plot of the asymmetric unit of compound $[\text{Bu}_4\text{N}]_2[\text{Ni}(\text{btdt})_2]$ (**4**), that contains one tetrabutylammoniumcation and half molecule of $[\text{Ni}(\text{btdt})_2]^{2-}$ ion. Hydrogen atoms are not shown for clarity (20% probability); (b) one dimensional hydrogen bonding chain characterized by $\text{C}-\text{H}\cdots\text{S}$ hydrogen bonding interactions; and (c) two dimensional supramolecular network is characterized by the combination of $\text{C}-\text{H}\cdots\text{S}$ and $\text{S}\cdots\text{S}$ interactions in the crystal structure of the compound **4**.

Crystal Structure Description of $[\text{Bu}_4\text{N}]_2[\text{Ni}(\text{btdt})_2]$ (**4**)

Black colored blocks type crystals of compound $[\text{Bu}_4\text{N}]_2[\text{Ni}(\text{btdt})_2]$ (**4**), suitable for single crystal X-ray structure analysis, were grown from vapor diffusion of diethyl ether into acetonitrile solution. Crystal structure of complex **4** crystallizes in triclinic space group $P-1$. The asymmetric unit in the crystal structure of compound **4** (represented as labeled atoms) contains half molecule of $[\text{Bu}_4\text{N}]_2[\text{Ni}(\text{btdt})_2]$ (**4**) shown as thermal ellipsoidal plot in Figure 3.20(a). The structure of complex **4** shows square planar geometry around the Ni(II) ion, there is no deviation between the two SMS planes with average Cu–S bond distance of 2.162 ± 0.001 Å. However, there is a small deviation in the planarity of dithiolate-chelated ring with an angle of 1.56° between S1Ni1S1 and S1C1C6S2 planes present in the Ni1S1C1C6S2 dithiolate-chelated ring as shown in Figure 3.21(a).

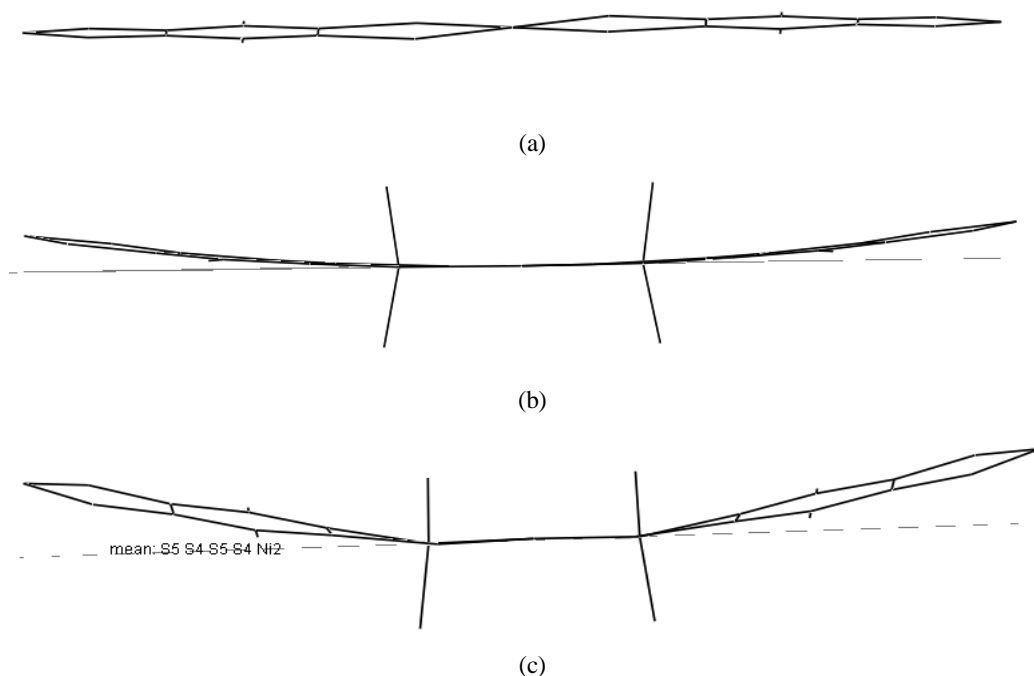


Figure 3.21. Anionic complex units through side view of: (a) complex **4** {Ni1S4} plane; (b) complex **5** {Ni1S4} plane; (c) {Ni2S4} plane.

In the molecular packing diagram of the complex **4**, both cation $[\text{Bu}_4\text{N}]^+$ and anion $[\text{Ni}(\text{btdt})_2]^{2-}$ are involved in $\text{C}-\text{H}\cdots\text{S}$ hydrogen bonding interactions resulting in a one dimensional supramolecular chain as shown in Figure 3.20(b). The relevant hydrogen bonding geometrical parameters are listed in the Table 3.6. Each tetrabutylammonium

cation is characterized by three C–H···S hydrogen bonding contacts with two surrounding $[\text{Ni}(\text{btdt})_2]^{2-}$ anions as shown in Figure 3.20(b). Wherein, two of them are described as C–H···S interactions with S2 atom of surrounding anions, positioned at $-x+1, -y+1, -z+1$ symmetry. The remaining one is described as C–H···S weak interaction with S1 atom of other anion positioned at $x, y-1, z$ symmetry. As shown in the packing diagram (Figure 3.20(b)), each dithiolate ligand connects with two distinct tetrabutylammonium cations, characterized by three weak C–H···S hydrogen bonding interactions. Thus, each metal-dithiolate anion is surrounded by four discrete tetrabutylammonium cations. Interestingly, this one-dimensional supramolecular chain is further characterized by S···S contacts resulting in a two dimensional supramolecular sheet as shown in Figure 3.20(c). The S···S contact distance is 3.734 Å.

Crystal Structure Description of $[\text{Bu}_4\text{N}]_2[\text{Ni}(\text{btdtO}_4)_2] \cdot \text{H}_2\text{O}$ (**5**)

Red colored needles of Ni-sulfonate complex $[\text{Bu}_4\text{N}]_2[\text{Ni}(\text{btdtO}_4)_2] \cdot \text{H}_2\text{O}$ (**5**), suitable for single crystal X-ray structure analysis, were grown from vapor diffusion of diethyl ether into acetonitrile solution, which crystallizes in monoclinic system with $C2/c$ space group. The asymmetric unit in the crystal structure complex **5** contains two half molecules of $[\text{Ni}(\text{btdtO}_4)_2]^{2-}$ anions, two tetrabutylammonium cations and one lattice water molecule shown as thermal ellipsoidal plot in Figure 3.22.

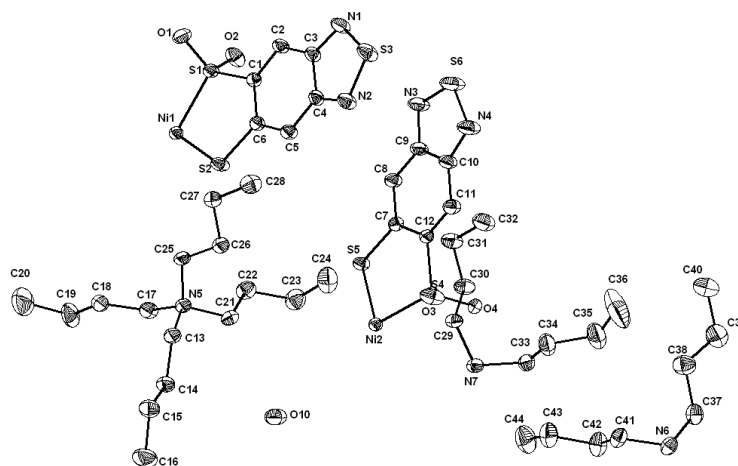


Figure 3.22. (a) Thermal ellipsoidal plot of the asymmetric unit of compound $[\text{Bu}_4\text{N}]_2[\text{Ni}(\text{btdtO}_4)_2] \cdot \text{H}_2\text{O}$ (**5**), that contains two tetrabutylammonium cations, two half molecules of $[\text{Ni}(\text{btdtO}_4)_2]^{2-}$ ions and one lattice water molecule. Hydrogen atoms are not shown for clarity (30% probability).

In the crystal structure, the geometry around Ni(II) ions, are surrounded by four sulfur atoms with distorted from square-planar geometry, and there are dihedral angles of 0.80° and 2.24° between the two SMS planes present in the both molecules containing Ni(1) and Ni(2), ions, respectively. In addition to these small deviations from the square planar geometry around the metal ion, dithiolate complexes present in the complex **5** largely suffers from the planarity in the dithiolene chelated rings. The bending deviations (η) between the {S1Ni1S2} and {S1C1C6S2} planes, {S4Ni2S5} and {S4C12C7S5} planes, are characterized by the angles of 2.09° and 10.40° present in {Ni1S1S2C1C6} and {Ni2S4S5C7C12} dithiolate-chelated rings, respectively as shown Figures 3.21(b) and 3.21(c). As shown in Figure 3.21(a) in parallel view of $[\text{Ni}(\text{btdt})_2]^{2-}$ anion in complex **4**, there is no deviation to the molecular plane. But in complex **5**, both molecules $[\text{Ni}(\text{btdtO}_4)_2]^{2-}$ are bent from the molecular plane, leading to the boat shapes as shown in Figures 3.21(b) and 3.21(c). The oxygen atoms of sulfinates are involved in C–H \cdots O hydrogen bonding interaction, that is the reason why $[\text{Ni}(\text{btdtO}_4)_2]^{2-}$ molecules are bending into boat shapes.

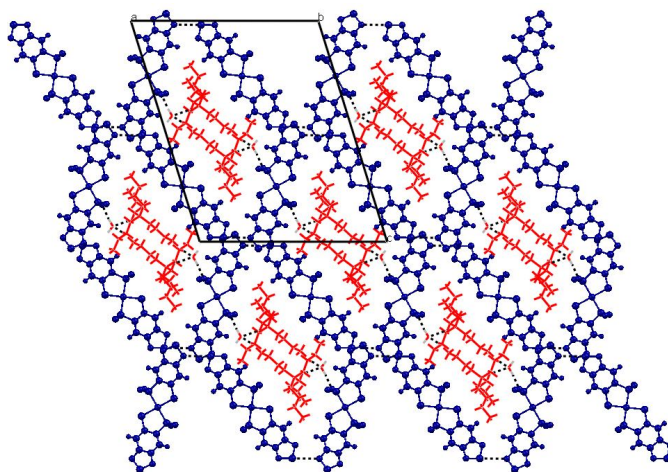


Figure 3.23. (b) Two-dimensional supramolecular network as a result of combination of S \cdots N non-covalent interactions and C–H \cdots O and O–H \cdots O hydrogen bonding interactions in the crystal structure of complex **5**.

If the bottom of boat shape is considered as molecular plane containing S(1)S(2)Ni(1)S(1#)S(2#) atoms in complex **5**, the plane containing 2,1,3-benzenethiadiazole atoms, is bent from the molecular plane by an angle 5.97° , but the molecular plane of other molecule (S(4)S(5)Ni(1)S(4#)S(5#)) is more bending than previous one, which is an angle of 13.12° . In this molecule of Ni(2) complexing unit, the

oxygen atoms of sulfinates are involved in O–H \cdots O interaction with lattice water molecule along with C–H \cdots O hydrogen bonding interactions. In disulfinate complex **5**, average Ni–S distances (Ni(1)–S and Ni(2)–S bond distances are 2.149 ± 0.001 Å and 2.156 ± 0.01 Å, respectively) are less than those in complex **4** (2.162 ± 0.001). The S–O bond distances are in the range of reported sulfinato complexes of dithiolene.^{18–22} The molecular packing diagram of the complex **5**, characterized by C–H \cdots O and O–H \cdots O hydrogen bonding and S \cdots N non-covalent interactions resulting in a two dimensional supramolecular network view down to crystallographic *b* axis, is shown in Figure 3.23. The relevant hydrogen bonding geometrical parameters are listed in the Table 3.6, and S \cdots N interactions are in the range from 3.194 to 3.513 Å.

3.4. Conclusions

We have described here, new metal bis(dithiolene) complexes $[\text{Bu}_4\text{N}][\text{M}^{\text{III}}(\text{btdt})_2]$ [$\text{M} = \text{Cu}$ (**1**), Au (**2**)] and $[\text{Bu}_4\text{N}]_2[\text{M}^{\text{II}}(\text{btdt})_2]$ [$\text{M} = \text{Pt}$ (**3**), Ni (**4**)] based on H_2btdt ($\text{btdt}^{2-} = 2,1,3\text{-benzenethiadiazole-5,6-dithiolate}$) ligand, and the solid state structures of these compounds have been characterized by single crystal X-ray crystallography. We have explained distortion in square-planar geometry of compounds **1–4**, in the terms of dihedral angle (λ) between two SMS planes, bending angle (η) (between the SMS and CSSC planes) of dithiolene chelate ring system and $c_1\text{--M--}c_2$ angles (where c_1 and c_2 are midpoints between the two coordinated sulfur atoms of each dithiolene ligand). Solution absorption spectra of these compounds have been described, in which the solvent sensitive broad band is observed for the complex **3** and **4**; this is assigned as charge transfer (CT) transition involving electronic excitation from a HOMO which is a mixture of dithiolate (π) and metal (d) orbital character to a LUMO which is a π^* orbital of the dithiolate. The electrochemistry of the copper(III) complex **1** is very interesting in the sense that these complexes get reduced more easily. This indicates that the complex **1** might act as oxidation catalyst for organic transformations / oxidation reactions of industrial importance. The S \cdots S non covalent intermolecular interactions among the complexes are very important to get the promising materials such as conducting and magnetic materials. The compounds **2** and **4** are characterized by S \cdots S non covalent interactions between the dithiolate molecules. To our knowledge, we have described for the first time sulfur oxygenated product **5** of metal bis(dithiolene) complex by simple air oxidation of

compound **4** at room light. Interestingly Ni-compound **4** is oxidized electrochemically at very low oxidation potentials.

Table 3.1. Crystal Data and Structural Refinement for Compounds **1–3**

	1	2	3
Empirical formula	C ₂₈ H ₄₀ N ₅ S ₆ Cu	C ₂₈ H ₄₀ N ₅ S ₆ Au	C ₄₄ H ₇₆ N ₆ S ₆ Pt
Formula weight	702.55	835.98	1076.56
T [K], λ [Å]	298(2), 0.71073	100(2), 0.71073	298(2), 0.71073
Crystal system, Space group	Triclinic, <i>P</i> -1	Monoclinic, <i>P</i> 2(1)/c	Monoclinic, <i>C</i> 2/c
<i>a</i> [Å]	10.5295(9)	23.281(8)	23.092(3)
<i>b</i> [Å]	12.7015(11)	12.001(4)	10.1561(11)
<i>c</i> [Å]	13.9428(12)	25.913(8)	21.949(2)
α [deg]	72.887(10)	90.000	90.000
β [deg]	80.949(10)	109.832(5)	93.579(2)
γ [deg]	72.642(10)	90.000	90.000
<i>V</i> [Å ³]	1696.1(3)	6811(4)	5137.5(10)
<i>Z</i> , <i>D</i> _{calc} [Mg m ⁻³]	2, 1.376	8, 1.631	4, 1.392
μ [mm ⁻¹], F(000)	1.040, 736	4.715, 3344	3.010, 2224
Crystal size [mm ³]	0.34 x 0.24 x 0.06	0.40 x 0.24 x 0.12	0.34 x 0.24 x 0.12
θ range for data collection [deg]	1.53 to 25.97	1.61 to 25.12	1.77 to 25.06
Reflections collected / unique	15724/6551	63523/12099	23386/4532
R(int)	0.0248	0.0710	0.0509
Data / restraints / parameters	6551/0/368	12099/0/729	4532/0/262
Goodness-of-fit on F ²	1.022	1.033	1.065
R ₁ /wR ₂ [I > 2 σ (I)]	0.0425/0.1019	0.0414/0.1004	0.0416/0.1041
R ₁ /wR ₂ (all data)	0.0573/0.1097	0.0605/0.1109	0.0723/0.1254
Largest diff. Peak/hole [e Å ⁻³]	0.382/-0.259	1.297/-0.877	1.339/-0.786

Table 3.2. Crystal Data and Structural Refinement for Compounds **4** and **5**

	4	5
Empirical formula	C ₄₄ H ₇₆ N ₆ S ₆ Ni	C ₄₄ H ₇₈ N ₆ O ₅ S ₆ Ni
Formula weight	940.18	1022.19
T [K], λ [Å]	298(2), 0.71073	298(2), 0.71073
Crystal system, Space group	Triclinic, <i>P</i> -1	Monoclinic, <i>C</i> 2/c
<i>a</i> [Å]	7.7925(16)	21.927(4)
<i>b</i> [Å]	12.946(3)	18.645(4)
<i>c</i> [Å]	12.957(3)	27.178(5)
α [deg]	86.80(3)	90.000
β [deg]	83.34(3)	107.26(3)
γ [deg]	82.19(3)	90.000
<i>V</i> [Å ³]	1285.2(5)	10611(4)
<i>Z</i> , <i>D</i> _{calc} [Mg m ⁻³]	1, 1.215	8, 1.280
μ [mm ⁻¹], F(000)	0.656, 506	0.648, 4384
Crystal size [mm ³]	0.34 x 0.22 x 0.10	0.38 x 0.10 x 0.06
θ range for data collection [deg]	1.58 to 25.00	1.46 to 25.00
Reflections collected / unique	12361/4513	50482/9340
R(int)	0.0243	0.1460
Data / restraints / parameters	4513/0/263	9340/0/577
Goodness-of-fit on F ²	1.041	0.934
R ₁ /wR ₂ [I > 2 σ (I)]	0.0495/0.1291	0.0561/0.1091
R ₁ /wR ₂ (all data)	0.0665/0.1418	0.1379/0.1347
Largest diff. Peak/hole [e Å ⁻³]	0.386/-0.201	0.676/-0.330

Table 3.3. Selected Bond Lengths (Å) and Bond Angles (°) for compounds **1–3**

Compound 1			
Cu(1)-S(1)	2.1595(8)	Cu(1)-S(1)#1	2.1595(8)
Cu(1)-S(2)#1	2.1769(8)	Cu(1)-S(2)	2.1769(8)
Cu(2)-S(4)#2	2.1656(8)	Cu(2)-S(4)	2.1656(8)
Cu(2)-S(5)	2.1736(7)	Cu(2)-S(5)#2	2.1736(7)
S(1)-Cu(1)-S(1)#1	180.0	S(1)-Cu(1)-S(2)#1	87.80(3)
S(1)#1-Cu(1)-S(2)#1	92.20(3)	S(1)-Cu(1)-S(2)	92.20(3)
S(1)#1-Cu(1)-S(2)	87.80(3)	S(2)#1-Cu(1)-S(2)	180.0
S(4)#2-Cu(2)-S(4)	180.0	S(4)#2-Cu(2)-S(5)	87.97(3)
S(4)-Cu(2)-S(5)	92.03(3)	S(4)#2-Cu(2)-S(5)#2	92.03(3)
S(4)-Cu(2)-S(5)#2	87.97(3)	S(5)-Cu(2)-S(5)#2	180.0(2)
C(1)-S(1)-Cu(1)	105.14(10)	C(6)-S(2)-Cu(1)	104.78(9)
C(7)-S(4)-Cu(2)	104.98(9)	C(12)-S(5)-Cu(2)	104.73(9)
Compound 2			
Au(1)-S(2)	2.2965(16)	Au(1)-S(3)	2.2966(17)
Au(1)-S(1)	2.3030(17)	Au(1)-S(4)	2.3090(16)
Au(2)-S(7)	2.3011(17)	Au(2)-S(8)	2.3020(16)
Au(2)-S(10)	2.3098(17)	Au(2)-S(9)	2.3101(16)
S(2)-Au(1)-S(3)	177.68(8)	S(2)-Au(1)-S(1)	89.28(6)
S(3)-Au(1)-S(1)	91.16(6)	S(2)-Au(1)-S(4)	90.41(6)
S(3)-Au(1)-S(4)	89.31(6)	S(1)-Au(1)-S(4)	175.99(7)
S(7)-Au(2)-S(8)	90.01(6)	S(7)-Au(2)-S(10)	178.38(7)
S(8)-Au(2)-S(10)	89.65(6)	S(7)-Au(2)-S(9)	90.74(6)
S(8)-Au(2)-S(9)	179.18(6)	S(10)-Au(2)-S(9)	89.61(6)
C(1)-S(1)-Au(1)	104.1(2)	C(2)-S(2)-Au(1)	104.28(19)
C(7)-S(3)-Au(1)	104.8(2)	C(8)-S(4)-Au(1)	103.1(2)
C(17)-S(7)-Au(2)	103.7(2)	C(18)-S(8)-Au(2)	104.40(19)
C(19)-S(9)-Au(2)	103.6(2)	C(20)-S(10)-Au(2)	103.5(2)
Compound 3			
Pt(1)-S(1)#3	2.2785(19)	Pt(1)-S(1)	2.2785(19)
Pt(1)-S(2)	2.2829(17)	Pt(1)-S(2)#3	2.2830(17)
S(1)#3-Pt(1)-S(1)	91.25(10)	S(1)#3-Pt(1)-S(2)	177.27(6)
S(1)-Pt(1)-S(2)	88.52(7)	S(1)#3-Pt(1)-S(2)#3	88.52(6)
S(1)-Pt(1)-S(2)#3	177.26(6)	S(2)-Pt(1)-S(2)#3	91.83(8)
C(6)-S(2)-Pt(1)	105.8(2)	C(1)-S(1)-Pt(1)	105.7(2)

Symmetry transformations used to generate equivalent atoms: #1 -x+2,-y+1,-z+2; #2 -x+1,-y+1,-z+1; #3 -x+1,y,-z+3/2.

Table 3.4. Selected Bond Lengths (Å) and Bond Angles (°) for compounds **4** and **5**

Compound 4			
Ni(1)-S(2)	2.1614(9)	Ni(1)-S(2)#1	2.1614(9)
Ni(1)-S(1)#1	2.1629(10)	Ni(1)-S(1)	2.1629(10)
S(2)-Ni(1)-S(2)#1	180.0	S(2)-Ni(1)-S(1)#1	88.87(4)
S(2)#1-Ni(1)-S(1)#1	91.13(4)	S(2)-Ni(1)-S(1)	91.13(4)
S(2)#1-Ni(1)-S(1)	88.87(4)	S(1)#1-Ni(1)-S(1)	179.99(14)
C(1)-S(1)-Ni(1)	106.16(11)	C(6)-S(2)-Ni(1)	106.26(10)
C(1)-S(1)-Ni(1)	106.16(11)	C(6)-S(2)-Ni(1)	106.26(10)
Compound 5			
O(1)-S(1)	1.471(3)	O(2)-S(1)	1.453(3)
O(4)-S(4)	1.470(3)	O(3)-S(4)	1.452(3)
Ni(1)-S(1)#3	2.1479(13)	Ni(1)-S(1)	2.1479(12)
Ni(1)-S(2)	2.1498(11)	Ni(1)-S(2)#3	2.1499(11)
Ni(2)-S(4)#2	1.458(12)	Ni(2)-S(4)	2.1458(12)
Ni(2)-S(5)#2	2.1666(13)	Ni(2)-S(5)	2.1667(12)
S(1)#3-Ni(1)-S(1)	179.40(8)	S(1)#3-Ni(1)-S(2)	88.19(5)
S(1)-Ni(1)-S(2)	91.81(5)	S(1)#3-Ni(1)-S(2)#3	91.81(5)
S(1)-Ni(1)-S(2)#3	88.19(5)	S(2)-Ni(1)-S(2)#3	179.51(8)
S(4)#2-Ni(2)-S(4)	178.71(8)	S(4)#2-Ni(2)-S(5)#2	90.99(5)
S(4)-Ni(2)-S(5)#2	88.99(5)	S(4)#2-Ni(2)-S(5)	89.00(5)
S(4)-Ni(2)-S(5)	90.99(5)	S(5)#2-Ni(2)-S(5)	178.18(8)
O(3)-S(4)-Ni(2)	116.80(15)	O(4)-S(4)-Ni(2)	110.64(14)
C(12)-S(4)-Ni(2)	105.96(14)	O(2)-S(1)-Ni(1)	114.09(14)
O(1)-S(1)-Ni(1)	112.57(14)	C(1)-S(1)-Ni(1)	105.89(14)
C(7)-S(5)-Ni(2)	106.15(14)	C(6)-S(2)-Ni(1)	106.37(14)

Symmetry transformations used to generate equivalent atoms: #1 -x,-y+2,-z+1; #2 -x+2,y,-z+1/2; #3 -x+1,y,-z+1/2

Table 3.5. Hydrogen Bonds for Compounds **1–3**

D-H...A	d(D...H)	d(H...A)	d(D...A)	<(DHA)
Compound 1				
C(8)-H(8)...N(3)#1	0.93	2.67	3.578(4)	164.0
C(13)-H(13A)...N(2)#2	0.97	2.62	3.570(4)	166.7
Compound 2				
C(45)-H(45B)...N(1)#3	0.97	2.69	3.621(13)	162.1
Compound 3				
C(15)-H(15B)...S(2)	0.97	2.81	3.751(7)	162.9
C(7)-H(7A)...N(1)#4	0.97	2.59	3.551(9)	172.7

Symmetry transformations used to generate equivalent atoms: #1 -x+1,-y+2,-z+1; #2 -x+1,-y+1,-z+2; #3 x,y,-1,z; #4 x,-y+1,z+1/2.

Table 3.6. Hydrogen Bonds for Compounds **4** and **5**

D–H...A	d(D...H)	d(H...A)	d(D...A)	<(DHA)
Compound 4				
C(11)-H(11B)...S(2)#1	0.97	2.94	3.850(4)	157.4
C(8)-H(8A)...S(2)#1	0.97	2.92	3.714(4)	140.1
C(19)-H(19B)...S(1)#2	0.97	2.87	3.754(3)	152.3
Compound 5				
C(8)-H(8)...N(2)	0.93	2.65	3.431(6)	142.2
O(10)-H(10O)...O(4)#3	0.97	1.95	2.884(5)	162.6
C(14)-H(14A)...O(10)	0.97	2.60	3.561(6)	169.7
C(21)-H(21B)...O(10)	0.97	2.53	3.290(6)	135.1
C(18)-H(18A)...O(1)#4	0.97	2.70	3.283(6)	119.2
C(13)-H(13B)...O(3)#3	0.97	2.64	3.582(5)	163.1
C(33)-H(33B)...O(1)#5	0.97	2.60	3.538(6)	163.7

Symmetry transformations used to generate equivalent atoms: #1 -x+1,-y+1,-z+1; #2 x,y-1,z; #3 -x+2,y,-z+1/2; #4 -x+1,y,-z+1/2; #5 x+1/2,y-1/2,z.

3.5. References

- 1 Karlin, K. D.; Stiefel, E. I. *Prog. Inorg. Chem.* John Wiley, New York, **2004**, Volume 52.
- 2 (a) Kato, R. *Chem. Rev.* **2004**, *104*, 5319–5346. (b) Mercuri, M. L.; Deplano, P.; Pilia, L.; Serpe, A.; Artizzu, F. *Coord. Chem. Rev.* **2010**, *254*, 1419–1433. (c) Coomber, A. T.; Beljonne, D.; Friend, R. H.; Brédas, J. L.; Charlton, A.; Robertson, N.; Underhill, A. E.; Kurmoo, M. Day, P. *Nature* **1996**, *380*, 144–146. (d) Ren, X. M.; Nishihara, S.; Akutagawa, T.; Noro, S.; Nakamura, T. *Inorg. Chem.* **2006**, *45*, 2229–2234. e) Robertson, N.; Cronin, L. *Coord. Chem. Rev.* **2002**, *227*, 93–127.
- 3 (a) Deplano, P.; Pilia, L.; Espa, D.; Mercuri, M. L.; Serpe, A. *Coord. Chem. Rev.* **2010**, *254*, 1434–1447. (b) Serrano-Andrés, L.; Avramopoulos, A.; Li, J.; labéguerie, P.; Bégué, D.; Kellö, V.; Papadopoulos, M. G. *J. Chem. Phys.* **2009**, *131*, 134312. (c) Chen, C.-T.; Liao, S.-Y.; Lin, K.-J.; Lai, L.-L. *Adv. Mater.* **1998**, *3*, 334–338.

- 4 (a) Mueller-Westerhoff, U. T.; Vance, B.; Yoon, D. I. *Tetrahedron* **1991**, *47*, 909–932. (b) deplano, P.; Mercuri, M. L.; Pintus, G.; Trogu, E. F. *Comments Inorg. Chem.* **2001**, *22*, 353–374. (c) Bai, J.-F.; Zuo, J.-L.; Tan, W.-L.; Ji, W.; Shen, Z.; Fun, H.-K.; Chinnakali, K.; Razak, I. A.; You, X.-Z.; Che, C.-M. *J. Mater. Chem.* **1999**, *9*, 2419–2423. (d) Aragoni, M. C.; Arca, M.; Cassano, T.; Denotti, C.; Devillanova, F. A.; Frau, R.; Isaia, F.; Lelj, F.; Lippolis, V.; Nitti, L.; Romaniello, P.; Tommasi, R.; Verani, G. *Eur. J. Inorg. Chem.* **2003**, 1939–1947.
- 5 (a) Hine, F. J.; Taylor, A. J.; Garner, C. D. *Coord. Chem. Rev.* **2010**, *254*, 1570–1579 (b) Rees, D. C.; Hu, Y.; Kisker, C.; Sahindelin, H. *J. Chem. Soc., Dalton. Trans.* **1997**, 3909–3914. (c) Rudolph, M. J.; Wuebbens, M. M.; Rajagopalan, K. V.; Sahindelin, H. *Nat. Struct. Biol.* **2001**, *8*, 42.
- 6 (a) Johnson, J. L.; Rajagopalan, K. V. *Proc. Natl. Acad. Sci. USA* **1982**, *79*, 6856–6860. (b) Johnson, J. L.; Hainline, B. E.; Rajagopalan, K. V.; Arison, B. H. *J. Biol. Chem.* **1984**, *259*, 5414–5422. (c) Boyde, S.; Garner, C. D.; Enemark, J. H.; Bruck, M. A.; Kristofzski, J. G. *J. Chem. Soc. Dalton. Trans.* **1987**, 2267–2271. (d) Boyde, S.; Garner, C. D.; Enemark, J. H.; Ortega, R. B. *J. Chem. Soc., Dalton. Trans.* **1987**, 297–302. (e) Boyde, S.; Garner, C. D.; Enemark, J. H.; Ortega, R. B. *Polyhedron* **1986**, *5*, 377–379.
- 7 (a) Rignedoli, A.; Peyronel, G.; Malavasi, W. *J. Inorg. Nucl. Chem.* **1976**, *38*, 1963. (b) Theriot, L. J.; Ganguli, K. K.; Kavarnos, S.; Bernal, I. *J. Inorg. Nucl. Chem.* **1969**, *31*, 3133. (c) Boyde, S.; Garner, C. D. *J. Chem. Soc. Dalton. Trans.* **1991**, 713.
- 8 Bruke, R. W.; Deardorff, E. R. *Talanta* **1970**, *17*, 255–264.
- 9 Ryabushko, O. P.; Pilipenko, A. T.; Batkovskaya, L. A.; Savin, Y. S. *Ukr. Khim. Zh.* **1988**, *54*, 1172–1176.
- 10 (a) Cummings, S. D.; Eisenberg, R. *Inorg. Chem.* **1995**, *34*, 2007–2014. (b) Cummings, S. D.; Eisenberg, R. *Inorg. Chem.* **1995**, *34*, 3396–3403.
- 11 Wang, J.-J.; Groysman, S.; Lee, S. C.; R. H. Holm, R. H. *J. Am. Chem. Soc.* **2007**, *129*, 7512.

- 12 (a) Mrkvová, K.; Kameníček, J.; Šindelář, Z.; Kvítek, L. *Transition. Met. Chem.* **2004**, 29, 238. (b) Walla, J.; Smékal, Z.; Kameníček, J. *Acta Univ. Palacki. Olom.*, **1998**, 37.
- 13 Schiødt, N. C.; Bjørnholm, T.; Bechgaard, K.; Neumeier, J. J.; Allgeier, C.; Jacobsen, C. S.; Thorup, N. *Phys. Rev. B* **1996**, 53, 1773.
- 14 Schiødt, N. C.; Sommer-Larsen, P.; Bjørnholm, T.; Nielsen, M. F.; Larsen, J.; Bechgaard, K. *Inorg. Chem.* **1995**, 34, 3688.
- 15 Bolligarla, R.; Das, S. K. *CrystEngComm* **2010**, 12, 3409–3412.
- 16 (a) van der Zwaan, J. W.; Coremans, J. M. C. C.; Bouwens, E. C.; Albracht, S. P. J. *Biochim. Biophys. Acta.* **1990**, 1041, 101. (b) Coremans, J. M. C. C.; van der Zwaan, J. W.; Albracht, S. P. J. *Biochim. Biophys. Acta.* **1992**, 1119, 157.
- 17 Shin, W.; Lindahl, P. A.; *Biochim. Biophys. Acta.* **1993**, 1161, 317.
- 18 (a) Grapperhaus, C. A.; Darensbourg, M. Y. *Acc. Chem. Res.* **1998**, 31, 451–459. (b) Buonomo, R. M.; Font, I.; Maguire, M. J.; Reibenspies, J. H.; Tuntulani, T.; Darensbourg, M. Y. *J. Am. Chem. Soc.* **1995**, 117, 963–973. (c) Tuntulani, T.; Musie, G.; Reibenspies, J. H.; Darensbourg, M. Y. *Inorg. Chem.* **1995**, 34, 6279–6286. (d) Grapperhaus, C. A.; Maguire, M. J.; Tuntulani, T.; Darensbourg, M. Y. *Inorg. Chem.* **1997**, 36, 1860–1866. (e) Darensbourg, M. Y.; Tuntulani, T.; Reibenspies, J. H. *Inorg. Chem.* **1995**, 34, 6287–6294. (f) Bellefeuille, J. A.; Grapperhaus, C. A.; Buonomo, R. M.; Reibenspies, J. H.; Darensbourg, M. Y. *Organometallics* **1998**, 17, 4813–4821. (g) Kaasjager, V. E.; Bouwman, E.; Gorter, S.; Reedijk, J.; Grapperhaus, C. A.; Reibenspies, J. H.; Smee, J. J.; Darensbourg, M. Y.; Derecskei-Kovacs, A.; Thomson, L. M. *Inorg. Chem.* **2002**, 41, 1837–1844.
- 19 Henderson, R. K.; Bouwman, E.; Spek, A. L.; Reedijk, J. *Inorg. Chem.* **1997**, 36, 4616–4617.
- 20 Connick, W. B.; Gray, H. B. *J. Am. Chem. Soc.* **1997**, 119, 11620–11627.
- 21 (a) Cocker, T. M.; Bachman, R. E. *Inorg. Chem.* **2001**, 40, 1550–1556. (b) T. M. Cocker, R. E. Bachman, *Chem. Commun.* **1999**, 875–876.
- 22 (a) Robertson, N.; Parsons, S.; Awaga, K.; Fujita, W. *CrystEngComm* **2000**, 2, 121–124. (b) Lee, C.-M.; Hsieh, C.-H.; Dutta, A.; Lee, G.-H.; Liaw, W.-F. *J. Am. Chem. Soc.* **2003**, 125, 11492–11493.

- 23 Brusso, J. L.; Clements, O. P.; Haddon, R. C.; Itkis, M. E.; Leitch, A. A.; Oakley, R. T.; Reed, R. W.; Richardson, J. F. *J. Am. Chem. Soc.* **2004**, *126*, 8256.
- 24 Bruker. *SADABS*, *SMART*, *SAINT* and *SHELXTL*, **2000** (Bruker AXS Inc., Madison, Wisconsin, USA).
- 25 Sheldrick, G. M. *Acta Crystallogr. Sect. A* **2008**, *64*, 112–122.
- 26 Ribas, X.; Dias, J.; Morgado, J.; Wurst, K.; Almeida, M.; Veciana, J.; Rovira, C. *CrystEngComm* **2002**, *4*, 564.
- 27 Madhu, V.; Das, S. K. *Inorg. Chem.* **2006**, *45*, 10037.
- 28 Shupack, S. I.; Billig, E.; Clark, R. J. H.; Williams, R.; Gray, H. B. *J. Am. Chem. Soc.* **1964**, *86*, 4594.
- 29 Papavassiliou, G. C.; Cotsilios, A. M.; Jacobsen, C. S. *J. Mol. Struct.* **1984**, *115*, 41.
- 30 Bondi, A. *J. Phys. Chem.* **1964**, *68*, 441.

Acid-Base Behavior of a Simple and Nitrogen Rich Metal Bis(Dithiolene) System: Syntheses, Crystal Structures and Spectroscopy of $[\text{Bu}_4\text{N}]_2[\text{M}^{\text{II}}(\text{ppdt})_2]$ ($\text{M} = \text{Ni}, \text{Pt}$; $\{\text{Ppdt}\}^{2-} = \text{Pyrido}[2,3-b]\text{pyrazine-2,3-dithiolate}$)

4 Chapter

Abstract:- The syntheses, crystal structures and properties of compounds $[\text{Bu}_4\text{N}]_2[\text{Ni}(\text{ppdt})_2]$ (**1**) and $[\text{Bu}_4\text{N}]_2[\text{Pt}(\text{ppdt})_2]$ (**2**) ($\{\text{ppdt}\}^{2-} = \text{pyrido}[2,3-b]\text{pyrazine-2,3-dithiolate}$) have been described. Compound **1** crystallizes in $P2_1/c$ space group (monoclinic system), whereas compound **2** crystallizes in $C2/c$ space group (monoclinic system). The crystal structures of both compounds **1** and **2** have been characterized by C–H...S and C–H...N hydrogen bonding interactions between cation and anions resulting in 3-dimensional supramolecular networks in the crystals of **1** and **2**, respectively. The acid–base behavior of the ground states of both **1** and **2** also the excited state of compound **2** in solutions has been studied. The pH dependent changes in the charge-transfer absorption and emission spectra are attributed to the protonation on an imine nitrogen of the ppdt ligand. The ground–state basicity constants of the two complexes **1** and **2** have been determined from spectrophotometric analysis by titrating with a weak acid, yielding $\text{p}K_{\text{b}1} = 8.0$ for complex **1** and $\text{p}K_{\text{b}1} = 7.8$ for complex **2**. The excited–state basicity constant $\text{p}K_{\text{b}1}^*$ for complex **2** has been determined by a thermodynamic equation using a Förster analysis yielding the value of 1.8. The complex **1** is electrochemically quasi-reversible with an oxidation potential of $E_{1/2} = +0.46 \text{ V vs Ag/AgCl}$ ($\Delta E = 0.12 \text{ V}$), whereas the complex **2** is electrochemically irreversible with an oxidation potential of $E_{1/2} = +0.41 \text{ V vs Ag/AgCl}$ in methanol solutions.

4.1. Introduction

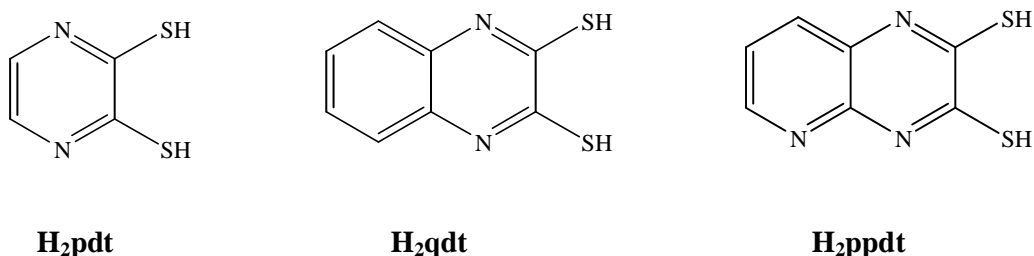
Chemical research on metal-dithiolene complexes has always remained active, since its inception in the early of 1960s, because the relevant transition metal coordination complexes have distinctive redox characteristics.¹ Today, dithiolene chemistry is more recognized by its relations to materials science in the context of molecular electronic conductors and NLO materials.²⁻⁸ Choosing a dithiolate ligand is very important in obtaining a successful dithiolene based material. Recently, the scope of metal dithiolene complexes has extended to bioinorganic modeling studies because of the existence of metal-dithiolene moiety in many metallo-enzymes.⁹ In this regard, nitrogen atom containing heterocyclic based dithiolene complexes are present in “molybdopterin” that constitutes the molybdenum cofactor of these hydroxylase type molybdo-enzymes.¹⁰ For example, one of the nitrogen containing dithiolene ligands, namely, qdt^{2-} and its molybdenum-oxo complexes have been investigated for modeling the active sites of molybdenum hydroxylase enzymes.¹¹ These studies have explored the changes in the redox properties¹² and the electronic absorption spectra of relevant metal dithiolene

complexes upon reversible protonation of the coordinated qdt ligand.¹³ One or both nitrogen atoms of the $\{\text{qdt}\}^{2-}$ ligand in their complexes could be protonated and again deprotonated, meaning that it shows acid–base behavior, as observed in the Ni(II)-,¹³⁻¹⁴ Pt(II)-¹⁵ and Mo(IV)-qdt complexes.¹⁶

A metal dithiolene complex, exhibiting acid-base behavior, is important to study, because understanding proton transfer reactions are essential for maintaining cellular life and they are part of the metabolic processes taking part in extra- and intra-cellular fluids.¹⁷ For example, the energy needed for maintaining the cell alive is produced by a cycle of reactions implying proton transfer(s).¹⁷ Enzymes are essential in the metabolic processes and their three-dimensional structures determine the reactivity. In turn, this structure depends both on the temperature and on the acidity level, which consequently influences the reactivity of proteins. The latter is optimum for a given acidity level.¹⁷ For example, trypsin, a digestive enzyme located in the intestine, has an optimal activity when its acidity level is low. When the acidity level increases, the enzyme is denatured, as observed in majority of the enzymes. On the other hand, pepsin, a digestive enzyme of the stomach, has an optimal activity when the acidity level is high; it is perfectly adapted to the acidic environment of the stomach. In the same way, within the active site of the enzyme, the catalytic reaction implies specific functional groups of some amino acids, for example, a carboxylate group. When the level of acidity is increased, this group will be protonated and will no more be able to play a role in the reaction, resulting in inhibition of the enzymatic activity. Because of this significance of the proton transfer reactions in biology, we are interested to study the acid-base properties for the nitrogen containing heterocyclic based metal-dithiolene complexes.

In literature, there is only report (in the area of metal dithiolene systems) by Cummings and Eisenberg that described the detailed pH dependent absorption and emission studies of a Pt(II) quinoxaline-2,3-dithiolate ($\{\text{qdt}\}^{2-}$, Scheme 4.1) complex $[\text{Bu}_4\text{N}]_2[\text{Pt}(\text{qdt})_2]$.¹⁵ With the aim of understanding the acid-base behavior for the metal-dithiolene complexes, we have synthesized $[\text{Bu}_4\text{N}]_2[\text{M}(\text{ppdt})_2]$ ($\text{M} = \text{Ni}$ (**1**), Pt (**2**); $\{\text{ppdt}\}^{2-} = \text{pyrido}[2,3-b]\text{pyrazine-2,3-dithiolate}$, Scheme 4.1) and described pH dependent absorption and emission studies by the protonation and deprotonation of imine nitrogen atom of $\{\text{ppdt}\}^{2-}$ ligand present in the metal complex. This pH dependent absorption and emission studies have been studied by adding with weak acids and weak bases as well as the strong acids and strong bases. In this chapter, we have described syntheses,

electrochemical characterization, crystal structures, pH dependent absorption and emission studies and the supramolecular features of compounds **1** and **2** in the solid state emphasizing C–H...S and C–H...N weak interactions.



Scheme 4.1. Structural representation of some N-heterocyclic based dithiolene ligands.

4.2. Experimental Details

4.2.1. General methods

Micro analytical (C, H, N) data were obtained with a FLASH EA 1112 Series CHNS Analyzer. Infrared (IR) spectra were recorded on KBr pellets with a JASCO FT/IR-5300 spectrometer in the region of 400-4000cm⁻¹. ¹H NMR spectra of compounds were recorded on Bruker DRX- 400 spectrometer using Si(CH₃)₄ [TMS] as an internal standard. Electronic absorption spectra were recorded on a Cary 100 Bio UV-Visible spectrophotometer. The emission spectra for the samples in solutions were recorded at room temperature on a Horiba Jobin Yvon Fluoromax-4 spectrofluorometer. In the measurements of emission and excitation spectra, the pass width was 5 nm. All the measurements were carried out under the same experiment conditions. A Cypress model CS-1090/CS-1087 electro analytical system was used for cyclic voltammetric experiments. The electrochemical experiments were measured in MeOH containing [Bu₄N][ClO₄] as a supporting electrolyte, using a conventional cell consisting of two platinum wires as working and counter electrodes, and a Ag/AgCl electrode as a reference. The potentials reported here are uncorrected for junction contributions.

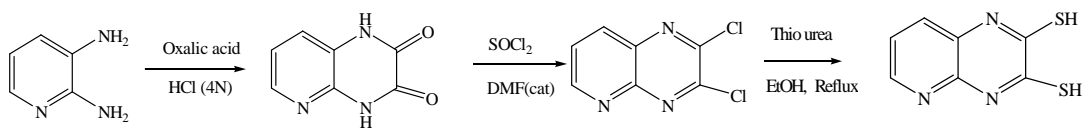
4.2.2. Materials

2,3-Dichloropyrido[2,3-*b*]pyrazine was prepared according to literature procedure.¹⁸ Syntheses of metal complexes were performed under N₂ using standard inert-atmosphere techniques. Solvents were dried by standard procedures.

4.2.3. Synthesis and Characterization

Synthesis of Pyrido[2,3-*b*]Pyrazine-2,3-Dithiol (H_2ppdt)

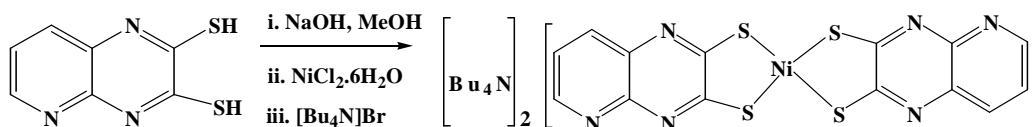
Pyrido[2,3-*b*]pyrazine-2,3-dithiol (H_2ppdt) was prepared according modified literature procedure.¹⁹ 1.05 g (5.249 mmol) of 2,3-Dichloropyrido[2,3-*b*]pyrazine and 2.2 g (28.9 mmol) of thiourea were suspended in 25 mL of absolute ethanol and this mixture was reflux for 1 h. The solution was concentrated to a small volume. It was then diluted with 60 mL of water and made alkaline by the addition of 6.25 g NaOH. This was refluxed for half an hour. On acidifying with acetic acid, a brownish orange product was formed which was separated by filtration, washed with water and dried under vacuum. Yield: 1.004 g (98 %). IR (KBR pellet) (ν/cm^{-1}): 1665, 1601, 1555, 1433, 1404, 1350, 1296, 1157, 1071, 912, 806, 625, 536. 1H NMR (400 MHz, δ ppm) (DMSO- d_6): 7.3(d, 1H), 8.211(d, 1H), 8.262(d, 1H), 14.275(s, 1H), 14.562(s, 1H). Anal. Calcd. for $C_7H_5N_3S_2$: C, 43.06; H, 2.58; N, 21.52%. Found: C, 43.12; H, 2.48; N, 21.46%.



Scheme 4.2. Schematic representation for the synthesis of ligand (H_2ppdt).

Synthesis of $[Bu_4N]_2[Ni(ppdt)_2]$ (**1**)

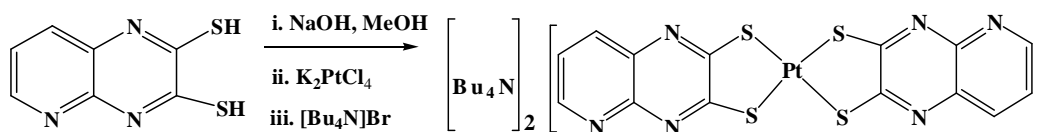
The $ppdt$ dianion is generated *in situ* by treatment with H_2ppdt (0.100 g, 0.512 mmol) with NaOH (0.045 g, 1.125 mmol) in MeOH (10 mL). To the resulting clear yellow solution, solid $NiCl_2 \cdot 6H_2O$ (0.061 g, 0.257 mmol) was added; the resulting dark blue solution was stirred for 10 minutes. Reddish brown micro crystals were precipitated by adding tetrabutylammonium bromide (0.2 g, 0.62 mmol); the microcrystals were filtered, washed with water followed by diethyl ether and dried at room temperature. It was recrystallized from acetonitrile solution by diffusing diethyl ether. Yield: 0.250 g (52.0% based on Ni). IR (KBR pellet) (ν/cm^{-1}): 2959, 2866, 1578, 1547, 1470, 1453, 1395, 1354, 1296, 1240, 1217, 1155, 1107, 880, 777, 739, 594, 424, 411. Anal. Calcd. for $C_{46}H_{78}N_8S_4Ni$: C, 59.40; H, 8.45; N, 12.05%. Found: C, 59.01; H, 8.42; N, 12.11%. 1H NMR (400 MHz, δ ppm) (DMSO- d_6): 0.91(t, 24H), 1.28-1.30(m, 16H), 1.56(b, 16H), 3.17(t, 16H), 7.23(s, 2H), 7.83(s, 2H), 8.44(s, 2H).



Scheme 4.3. Schematic representation for the synthesis of compound $[\text{Bu}_4\text{N}]_2[\text{Ni}(\text{ppdt})_2]$ (**1**).

Synthesis of $[\text{Bu}_4\text{N}]_2[\text{Pt}(\text{ppdt})_2]$ (**2**)

The *insitu* generation of ppdt dianion by the treatment of H_2ppdt (0.100 g, 0.512 mmol) with NaOH (0.045 g, 1.125 mmol) in MeOH (10 mL). To the resulting clear yellow solution, K_2PtCl_4 solution [prepared by dissolving K_2PtCl_4 (0.106 g, 0.256 mmol) compound in water (5.0 mL) for 2 h at room temperature] was added; the resulting dark red solution was stirred for 2 h at 55-60°C. Dark red micro crystals were precipitated by adding tetrabutylammonium bromide (0.2 g, 0.621 mmol); the micro crystals were filtered, washed with water followed by diethyl ether, and dried at room temperature. It was recrystallized from acetonitrile solution by vapor diffusion with diethyl ether. Yield: 0.180 g (66.0% based on Pt). IR (KBR pellet) (ν/cm^{-1}): 2959, 2866, 1578, 1547, 1470, 1453, 1354, 1296, 1155, 1107, 880, 777, 594, 424. Anal. Calcd. for $\text{C}_{46}\text{H}_{78}\text{N}_8\text{S}_4\text{Pt}$: C, 51.80; H, 7.37; N, 10.51%. Found: C, 51.10; H, 7.25; N, 10.67%. ^1H NMR (400 MHz, δ ppm) (CDCl_3): 0.737(t, 24H), 1.18-1.23(m, 16H), 1.45-1.53(m, 16H), 3.27(t, 16H), 7.19(dd, 2H), 8.01(d, 2H), 8.57(d, 2H).



Scheme 4.4. Schematic representation for the synthesis of compound $[\text{Bu}_4\text{N}]_2[\text{Pt}(\text{ppdt})_2]$ (**2**).

4.2.4. Single Crystal Structure Determination

Single crystals suitable for facile structural determination for the compounds (**1** and **2**), were measured on a three circle Bruker SMART APEX CCD area detector system under Mo- $\text{K}\alpha$ ($\lambda = 0.71073 \text{ \AA}$) graphite monochromatic X-ray beam. The frames were recorded with an ω scan width of 0.3° , each for 8 s, crystal-detector distance 60 mm, collimator 0.5 mm. Data reduction performed by using SAINTPLUS.²⁰ Empirical absorption corrections using equivalent reflections performed program SADABS.²⁰ The Structures were solved by direct methods and least-square refinement on F^2 for the compounds **1** and **2** by using SHELXS-97.²¹ All non-hydrogen atoms were refined anisotropically. The hydrogen atoms

were included in the structure factor calculation by using a riding model. The crystallographic parameters, data collection and structure refinement of the compounds **1** and **2** are summarized in Table 4.1. Selected bond lengths and angles for the compounds **1** and **2** are listed in Table 4.2.

4.3. Results and Discussion

4.3.1. Synthesis and Characterization

The synthetic route for the synthesis of ligand (H₂ppdt) has been shown Scheme 4.2, started from *o*-phenylenediamine in three steps. Synthesis of metal complexes was performed through a general common procedure, as shown in Schemes 4.3, and the {ppdt}²⁻ ions are generated, *in situ*, by the reaction of ligand (H₂ppdt) in basic medium containing MeOH solution, which are reacted with corresponding metal chloride salts resulting the respective metal complexes **1** and **2** and isolated as tetrabutylammonium salts by the addition of Bu₄NBr. Metal complexes **1** and **2** were recrystallized from acetonitrile solution by the vapour diffusion of diethyl ether. Crystals of compounds **1** and **2** have been characterized by single crystal X-ray structure determination. Complexes **1** and **2** have been further characterized by NMR spectroscopy including their elemental analysis.

4.3.2. Electronic Absorption Spectra

The absorption spectra of complexes [Bu₄N]₂[Ni(ppdt)₂] (**1**) and [Bu₄N]₂[Pt(ppdt)₂] (**2**) in MeOH are shown in Figure 4.1. The broad band's observed in the visible region centered at ~565 nm ($\epsilon = 20400 \text{ L mol}^{-1}\text{cm}^{-1}$) for complex **1** and at ~540 nm ($\epsilon = 25700 \text{ L mol}^{-1}\text{cm}^{-1}$) for complex **2** are due to the charge transfer transitions involving electronic excitation from a HOMO which is a mixture of dithiolate (π) and metal (*d*) orbital character to a LUMO which is a π^* orbital of the dithiolate, that are characteristics of metal(II) bis dithiolene complexes.^{22,23} Comparison of these visible bands for complexes **1** and **2** with those of [M(qdt)₂]²⁻ (M = Ni, Pt), demonstrate that the present system (compounds **1** and **2**) undergo bathochromic shift with larger molar absorptivity {[Ni(qdt)]²⁻, $\lambda_{\text{max}} = 540 \text{ nm}$, $\epsilon = 17900 \text{ L mol}^{-1}\text{cm}^{-1}$ in MeOH; [Pt(qdt)]²⁻, $\lambda_{\text{max}} = 510 \text{ nm}$, $\epsilon = 25000 \text{ L mol}^{-1}\text{cm}^{-1}$ in MeOH}. In the present system having three nitrogen atoms in each dithiolate ligand, the relatively large molar absorptivity for the both complexes **1** and **2**, compared to that of “two-nitrogen-dithiolene” system [M(qdt)₂]²⁻ is probably due to the increase in the

delocalization of the nitrogen-lone paired electrons from three nitrogen atoms (complexes **1** and **2**) compared to the delocalization from two nitrogen atoms (each dithiolene ligand) in the qdt complexes $[\text{Ni}(\text{qdt})_2]^{2-}$ and $[\text{Pt}(\text{qdt})_2]^{2-}$. Because of the more delocalization of lone paired electrons from nitrogen atoms (complexes **1** and **2**), the energy gap between HOMO and LUMO is reduced and shifts to more low energy region compared to the corresponding metal-qdt complexes.

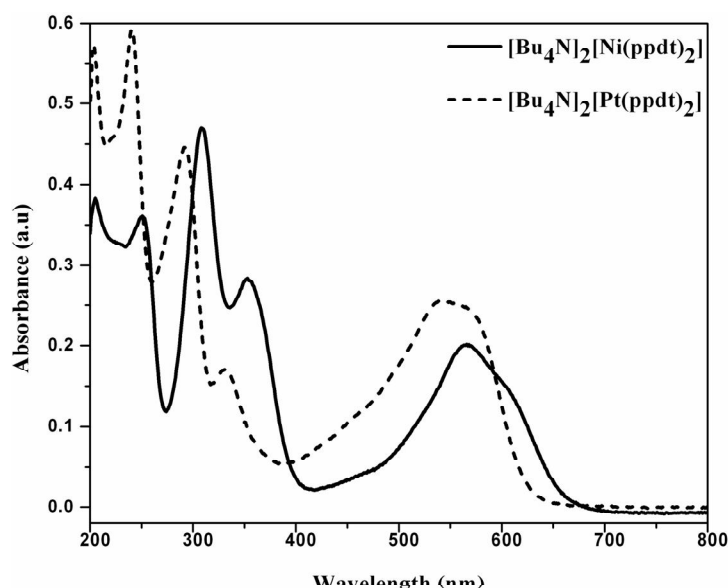


Figure 4.1. Electronic absorption spectra for the compounds **1** and **2** in MeOH ($1 \times 10^{-5} \text{M}$).

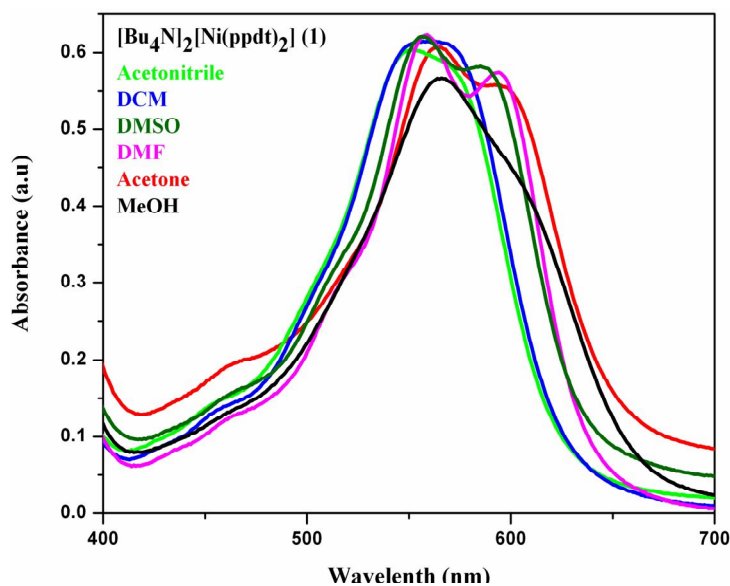


Figure 4.2. Solvatochromic effect on the absorption spectra of complex $[\text{Bu}_4\text{N}]_2[\text{Ni}(\text{ppdt})_2]$ (**1**).

Furthermore, comparison of the charge transfer transition visible bands among the complexes **1** and **2**, complex **1** absorbs in low energy region (565 nm) compared to that (540 nm) of complex **2**. This indicates metal orbital involvement in the transition. The ordering of MLCT energies as Pt(II) > Ni(II) is in accordance with that of several other homologous series of Ni(II), Pd(II), and Pt(II) square planar complexes containing cyanide and dithiolate ligands {Pd(II) > Pt(II) \approx Ni(II)}.^{22–24} The effect of solvent polarity on the absorption bands in the visible region for the complexes **1** and **2** are shown in Figures 4.2 and 4.3, respectively. When the solvent polarity increases, the absorption maxima shifts to lower energy region meaning that bathochromic shifts occur for the compounds **1** and **2**. The bathochromic shift is due to more stabilization of the excited state than ground state with increasing the polarity of solvent molecules. This reduces the energy gap between the ground state and excited state and it shifts to red region. In aprotic solvents, the broad band in the visible region is separated into two well-resolved maxima for the complex [Bu₄N]₂[Pt(ppdt)₂] (**2**), whereby it is not resolved in protic solvents, for example in MeOH, and shows a broad band in the visible region but absorption maxima shifts to higher energy region centered at \sim 540 nm as shown in Figure 4.3. The same observation was reported in the literature for Pt-qdt complex.²² In the case of nickel complex [Bu₄N]₂[Ni(ppdt)₂] (**1**), the broad band in the visible region is not well separated in contrast to well-separation in the case of corresponding Pt-ppdt complex. However, in protic solvents, compound **1** shows only broad feature in the visible region centered at \sim 565 nm as shown in Figure 4.2.

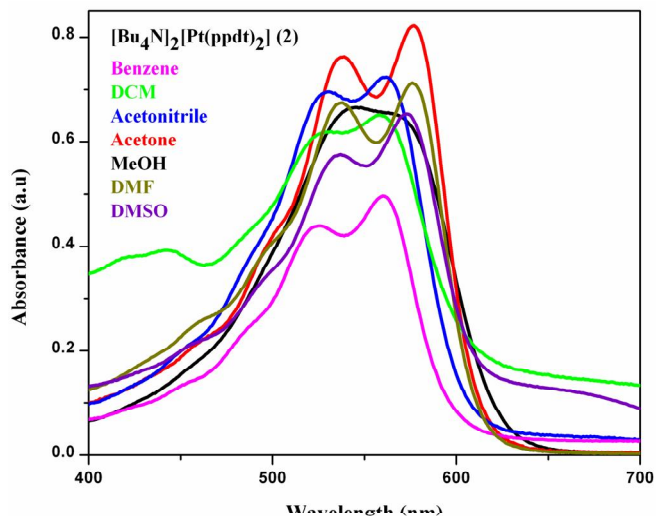


Figure 4.3. Solvatochromic effect on the absorption spectra of complex [Bu₄N]₂[Pt(ppdt)₂] (**2**).

pH-Dependant Absorption Spectral Studies of $[\text{Bu}_4\text{N}]_2[\text{Ni}(\text{ppdt})_2]$ (**1**)

Because of the presence of available lone pair of electrons on nitrogen atoms of dithiolene ligands, we performed pH dependent absorption spectral studies by titrating with both weak and strong acids. Figure 4.4 shows the spectral changes that occur upon the addition of 10 μL aliquots of a dilute CH_3COOH solution ($3.51 \times 10^{-1}\text{M}$ in methanol). The observed spectral changes contain a large red shift in visible region from wavelength 565 nm to 670 nm. The steady diminish in the absorption band at 565 nm is accompanied by the appearance of a new band feature with a maximum at 670 nm and a little increase in absorbance at 415 nm region as shown in Figure 4.4(a).

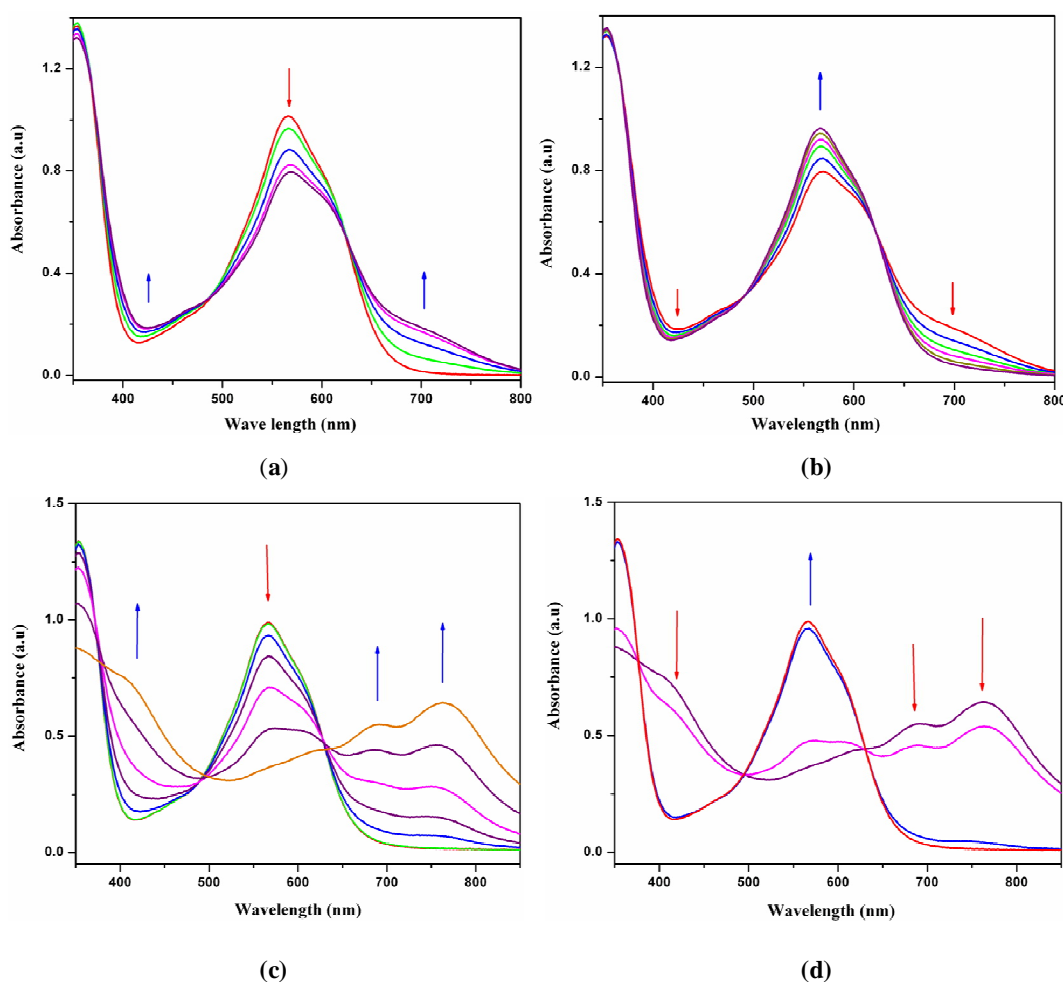


Figure 4.4. (a) Changes in the absorption spectra of $[\text{Bu}_4\text{N}]_2[\text{Ni}(\text{ppdt})_2]$ (**1**) ($4.3 \times 10^{-5}\text{M}$) upon addition of 10 μL aliquots of dilute CH_3COOH ($3.51 \times 10^{-1}\text{M}$) in methanol. (b) Spectral changes upon addition of 10 μL aliquots of dilute aq. NH_3 (1.068M) in methanol to the protonated species (blue colored) of **1** ($4.3 \times 10^{-5}\text{M}$). (c) Changes in the absorption spectra of $[\text{Bu}_4\text{N}]_2[\text{Ni}(\text{ppdt})_2]$ (**1**) ($4.3 \times 10^{-5}\text{M}$) upon addition of 10 μL aliquots of dilute HCl ($1.13 \times 10^{-1}\text{M}$) in methanol. (d) Back titration (spectral changes) upon addition of 10 μL aliquots of dilute NaOH (0.1875M) in methanol to the protonated species (blue colored) of **1** ($4.3 \times 10^{-5}\text{M}$).

Thus the complex **1** can be protonated by an acid at the imine nitrogen atoms of the ppdt ligand. During the titration with acetic acid, we observed clean isosbestic points that are maintained at 368, 488 and 623 nm [see Figure 4.4(a)]. This suggests that there are only two absorbing species in the concerned solution. The spectral changes, described above, are fully reversible upon addition of weak base such as aq. NH_3 . In the reverse titration with a weak base (aqueous NH_3), the same isosbestic points are maintained during the titration as shown in Figure 4.4(b).

When compound **1** was titrated with a strong acid, such as HCl in place of weak acid (CH_3COOH), additional changes are observed in the concerned electronic spectrum as shown in Figure 4.4(c). Thus, Figure 4.4(c) shows the changes in the absorption spectra of $[\text{Bu}_4\text{N}]_2[\text{Ni}(\text{ppdt})_2]$ (**1**) (4.3×10^{-5} M) upon addition of 10 μL aliquots of dilute HCl (1.13×10^{-1} M) in methanol. While titrating with HCl, the observed spectral changes contain large red shift with appearance of new absorption bands at 688, and 762 nm, with diminishing of the band at 565 nm. This is in contrast to the fact that only one new band (670 nm) appears by titrating **1** with acetic acid. The isosbestic points are maintained during the initial titration with HCl, which are identical to those seen with acetic acid; upon continuing the titration with HCl, it leads to loss of the original set of isosbestic points with the emergence of a new set of isosbestic points at 382, 494, 632 nm. This clearly indicates the involvement of second nitrogen atom in the acid base behavior in the case of strong acid. This is further corroborated by the appearance of a new set of isosbestic points as shown in Figure 4.4(c). This process is reversible by the back titration with dil. NaOH in methanol solution as shown in Figure 4.4(d). The identical results were obtained with other strong acid such as CF_3COOH .

pH-Dependent Absorption Spectra of $[\text{Bu}_4\text{N}]_2[\text{Pt}(\text{ppdt})_2]$ (2**)**

The red color of neutral solution of $[\text{Bu}_4\text{N}]_2[\text{Pt}(\text{ppdt})_2]$ (**2**) also turns to deep blue when it is treated with acetic acid. Therefore we performed pH dependent absorption spectral studies by titrating compound **2** with both weak and strong acids. Figure 4.5(a) shows changes in the absorption spectra of $[\text{Bu}_4\text{N}]_2[\text{Pt}(\text{ppdt})_2]$ (**2**) (3.56×10^{-5} M) upon addition of 10 μL aliquots of dilute CH_3COOH (3.51×10^{-1} M) in methanol. The observed spectral changes contain a large red shift in visible region from wavelength 545 nm to 645 nm. The steady diminish in the absorption band at 545 nm is accompanied by the appearance of a new band feature with a maximum at 645 nm and a little increase in absorbance at 390 nm

region as shown in Figure 4.5(a). Thus the complex **2** can be protonated by an acid at the imine nitrogen atoms of the ppdt ligand. During the titration with acetic acid, we observed clean isosbestic points that are maintained at 348, 470 and 593 nm [see Figure 4.5(a)]. This suggests that there are only two absorbing species in the concerned solution. The spectral changes, described above, are fully reversible upon addition of weak base such as aq. NH_3 . In the reverse titration with a weak base (aqueous NH_3), the same isosbestic points are maintained during the titration as shown in Figure 4.5(b).

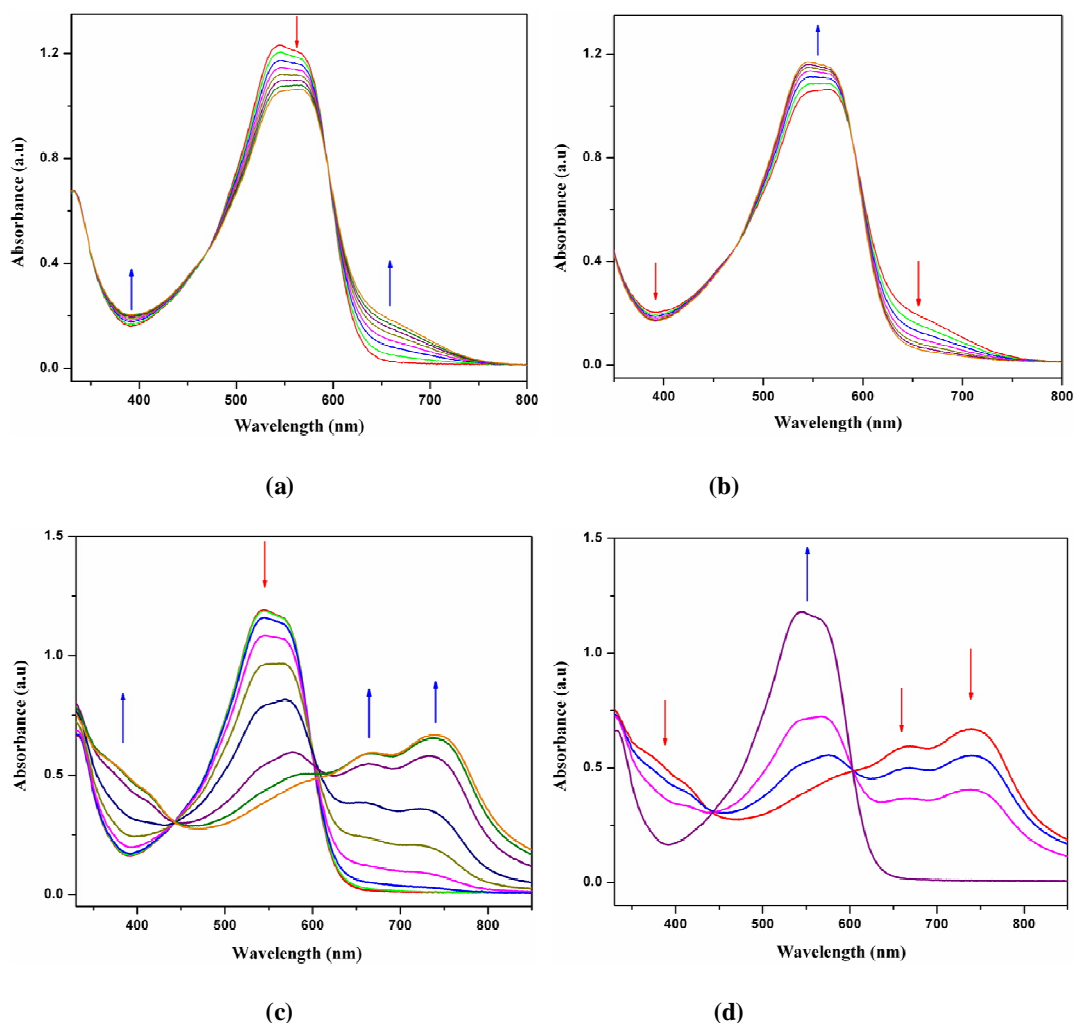


Figure 4.5. (a) Changes in the absorption spectra of $[\text{Bu}_4\text{N}]_2[\text{Pt}(\text{ppdt})_2]$ (**2**) (3.56×10^{-5} M) upon addition of 10 μL aliquots of dilute CH_3COOH (3.51×10^{-1} M) in methanol. (b) Back titration (spectral changes) upon addition of 10 μL aliquots of dilute aq. NH_3 (1.068 M) in methanol to the protonated species (blue colored) of **2** (3.56×10^{-5} M). (c) Changes in the absorption spectra of $[\text{Bu}_4\text{N}]_2[\text{Pt}(\text{ppdt})_2]$ (**2**) (3.56×10^{-5} M) upon addition of 10 μL aliquots of dilute HCl (1.13×10^{-1} M) in methanol. (d) Back titration (spectral changes) upon addition of 10 μL aliquots of dilute NaOH (0.1875 M) in methanol to the protonated species (blue colored) of **2** (3.56×10^{-5} M).

If the titration of the complex $[\text{Bu}_4\text{N}]_2[\text{Pt}(\text{ppdt})_2]$ (**2**) is performed with strong acid, such as HCl in place of weak acid (acetic acid), additional changes are observed in the relevant spectra as shown in Figure 4.5(c). Thus, Figure 4.5(c) shows the changes in the absorption spectra of $[\text{Bu}_4\text{N}]_2[\text{Pt}(\text{ppdt})_2]$ (**2**) (3.56×10^{-5} M) upon addition of 10 μL aliquots of dilute HCl (1.13×10^{-1} M) in methanol. While titrating with HCl, the observed spectral changes contain large red shift with appearance of new absorption bands at 670 and 740 nm, with diminishing the band at 545 nm, whereas only one new band appeared at 645 nm by the titrating with acetic acid. The isosbestic points are maintained during the initial titration with HCl, which are identical to those seen with acetic acid. Continuation of the titration with HCl leads to loss of the original set of isosbestic points and the emergence of a new set of isosbestic points at 350, 443, 618 nm. This again indicates the involvement of a second nitrogen atom of the ring for its protonation with a strong acid. This process is reversible by the back titration with dil. NaOH in methanol solution as shown in Figure 4.5(d). Qualitatively, the same results were obtained with other strong acid such as CF_3COOH .

4.3.3. Emission Spectra

The complex $[\text{Bu}_4\text{N}]_2[\text{Ni}(\text{ppdt})_2]$ (**1**) is not emissive. But the complex $[\text{Bu}_4\text{N}]_2[\text{Pt}(\text{ppdt})_2]$ (**2**) exhibits moderate emission at 635 nm (excited at 543 nm) at room temperature as shown in Figure 4.6. The similar emission was observed for reported $[\text{Bu}_4\text{N}]_2[\text{Pt}(\text{qdt})_2]$ complex.¹⁵ pH-Dependent emission spectral studies for compound **2** are described below. The emission spectra of compound **2** in MeOH in different concentrations are shown in Figure 4.6.

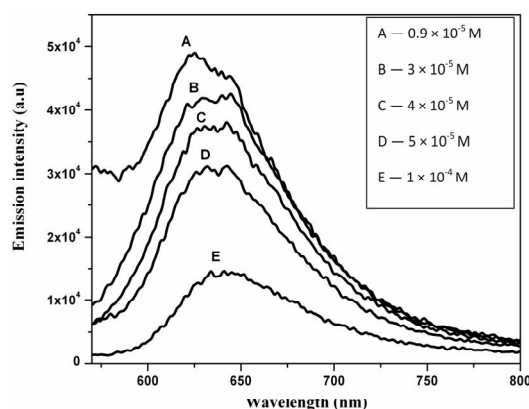


Figure 4.6. Emission spectrum of complex $[\text{Bu}_4\text{N}]_2[\text{Pt}(\text{ppdt})_2]$ (**2**) in MeOH in different concentrations at 298K.

pH-Dependent Emission Spectra of $[\text{Bu}_4\text{N}]_2[\text{Pt}(\text{ppdt})_2]$ (**2**)

We extended pH dependent spectral studies to emission spectroscopy for complex $[\text{Bu}_4\text{N}]_2[\text{Pt}(\text{ppdt})_2]$ (**2**) by titrating with both weak and strong acids. Figure 4.7(a) shows the changes in the emission spectra of $[\text{Bu}_4\text{N}]_2[\text{Pt}(\text{ppdt})_2]$ (**1**) (1.07×10^{-4} M) upon addition of 10 μL aliquots of dilute CH_3COOH (5.26×10^{-1} M) in methanol. While titrating with acetic acid, the observed spectral changes contain a red shift with appearance of new broad red feature at 750 nm, with the band at 642 nm diminishing. The new emission broad feature, observed at 750 nm upon protonation, is not very prominent compared to the initial band

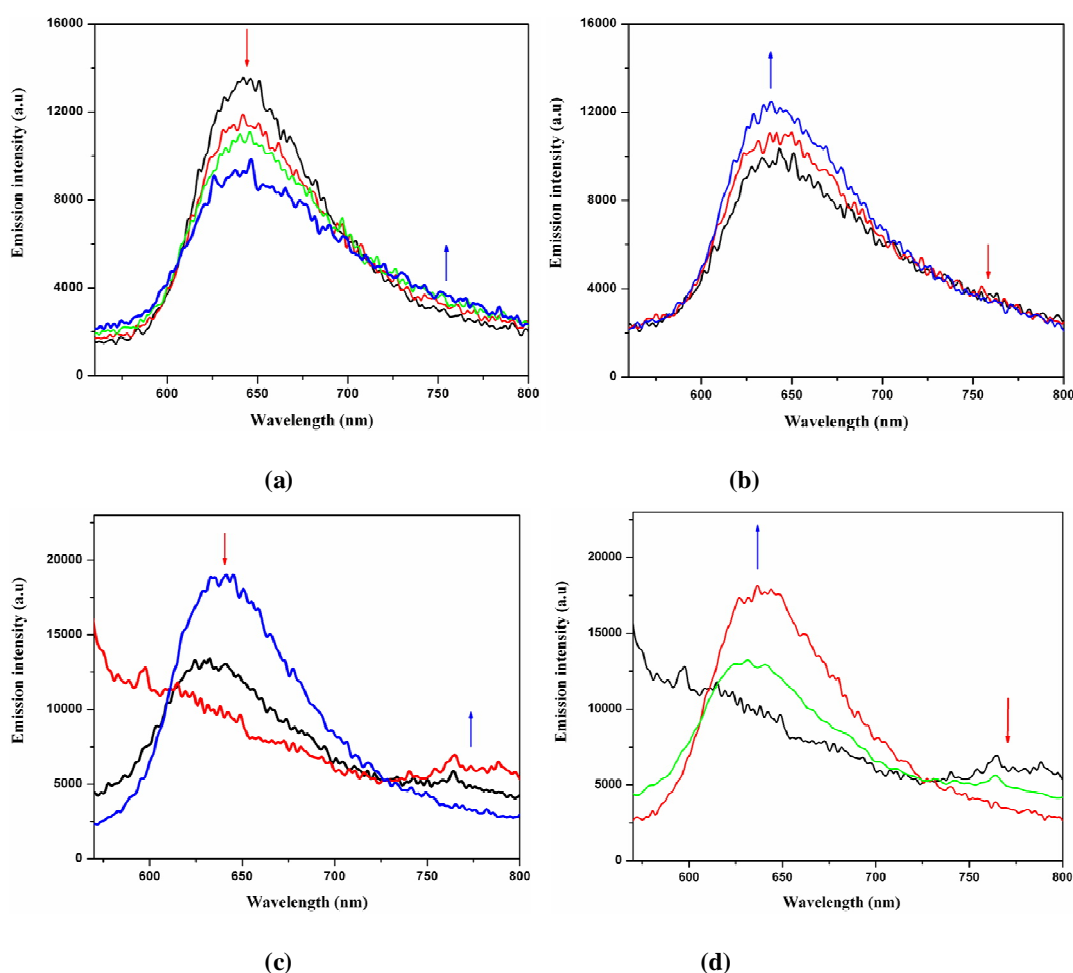


Figure 4.7. (a) Changes in the emission spectra of $[\text{Bu}_4\text{N}]_2[\text{Pt}(\text{ppdt})_2]$ (**2**) (1.07×10^{-4} M) upon addition of 10 μL aliquots of dilute CH_3COOH (5.26×10^{-1} M) in methanol. (b) Back titration (spectral changes) upon addition of 10 μL aliquots of dilute aq. NH_3 (5.34×10^{-1} M) in methanol to the protonated species of compound **2**. (c) Changes in the emission spectra of $[\text{Bu}_4\text{N}]_2[\text{Pt}(\text{ppdt})_2]$ (**2**) (1.07×10^{-4} M) upon addition of 10 μL aliquots of dilute HCl (5.0×10^{-2} M) in methanol. (d) Back titration (spectral changes) upon addition of 10 μL aliquots of dilute NaOH (5.14×10^{-2} M) in methanol to the protonated species of compound **2** (3.56×10^{-5} M).

without protonation. During the titration with acetic acid, we observed isosbestic points that are maintained at 607 and 710 nm [see Figure 4.7(a)]. In addition, the process is completely reversible with addition of base such as aq. NH_3 regenerating the initial emission profile as shown in Figure 4.7(b). When we titrate the complex $[\text{Bu}_4\text{N}]_2[\text{Pt}(\text{ppdt})_2]$ (**2**) with strong acid such as HCl in place of weak acid such as acetic acid, the emission spectrum diminishes leading to a featureless curve as shown in Figure 4.7(c). Thus, Figure 4.7(c) shows the changes in the emission spectra of $[\text{Bu}_4\text{N}]_2[\text{Pt}(\text{ppdt})_2]$ (**2**) (1.07×10^{-4} M) upon addition of 10 μL aliquots of dilute HCl (5.0×10^{-2} M) in methanol. Remarkably, even though the emission spectrum became featureless by the addition of HCl acid, this process is reversible by the back titration with dil. NaOH in methanol solution as shown in Figure 4.7(d), when the featureless curve regenerates to the original emission spectrum.

4.3.4. Determination of Basicity Constants

During the titration with acetic acid, complex **2** is singly protonated, because a set of clean isosbestic points is maintained throughout the conversion from the unprotonated dianionic complex to singly protonated monoanionic species. Thus, from this data we would be able to determine the basicity constant $\text{p}K_{\text{b1}}$. To determine the basicity constant $\text{p}K_{\text{b1}}$, we performed titration of complex $[\text{Bu}_4\text{N}]_2[\text{Pt}(\text{ppdt})_2]$ (**2**) with acetic acid, and plot the diagram of pH versus percent of change in absorbance as shown in Figure 4.8. Therefore, the inflection of the titration curve from the data in Figure 4.8 can be used to calculate ground state basicity constant $\text{p}K_{\text{b1}}$; the value of $\text{p}K_{\text{b1}}$ was found to be 7.8 and this value supports that the complex is moderately basic. The value of $\text{p}K_{\text{b1}} = 7.8$ of complex $[\text{Bu}_4\text{N}]_2[\text{Pt}(\text{ppdt})_2]$ (**2**), which is considerably smaller than the reported $\text{p}K_{\text{b1}}$ of complex $[\text{Bu}_4\text{N}]_2[\text{Pt}(\text{qdt})_2]$ (6.9). This means that the complex $[\text{Bu}_4\text{N}]_2[\text{Pt}(\text{ppdt})_2]$ (**2**) is less basic than the reported complex $[\text{Bu}_4\text{N}]_2[\text{Pt}(\text{qdt})_2]$.¹⁵

An estimate of the excited state basicity constant $\text{p}K_{\text{b}}^*$ can be calculated by using an equation which is developed by Förster, based on purely thermodynamic principles, and employed with varying success for many acid–base systems, which relates $\text{p}K_{\text{b}}^*$ to $\text{p}K_{\text{b}}$ using only the frequencies of the E_{0-0} transition for the basic (ν_{B}) and protonated (ν_{BH^+}) form of the complex.¹⁵

$$\text{p}K_{\text{b}}^* = \text{p}K_{\text{b}} - \frac{N\hbar}{2.303RT}(\nu_{\text{B}} - \nu_{\text{BH}^+})$$

Where N Avogadro's number, h is planck's constant, R is the gas constant, and T is the temperature. The use of absorption maxima for $[\text{Pt}(\text{ppdt})_2]^{2-}$ (545nm) and $[\text{Pt}(\text{ppdt})(\text{Hppdt})]^{1-}$ (645 nm) yields a $\Delta \text{p}K_b$ of 6.0 and an excited state basicity constant $\text{p}K_b^*$ of 1.8. Qualitatively, these results indicate that the Förster analysis predicts an excited state which is more basic than ground state.

To determine the basicity constant $\text{p}K_{b1}$ for the complex $[\text{Bu}_4\text{N}]_2[\text{Ni}(\text{ppdt})_2]$ (**1**), we performed titration with acetic acid, and plot the diagram of pH versus percent of change in absorbance as shown in Figure 4.8. Therefore, the inflection of the titration curve from the data in Figure 4.8 can be used to calculate ground state basicity constant $\text{p}K_{b1}$, which was found to be 8.0 and this value supports that the complex is moderately basic. The value of $\text{p}K_{b1} = 8.0$ of complex $[\text{Bu}_4\text{N}]_2[\text{Ni}(\text{ppdt})_2]$ (**1**) is closer to the $\text{p}K_{b1}$ of Pt-ppdt complex $[\text{Bu}_4\text{N}]_2[\text{Pt}(\text{ppdt})_2]$ (**2**).

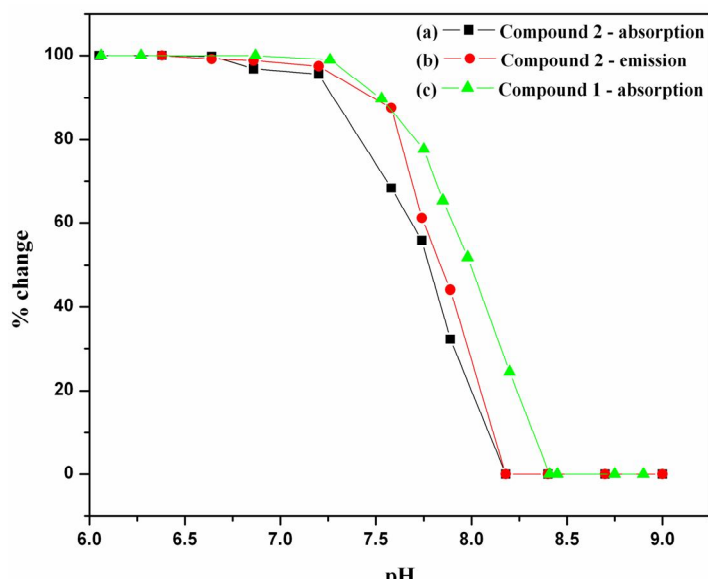


Figure 4.8. Titration curves for $[\text{Bu}_4\text{N}]_2[\text{Pt}(\text{ppdt})_2]$ (**2**) in water (10% MeOH added), using (a) percent change in absorbance at 513 nm (■) and (b) percent change in emission intensity at 650 nm (●) versus pH. (c) Titration curve for $[\text{Bu}_4\text{N}]_2[\text{Ni}(\text{ppdt})_2]$ (**1**) in water (10% MeOH added), using percent change in absorbance at 544 nm (▲) versus pH.

4.3.5. Electrochemistry

As shown in Figure 4.9, complex **1** undergoes quasi-reversible oxidation ($\Delta E = 0.12$ V) at $E_{1/2} = +0.46$ V vs Ag/AgCl, that corresponds the $[\text{Ni}(\text{ppdt})_2]^{1-}/[\text{Ni}(\text{ppdt})_2]^{2-}$ redox couple, indicating that Ni(III) complex $[\text{Ni}(\text{ppdt})_2]^{1-}$ is fairly stable in the electrochemical scale.

Similar oxidative response was observed for the qdt-based compound $[\text{Bu}_4\text{N}]_2[\text{Pt}(\text{qdt})_2]$.¹⁵ On the other hand, $[\text{Bu}_4\text{N}]_2[\text{Pt}(\text{ppdt})_2]$ (**2**) exhibit an irreversible oxidation at $E_{1/2} = +0.41 \text{ V}$ vs Ag/AgCl, suggesting that the $[\text{Pt}(\text{ppdt})_2]^{1-}$ is unstable in the electrochemical scale.

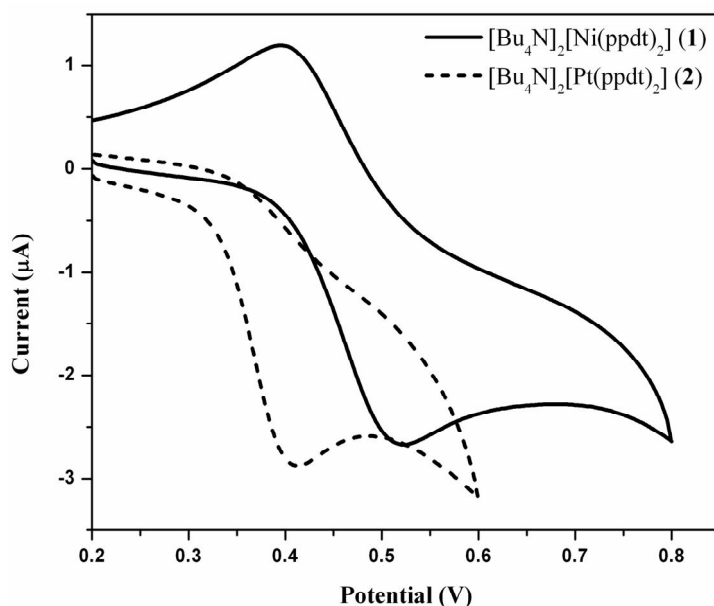


Figure 4.9. Cyclic voltammograms of compounds **1** and **2** in TBAP/MeOH at a scan rate 50 mV s^{-1} .

4.3.6. X-ray Crystallographic Studies

Crystal Structure Descriptions of Compounds **1** and **2**

The crystals of both compounds **1** and **2**, suitable for single crystal X-ray structure determination, were obtained from acetonitrile solution by the vapor diffusion of diethyl ether. Crystallographic analysis revealed that complex **1** crystallizes in monoclinic form with space group $P2_1/c$, whereas the complex **2** crystallizes in monoclinic space group $C2/c$. The relevant asymmetric unit of the complex **1** contains the full molecule of $[\text{Bu}_4\text{N}]_2[\text{Ni}^{\text{II}}(\text{ppdt})_2]$ (**1**) but in the asymmetric unit of the complex **2** contains half molecule of $[\text{Bu}_4\text{N}]_2[\text{Pt}(\text{ppdt})_2]$ (**2**) are shown in Figures 4.10 and 4.11, respectively. The crystallographic details and relevant bond lengths and angles for the compounds **1** and **2** are described in Tables 4.1 and 4.2, respectively. In the anion present in the complex **1**, the geometry around the nickel ion, which is coordinated by four sulfur atoms from two ppdt ligands, are almost square planar because S–Ni–S coordination angles are in the range of $88.50(5)^\circ$ to $91.48(5)^\circ$ (Table 4.2) and with a small dihedral angle 9.31° between two ppdt

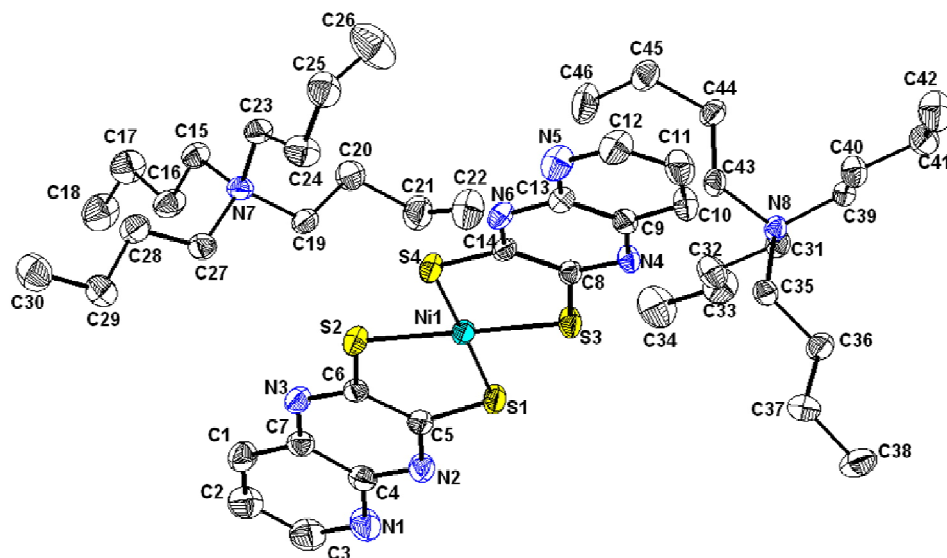


Figure 4.10. Thermal ellipsoidal plot of the asymmetric unit of compound $[\text{Bu}_4\text{N}]_2[\text{Ni}(\text{ppdt})_2]$ (**1**), that contains two tetrabutylammonium cations and one $[\text{Ni}(\text{ppdt})_2]^{2-}$ ion. Hydrogen atoms are not shown for clarity (20% probability).

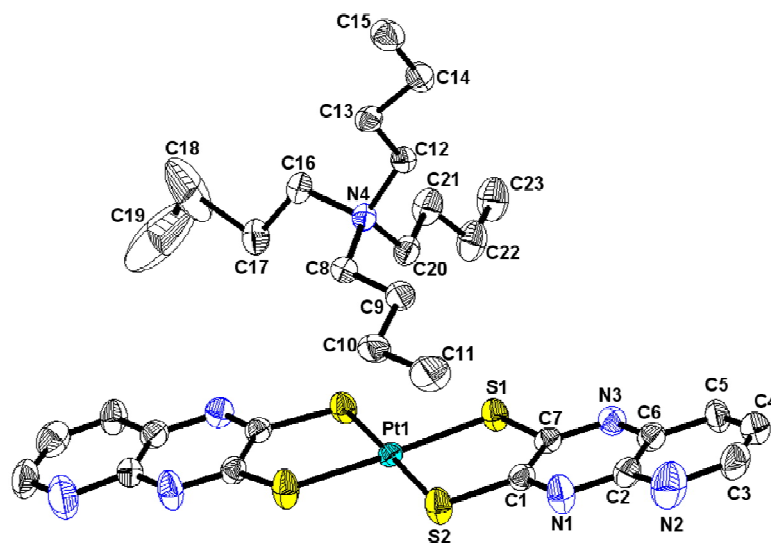


Figure 4.11. Thermal ellipsoidal plot of the asymmetric unit of compound $[\text{Bu}_4\text{N}][\text{Pt}(\text{ppdt})_2]$ (**2**), that contains one tetrabutylammonium cation and half molecule of $[\text{Pt}(\text{ppdt})_2]^{2-}$ ion. Hydrogen atoms are not shown for clarity (20% probability).

planes, which is comparable to that in nickel-qdt complex $[\text{Ni}(\text{qdt})_2]$.²⁵ But in the anion of the complex **2**, the geometry around the platinum ion, which is coordinated by four sulfur atoms from two ppdt ligands, are almost square planar because S–Pt–S coordination angles are in the range of $88.54(6)^\circ$ to $91.66(9)^\circ$ (Table 4.2) and with a small dihedral angle 1.16° between two ppdt planes, which is less than the dihedral angle found in the

crystal structure of nickel-ppdt complex **1**. This shows that when we go from nickel-ppdt complex (**1**) to platinum-ppdt (**2**) complex, the geometry around platinum ion becomes more planar in compound **2** because of increasing the size of the platinum ion (e.g., from Ni^{2+} to Pt^{2+}). The average bond distance of Pt-S is 2.280 ± 0.002 Å in compound **2**, which is relatively larger than that in compound $[\text{Bu}_4\text{N}]_2[\text{Ni}(\text{ppdt})_2]$ (**1**), for which the average bond distance of Ni-S is 2.171 ± 0.002 Å.

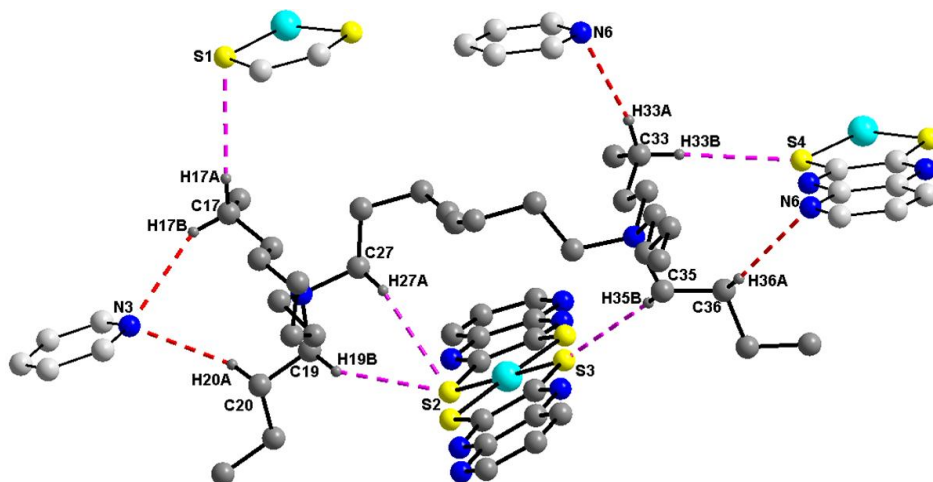


Figure 4.12. A View of the molecular structure of $[\text{Bu}_4\text{N}]_2[\text{Ni}(\text{ppdt})_2]$ (**1**) (thick solid lines) (some hydrogen atoms are removed for clarity) showing all the H-bonding intermolecular cation-anion contacts (dotted lines) with other surrounding moieties (thin solid lines).

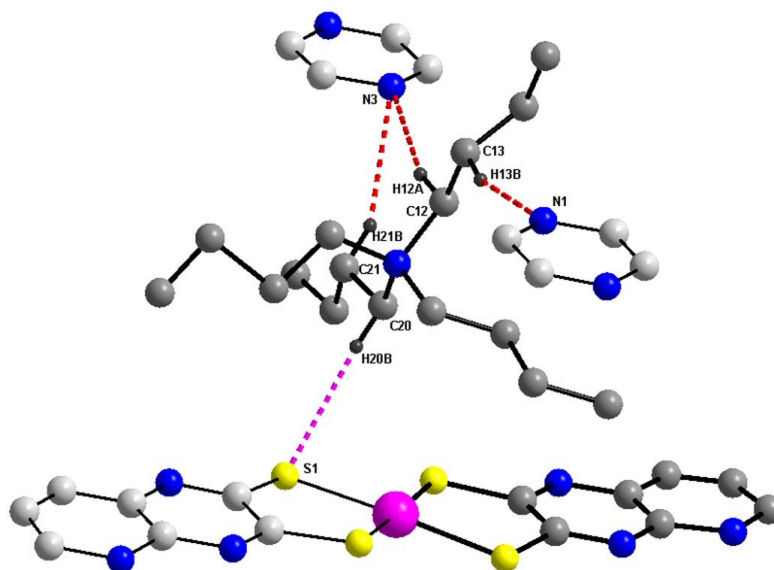


Figure 4.13. A View of the molecular structure of $[\text{Bu}_4\text{N}]_2[\text{Pt}(\text{ppdt})_2]$ (**2**) (thick solid lines) (some hydrogen atoms are removed for clarity) showing all the H-bonding intermolecular cation-anion contacts (dotted lines) with other surrounding moieties (thin solid lines).

In the crystal structures of the complexes **1** and **2**, both cations $[\text{Bu}_4\text{N}]^+$ and anions $[\text{M}(\text{ppdt})_2]^{2-}$ are involved in an extensive hydrogen bonding interactions resulting in a three dimensional supramolecular networks. The views of the building units for the formation of supramolecular networks of the complexes **1** and **2**, with the evidence of all the H-bonding intermolecular cation-anion contacts, are shown in Figures 4.12 and 4.13, respectively. The relevant hydrogen bonding geometrical parameters of the complexes **1** and **2** are listed in the Tables 4.3 and 4.4, respectively. The molecular packing of compound **1** is characterized by $\text{C}-\text{H}\cdots\text{S}$ and $\text{C}-\text{H}\cdots\text{N}$ weak interactions resulting in a three-dimensional supramolecular network as shown in Figures 4.14.

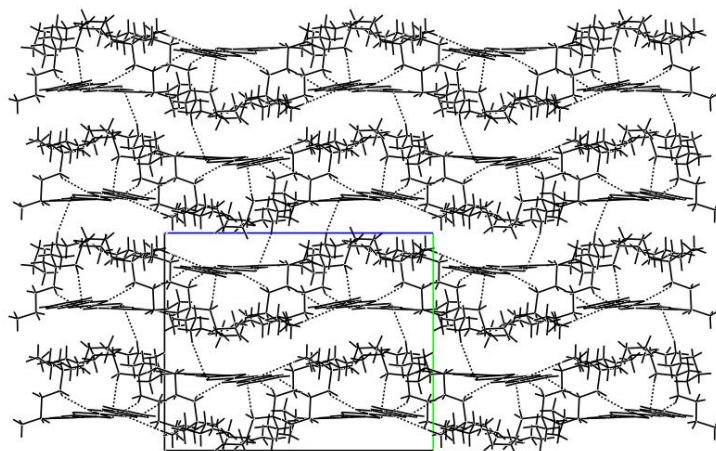


Figure 4.14. The molecular packing diagram of $[\text{Bu}_4\text{N}]_2[\text{Ni}(\text{ppdt})_2]$ (**1**) is characterized by $\text{C}-\text{H}\cdots\text{N}$ and $\text{C}-\text{H}\cdots\text{S}$ weak interactions, when viewed down to the crystallographic a axis.

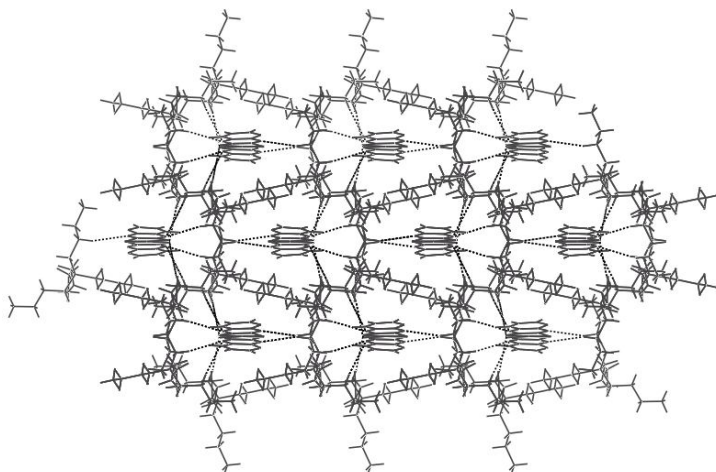


Figure 4.15. The molecular packing diagram of $[\text{Bu}_4\text{N}]_2[\text{Pt}(\text{ppdt})_2]$ (**2**) characterized by $\text{C}-\text{H}\cdots\text{N}$ and $\text{C}-\text{H}\cdots\text{S}$ weak interactions, when viewed down to the crystallographic a axis.

In the crystal structure of the complex **2**, each tetrabutylammonium cation is characterized by four H-bond contacts (one C–H...S and three C–H...N weak interactions) with three surrounding anions as shown in Figure 4.13. Wherein, three of them are described as C–H...N interactions with N1 and N3 atoms of two distinct anions, positioned at $x, -y, z+0.5$ and $0.5-x, 0.5-y, 1-z$ respectively. The remaining one is described as C–H...S weak interaction with S1 atom of other anion positioned at $-x, y, 0.5-z$ symmetry. The weak hydrogen bonding interactions between cation and anion due to ionic nature of compounds may induce the charge effect. The effective combination of the C–H...S and C–H...N hydrogen bonding interactions in the crystal structure of the complex **2** results in a three-dimensional supramolecular network having well defined channels as shown in Figure 4.15, that is viewed down to crystallographic a axis. As shown in the packing diagram (Figure 4.15), each dithiolate ligand connects with three distinct tetrabutylammonium cations characterized by four weak H-bonding interactions. Thus, each metal-dithiolene complex anion is surrounded by six discrete tetrabutylammonium cations.

4.4. Conclusion

In conclusion, we have described here for the first time a “three-nitrogen” based metal bis(dithiolene) system $[\text{Bu}_4\text{N}]_2[\text{M}(\text{ppdt})_2]$ [when $\text{M} = \text{Ni}$ (**1**), when $\text{M} = \text{Pt}$ (**2**)], that shows a very large molar absorptivity in the visible region. We have also described that the crystal structures of compounds **1** and **2** show three dimensional supramolecular hydrogen bonding network formed by C–H...S and C–H...N weak interactions. We have shown that both compounds $[\text{Bu}_4\text{N}]_2[\text{Ni}(\text{ppdt})_2]$ (**1**) and $[\text{Bu}_4\text{N}]_2[\text{Pt}(\text{ppdt})_2]$ (**2**) can be protonated by acids at the imine nitrogen of the ppdt ligand. This protonation is reflected by a red shift of the charge transfer (CT) bands of the respective complexes. A red shift of the CT absorption and emission bands is consistent with stabilization of the π^* orbital of ppdt ligand upon protonation. The easiness with which the compounds **1** and **2** are protonated is the result of their di-anionic charge. Compounds **1** and **2** represent a rare class of materials¹⁵ in the sense that such system may be of interest in developing visible light induced photocatalysts for proton reduction. Interestingly, this system can be easily protonated and has increased basicity upon excitation (in case of compound **2**), which are necessary criteria for a potential photocatalyst.

Table 4.1. Crystallographic Data and Structural Refinement for Compounds **1** and **2**

	1	2
Empirical formula	C ₄₆ H ₇₈ N ₈ S ₄ Ni	C ₄₆ H ₇₈ N ₈ S ₄ Pt
Formula weight	930.11	1066.49
Temperature (K)	298(2)	298(2)
Crystal size (mm)	0.36x 0.16 x 0.10	0.42 x 0.22 x 0.12
Crystal system	Monoclinic	Monoclinic
Space group	<i>P</i> 2(1)/ <i>c</i>	<i>C</i> 2/ <i>c</i>
Z	4	4
Wavelength(Å)	0.71073	0.71073
Unit cell dimensions		
<i>a</i> [Å]	16.406(2)	18.290(4)
<i>b</i> [Å]	15.904(2)	20.654(4)
<i>c</i> [Å]	20.180(3)	16.262(3)
β [°]	102.704(3)	122.57(3)
Volume[Å ³]	5136.4(13)	5177.0(18)
Calculated density(Mg/m ⁻³)	1.203	1.368
Reflections collected/ unique	48717/9038	24664 / 4577
R(int)	0.1025	0.0249
F(000)	2008	2208
Theta range for data collection(deg.)	1.27 to 25.00	1.65 to 25.00
Refinement method	Full-matrix least-squares on F ²	
Data / restraints / parameters	9038 / 0 / 540	4577 / 4 / 271
Goodness-of-fit on F ²	0.987	1.122
R ₁ /wR ₂ [I>2sigma(I)]	0.0594 / 0.1188	0.0372 / 0.1002
R ₁ /wR ₂ (all data)	0.1462 / 0.1518	0.0412 / 0.1022
Largest diff. peak and hole [e.Å ⁻³]	0.321 and -0.208	0.698 and -0.453

Table 4.2. Selected Bond Lengths [\AA] and Angles [$^\circ$] for Compounds **1** and **2**

1		2	
Ni(1)-S(1)	2.1736(13)	Pt(1)-S(2)#1	2.2786(17)
Ni(1)-S(2)	2.1723(13)	Pt(1)-S(2)	2.2787(17)
Ni(1)-S(3)	2.1687(13)	Pt(1)-S(1)	2.2834(16)
Ni(1)-S(4)	2.1718(13)	Pt(1)-S(1)#1	2.2834(16)
S(2)-Ni(1)-S(1)	91.48(5)	S(2)#1-Pt(1)-S(2)	91.66(9)
S(3)-Ni(1)-S(4)	91.41(5)	S(2)#1-Pt(1)-S(1)	177.23(8)
S(3)-Ni(1)-S(1)	88.63(5)	S(2)-Pt(1)-S(1)	88.54(6)
S(4)-Ni(1)-S(2)	88.50(5)	S(2)#1-Pt(1)-S(1)#1	88.54(6)
S(4)-Ni(1)-S(1)	178.44(6)	S(2)-Pt(1)-S(1)#1	177.23(8)
S(3)-Ni(1)-S(2)	179.40(6)	S(1)-Pt(1)-S(1)#1	91.39(8)

Symmetry transformations used to generate equivalent atoms: #1 -x, y, -z+1/2.

Table 4.3. Hydrogen Bonds for Compound **1**

D–H...A	d(D...H)	d(H...A)	d(D...A)	<(DHA)
C17–H17A...S1 #1	0.97	2.93	3.811(5)	152.0
C20–H20A...N3#2	0.97	2.77	3.692(7)	159.9
C17–H17B...N3#2	0.97	2.80	3.679(7)	151.5
C33–H33A...N6#3	0.97	2.72	3.676(7)	169.4
C36–H36A...N6#4	0.97	2.71	3.538(6)	143.7
C33–H33B...S4#4	0.97	2.96	3.918(6)	169.3
C35–H35B...S3#5	0.97	2.95	3.829(4)	150.8
C19–H19B...S2#5	0.97	2.95	3.837(4)	151.9
C27–H27A...S2#5	0.97	2.94	3.817(4)	150.3

Symmetry transformations used to generate equivalent atoms: #1 -x, y+0.5, -z+1.5; #2 x, -y+0.5, z+0.5; #3 -x+1, y+0.5, -z+1.5; #4 x, -y+0.5, z-0.5; #5 x, y, z.

Table 4.4. Hydrogen Bonds for Compound **2**

D–H···A	d(D···H)	d(H···A)	d(D···A)	<(DHA)
C13–H13B···N1 #1	0.97	2.58	3.516(8)	163.5
C12–H12A···N3#2	0.97	2.54	3.483(8)	164.2
C21–H21B···N3#2	0.97	2.70	3.609(10)	156.5
C20–H20B···S1#3	0.97	2.82	3.767(7)	165.7

Symmetry transformations used to generate equivalent atoms: #1 x, -y, z+0.5; #2 -x+0.5, -y+0.5, -z+1; #3 -x, y, -z+0.5.

4.5. References

- 1 Karlin, K. D.; Stiefel, E. I. *Prog. Inorg. Chem.* John Wiley, New York, **2004**, Volume 52.
- 2 Tanaka, H.; Okano, Y.; Kobayashi, H.; Suzuki, W. Kobayashi, A. *Science* **2001**, 291, 285.
- 3 Kato, R. *Chem. Rev.* **2004**, 104, 5319.
- 4 Coomber, A. T.; Beljonne, D.; Friend, R. H.; Brédas, J. L.; Charlton, A.; Robertson, N.; Underhill, A. E.; Kurmoo, M.; Day, P. *Nature* **1996**, 380, 144.
- 5 Robertson, N.; Cronin, L. *Coord. Chem. Rev.* **2002**, 227, 93.
- 6 Chen, C.-T.; Liao, S.-Y.; Lin, K.-J.; Lai, L.-L. *Adv. Mater.* **1998**, 3, 334.
- 7 Mueller-Westerhoff, U. T.; Vance, B.; Yoon, D. I. *Tetrahedron* **1991**, 47, 909.
- 8 Ren, X. M.; Nishihara, S.; Akutagawa, T.; Noro, S.; Nakamura, T. *Inorg. Chem.* **2006**, 45, 2229.
- 9 Majumdar, A.; Pal, K.; Sarkar, S. *J. Am. Chem. Soc.* **2006**, 128, 4196.
- 10 (a) Johnson, J. L.; Rajagopalan, K. V. *Proc. Natl. Acad. Sci. USA* **1982**, 79, 6856.
(b) Johnson, J. L.; Hainline, B. E.; Rajagopalan, K. V.; Arison, B. H. *J. Biol. Chem.* **1984**, 259, 5414.
- 11 (a) Boyde, S.; Garner, C. D.; Enemark, J. H.; Bruck, M. A.; Kristofzski, J. G. *J. Chem. Soc., Dalton. Trans.* **1987**, 2267. (b) Boyde, S.; Garner, C. D.; Enemark, J. H.; Ortega, R. B. *J. Chem. Soc., Dalton. Trans.* **1987**, 297. (c) Boyde, S.; Garner, C. D.; Enemark, J. H.; Ortega, R. B. *Polyhedron* **1986**, 5, 377.

- 12 Theriot, L. J.; Ganguli, K. K.; Kavarnos, S.; Bernal, I. *J. Inorg. Nucl. Chem.* **1969**, *31*, 3133.
- 13 Rignedoli, A.; Peyronel, G.; Malavasi, W. *J. Inorg. Nucl. Chem.* **1976**, *38*, 1963.
- 14 Mukhopadhyay, S.; Ray, D. *J. Chem. Soc., Dalton Trans.* **1993**, 1159.
- 15 Cummings, S. D.; Eisenberg, R. *Inorg. Chem.* **1995**, *34*, 3396.
- 16 Boyde, S.; Garner, C. D.; Enemark, J. H.; Ortega, R. B. *J. Chem. Soc., Dalton Trans.* **1987**, 297.
- 17 Bünzli, J. –C. G.; Chauvin, A. –S.; Imbert, D. *Module 4: Proton Transfer Reactions*.
- 18 Broceta, A. U.; Pineda-de-las-Infantas, M. J.; Mochón, J. J. D.; Romagnoli, R.; Baraldi, P. G.; Gallo, M. A.; Espinosa, A. *J. Org. Chem.* **2005**, *70*, 2878.
- 19 Morrison, D. C.; Furst, A. *J. Org. Chem.* **1955**, *21*, 470.
- 20 Bruker. *SADABS*, *SMART*, *SAINT* and *SHELXTL*, **2000** (Bruker AXS Inc., Madison, Wisconsin, USA).
- 21 Sheldrick, G. M. *Acta Crystallogr. Sect. A* **2008**, *64*, 112–122.
- 22 Cummings, S. D.; Eisenberg, R. *Inorg. Chem.* **1995**, *34*, 2007.
- 23 Shupack, S. I.; Billig, E.; Clark, R. J. H.; Williams, R.; Gray, H. B. *J. Am. Chem. Soc.* **1964**, *86*, 4594.
- 24 (a) Gray, H. B.; Bullhausen, C. J.; *J. Am. Chem. Soc.* **1963**, *85*, 260. (b) Werden, E. Billig, B. G.; Gray, H. B. *Inorg. Chem.* **1966**, *5*, 78. (c) Fackler, J. P. Jr.; Coucouvanis, D. *J. Am. Chem. Soc.* **1966**, *88*, 3913.
- 25 Zhao, Y.; Su, W.; Cao, R.; Hong, M. *Acta Cryst. E* **2001**, *57*, m229.

Nature of the Substituent Influences the Electronic and Electrochemical Properties of New Square-Planar Nickel-Bis(Quinoxaline-6,7-dithiolate) Complexes and Comparison of these Properties with Those of Existing $[\text{Bu}_4\text{N}]_2[\text{Ni}(\text{qdt})_2]$ (Qdt = Quinoxaline-2,3-dithiolate): Synthesis and Crystallographic study

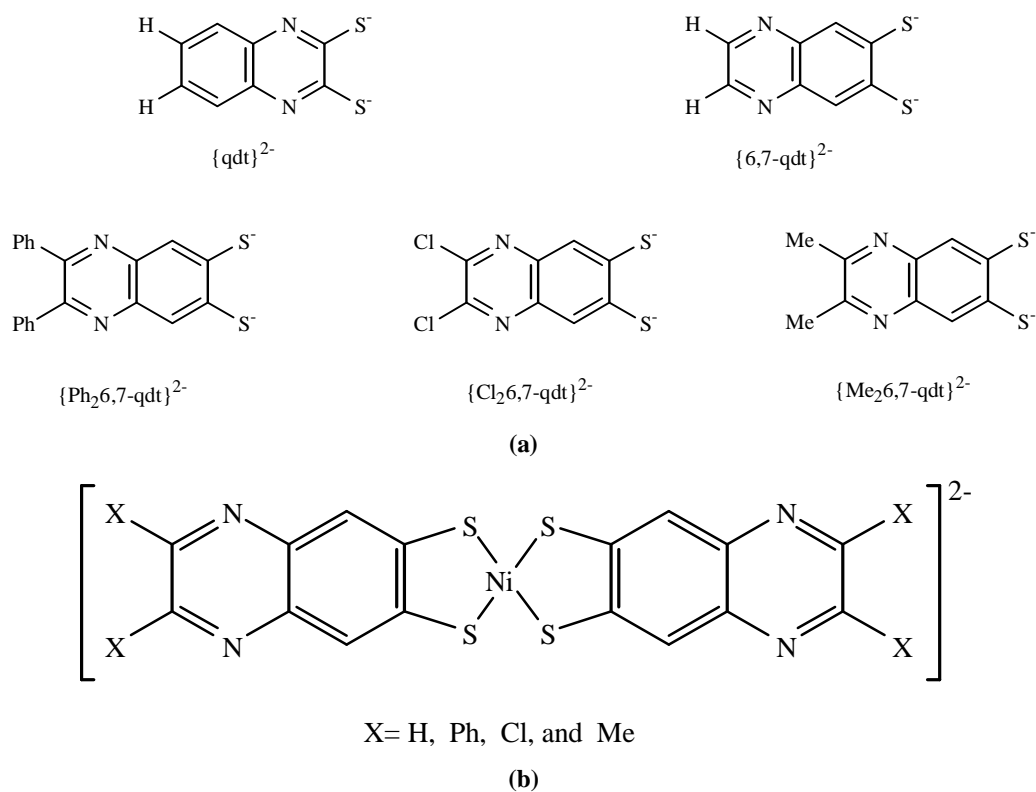
5 Chapter

Abstract:- We have described the syntheses and crystal structures of a series of square-planar nickel-bis(quinoxaline-6,7-dithiolate) complexes with the general formula $[\text{Bu}_4\text{N}]_2[\text{Ni}(\text{X}_2\text{6,7-qdt})_2]$, where X = H (**1a**), Ph = phenyl (**2a**), Cl (**3**) and Me = methyl (**4**) [$\{6,7\text{qdt}\}^{2-}$ = quinoxaline-6,7-dithiolate]. The solution and solid-state electronic absorption spectra and electrochemical properties of these compounds, are strongly dependent on the electron donating / accepting nature of the substituent. Particularly, the CT (charge transfer) transition bands observed in the visible region are greatly affected by the electronic nature of the substituent attached to the quinoxaline-6,7-dithiolate ring. The CT transition of $[\text{Bu}_4\text{N}]_2[\text{Ni}(6,7\text{-qdt})_2]$ absorb at low energy region in comparison to the CT band of the $[\text{Bu}_4\text{N}]_2[\text{Ni}(\text{qdt})_2]$ in the visible region. In addition to this, the observed CT bands in all the complexes are sensitive to the solvent polarity. Interestingly, complexes **1a**, **2a**, **3** and **4** undergo reversible oxidation at very low oxidation potentials appearing at $E_{1/2} = +0.12$ V, 0.033 V, 0.18 V and 0.044 V vs Ag/AgCl respectively, corresponding to the di-anionic complexes to mono-anionic complexes in MeOH solutions compared to that of $[\text{Ni}(\text{qdt})_2]^{2-}$ ($E_{1/2} = +0.41$ V vs Ag/AgCl). In addition to this, $[\text{PPh}_4]_2[\text{Ni}(\text{X}_2\text{6,7-qdt})_2]$ {X = H (**1b**), Ph (**2b**)} complexes also have been described. Compounds **1a**, **1b**, **2b**, **3** and **4** have been characterized unambiguously by single crystal X-ray structural analysis. The molecular structures of all the compounds exhibit weak C–H \cdots S and C–H \cdots N weak interactions.

5.1. Introduction

Metal-dithiolene complexes have been offering considerable interests to inorganic chemists for more than four decades due to their unique properties and they provide redox active ligands with the ability to form highly electron-delocalized complexes.¹ The increasing great attention in the design and synthesis of metal–dithiolene complexes is due to their potential applications in the areas of conducting-, magnetic-,² nonlinear optical-materials³ and near-infrared (NIR) dyes.⁴ The recent interests of metal dithiolene complexes in the area of bioinorganic modeling studies are owing to their existence of metal–dithiolene moiety in the active sites of many metallo-enzymes.⁵ Particularly in the area of bioinorganic modeling studies, nitrogen atom containing heterocyclic based dithiolene complexes are present in “molybdopterin” that constitutes the molybdenum cofactor of the active site of hydroxylase-type molybdo-enzymes.⁶ Predominately, qdt^{2-} (quinoxaline-2,3-dithiolate, Scheme 5.1) and its molybdenum-oxo complexes have been

investigated for modeling the active sites of molybdenum hydroxylase enzymes.⁷ Furthermore, heterocyclic based dithiolene systems containing N and S atoms offer coordination ability as secondary coordination in addition to dithiolate group.⁸ In recent years, the large potential for achieving novel coordination structures by exploring the coordination ability of both S and N atoms has stimulated, for the preparation of several dithiolene ligands with nitrogen coordinating groups of increasing complexity.⁹ In addition to this, qdt-based systems have been used in the development of field-effect transistors by introducing the fused qdt-based systems to the TTF-skeleton.¹⁰ The photo-physical (luminescence) properties of platinum complexes of qdt-type ligand have been studied extensively by Eisenberg's group.¹¹ Additionally, qdt-type ligands are useful in the area of analytical chemistry to analyze the metal quantification in ppm levels due to their absorption in visible region with large molar extension coefficient values.¹² The utility of qdt- complexes as ion-active substances of membrane electrodes has also been reported in literature.¹³ These facts prompted us to design and synthesize new type of qdt-based



Scheme 5.1. (a) Structural representation of quinoxaline dithiolate ligands; (b) General structural representation of newly synthesized nickel(II)-bis(quinoxaline-6,7-dithiolate) system.

ligands and to synthesize its metal bis(dithiolene) complexes, so that we can compare the chemistry of this new qdt-system with that of existing qdt compounds. Furthermore, H. B. Gray *et al.* studied the effect of different substituents on the electronic structure of the {MS₄} group systematically.¹⁴ This encourages us to design, synthesize, and perform comparative physical studies of new quinoxaline-dithiolate systems. In the present chapter, we have synthesized four new quinoxaline based dithiolate-ligands ($\{6,7\text{-qdt}\}^{2-}$, $\{\text{Ph}_26,7\text{-qdt}\}^{2-}$, $\{\text{Cl}_26,7\text{-qdt}\}^{2-}$) and $\{\text{Me}_26,7\text{-qdt}\}^{2-}$ [Scheme 5.1(a)] and their nickel square-planar bis(dithiolene) complexes. This new series of square-planar bis(dithiolene) complexes $\{[\text{Ni}(\text{X}_26,7\text{-qdt})_2]$, Scheme 5.1(b) $\}$ give an opportunity to their comparative studies of electronic and electrochemical properties and also comparison with the existing complex $[\text{Bu}_4\text{N}]_2[\text{Ni}(\text{qdt})_2]$. Particularly, we have demonstrated the comparison of their electronic and electrochemical studies with our new compound $[\text{Bu}_4\text{N}]_2[\text{Ni}(6,7\text{-qdt})_2]$ (**1a**) and existed compound $[\text{Bu}_4\text{N}]_2[\text{Ni}(\text{qdt})_2]$.

5.2. Experimental Details

5.2.1. General methods

Micro analytical (C, H, N, S) data were obtained with a FLASH EA 1112 Series CHNS Analyzer. Infrared (IR) spectra were recorded on KBr pellets with a JASCO FT/IR-5300 spectrometer in the region of 400-4000 cm⁻¹. ¹H NMR spectra of compounds were recorded on Bruker DRX- 400 spectrometer using Si(CH₃)₄ [TMS] as an internal standard. Electronic absorption spectra were recorded on a Cary 100 Bio UV-Visible spectrophotometer. A Cypress model CS-1090/CS-1087 electro analytical system was used for cyclic voltammetric experiments. The electrochemical experiments were measured in MeOH containing $[\text{Bu}_4\text{N}][\text{ClO}_4]$ as a supporting electrolyte, using a conventional cell consisting of two platinum wires as working and counter electrodes, and a Ag/AgCl electrode as a reference. The potentials reported here are uncorrected for junction contributions.

5.2.2. Materials

All the chemicals for the syntheses were commercially available and used as received. 1,2-Diaminobenzene-bis(thiocyanate) (**A**),¹⁵ 5,6-Diamino-benzo[1,3]dithiole-2-thione (**D**),¹⁶ and $[\text{Bu}_4\text{N}]_2[\text{Ni}(\text{qdt})_2]$ ¹⁷ were prepared according to literature procedures. Syntheses of

metal complexes were performed under N₂ using standard inert-atmosphere techniques. Solvents were dried by standard procedures.

5.2.3. Synthesis and Characterization

Synthesis of 6,7-Bis-thiocyanato-quinoxaline (B)

Glyoxal (0.648 g, 13.51 mmol, 1.28 ml) was added to the slurry of recrystallized 1,2-diaminobenzene-bis(thiocyanate) (**A**) (2.5 g, 11.260 mmol) in 200 mL of methanol and the reaction mixture was refluxed for 20 hrs. The precipitate, thus obtained, was filtered, washed with MeOH (little amount) followed by hexane (several amount) and dried. Yield: 1.815 g (71.0%). Anal. Calcd. for C₁₀H₄N₄S₂: C, 49.16; H, 1.65; N, 22.93%. Found: C, 49.49; H, 1.82; N, 22.44%. IR (KBr, cm⁻¹): 3383, 3045, 2158, 1579, 1508, 1452, 1335, 1302, 1188, 1090, 1018, 920, 891, 686, 545, 522 cm⁻¹. ¹H NMR (400 MHz, δ ppm) (CDCl₃): 8.64(s, 2H), 9.00(s, 2H). LC–MS (negative mode): m/z = 243 (M⁺–H)⁺.

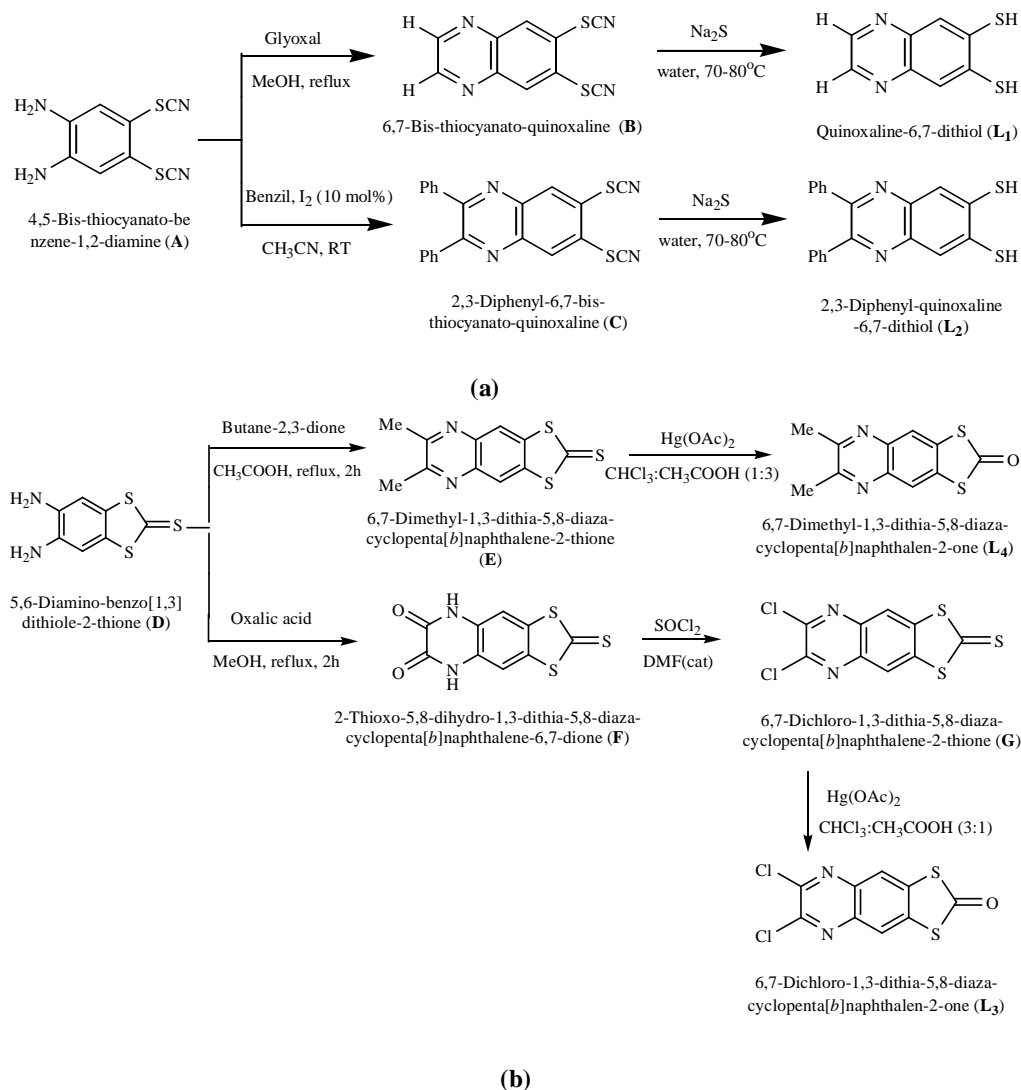
Synthesis of 2,3-Diphenyl-6,7-bis-thiocyanato-quinoxaline (C)

A mixture of solution containing 1,2-diaminobenzene-bis(thiocyanate) (**A**) (300 mg, 1.35 mmol), benzil (316 mg, 1.50 mmol) and iodine (10 mol%) in CH₃CN (10.0 mL) was stirred for 1 h. The resulting yellow precipitate was separated by filtration, washed with little CH₃CN, and dried in vacuum. Yield: 0.450 g (84.0%); Yellow solid; IR (KBr, cm⁻¹): 3067 (C–H Str, Ar), 2160 (C \equiv N str), 1653, 1597, 1537, 1435, 1390, 1338, 1253, 1194, 1057, 1022, 952, 893, 871, 769, 723, 698, 597, 543, 493; ¹H NMR (400 MHz, CDCl₃): δ 8.66 (s, 2H), 7.55 (d, 4H), 7.36-7.46 (m, 6H) ppm; ¹³C NMR (CDCl₃): δ 156.32, 141.47, 137.75, 134.35, 129.95, 129.88, 128.53, 126.72, 107.91 ppm; LC–MS (negative mode): m/z = 395 (M⁺–H)⁺; Anal. Calcd. for C₂₂H₁₂N₄S₂: C, 66.64; H, 3.05; N, 14.13%. Found: C, 65.88; H, 3.40; N, 14.33 %.

Synthesis of 6,7-Dimethyl-1,3-dithia-5,8-diaza-cyclopenta[b]naphthalen-2-thione (E)

5,6-Diamino-benzo[1,3]dithiole-2-thione (**D**) (150 mg, 0.7 mmol) and butane-2,3-dione (0.67 ml, 0.77 mmol) were dissolved in acetic acid (15.0 mL) and the reaction mixture was refluxed for 1.5 h. The resulting yellow precipitate was washed with MeOH for several times and dried in vacuum, to give yellow colored solid. This compound can be directly used for the preparation of ligand **L₄**. Yield: 0.180 (96.0%); Pale yellow solid; IR (KBr,

cm^{-1}): 3059, 1450, 1398, 1321, 1182, 1068 (C=S), 883, 844, 758, 509, 424; ^1H NMR (400 MHz, CDCl_3): δ 8.08 (s, 2H), 2.77 (s, 6H) ppm; LC-MS (positive mode): m/z = 265 ($\text{M}^+ + \text{H}^+$); Anal. Calcd. for $\text{C}_{11}\text{H}_8\text{N}_2\text{S}_3$: C, 49.97; H, 3.05; N, 10.60%. Found: C, 50.23; H, 2.84; N, 10.85 %.



Scheme 5.2. Synthesis of quinoxaline dithiolate ligands (a) L_1 and L_2 (b) L_3 and L_4 .

Synthesis of 2-Thioxo-5,8-dihydro-1,3-dithia-5,8-diazacyclopenta[b]naphthalene-6,7-dione (F)

A solution of 5,6-Diaminobenzene-1,3-dithiole-2-thione (compound **D**, 100 mg, 0.467 mmol) and oxalic acid (65 mg, 0.515 mmol) in MeOH (15 mL) were refluxed for 24 h under N_2 . After filtration, the pale yellow precipitate was washed with cold MeOH, and then air dried. Pale yellow solid; Yield = 66%; IR (KBr, cm^{-1}): 3261 (N-H str),

3049, 2914, 1693, (C=O), 1444, 1379, 1271, 1059 (C=S), 877, 841, 790, 677, 555, 511; ^1H NMR (400 MHz, DMSO- d_6): δ 12.22 (s, 2H), 7.48 (s, 2H) ppm; ^{13}C NMR (100 MHz, DMSO- d_6): δ 213.09 (C=S), 155.29 (C=O), 134.92, 126.95, 108.82 ppm; LC–MS (positive mode): m/z = 269 ($\text{M}^+ + \text{H}$) $^+$; Anal. Calcd. for $\text{C}_9\text{H}_4\text{N}_2\text{O}_2\text{S}_3$: C, 40.28; H, 1.50; N, 10.44%. Found: C, 40.02; H, 1.78; N, 10.56%.

Synthesis of 6,7-Dichloro-1,3-dithia-5,8-diaza-cyclopenta[b]naphthalene-2-thione (G)

To a solution of compound **F** (142 mg, 0.529 mmol) in thionyl chloride (4 mL) was added dropwise DMF (0.05 mL). The reaction mixture was refluxed for 15 h and then concentrated under vacuum. The resulting residue was evaporated with dichloromethane several times, dissolved in dichloromethane (20 mL) and poured into ice-water. The organic layer was collected, washed with saturated aqueous NaCl, dried over Na_2SO_4 , and then evaporated to provide compound **G** as a light yellow solid, which was used without further purification in the next step; Yellow solid; Yield = 65%; IR (KBr, cm^{-1}): 1527, 1444, 1257, 1180, 1070 (C=S) 878, 568, 436; ^1H NMR (400 MHz, CDCl_3): δ 8.15 (s, 2H) ppm; ^{13}C NMR: We could not record the ^{13}C NMR spectrum because of the poor solubility of the compound in common organic solvents; LC–MS (positive mode): m/z = 306 ($\text{M}^+ + \text{H}$) $^+$, 308 [$(\text{M}+2)^+ + \text{H}$] $^+$; Anal. Calcd. for $\text{C}_9\text{H}_2\text{N}_2\text{S}_3\text{Cl}_2$: C, 35.42; H, 0.66; N, 9.18%. Found: C, 35.22; H, 0.79; N, 9.46%.

Synthesis of Quinoxaline-6,7-dithiol (L_1)

Compound **B** (1.815 g, 8.0 mmol) was added as a solid to a solution of Na_2S (2.93, 36mmol) in 100 mL of degassed water and the mixture heated to 70-80 °C for 60 min to produce a clear, orange-red solution. The mixture was cooled to room temperature, and 20 mL of 10% HCl was added drop wise to afford a heavy, brown precipitate. The precipitate was filtered off, washed with water, and air-dried. Thus dithiol ligand L_1 is obtained. Yield 1.25 g (80.0%). Anal. Calcd for $\text{C}_8\text{H}_6\text{N}_2\text{S}_2$: C, 49.46; H, 3.11; N, 14.41%. Found: C, 49.12; H, 3.34; N, 14.32%. IR (KBr, cm^{-1}): 3405(w), 3040(w), 1626 (w), 1579(m), 1489(m), 1446(s), 1278(s), 1186(m), 1022(s), 918(s), 893(s), 418(m). ^1H NMR (400 MHz, δ ppm) (CD_3OD): 8.93(s, 2H), 8.38(s, 2H). LC–MS (positive mode): m/z = 195 ($\text{M}^+ + \text{H}$) $^+$.

Synthesis of 2,3-Diphenyl-quinoxaline-6,7-dithiol (L_2)

2,3-Diphenyl-6,7-bis-thiocyanato-quinoxaline (**C**) (0.3 g, 0.757 mmol) was added as a solid to a solution of Na_2S (0.3 g, 3.85 mmol) in 100 mL of degassed water and the mixture was heated to 70-80 °C for 24 h, to produce a clear, orange-red solution. The mixture was then cooled to room temperature, and 20 mL of 10% HCl was added drop wise to afford a heavy, brown precipitate. The precipitate was filtered off, washed with water, and air-dried. Thus the dithiol ligand L_2 was obtained. Yield 0.180 g (68.6%). IR (KBr, cm^{-1}): 3057 (C–H Str, Ar), 2530 (S–H str), 1581, 1533, 1433, 1388, 1338, 1253, 1188, 1059, 1022, 960, 869, 765, 727, 694, 596, 543; LC–MS (positive mode): m/z = 347 ($M^+ + H$)⁺; Anal. Calcd. for $C_{20}H_{14}N_2S_2$: C, 69.33; H, 4.07; N, 8.09%. Found: C, 69.86; H, 3.92; N, 7.82%.

Synthesis 6,7-Dichloro-1,3-dithia-5,8-diaza-cyclopenta[b]naphthalen-2-one (L_3)

To a solution of 6,7-Dichloro-1,3-dithia-5,8-diaza-cyclopenta[b]naphthalene-2-thione (**G**) (90 mg, 0.29 mmol) in chloroform and acetic acid (3:1, v/v, 28.0 mL), $Hg(OAc)_2$ (332 mg, 1.038 mmol) was added and it was stirred for 15 h at room temperature under N_2 atmosphere. The precipitate was filtered off using celite and washed with chloroform. The filtrate was extracted with saturated $NaHCO_3$ solution (3×33 mL) and water (50.0 mL). To remove any traces of water, anhydrous Na_2SO_4 was added. The solvent was removed in vacuum, which produces pale yellow colored compound L_3 as product. Yield = 95%; Pale yellow solid; IR (KBr, cm^{-1}): 1732 (C=O), 1660, 1523, 1446, 1257, 1147, 999, 862, 561, 435; 1H NMR (400 MHz, $CDCl_3$): δ 8.15 (s, 2H) ppm; ^{13}C NMR (100 MHz, $CDCl_3$): δ 187.75 (C=O), 146.20, 138.89, 137.57, 121.57 ppm; LC–MS (positive mode): m/z = 290 ($M^+ + H$)⁺, 292 [$(M+2)^+ + H$]⁺; Anal. Calcd. for $C_9H_2N_2OS_2Cl_2$: C, 37.38; H, 0.70; N, 9.69%. Found: C, 37.02; H, 0.78; N, 9.86%.

Synthesis of 6,7-Dimethyl-1,3-dithia-5,8-diaza-cyclopenta[b]naphthalen-2-one (L_4)

To a solution of 6,7-dimethyl-1,3-dithia-5,8-diaza-cyclopenta[b]naphthalen-2-thione (**E**) (135 mg, 0.511 mmol) in chloroform and acetic acid (3:1, v/v, 40 mL), $Hg(OAc)_2$ (521 mg, 1.63 mmol) was added and it was stirred for 12 h at room temperature under N_2 atmosphere. The precipitate was filtered off using celite and washed with chloroform. The filtrate was extracted with saturated $NaHCO_3$ solution (3×33 mL) and water (50 mL). To

remove any traces of water, anhydrous Na₂SO₄ was added. The solvent was removed in vacuum, which produces pale yellow colored compound **L₄** as product. Yield: 115 mg (91.0%); Pale yellow solid; IR (KBr, cm⁻¹): 3057, 2916, 1745 (C=O), 1653, 1454, 1398, 1319, 1178, 1093, 869, 844, 756, 582, 439; ¹H NMR (400 MHz, CDCl₃): δ 8.10 (s, 2H), 2.75 (s, 6H) ppm; LC-MS (positive mode): *m/z* = 249 (M⁺+H)⁺; Anal. Calcd. for C₁₁H₈N₂OS₂: C, 53.20; H, 3.25; N, 11.28%. Found: C, 53.67; H, 3.01; N, 10.98%.

Synthesis of [Bu₄N]₂[Ni(6,7,-qdt)₂] (1a)

The 6,7,-qdt dianion is generated, *in situ*, by treatment with H₂(6,7-qdt) (0.060 g, 0.309 mmol) with NaOH (0.029 g, 0.725 mmol) in MeOH (10mL). To the resulting clear red solution, NiCl₂·6H₂O (0.035 g, 0.15 mmol) was added; the resulting dark blue solution was stirred for 30 min. Dark blue micro crystals were precipitated by adding tetrabutylammonium bromide (0.1 g, 0.310 mmol); the micro crystals were filtered, washed with water followed by diethyl ether, and dried at room temperature. It was recrystallized from acetonitrile solution by vapor diffusion with diethyl ether. Yield: 0.116 g (83.3% based on Ni). Anal. Calcd. for C₄₈H₈₀N₆S₄Ni: C, 62.12; H, 8.69; N, 9.05%. Found: C, 62.88; H, 8.24; N, 9.28%. IR (KBR pellet) (ν/cm⁻¹): 2957(s), 2866(m), 1557(m), 1439(s), 1412(s), 1178(s), 1078(s), 1028(s), 929(s), 873(s), 781(s). ¹H NMR (400 MHz, δ ppm) (CD₃CN): 0.93(t, 24H), 1.31-1.37(m, 16H), 1.59-1.61(m, 16H), 3.15(t, 16H), 7.41(s, 4H), 8.18(s, 4H).

Synthesis of [PPh₄]₂[Ni(6,7-qdt)₂] (1b)

The dianion of 6,7-qdt was generated, *in situ*, by the reaction of quinoxaline-6,7-dithiol (**L₁**) (0.104 g, 0.536 mmol) with NaOH (0.060 g, 1.5 mmol) in MeOH (10 mL) under nitrogen atmosphere. To the resulting clear red solution, solid NiCl₂·6H₂O (0.064 g, 0.269 mmol) was added; the resulting dark red solution was stirred for 15 min at room temperature. Dark brown micro crystals were precipitated by adding tetraphenylphosphonium bromide (0.292 g, 0.696 mmol); the micro crystals were filtered, washed with water followed by diethyl ether, and dried at room temperature. It was recrystallized from acetonitrile solution by vapor diffusion with diethyl ether. Yield: 0.350 g (71.3% based on Ni). Anal. Calcd. for C₆₄H₄₈N₄S₄P₂Ni: C, 68.51; H, 4.31; N, 4.99%. Found: C, 68.23; H, 4.12; N, 5.36%. IR (KBR pellet) (ν/cm⁻¹): 3040, 1660, 1583, 1483,

1435, 1412, 1340, 1174, 1107, 1078, 1024, 925, 779, 752, 721, 688, 524; ^1H NMR (400 MHz, δ ppm) (CD_3CN): 7.67-7.76 (m, 40H), 7.90-7.93 (m, 8H).

Synthesis of $[\text{Bu}_4\text{N}]_2[\text{Ni}(\text{Ph}_2\text{-6,7-qdt})_2]$ (**2a**)

The dianion of 2,3-diphenyl-6,7-qdt was generated, *in situ*, by the treatment of 2,3-diphenyl-quinoxaline-6,7-dithiol (**L**₂) (0.052 g, 0.15 mmol) with NaOH (0.020 g, 0.5 mmol) in methanol (7.0 mL). To the resulting clear red solution, solid $\text{NiCl}_2 \cdot 6\text{H}_2\text{O}$ (0.018 g, 0.075 mmol) was added; the resulting dark brown solution was stirred for 15 min at room temperature. Black colored micro crystals were precipitated by adding tetrabutylammonium bromide (0.07 g, 0.215 mmol); the micro crystals were filtered, washed with water followed by diethyl ether, and dried at room temperature. It was recrystallized from acetonitrile solution by vapor diffusion with diethyl ether. Yield: 0.200 g (74.1% based on Ni). Anal. Calcd. for $\text{C}_{72}\text{H}_{96}\text{N}_6\text{S}_4\text{Ni}$: C, 70.16; H, 7.85; N, 6.82%. Found: C, 70.57; H, 7.29; N, 6.49%. IR (KBR pellet) (ν/cm^{-1}): 2959, 2918, 2860, 1595, 1483, 1423, 1340, 1192, 1072, 1024, 858, 821, 698. ^1H NMR (400 MHz, δ ppm) (CD_3CN): 0.949 (t, 24H), 1.32-1.37 (m, 16H), 1.60 (bs, 16H), 3.10 (t, 16H), 7.15-7.37 (m, 24H).

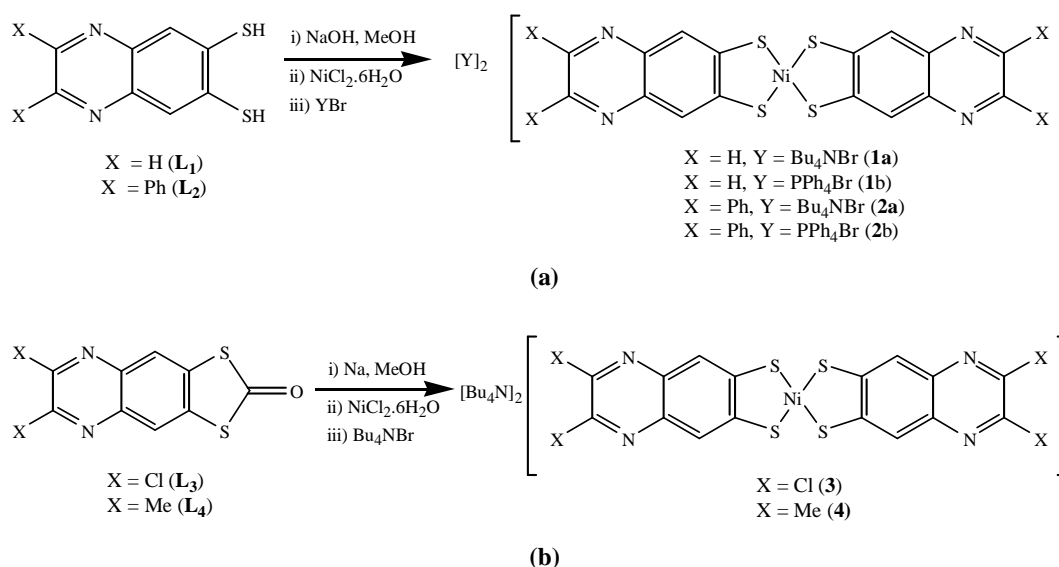
Synthesis of $[\text{PPh}_4]_2[\text{Ni}(\text{Ph}_2\text{6,7-qdt})_2]$ (**2b**)

This compound was prepared by using above procedure for the preparation of compound **2a**, but tetraphenylphosphonium bromide was added in place of tetrabutylammonium bromide and separated as tetraphenylphosphonium salt. It was recrystallized from DMF solution by vapor diffusion with diethyl ether. Yield: 79.4% based on Ni. Anal. Calcd. for $\text{C}_{97}\text{H}_{85}\text{N}_7\text{O}_3\text{P}_2\text{S}_4\text{Ni}$: C, 70.79; H, 5.21; N, 5.96%. Found: C, 70.25; H, 5.34; N, 6.18%. IR (KBR pellet) (ν/cm^{-1}): 3059, 2953, 2924, 1670, 1425, 1340, 1195, 1107, 1082, 1020, 723, 690, 520; ^1H NMR (400 MHz, δ ppm) (CD_3CN): 7.31-7.48 (m, 20H), 7.70-7.77 (m, 40H), 7.90-7.93 (m, 4H).

Synthesis of $[\text{Bu}_4\text{N}]_2[\text{Ni}(\text{Cl}_2\text{-6,7-qdt})_2]$ (**3**)

The dianion of 2,3-dichloro-6,7-qdt is generated, *in situ*, by the treatment of 6,7-dichloro-1,3-dithia-5,8-diaza-cyclopenta[*b*]naphthalen-2-one (**L**₃) (0.080 g, 0.277 mmol) with Na metal (0.020 g, 0.877 mmol) in methanol (10 mL). To the resulting clear brown solution,

solid $\text{NiCl}_2 \cdot 6\text{H}_2\text{O}$ (0.034 g, 0.143 mmol) was added; the resulting dark brown solution was stirred for 15 min at room temperature. To this, tetrabutylammonium bromide (0.1 g, 0.310 mmol) was added followed by addition 30 mL of deionised water resulting in the precipitation of black colored micro crystals; the micro crystals were filtered, washed with water followed by diethyl ether, and dried at room temperature. It was recrystallized from acetonitrile solution by vapor diffusion with diethyl ether. Yield: 0.190 g (52.9% based on Ni). Anal. Calcd. for $\text{C}_{48}\text{H}_{76}\text{N}_6\text{S}_4\text{Cl}_4\text{Ni}$: C, 54.09; H, 7.19; N, 7.88%. Found: C, 54.41; H, 7.25; N, 7.51%. IR (KBR pellet) (ν/cm^{-1}): 2959, 2872, 1562, 1433, 1377, 1315, 1194, 1149, 1078, 983, 862, 738, 570, 518. ^1H NMR (400 MHz, δ ppm) (CD_3CN): 0.946 (t, 24H), 1.34 (bs, 16H), 1.59 (bs, 16H), 3.08 (t, 16H), 7.42 (s, 4H).



Scheme 5.3. Synthesis of nickel 6,7-quinoxaline-dithiolate complexes (a) **1a**, **1b**, **2a** and **2b**; (b) **3** and **4**.

Synthesis of $[\text{Bu}_4\text{N}]_2[\text{Ni}(\text{Me}_2\text{-6,7-qdt})_2] (\mathbf{4})$

The dianion of 2,3-dimethyl-6,7-qdt is generated, *in situ*, by the reaction of 6,7-dimethyl-1,3-dithia-5,8-diaza-cyclopenta[*b*]naphthalen-2-one (**L₄**) (0.100 g, 0.401 mmol) with Na (0.046 g, 1.0 mmol) in MeOH (10mL) under nitrogen atmosphere. To the resulting clear red solution, $\text{NiCl}_2 \cdot 6\text{H}_2\text{O}$ (0.048 g, 0.201 mmol) was added; the resulting dark red solution was stirred for 15 min at room temperature. Dark red micro crystals were precipitated by adding tetrabutylammonium bromide (0.2 g, 0.621mmol); the micro crystals were filtered, washed with water followed by diethyl ether, and dried at room temperature. It was

recrystallized from acetonitrile solution by vapor diffusion with diethyl ether. Yield: 0.295 g (71.2% based on Ni). Anal. Calcd. for $C_{52}H_{88}N_6S_4Ni$: C, 63.46; H, 9.01; N, 8.54%. Found: C, 63.25; H, 8.89; N, 8.81%. IR (KBR pellet) (ν/cm^{-1}): 2957, 2924, 2866, 1736, 1635, 1570, 1448, 1423, 1325, 1168, 1076, 989, 839, 748, 588; 1H NMR (400 MHz, δ ppm) (CD_3CN): 0.93 (bs, 24H), 1.32 (bs, 16H), 1.58 (bs, 16H), 2.56 (s, 12H) 3.09 (bs, 16H), 8.15 (s, 4H).

5.2.4. Single Crystal Structure Determination

Single crystals suitable for facile structural determination for the compounds **1a**, **1b**, **2b**, **3** and **4** were measured on a three circle Bruker SMART APEX CCD area detector system under Mo-K α ($\lambda = 0.71073$ Å) graphite monochromatic X-ray beam. The frames were recorded with an ω scan width of 0.3° , each for 10 s, crystal-detector distance 60 mm, collimator 0.5 mm. Data reduction performed by using SAINTPLUS.¹⁸ Empirical absorption corrections using equivalent reflections performed program SADABS.¹⁸ The Structures were solved by direct methods and least-square refinement on F^2 for all the compounds by using SHELXS-97.¹⁹ All non-hydrogen atoms were refined anisotropically. The hydrogen atoms were included in the structure factor calculation by using a riding model.

5.3. Results and Discussion

5.3.1. Synthesis and Characterization

The synthetic route for the synthesis of four dithiolate-ligands (**L**₁–**L**₄) has been shown Scheme 5.2. The intermediate precursor for the synthesis of ligands **L**₁–**L**₄ were obtained by the simple condensation reactions of amines (**A**) and (**D**) with respective di-ones. The ligands **L**₁ and **L**₂ have been synthesized by the reaction of the condensed products **B** and **C** with Na₂S at 70-80 °C respectively, and followed by protonation in acidic conditions as shown in Scheme 5.2(a). Compound 6,7-bis-thiocyanato-quinoxaline (**B**) was prepared by simple condensation reaction between the 1,2-diaminobenzene-bis(thiocyanate) (**A**) with glyoxal under refluxing conditions for 20 h gives a reasonable yield 71%. Compound 2,3-diphenyl-6,7-bis-thiocyanato-quinoxaline (**C**) was prepared according to modified literature procedure,²⁰ which was obtained by a condensation reaction between the 1,2-

diaminobenzene-bis(thiocyanate) (**A**) and benzil by using iodine as catalyst in acetonitrile solution for 1 h at room temperature resulting in quantitative yield 84%.

The synthesis of dithiolate-ligands **L**₃ and **L**₄ have been started from the 5,6-diaminobenzo[1,3]dithiole-2-thione (**D**), as shown in Scheme 5.2(b). The condensation reaction of **D** with oxalic acid under refluxing conditions in MeOH solution results in the formation of compound **F**, and it was subjected to chlorination with SOCl₂ giving thione compound **G** in quantitative yield. The thione derivative **G** was used for the synthesis of ligand **L**₃ by using Hg(OAc)₂ in CHCl₃ : CH₃COOH (3:1) in good yield (95%) as shown in Scheme 5.2(b). In the same way, ligand **L**₄ was obtained in two steps starting from 5,6-diaminobenzo[1,3]dithiole-2-thione (**D**). In the first step, 6,7-dimethyl-1,3-dithia-5,8-diazacyclopenta[*b*]naphthalen-2-thione (**E**) was prepared according to modified literature procedure,²¹ which was obtained by the condensation reaction of 5,6-diaminobenzo[1,3]dithiole-2-thione (**C**) with butane-2,3-dione in acetic acid at refluxing conditions in quantitative yields [Scheme 5.2(b)]. In the second step of the synthesis, the 1,3-dithia-2-thione derivative (**E**) was converted into corresponding 1,3-dithia-2-one derivative (**L**₄) by using Hg(OAc)₂ in CHCl₃ : CH₃COOH (3:1) in good yield (98%) as presented in Scheme 5.2(b). All the newly synthesized materials have been characterized by NMR spectroscopy including elemental and LC-MS analyses.

Synthesis of metal complexes was performed through a general common procedure, similar to previously described procedures²² as shown in Scheme 5.3(a) and 5.3(b). The {X₂6,7qdt}²⁻ ions are generated, *in situ*, by the reaction of ligands (**L**₁–**L**₄) in basic medium containing MeOH solution, which are reacted with nickel chloride salt resulting in the formation of the respective nickel complexes and precipitated as tetrabutylammonium salts by the addition of Bu₄NBr [compounds **1a**, **2a**, **3**, and **4**]. Tetraphenylphosphonium bromide was added instead of adding tetrabutylammonium bromide for the precipitation of nickel complexes of ligands **L**₁ and **L**₂ resulting in the complexes of **1b** and **2b**, respectively as shown Scheme 5.3(a). Metal complexes **1a**, **1b**, **2a**, **3** and **4** were recrystallized from acetonitrile solution by the vapour diffusion of diethyl ether. Complex **2b** was recrystallized from DMF solution by the vapour diffusion of diethyl ether. Crystals of compounds **1a**, **1b**, **2b**, **3** and **4** have been characterized by single crystal X-ray structure determination. But the crystals of compound **2a** were not suitable

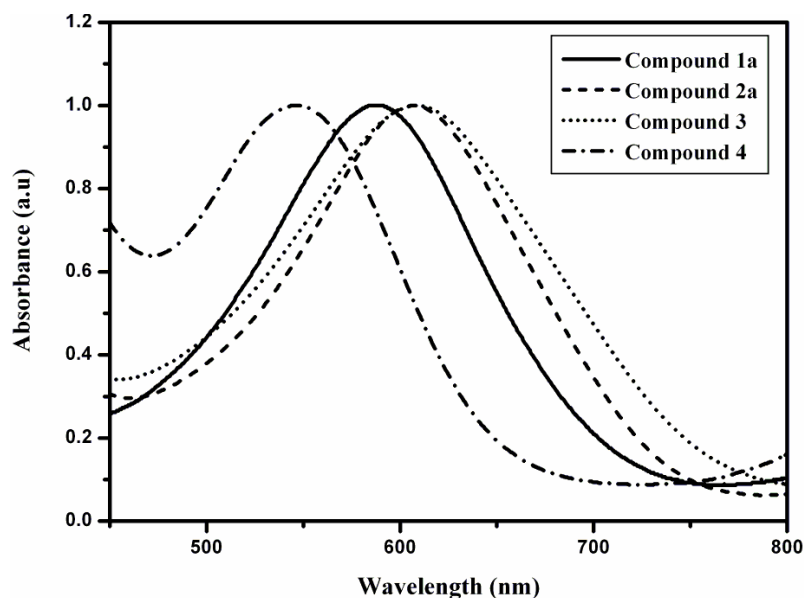
for single crystal X-ray structure analysis. All the complexes have been further characterized by NMR spectroscopy including their elemental analysis.

5.3.2. Electronic Absorption Spectroscopy

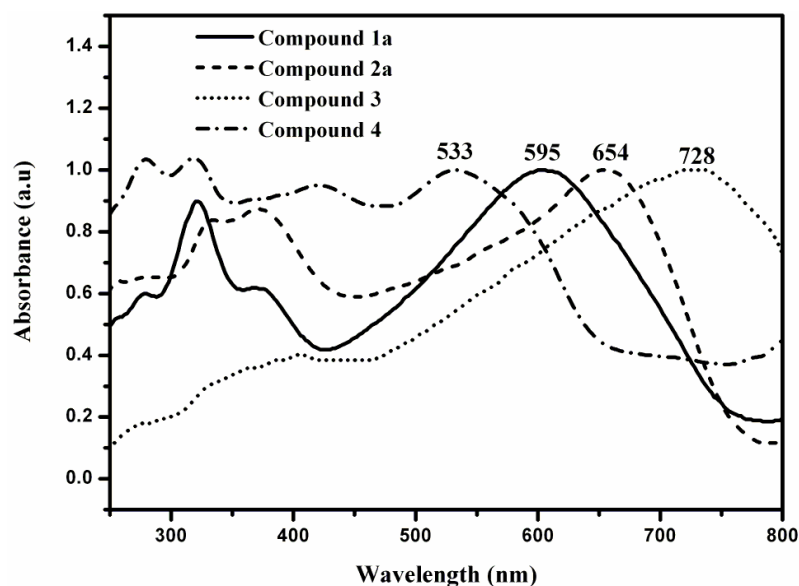
Effect of the Nature of the Substitution on the Absorption

The electronic absorption spectra of complexes **1a**, **2a**, **3** and **4** in MeOH solutions are shown in Figure 5.1(a). The broad bands are observed in the visible region centered at ~588 nm ($\epsilon = 35000 \text{ L mol}^{-1}\text{cm}^{-1}$), ~607 nm ($\epsilon = 21,000 \text{ L mol}^{-1}\text{cm}^{-1}$), ~610 nm ($\epsilon = 34,600 \text{ L mol}^{-1}\text{cm}^{-1}$) and ~547 nm ($\epsilon = 24,200 \text{ L mol}^{-1}\text{cm}^{-1}$) for complexes **1a**, **2a**, **3** and **4**, respectively. These broad bands are due to the charge transfer (CT) transitions involving electronic excitation from a HOMO which is a mixture of dithiolate (π) and metal (d) orbital character to a LUMO which is a π^* orbital of the dithiolate, which are characteristics of metal(II) bis (dithiolene) complexes.^{23,11a} Interestingly, this CT band alters the energy of absorption, by simple changing of phenyl, chloro and methyl substitutions to the dithiolate core moiety present in complex **1a**, resulting in complexes **2a**, **3** and **4**, respectively [Scheme 5.1(a)]. The electron donating group such as methyl present in the complex **4** compared to the hydrogen present in complex **1a**, results in variation of CT band absorption maxima shifts to higher energy region in different solvents as well as in solid state (Table 5.1). In other words, the electron withdrawing groups, such as, phenyl and chloro substituents present in complexes **2a** and **3**, respectively, compared to hydrogen present in the complex **1a**, results in shift of CT band absorption maxima shifts to lower energy region in various solvents as well as in solid-state (Table 5.1).

Thus the red shift of the both complexes **2a** and **3** depends upon electron withdrawing capability. By changing it to a more electron withdrawing chloro substituent compared to the phenyl group, position of the absorption maxima shifts to more towards to red region. From this, we conclude that the electron donating groups alters the position of the absorption maxima shifts to blue region and electron-withdrawing groups, alter the position of the absorption maxima shifted to red region. The maximum shifts are observed for all the complexes in diffuse reflectance spectra rather than in solution state as shown in Table 5.1, and the diffuse reflectance spectra of compound **1a**, **2a**, **3** and **4** as shown in



(a)



(b)

Figure 5.1. (a) Electronic absorption spectra in solution (MeOH) and (b) diffuse reflectance of solid compounds **1a**, **2a**, **3** and **4**.

Figure 5.1(b). By the substitution of electron donating group such as methyl- to the dithiolenic core moiety may decrease the charge acceptor ability and results in blue shift. On the other hand, electron withdrawing groups such as phenyl- and chloro- substitutions lead to red shifts, probably due to the increasing charge acceptor ability by decreasing the electron density on the dithiolenic core moiety. Among two electron withdrawing

groups, phenyl- and chloro- substituents, and the latter one has more withdrawing nature and decreases the more electron density on dithiolene core, consequently causes more red shift. Furthermore, the CT bands of all these complexes are sensitive to the solvent polarity of the solvents as shown in Table 5.1. In DMF and acetone solvents, the CT bands are observed lower energy region, on other hand in DCM and acetonitrile solvents the CT bands absorbs at higher energy region for all the complexes **1a**, **2a**, **3** and **4**.

Table 5.1. Nature of the electron donating and withdrawing groups influences the shifting of absorption position maxima of the CT bands in the visible region

S.No	Solvent/Solid	CT band of the compounds, λ_{max} (nm)			
		1a	2a	3	4
1	MeOH	588	607	609	547
2	DCM	593	623	642	560
3	Acetonitrile	593	624	640	566
4	DMF	619	662	707	593
5	Acetone	619	660	709	589
6	Solid-state	595	654	728	533

Comparison of Electronic Absorption Properties Between the $[\text{Bu}_4\text{N}]_2[\text{Ni}(\text{6,7-qdt})_2]$ (**1a**) and $[\text{Bu}_4\text{N}]_2[\text{Ni}(\text{qdt})_2]$

The absorption spectra of the compounds $[\text{Bu}_4\text{N}]_2[\text{Ni}(\text{6,7-qdt})_2]$ (**1a**) and $[\text{Bu}_4\text{N}]_2[\text{Ni}(\text{qdt})_2]$ in MeOH is shown in Figure 5.2(a). The dominated broad bands in the visible region centered at ~588 nm ($\epsilon = 35000 \text{ L mol}^{-1}\text{cm}^{-1}$) and ~540 nm ($\epsilon = 17900 \text{ L mol}^{-1}\text{cm}^{-1}$) for complex **1a** and $[\text{Bu}_4\text{N}]_2[\text{Ni}(\text{qdt})_2]$ are due to the charge transfer (CT) transitions. The CT band of the compound (present system) in the visible region absorbs at considerably lower energy with the large molar extension coefficient value ($\lambda_{\text{max}} = 588 \text{ nm}$, $\epsilon = 35000 \text{ L mol}^{-1}\text{cm}^{-1}$ in MeOH) as compared to the metal complexes of qdt ligand $\{[(\text{Ni}(\text{qdt}))^{2-}, \lambda_{\text{max}} = 540 \text{ nm}, \epsilon = 17900 \text{ L mol}^{-1}\text{cm}^{-1} \text{ in MeOH}, [(\text{Pd}(\text{qdt}))^{2-}, \lambda_{\text{max}} = 441 \text{ nm}, \epsilon = 21300 \text{ L mol}^{-1}\text{cm}^{-1} \text{ in MeOH}, [(\text{Pt}(\text{qdt}))^{2-}, \lambda_{\text{max}} = 510 \text{ nm}, \epsilon = 19600 \text{ L mol}^{-1}\text{cm}^{-1} \text{ in MeOH}]\}^{11a}$. The comparison of this situation for two kinds of nickel complexes was made in Figure 5.2(a).

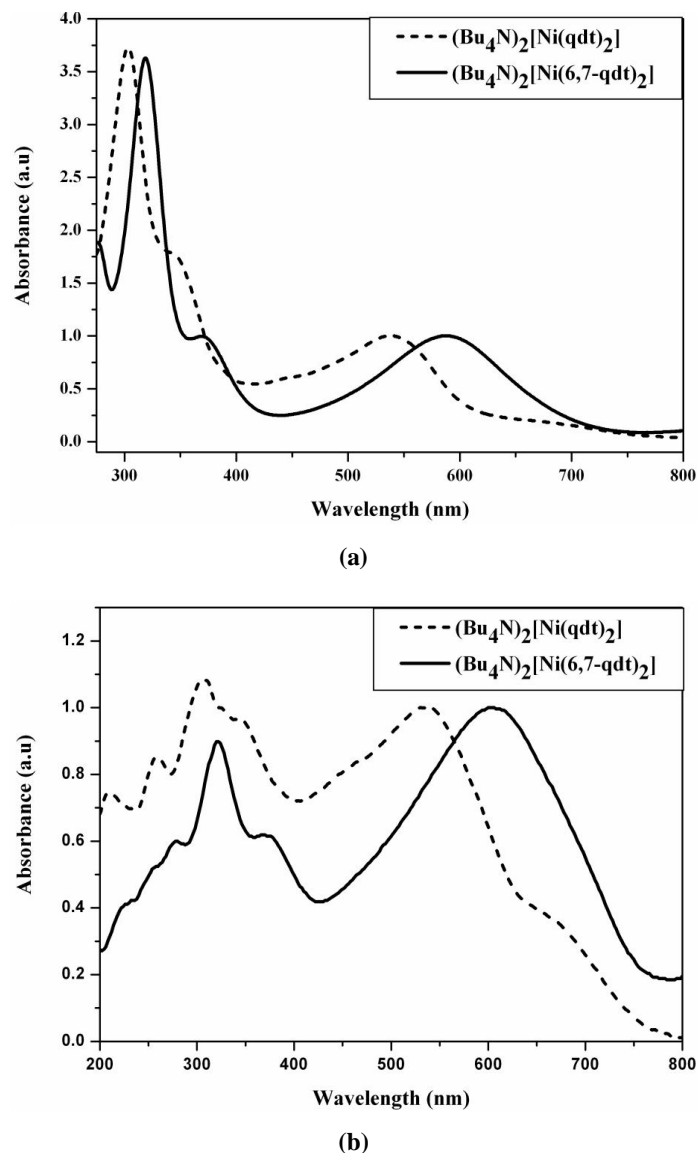
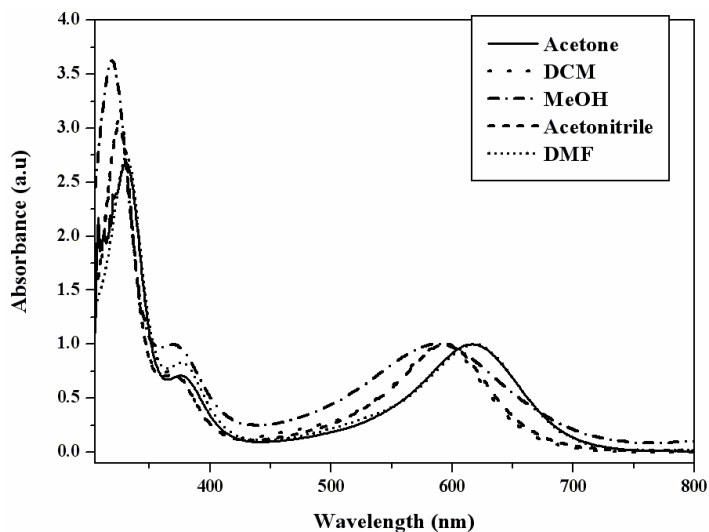


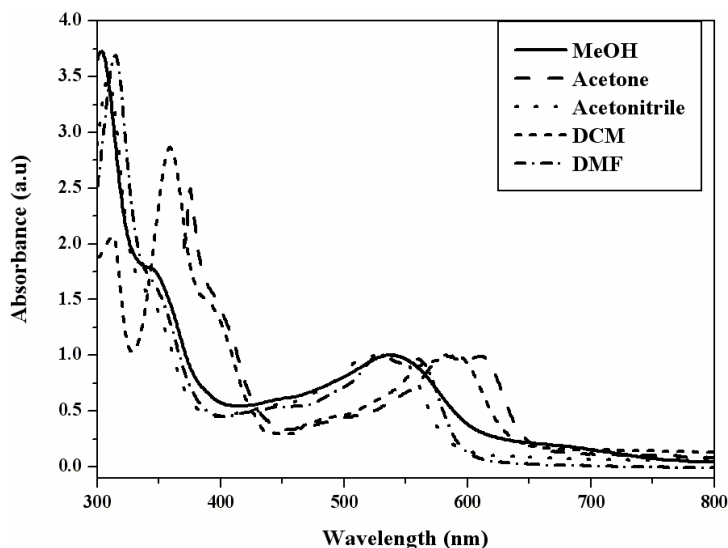
Figure 5.2. (a) Electronic absorption spectra for the compounds **1a** and $[\text{Bu}_4\text{N}]_2[\text{Ni}(\text{qdt})_2]$ in MeOH solutions (CT band normalized to 1); (b) Diffuse reflectance spectra of the compounds **1a** and $[\text{Bu}_4\text{N}]_2[\text{Ni}(\text{qdt})_2]$.

The effect of solvent polarity on the absorption bands in the visible region for the complex **1a** is shown in Figure 5.3(a). The CT band is sensitive to the solvent polarity, shifting significantly to higher energy region in less polar solvents, which is further considerable charge-transfer character. The same phenomena is also observed for the $(\text{Bu}_4\text{N})_2[\text{Ni}(\text{qdt})_2]$ complex, which is shown in Figure 5.3(b). In polar aprotic solvents, the CT band for the $(\text{Bu}_4\text{N})_2[\text{Ni}(\text{qdt})_2]$ possess two well resolved maxima in the visible region. It is worth mentioning that, in MeOH (protic solvent), the band is not resolved but

observed as broad band for $(\text{Bu}_4\text{N})_2[\text{Ni}(\text{qdt})_2]$. But in the case of complex **1a**, the CT bands show only broad bands in the visible region. The diffuse reflectance spectra of complex **1a** and $(\text{Bu}_4\text{N})_2[\text{Ni}(\text{qdt})_2]$ are shown in Figure 5.2(b). The observed bands in the visible region match exactly with the solution spectra of the both compounds. Complex **1a** shows a very broad band centered at 592 nm but the complex $(\text{Bu}_4\text{N})_2[\text{Ni}(\text{qdt})_2]$ absorbs at 535 nm along one shoulder at 645 nm in the diffuse reflectance spectra.



(a)



(b)

Figure 5.3. (a) Electronic absorption spectra (normalized to 1) of (a) complex $[\text{Bu}_4\text{N}]_2[\text{Ni}(6,7\text{-qdt})_2]$ (**1a**) and (b) complex $[\text{Bu}_4\text{N}]_2[\text{Ni}(\text{qdt})_2]$ in different solvents.

5.3.3. Electrochemical Studies

Effect of the Nature of the Substitution on the Electrochemical Properties

Interestingly, complexes **1a**, **2a**, **3** and **4** undergo reversible oxidation at very low oxidation potentials in MeOH solutions as shown in Figure 5.4. The first oxidation potentials appears at $E_{1/2} = +0.12$ V vs Ag/AgCl ($\Delta E = 74$ mV), $E_{1/2} = +0.033$ V ($\Delta E = 65$ mV), $E_{1/2} = +0.18$ V ($\Delta E = 77$ mV) and $E_{1/2} = +0.044$ V ($\Delta E = 89$ mV) vs Ag/AgCl, corresponds to the di-anionic complex to mono-anionic complex for the complexes **1a**, **2a**, **3** and **4**, respectively. The electrochemical properties (the first oxidation potentials) of the present system $[\text{Bu}_4\text{N}]_2[\text{Ni}(\text{X}_2\text{6,7-qdt})_2]$ are dependent on the nature of the electron donating / withdrawing groups attached to the 6,7-quinoxaline dithiolene core moiety. From these results, we conclude that the ligand must be participating to a large extent in electron transfer processes. In addition to this, complexes **1a**, **2a**, **3** and **4**, show some irreversible oxidations as shown in Table 5.2 and the respective CV diagrams are shown in Figure 5.5.

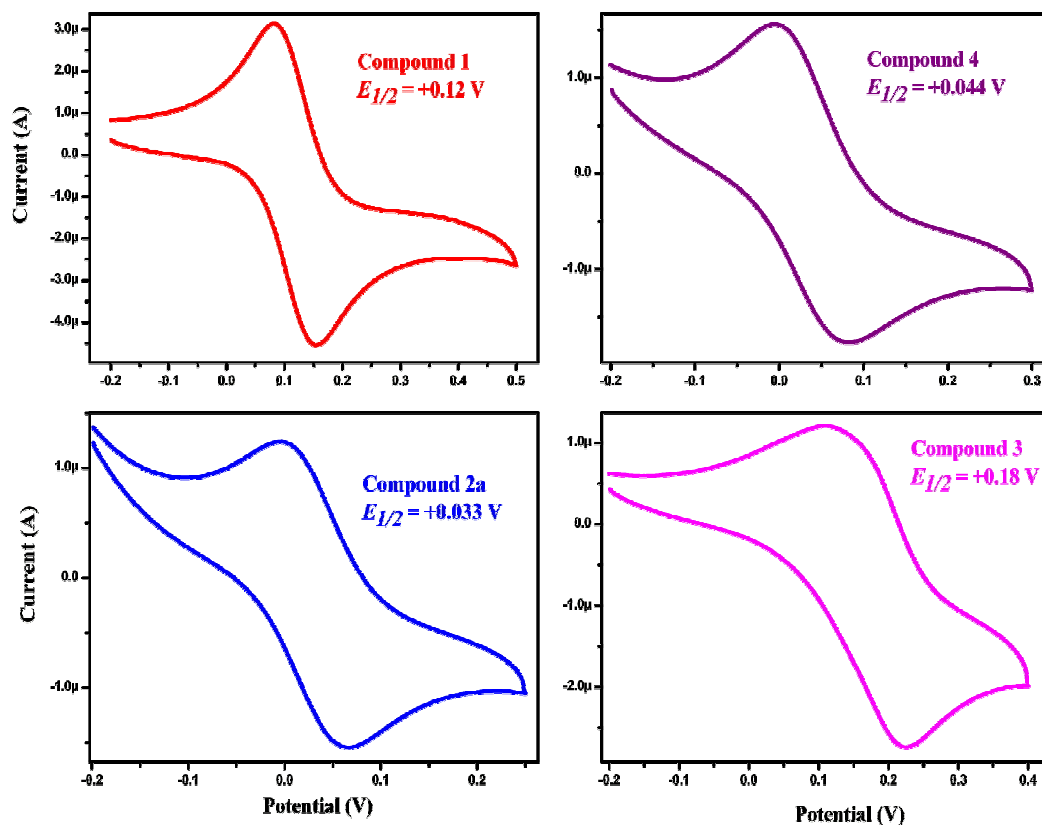
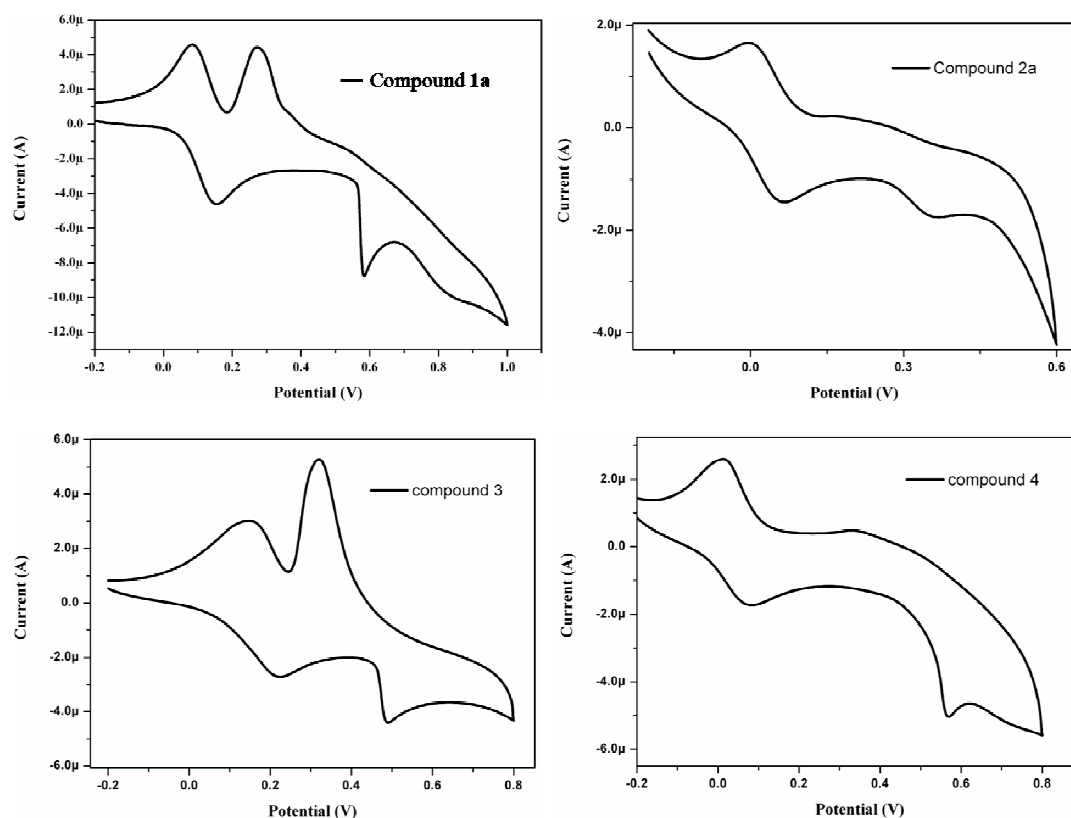


Figure 5.4. Cyclic voltammograms of compounds **1a**, **2a**, **3** and **4** in MeOH solutions at scan rate 50 mV s^{-1} , V vs Ag/AgCl.

Table 5.2. Electrochemical data of the compounds **1a**, **2a**, **3** and **4**.

	1a	2a	3	4
$E_{1/2}^{\text{oxd}}$ (V)	+0.12(rev)	+0.033(rev)	+0.18(rev)	+0.044(rev)
$E^{\text{2 oxd}}$ (V)	+0.27(irr)	—	+0.32(irr)	—
$E^{\text{3 oxd}}$ (V)	+0.58(irr)	+0.36(irr)	+0.49(irr)	+0.57(irr)

**Figure 5.5.** Cyclic voltammogram of compounds **1a**, **2a**, **3** and **4** in TBAP/MeOH at a scan rate 50 mV s⁻¹.

Comparison of Electrochemical Properties Between the [Bu₄N]₂[Ni(6,7-qdt)₂] (**1a**) and [Bu₄N]₂[Ni(qdt)₂]

Interestingly, complex **1a** undergoes reversible oxidation at very low oxidation potential compared to the [Ni(qdt)₂]²⁻ in MeOH solutions as shown in Figure 5.6. This shows $E_{1/2} = +0.12$ V *vs* Ag/AgCl ($\Delta E = 74$ mV), that corresponds the [Ni(6,7-dt)₂]¹⁻/ [Ni(6,7-dt)₂]²⁻ redox couple for the complex **1a**. But the first oxidation for the complex (Bu₄N)₂[Ni(qdt)₂] appears at $E_{1/2} = +0.41$ V *vs* Ag/AgCl ($\Delta E = 89$ mV), that corresponds the [Ni(qdt)₂]¹⁻/ [Ni(qdt)₂]²⁻ redox couple in the electrochemical scale. This clearly indicates that complex

1a is easily oxidized from di-anion to mono-anion compared to the $(\text{Bu}_4\text{N})_2[\text{Ni}(\text{qdt})_2]$ complex. This means that the ligand $\{6,7\text{-qdt}\}^{2-}$ is more electron releasing towards the metal ion than the $\{\text{qdt}\}^{2-}$ ligand. Thus the location of the ring nitrogen atoms of $\{\text{qdt}\}^{2-}$ ligand can tune the redox potential of the concerned complex.

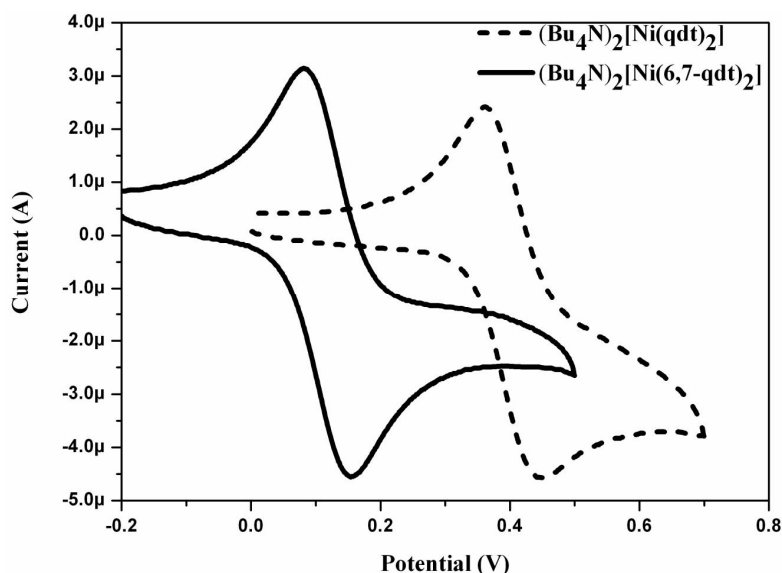


Figure 5.6. Cyclic voltammograms of compounds **1a** and $[\text{Bu}_4\text{N}]_2[\text{Ni}(\text{qdt})_2]$ in TBAP/MeOH at a scan rate 50 mV s^{-1} .

5.3.4. X-ray Crystallographic Studies

Crystal Structure Description of $[\text{Bu}_4\text{N}]_2[\text{Ni}(6,7\text{-qdt})_2]$ (**1a**)

The crystals of compound **1a**, suitable for single crystal X-ray structure determination, were obtained from acetonitrile solution by vapor diffusing with diethyl ether. Compound **1a** crystallizes in monoclinic space group $P2_1/c$. The relevant asymmetric unit contains half molecule of $[\text{Bu}_4\text{N}]_2[\text{Ni}(6,7\text{-qdt})_2]$ (**1a**) as shown in Figure 5.7. The crystallographic parameters, data collection and structure refinement of the compounds **1a** are summarized in Table 5.3. Selected bond lengths and angles for the compounds **1a** are listed in Table 5.5. In the complex anion $[\text{Ni}(6,7\text{-qdt})_2]^{2-}$, the geometry around the Ni^{2+} ion, which is coordinated by four sulfur atoms from two 6,7-qdt ligands, is almost square planar because S–Ni–S coordination angles are in the range of $88.41(13)^\circ$ to $91.59(13)^\circ$ (close to 90°) and there is no deviation between two 6,7-qdt planes. These coordination angles are comparable to the coordination angles in nickel-qdt complex $[\text{Ni}(\text{qdt})_2]^{2-}$ [$88.33(5)^\circ$ and

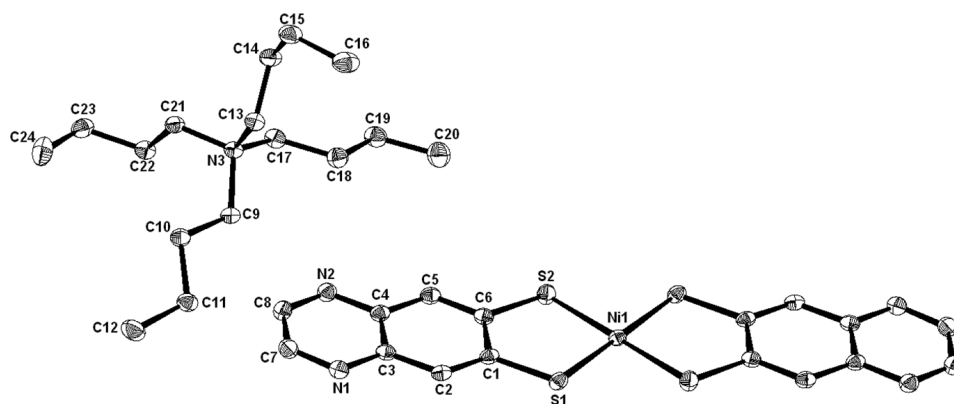


Figure 5.7. Thermal ellipsoidal plot of the asymmetric unit of compound $[\text{Bu}_4\text{N}]_2[\text{Ni}(6,7\text{-qdt})_2]$ (**1a**), that contains one tetrabutylammonium cation and half molecule of $[\text{Ni}(6,7\text{-qdt})_2]^{2-}$ ion. Hydrogen atoms are not shown for clarity (50% probability).

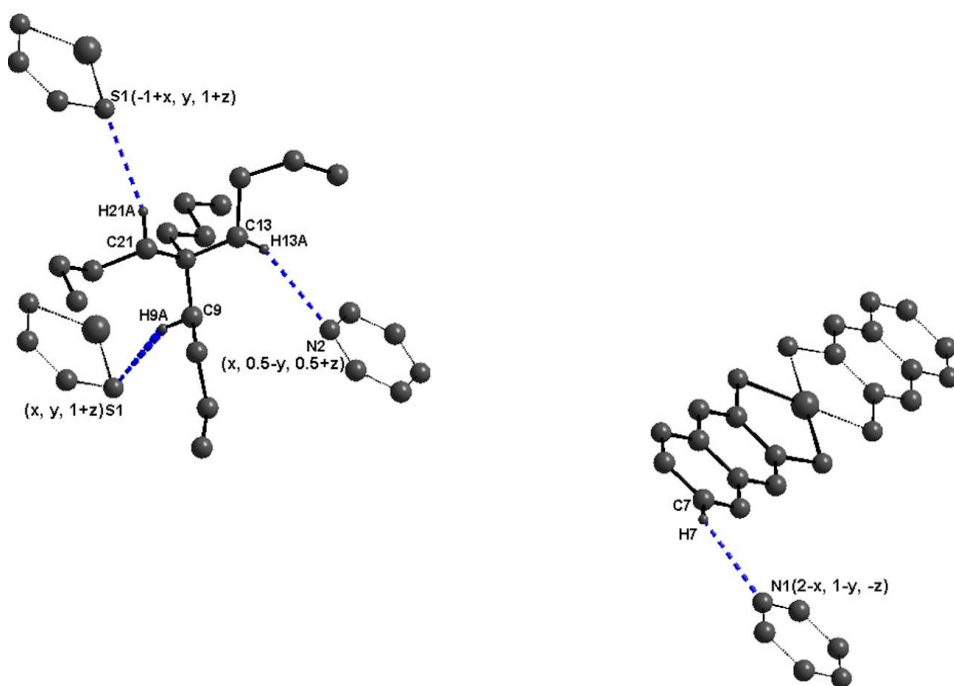


Figure 5.8. View of the asymmetric unit of $[\text{Bu}_4\text{N}]_2[\text{Ni}(6,7\text{-qdt})_2]$ (**1a**) (solid lines) (some of the hydrogen atoms are removed for clarity) showing all the H-bonding intermolecular cation-anion contacts and anion-anion contacts with other surrounding moieties (dotted lines).

$91.67(5)^\circ$].¹⁷ The average bond distance of Ni–S in the present study is $2.165 \pm 0.003 \text{ \AA}$, which is slightly shorter than average bond distance of Ni–S ($2.175 \pm 0.010 \text{ \AA}$) in nickel-qdt complex $[\text{Ni}(\text{qdt})_2]^{2-}$.¹⁷ In the crystal structure of compound **1a**, both cation $[\text{Bu}_4\text{N}]^+$ and anion $[\text{Ni}(6,7\text{-qdt})_2]^{2-}$ are involved in an extensive C–H \cdots S and C–H \cdots N hydrogen bonding interactions resulting in a three dimensional supramolecular network (*vide infra*).

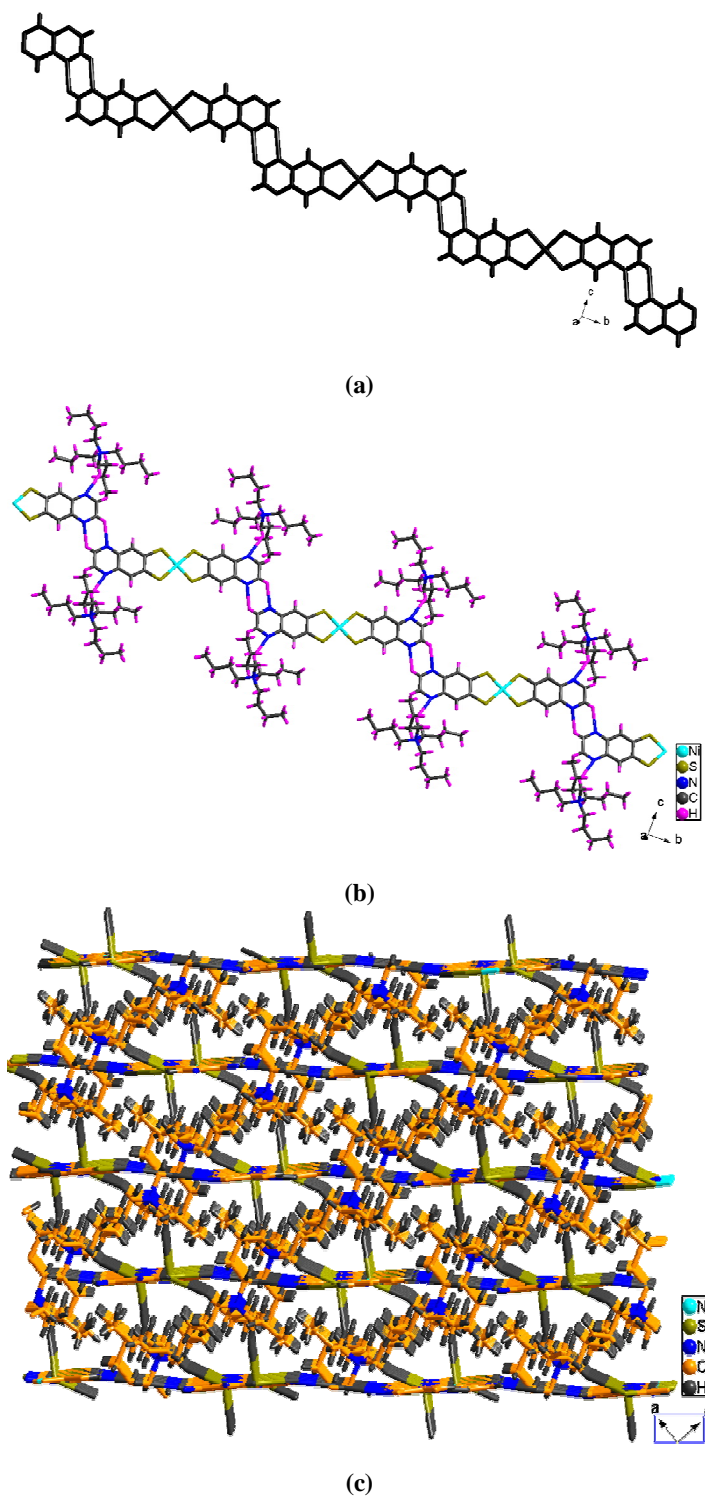


Figure 5.9. (a) One-dimensional supramolecular chain of $[\text{Bu}_4\text{N}]_2[\text{Ni}(\text{6,7-qdt})_2]$ (**1a**) characterized by C–H \cdots N weak interactions; (b) One dimensional supramolecular chain of $[\text{Bu}_4\text{N}]_2[\text{Ni}(\text{6,7-qdt})_2]$ (**1a**) characterized by two C–H \cdots N (N1 and N2 positioned at 2-*x*, 1-*y*, -*z* and *x*, 0.5-*y*, 0.5+*z* symmetry) H-bonding interactions; (c) Three dimensional supramolecular network of $[\text{Bu}_4\text{N}]_2[\text{Ni}(\text{6,7-qdt})_2]$ (**1a**) characterized by C–H \cdots N and C–H \cdots S weak interactions, when viewed down to the crystallographic *b* axis.

A view of the building unit for the formation of supramolecular network of $[\text{Bu}_4\text{N}]_2[\text{Ni}(\text{6,7-qdt})_2]^{2-}$ (**1a**), with the evidence of all the H-bonding intermolecular cation-anion and anion-anion contacts, is shown in Figure 5.8. The relevant hydrogen bonding geometrical parameters are listed in the Table 5.6. The C–H \cdots N (N1 positioned at 2-x, 1-y, -z symmetry) hydrogen bonding contact between the anions results in a one-dimensional supramolecular chain, as shown in Figure 5.9(a). This supramolecular chain involves C–H \cdots N hydrogen bonding interactions with surrounding tetrabutylammonium cations as shown in Figure 5.9(b). Each tetrabutylammonium cation is characterized by three H-bond contacts with three surrounding anions as shown in Figure 5.8; two of them are described as C–H \cdots S interactions with S1 atoms of two distinct anions, positioned at x, y, z+1 and x-1, y, z+1 symmetries respectively. The remaining one is described as C–H \cdots N weak interaction with N2 atom of other anion positioned at x, 0.5-y, 0.5+z symmetry. The weak H-bonding interactions between cation and anion due to ionic nature of compounds may induce the charge effect. The effective combination of the C–H \cdots S and C–H \cdots N hydrogen bonding interactions in the crystal structure results in a three-dimensional supramolecular network as shown in Figure 5.9(c), that is viewed down to crystallographic *b* axis.

Crystal Structure Description of $[\text{PPh}_4]_2[\text{Ni}(\text{6,7-qdt})_2]$ (**1b**)

The crystals of compound **1b**, suitable for single crystal X-ray structure determination, were obtained from acetonitrile solution by the vapour diffusion of diethyl ether. Crystallographic analysis revealed that compound **1b** crystallizes in monoclinic form with space group *C2/c* whereas compound **1a** crystallizes in *P2(1)/c*. The relevant asymmetric unit of the compound **1b** contains half molecule of $[\text{Ni}(\text{6,7-qdt})_2]^{2-}$ anion and one tetraphenylphosphonium cation. Thermal ellipsoid diagram of compound **1b** containing the anion complex unit is shown in Figure 5.10(a). The crystallographic parameters, data collection and structure refinement of the compounds **1b** are summarized in Table 5.3. Selected bond lengths and angles for the compounds **1b** are listed in Table 5.5. Eventhough, both complexes **1a** and **1b** form almost square planar geometry around the Ni^{2+} ion, which is coordinated by four sulphur atoms from two 6,7-qdt ligands between the two SMS planes, but there is a more deviation in the planar nature of the dithiolate-chelate present in the complex **1b**, which shows less deviation in the case of complex **1a**, as shown in Figures 5.10(b) and 5.10(c). The coordination angles are in the range of

88.41(13)°–91.59(13)° in complex **1a**, and 88.65(4)°–91.35(4)° in complex **1b**, which are very close to 90.0° and other coordination angles are 180.0° in both the complexes **1a** and **1b**, which are not deviated. The bending deviation (η) between the SMS plane and SCCS plane are characterized by the angle of 11.93° present in the {Ni1S1S2C1C2} chelate of the complex **1b**, whereas in complex **1a** this bending deviation is 1.88°. The deviation in the planar nature of the dithiolate-chelate may be due to the more bulkiness of tetraphenylphosphonium counter cations present in complex **1b**, compared to the tetrabutylammonium cations present in complex **1a**.

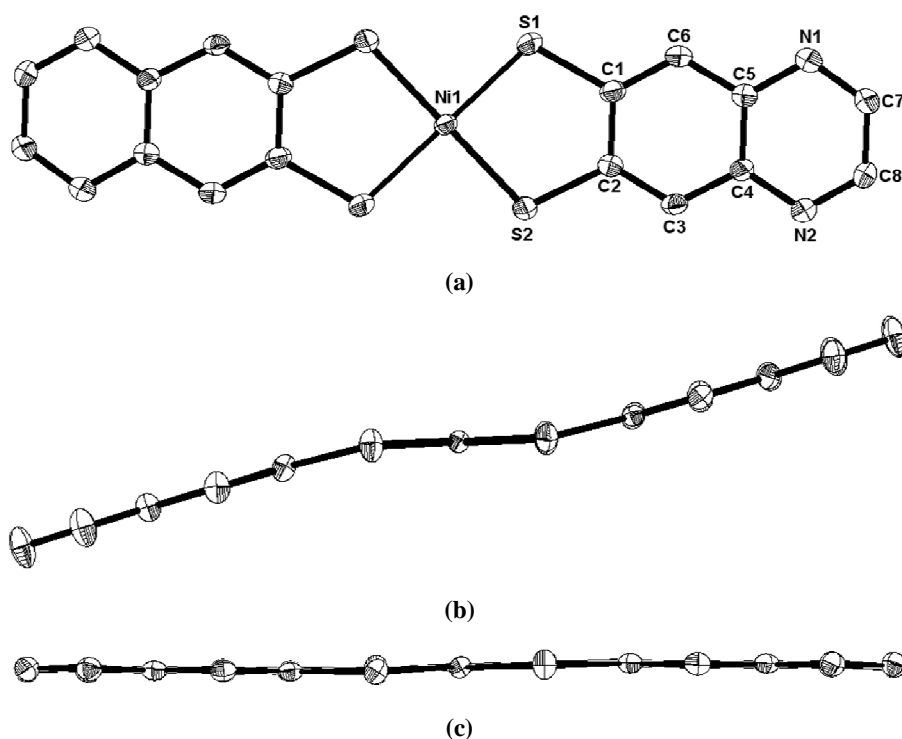


Figure 5.10. (a) Thermal ellipsoidal diagram of compound **1b** containing complexic unit (40% probability); and side view representation of complexes (b) **1b** and (c) **1a**.

In the crystal structure of compound **1b**, both cation $[\text{Bu}_4\text{N}]^+$ and anion $[\text{Ni}(6,7\text{-qdt})_2]^{2-}$ are involved in C–H...S and C–H...N hydrogen bonding interactions resulting in a one dimensional supramolecular network (*vide infra*). A view of the building unit for the formation of supramolecular network of $[\text{Bu}_4\text{N}]_2[\text{Ni}(6,7\text{-qdt})_2]^{2-}$ (**1**), with the evidence of all the H-bonding intermolecular cation-anion and anion-anion contacts, is shown in Figure 5.11(a). The relevant hydrogen bonding geometrical parameters are listed in the

Table 5.6. The C–H···N (N1 positioned at $-x, y, 0.5-z$ symmetry) hydrogen bonding contact between the anions results in a one-dimensional supramolecular chain. This supramolecular chain engages C–H···S weak hydrogen bonding interactions with surrounding tetraphenylphosphonium cations as shown in Figure 5.11(b).

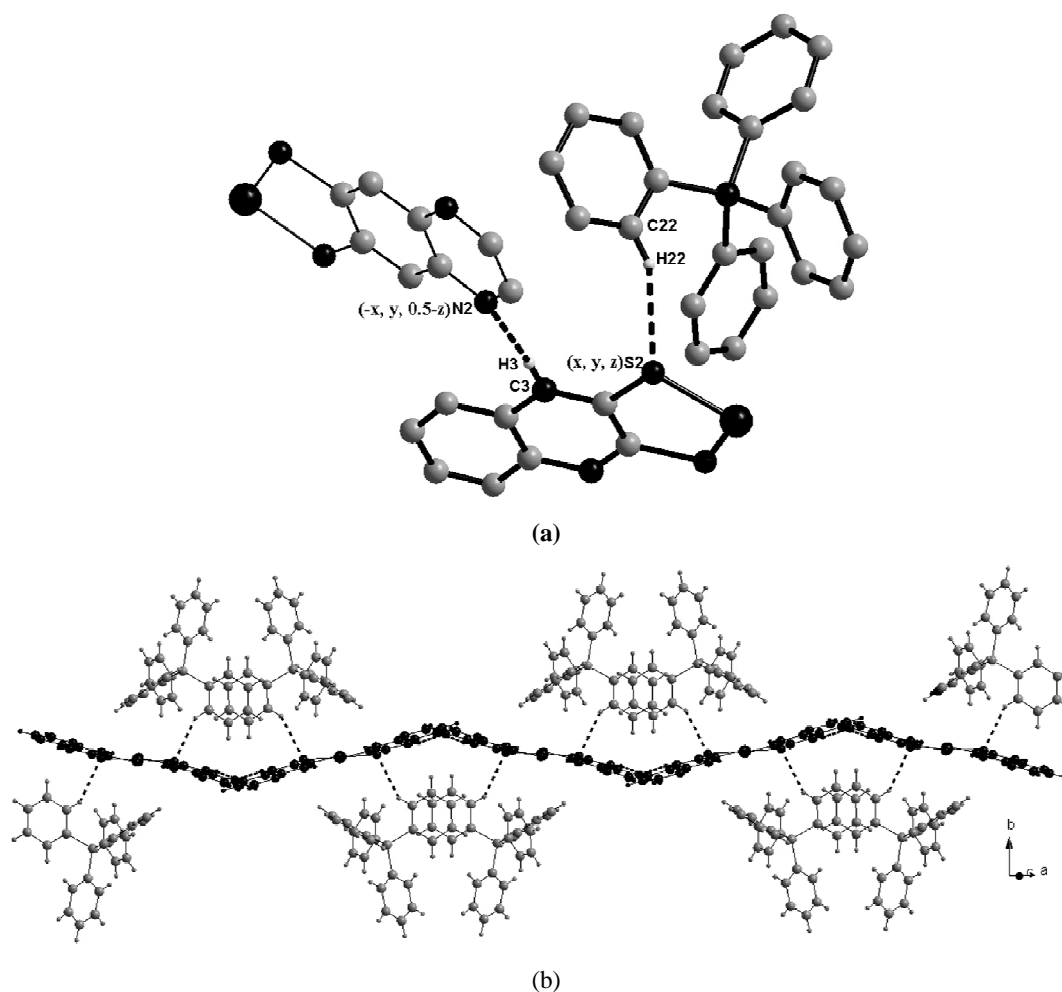


Figure 5. 11. (a) View of the asymmetric unit of $[\text{Bu}_4\text{N}]_2[\text{Ni}(\text{6,7-qdt})_2]$ (**1b**) (thick solid lines) (some of the hydrogen atoms are removed for clarity) showing all the H-bonding intermolecular cation-anion and anion-anion contacts (dotted lines) with other surrounding moieties (thin solid lines); (b) One dimensional supramolecular chain of compound **1b** characterized by C–H···N and C–H···S weak interactions.

Crystal Structure Description of $[\text{PPh}_4]_2[\text{Ni}(\text{Ph}_2\text{6,7-qdt})_2]$ (**2b**)

The crystals of compound **2b**, suitable for single crystal X-ray structure determination, were obtained from DMF solution by the vapor diffusion of diethyl ether. Crystallographic analysis revealed that compound **2b** crystallizes in monoclinic space group $C2/c$.

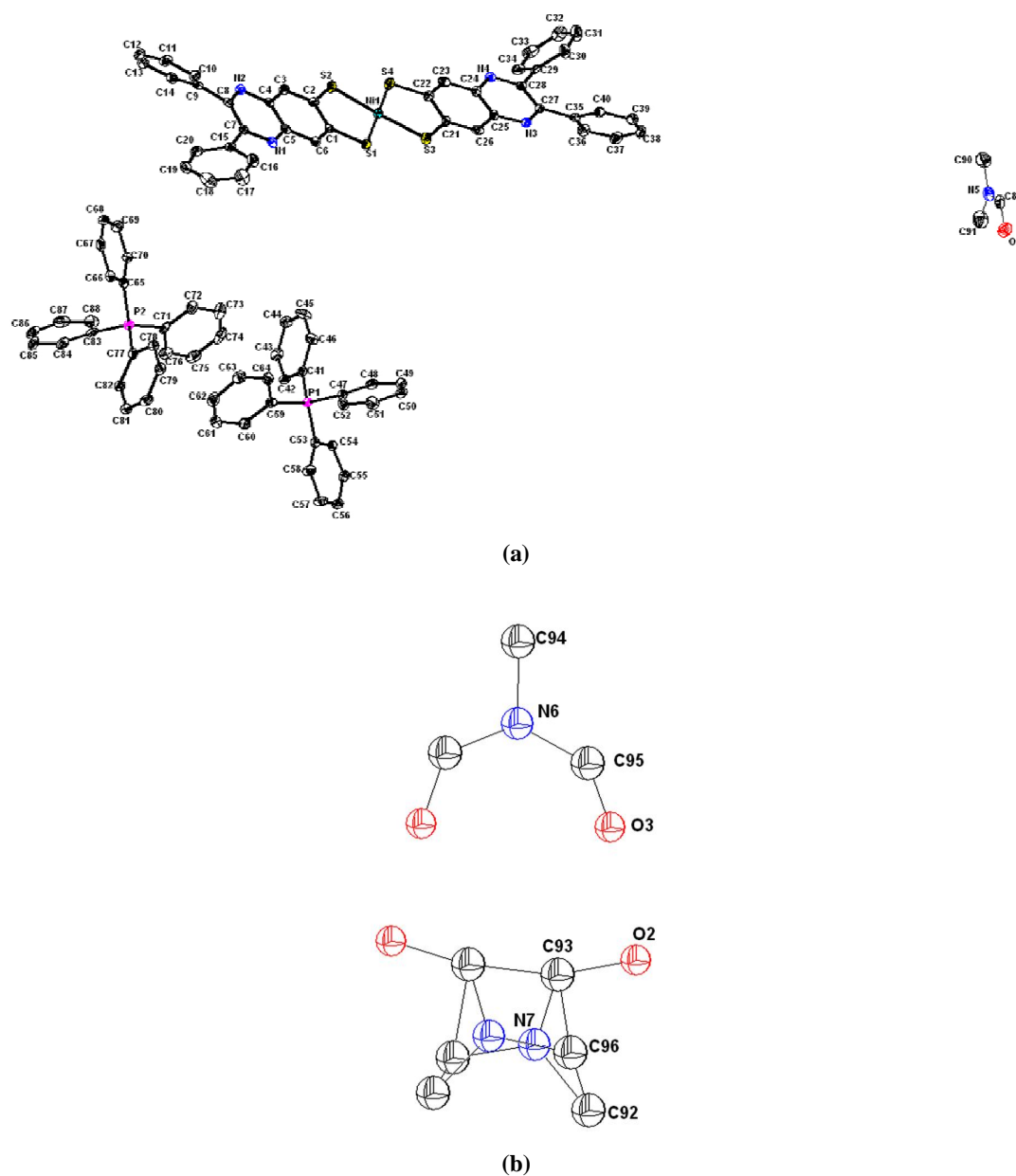


Figure 5.12. (a) Thermal ellipsoidal diagram of asymmetric unit of the compound **2b** (50% probability) (the two disordered DMF molecules and hydrogen atoms are removed for clarity; (b) The disordered two DMF solvent molecules (we could not perform anisotropic corrections).

The crystallographic parameters, data collection and structure refinement of the compounds **2b** are summarized in Table 5.3. Selected bond lengths and angles for the compounds **2b** are listed in Table 5.5. The relevant asymmetric unit of the compound **2b** contain one molecule of $[\text{Ni}(\text{Ph}_2\text{6,7-qdt})_2]^{2-}$ anionic complex and two tetraphenylphosphonium cations as shown Figure 5.12(a). In addition to this, three DMF

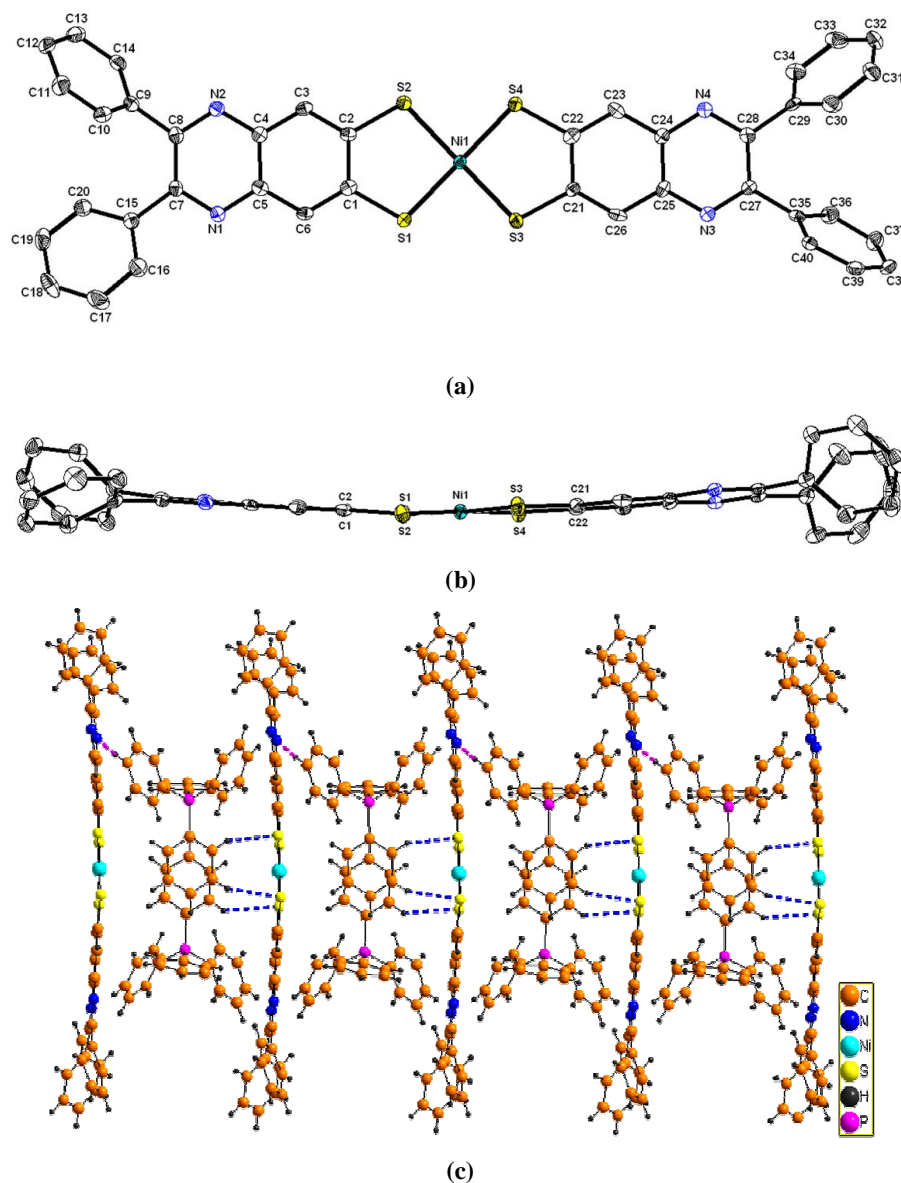


Figure 5.13. (a) Thermal ellipsoidal diagram of compound **2b** containing complexic unit (50% probability); and its (b) sideview representation; (c) one dimensional supramolecular chain of compound **2b** characterized by C–H...N and C–H...S weak interactions.

solvent molecules are crystallized in the crystal structure of the compound **2b**, in which, two of them are present in two fold axis of symmetry. These two DMF solvent molecules suffer from significant disorder; due to this we could not perform anisotropic refinement for these two solvent molecules as shown in Figure 5.12(b). Thermal ellipsoidal diagram of the $[\text{Ni}(\text{Ph}_2\text{6,7-qdt})_2]^{2-}$ anion in compound **2b** is shown in Figure 5.13(a). The dihedral angle between the two SMS planes is 2.70° and the geometry around the Ni^{2+} ion, which is coordinated by four sulfur atoms from two $\{\text{Ph}_2\text{6,7-qdt}\}^{2-}$ ligands shows slightly

distorted from square planar geometry as shown in Figure 5.13(b). The coordination angles are in the range of $177.81(6)^\circ$ – $178.36(6)^\circ$ and $88.51(5)^\circ$ – $91.51(5)^\circ$, which are slightly deviated from angles of 180.0° and 90.0° respectively. In addition to the dihedral angle, complex **2b** shows bending deviations in the planar nature of the dithiolate-chelates. The bending deviations (η) between the {S1Ni1S2} and {S1C1C2S2} planes, and {S3Ni1S4} and {S3C21C22S4} planes, are characterized by the angles of 5.80° and 0.26° present in {Ni1S1S2C1C2} and {Ni1S3S4C21C22} dithiolate-chelates, respectively. The crystal structure of the compound **2b** is characterized by three C–H...S weak interactions and one C–H...N weak interaction between the anion and cations resulting in a one dimensional supramolecular chain as shown Figure 5.13(c). The relevant hydrogen bonding geometrical parameters are listed in the Table 5.6. The weak C–H...S interactions may causes in the deviation in the dihedral angles around the metal ion and bending deviation of dithiolate-chelated ring.

Crystal Structure Description of [Bu₄N]₂[Ni(Cl₂6,7-qdt)₂] (3**)**

The crystals of compound **3**, for single crystal X-ray structure determination, were recrystallized from acetonitrile solution by the vapour diffusion of diethyl ether. X-ray crystal structure analysis shows that compound **3** crystallizes in monoclinic space group $P2(1)/c$. The crystallographic parameters, data collection and structure refinement of the compounds **3** are summarized in Table 5.4. Selected bond lengths and angles for the compounds **3** are listed in Table 5.5. The relevant asymmetric unit of the compound **3** contains half molecule of $[\text{Ni}(\text{Cl}_2\text{6,7-qdt})_2]^{2-}$ anion and one molecule of tetrabutylammonium cation. The thermal ellipsoidal diagram of the $[\text{Ni}(\text{Cl}_2\text{6,7-qdt})_2]^{2-}$ anion present in the compound **3** is shown in Figure 5.14(a). Because of the poor quality of the crystal, tetrabutylammonium cation present in the crystal structure of the compound **3** suffers significant disorder problem as shown Figure 5.15. Due to this, we could not study weak interactions between the cations and anions. Despite of few attempts of the recrystallization in various techniques, we could not get better quality of the single crystals of this compound. In the anion of the complex **3**, the geometry around the Ni^{2+} ion, which is coordinated by four sulfur atoms from two {Cl₂6,7-qdt} ligands, shows approximately square planar geometry, because the coordination angles are in the range of and $88.42(10)^\circ$ – $91.58(10)^\circ$ which are very close to 90.0° and other coordination angles are

180.0° without any deviation as shown in Figure 5.14(b). However, there is a deviation in the planar nature of the dithiolene-ligand (chelate) present in the complex **3**. The bending deviation (η) between the SMS plane and SCCS plane are characterized by the angle of 5.32° present in the {Ni1S1S2C1C2} chelate containing the complex **3**.

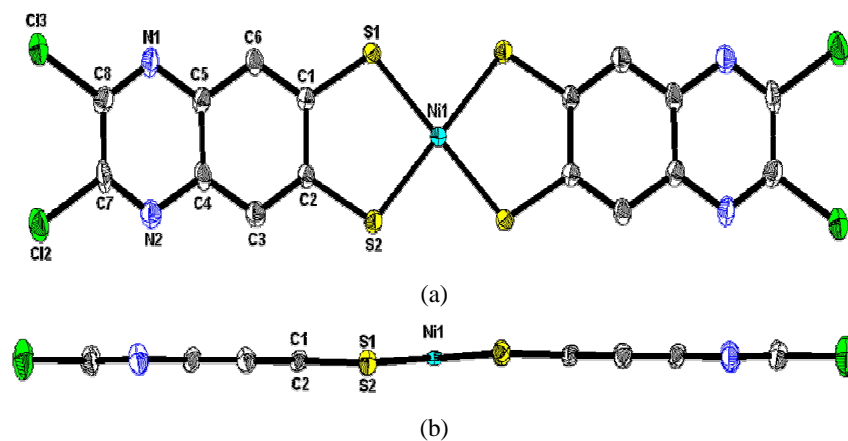


Figure 5.14. Thermal ellipsoidal diagram of compound **3** containing complexic unit (20% probability); and its (b) side view representation.

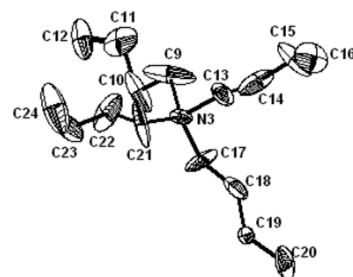
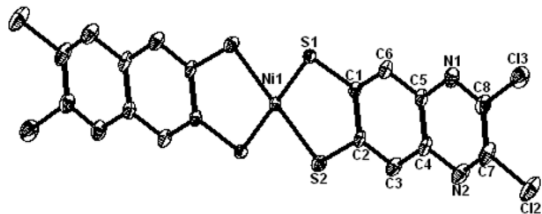


Figure 5.15. Thermal ellipsoidal diagram of asymmetric unit of the compound **3** (20% probability) (tetrabutylammonium cation present in the crystal structure suffers significant disorder problem, Hydrogen atoms removed for clarity).

Crystal Structure Description of $[\text{Bu}_4\text{N}]_2[\text{Ni}(\text{Me}_2\text{6,7-qdt})_2]$ (4**)**

The crystals of compound **4**, suitable for single crystal X-ray structure determination, were obtained from acetonitrile solution by the vapour diffusion of diethyl ether. Crystallographic analysis revealed that compound **4** crystallizes in monoclinic space group $P-1$. The crystallographic parameters, data collection and structure refinement of the compounds **4** are summarized in Table 5.4. Selected bond lengths and angles for the compounds **4** are listed in Table 5.5. The relevant asymmetric unit of the compound **4** contains one molecule of $[\text{Ni}(\text{Me}_2\text{6,7-qdt})_2]^{2-}$ anion and two molecules of tetrabutylammonium cations. The thermal ellipsoidal diagram of the $[\text{Ni}(\text{Me}_2\text{6,7-qdt})_2]^{2-}$ anion present in the compound **4** is shown in Figure 5.16(a).

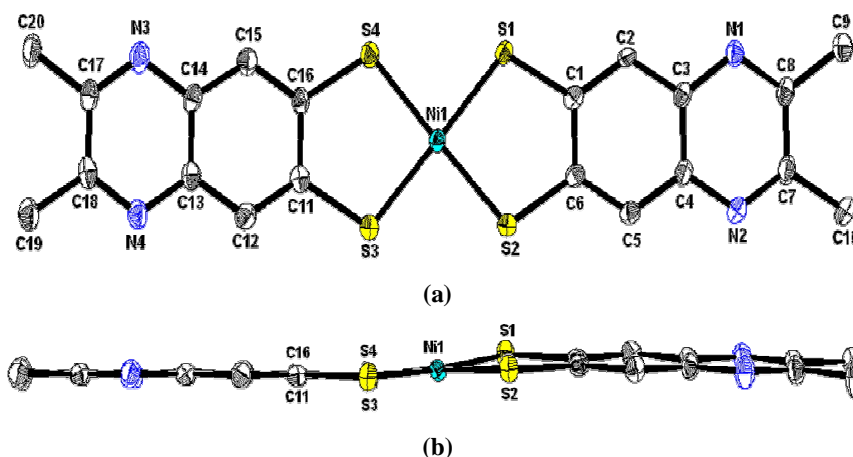


Figure 5.16. (a) Thermal ellipsoidal diagram of compound **4** containing complexic unit (40% probability); and its (b) side view representation.

In the anion of the complex **4**, the geometry around the Ni^{2+} ion, which is coordinated by four sulfur atoms from two $\{\text{Me}_2\text{6,7-qdt}\}^{2-}$ ligands, shows distorted from square planar geometry between the two SMS planes with a dihedral angle of 4.87° , because the coordination angles are in the range of $175.30(5)^\circ$ – $177.89(5)^\circ$ and $87.93(4)^\circ$ – $91.22(4)^\circ$ which are deviated from 180.0° and 90.0° , respectively. As shown in Figure 5.16(b), the distortion of the NiS_4 from square planar geometry clearly has shown the side view of anionic complex **4**, whereas complexes **1a** and **1b** do not show any distortion from square planar geometry as clearly shown by their side view diagrams of the complexes. The reason for the distortion from the square planar geometry may be due to involvement the sulfur atoms in an extensive $\text{C-H}\cdots\text{S}$ hydrogen bonding interactions, present in the

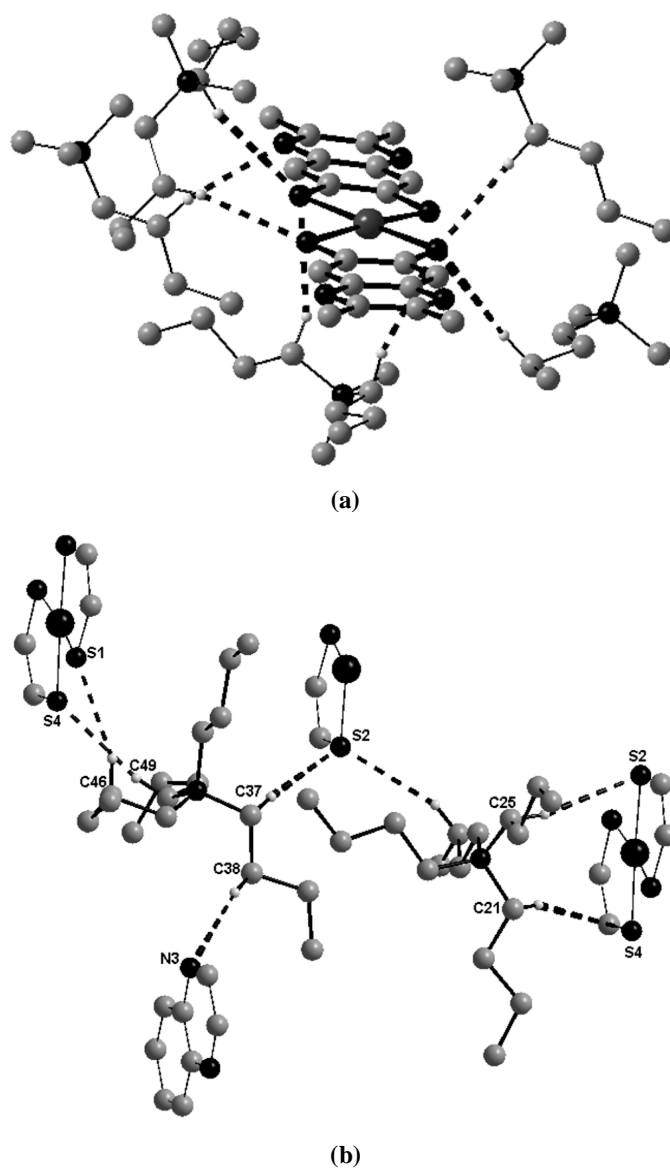


Figure 5.17. (a) Anionic complexic unit of the compound **4** (thick solid lines) showing all the H-bonding intermolecular cation-anion contacts (dotted lines) with other surrounding cations (thin solid lines); (b) View of the asymmetric unit of compound **4** (thick solid lines) (some of the hydrogen atoms are removed for clarity) showing all the H-bonding intermolecular cation-anion contacts (dotted lines) with other surrounding moieties (thin solid lines).

complex **4** compared to the previous complexes **1a** and **1b**, with less involvement of sulfur atoms in C–H...S hydrogen bonding interactions with surrounding tetrabutylammonium cations. Along with the more dihedral angle, complex **4** suffer from the bending deviations in the planar nature of the dithiolate-chelates. The bending deviations (η) between the {S1Ni1S2} and {S1C1C6S2} planes, and {S3Ni1S4} and {S3C11C16S4} planes, are

characterized by the angles of 6.24° and 4.53° present in $\{\text{Ni1S1S2C1C6}\}$ and $\{\text{Ni1S3S4C11C16}\}$ dithiolate-chelated rings, respectively.

In the crystal structure of the compound **4**, each dithiolate anionic complex containing three out of four sulfur atoms are characterized by six $\text{C-H}\cdots\text{S}$ hydrogen bonding contacts with four surrounding $[\text{Bu}_4\text{N}]^+$ cations and one $\text{C-H}\cdots\text{N}$ hydrogen bonding contact with one $[\text{Bu}_4\text{N}]^+$ cation as shown Figure 5.17(a). The asymmetric unit of the crystal structure contains two types of $[\text{Bu}_4\text{N}]^+$ cations, described by six $\text{C-H}\cdots\text{S}$ hydrogen-bond contacts with three surrounding anions and one $\text{C-H}\cdots\text{N}$ hydrogen-bonding contact with one anion is shown in Figure 5.17(b). The relevant hydrogen bonding geometrical parameters are listed in the Table 5.6. The effective combination of $\text{C-H}\cdots\text{S}$ and $\text{C-H}\cdots\text{N}$ weak hydrogen bonding interactions between the cation and anions are results in a two dimensional supramolecular network as shown in Figure 5.18.

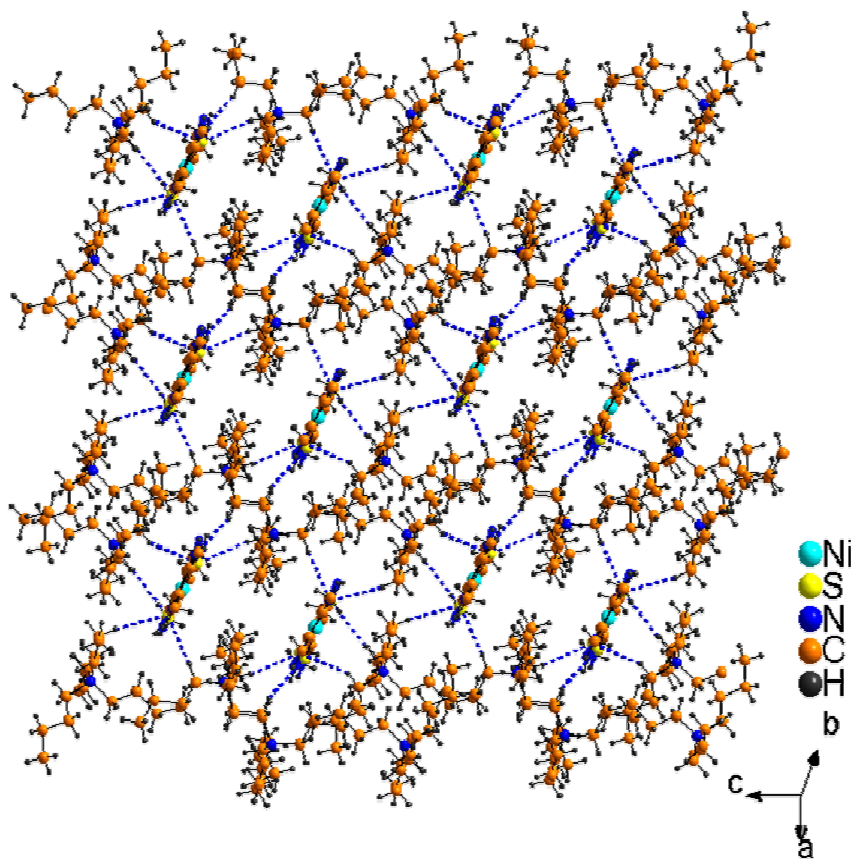


Figure 5.18. Three dimensional supramolecular network of compound **4** is characterized by $\text{C-H}\cdots\text{N}$ and $\text{C-H}\cdots\text{S}$ weak interactions.

Table 5.3. Crystal Data and Structural Refinement for Compounds **1a**, **1b** and **2b**

	1a	1b	2b
Empirical formula	C ₄₈ H ₈₀ N ₆ S ₄ Ni	C ₆₄ H ₄₈ N ₄ P ₂ S ₄ Ni	C ₉₇ H ₈₅ N ₇ O ₃ P ₂ S ₄ Ni
Formula weight	928.13	1121.95	1645.61
T [K], λ [Å]	100(2), 0.71073	100(2), 0.71073	100(2), 0.71073
Crystal system	Monoclinic	Monoclinic	Monoclinic
Space group	<i>P</i> 2(1)/ <i>c</i>	<i>C</i> 2/ <i>c</i>	<i>C</i> 2/ <i>c</i>
<i>a</i> [Å]	8.1456(8)	26.993(2)	19.6540(12)
<i>b</i> [Å]	16.3363(15)	13.2302(9)	19.3493(12)
<i>c</i> [Å]	18.6154(17)	16.4171(11)	41.897(3)
α [deg]	90.000	90.000	90.000
β [deg]	93.100(10)	117.476(2)	102.767(10)
γ [deg]	90.000	90.000	90.000
<i>V</i> [Å ³]	2473.5(4)	5201.6(7)	15539.2(17)
<i>Z</i> , <i>D</i> _{calc} [Mg m ⁻³]	2, 1.246	4, 1.433	8, 1.407
μ [mm ⁻¹], F[000]	0.600, 1004	0.643, 2328	0.459, 6896
Crystal size [mm ³]	0.58 x 0.20 x 0.14	0.46 x 0.20 x 0.08	0.50 x 0.26 x 0.04
θ range for data collection [deg]	1.66 to 26.00	1.70 to 26.48	1.50 to 26.03
Reflections collected / unique	25078/4833	27521/5393	79828/15262
R(int)	0.0269	0.0548	0.0862
Data / restraints / parameters	4833/0/272	5393/0/340	15262/ 0/ 972
Goodness-of-fit on F ²	1.059	1.112	1.112
R ₁ /wR ₂ [I > 2 σ (I)]	0.0291/0.0727	0.0804/0.1970	0.0875/0.1805
R ₁ /wR ₂ (all data)	0.0304/0.0736	0.0921/0.2052	0.1120/0.1924
Largest diff. Peak/hole [e Å ⁻³]	0.317/-0.344	1.834/-0.449	0.821/-0.984

Table 5.4. Crystal Data and Structural Refinement for Compounds **3** and **4**

	3	4
Empirical formula	C ₄₈ H ₇₆ N ₆ S ₄ Cl ₄ Ni	C ₅₂ H ₈₈ N ₆ S ₄ Ni
Formula weight	1065.94	984.23
T [K], λ [Å]	100(2), 0.71073	100(2), 0.71073
Crystal system	Monoclinic	Triclinic
Space group	<i>P</i> 2(1)/ <i>c</i>	<i>P</i> -1
<i>a</i> [Å]	13.8484(15)	13.0326(11)
<i>b</i> [Å]	8.5484(9)	14.3918(12)
<i>c</i> [Å]	22.521(3)	15.8859(13)
α [deg]	90.000	114.6950(10)
β [deg]	101.239(3)	94.4320(10)
γ [deg]	90.000	100.2510(10)
<i>V</i> [Å ³]	2614.9(5)	2625.3(4)
<i>Z</i> , <i>D</i> _{calc} [Mg m ⁻³]	2, 1.262	2, 1.245
μ [mm ⁻¹], F[000]	0.771, 988	0.569, 1068
Crystal size [mm ³]	0.24 x 0.10 x 0.06	0.38 x 0.10 x 0.06
θ range for data collection [deg]	1.50 to 24.94	1.43 to 26.08
Reflections collected / unique	23914/4580	27356/10289
R(int)	0.0771	0.0554
Data / restraints / parameters	4580/0/286	10289/0/580
Goodness-of-fit on F ²	1.249	1.089
R ₁ /wR ₂ [I > 2 σ (I)]	0.1690/0.3640	0.0786/0.1801
R ₁ /wR ₂ (all data)	0.1830/0.3733	0.1049/0.1942
Largest diff. Peak/hole [e Å ⁻³]	1.377/-0.791	1.910/-0.451

Table 5.5. Selected Bond Lengths and Bond Angles for compounds **1a**, **1b**, **2b**, **3** and **4**

Compound 1a			
Ni(1)-S(1)	2.1662(4)	Ni(1)-S(1)#1	2.1662(4)
Ni(1)-S(2)	2.1699(3)	Ni(1)-S(2)#1	2.1700(3)
S(1)-Ni(1)-S(1)#1	180.000(8)	S(1)-Ni(1)-S(2)	91.591(13)
S(1)#1-Ni(1)-S(2)	88.409(13)	S(1)-Ni(1)-S(2)#1	88.410(13)
S(1)#1-Ni(1)-S(2)#1	91.590(13)	S(2)-Ni(1)-S(2)#1	180.0
C(6)-S(2)-Ni(1)	105.48(5)	C(1)-S(1)-Ni(1)	105.63
Compound 1b			
Ni(1)-S(2)#1	2.1578(11)	Ni(1)-S(2)	2.1578(11)
Ni(1)-S(1)#1	2.1664(12)	Ni(1)-S(1)	2.1665(12)
S(2)#1-Ni(1)-S(2)	180.00(6)	S(2)#1-Ni(1)-S(1)#1	91.35(4)
S(2)-Ni(1)-S(1)#1	88.65(4)	S(2)#1-Ni(1)-S(1)	88.65(4)
S(2)-Ni(1)-S(1)	91.35(4)	S(1)#1-Ni(1)-S(1)	180.00(4)
C(1)-S(1)-Ni(1)	104.89(15)	C(2)-S(2)-Ni(1)	104.92(15)
Compound 2b			
Ni(1)-S(1)	2.1592(13)	Ni(1)-S(4)	2.1622(13)
Ni(1)-S(2)	2.1746(13)	Ni(1)-S(3)	2.1746(13)
S(1)-Ni(1)-S(4)	178.36(6)	S(1)-Ni(1)-S(2)	91.54(5)
S(4)-Ni(1)-S(2)	88.53(5)	S(1)-Ni(1)-S(3)	88.51(5)
S(4)-Ni(1)-S(3)	91.48(5)	S(2)-Ni(1)-S(3)	177.81(6)
C(1)-S(1)-Ni(1)	105.29(16)	C(21)-S(3)-Ni(1)	105.61(15)
C(22)-S(4)-Ni(1)	105.56(16)	C(2)-S(2)-Ni(1)	105.24(16)
Compound 3			
Ni(1)-S(2)	2.160(3)	Ni(1)-S(2)#2	2.160(3)
Ni(1)-S(1)#2	2.163(3)	Ni(1)-S(1)	2.163(3)
S(2)-Ni(1)-S(2)#2	179.998(1)	S(2)-Ni(1)-S(1)#2	88.42(10)
S(2)#2-Ni(1)-S(1)#2	91.58(10)	S(2)-Ni(1)-S(1)	91.58(10)
S(2)#2-Ni(1)-S(1)	88.42(10)	S(1)#2-Ni(1)-S(1)	180.0
C(1)-S(1)-Ni(1)	105.8(4)	C(2)-S(2)-Ni(1)	105.4(4)
Compound 4			
Ni(1)-S(4)	2.1599(12)	Ni(1)-S(2)	2.1675(12)
Ni(1)-S(1)	2.1699(12)	Ni(1)-S(3)	2.1786(12)
S(4)-Ni(1)-S(2)	177.89(5)	S(4)-Ni(1)-S(1)	87.93(4)
S(2)-Ni(1)-S(1)	90.83(4)	S(4)-Ni(1)-S(3)	91.22(4)
S(2)-Ni(1)-S(3)	90.15(4)	S(1)-Ni(1)-S(3)	175.30(5)
C(1)-S(1)-Ni(1)	105.77(14)	C(6)-S(2)-Ni(1)	105.55(14)
C(16)-S(4)-Ni(1)	105.91(15)	C(11)-S(3)-Ni(1)	105.20(15)

Symmetry transformations used to generate equivalent atoms: #1 -x+1/2,-y+3/2,-z+1; #2 -x+2,-y+2,-z.

Table 5.6. Hydrogen Bonds for Compounds **1a**, **1b**, **2b** and **4**

D–H...A	d(D...H)	d(H...A)	d(D...A)	<(DHA)
Compound 1a				
C(13)-H(13A)...N(2) ^a	0.97	2.70	3.4778(17)	137.6
C(7)-H(7)...N(1) ^b	0.93	2.66	3.2852(18)	124.8
C(21)-H(21A)...S(1) ^c	0.97	2.83	3.7573(13)	161.3
C(9)-H(9A)...S(1) ^d	0.97	2.77	3.6759(13)	155.3
Compound 1b				
C(3)-H(3)...N(2) ^e	0.93	2.61	3.531(6)	170.1
C(22)-H(22)...S(2)	0.93	2.88	3.650(6)	141.4
Compound 2b				
C(76)-H(76)...S(2) ^f	0.93	2.99	3.769(6)	142.9
C(61)-H(61)...S(1) ^f	0.93	2.94	3.801(5)	154.8
C(60)-H(60)...S(3) ^f	0.93	2.91	3.722(5)	147.3
C(54)-H(54)...O(1) ^g	0.93	2.62	3.469(6)	152.9
C(48)-H(48)...O(1) ^g	0.93	2.68	3.583(6)	164.6
C(50)-H(50)...N(4) ^h	0.93	2.72	3.576(6)	153.8
C(12)-H(12)...O(1) ⁱ	0.93	2.68	3.316(6)	125.8
Compound 4				
C(25)-H(25A)...S(2) ^k	0.97	2.86	3.814(4)	167.1
C(21)-H(21A)...S(4) ^k	0.97	2.88	3.778(4)	154.4
C(46)-H(46B)...S(1) ^l	0.97	2.76	3.669(4)	156.9
C(49)-H(49B)...S(4) ^l	0.97	2.83	3.780(4)	166.9
C(38)-H(38A)...N(3) ^m	0.97	2.64	3.584(6)	163.6
C(37)-H(37B)...S(2) ⁿ	0.97	2.65	3.609(4)	169.5
C(31)-H(31B)...S(2) ⁿ	0.97	2.90	3.785(5)	152.1

Symmetry transformations used to generate equivalent atoms: Symmetry transformations used to generate equivalent atoms: a) $x, -y+1/2, z+1/2$; b) $-x+2, -y+1, -z$; c) $x-1, y, z+1$; d) $x, y, z+1$; e) $-x, y, -z+1/2$; f) $x, y-1, z$; g) $x, -y+1, z+1/2$; h) $x+1/2, y-1/2, z$; i) $x, y, z+1$; k) $-x+1, -y+1, -z+1$; l) $-x+1, -y+1, -z$; m) $x, y+1, z$; n) $x-1, y+1, z$.

5.4. Conclusions

In design of new quinoxaline dithiolate ligands and its metal complexes, we have synthesized a new series of square-planar nickel-bis(quinoxaline-6,7-dithiolate) complexes with the general formula $[\text{Bu}_4\text{N}]_2[\text{Ni}(\text{X}_2\text{6,7-qdt})_2]$, where X = H (**1a**), Ph (**2a**), Cl (**3**) and Me (**4**). Solution and solid state absorption spectra of all these compounds show broad bands in the visible region which are due to the charge transfer (CT) transitions involving electronic excitation from a HOMO which is a mixture of dithiolate (π) and metal (d) orbital character to a LUMO which is a π^* orbital of the dithiolate, that are characteristics of metal(II) bis(dithiolene) complexes.^{23,11a} Interestingly, the absorption position maxima of these bands are strongly influenced by the nature of the electron donating / withdrawing groups attached to the 6,7-quinoxaline dithiolene core moiety. Cyclic voltammetric studies of complexes **1a**, **2a**, **3** and **4** undergo reversible oxidation at very low oxidation potentials compared to the existing Ni-qdt system (qdt = quinoxaline-2,3-dithiolate) corresponding to the di-anionic complexes to mono-anionic complexes, in MeOH solutions. This is probably due to the position of the nitrogen atom present in the qdt systems (qdt versus 6,7-qdt) that causes the difference in the withdrawing ability on the electron density in the vicinity of the metal atom. We also have described that the comparison studies of electronic and electrochemical properties between the nickel complexes of 6,7-qdt system and nickel complex of existed qdt-(quinoxaline-2,3-dithiolate) system. The electrochemical properties (the first oxidation potentials) of the present system $[\text{Bu}_4\text{N}]_2[\text{Ni}(\text{X}_2\text{6,7-qdt})_2]$ are dependent on the nature of the electron donating / withdrawing groups attached to the 6,7-quinoxaline dithiolene core moiety. From these results, we conclude that the ligand must be participating to a large extent in electron transfer process.

5.5. References

1. Karlin, K. D.; Stiefel, E. I. *Prog. Inorg. Chem.* John Wiley, New York, **2004**, Volume 52.
2. (a) Kato, R. *Chem. Rev.* **2004**, *104*, 5319–5346. (b) Mercuri, M. L.; Deplano, P.; Pilia, L.; Serpe, A.; Artizzu, F. *Coord. Chem. Rev.* **2010**, *254*, 1419–1433. (c) Coomber, A. T.; Beljonne, D.; Friend, R. H.; Brédas, J. L.; Charlton, A.; Robertson, N.; Underhill, A. E.; Kurmoo, M. Day, P. *Nature* **1996**, *380*, 144–146. (d) Ren, X. M.; Nishihara, S.; Akutagawa, T.; Noro, S.; Nakamura, T. *Inorg. Chem.* **2006**, *45*, 2229–2234. (e) Robertson, N.; Cronin, L. *Coord. Chem. Rev.* **2002**, *227*, 93–127.
3. (a) Deplano, P.; Pilia, L.; Espa, D.; Mercuri, M. L.; Serpe, A. *Coord. Chem. Rev.* **2010**, *254*, 1434–1447. (b) Serrano-Andrés, L.; Avramopoulos, A.; Li, J.; labéguerie, P.; Bégué, D.; Kellö, V.; Papadopoulos, M. G. *J. Chem. Phys.* **2009**, *131*, 134312. (c) Chen, C.-T.; Liao, S.-Y.; Lin, K.-J.; Lai, L.-L. *Adv. Mater.* **1998**, *3*, 334–338.
4. (a) Mueller-Westerhoff, U. T.; Vance, B.; Yoon, D. I. *Tetrahedron* **1991**, *47*, 909–932. (b) deplano, P.; Mercuri, M. L.; Pintus, G.; Trogu, E. F. *Comments Inorg. Chem.* **2001**, *22*, 353–374. (c) Bai, J.-F.; Zuo, J.-L.; Tan, W.-L.; Ji, W.; Shen, Z.; Fun, H.-K.; Chinnakali, K.; Razak, I. A.; You, X.-Z.; Che, C.-M. *J. Mater. Chem.* **1999**, *9*, 2419–2423. (d) Aragoni, M. C.; Arca, M.; Cassano, T.; Denotti, C.; Devillanova, F. A.; Frau, R.; Isaia, F.; Lelj, F.; Lippolis, V.; Nitti, L.; Romaniello, P.; Tommasi, R.; Verani, G. *Eur. J. Inorg. Chem.* **2003**, 1939–1947.
5. (a) Hine, F. J.; Taylor, A. J.; Garner, C. D. *Coord. Chem. Rev.* **2010**, *254*, 1570–1579. (b) Rees, D. C.; Hu, Y.; Kisker, C.; Sahindelin, H. *J. Chem. Soc., Dalton. Trans.* **1997**, 3909–3914. (c) Rudolph, M. J.; Wuebbens, M. M.; Rajagopalan, K. V.; Sahindelin, H. *Nat. Struct. Biol.* **2001**, *8*, 42.
6. (a) Johnson, J. L.; Rajagopalan, K. V. *Proc. Natl. Acad. Sci. USA* **1982**, *79*, 6856–6860. (b) Johnson, J. L.; Hainline, B. E.; Rajagopalan, K. V.; Arison, B. H. *J. Biol. Chem.* **1984**, *259*, 5414–5422.
7. (a) Boyde, S.; Garner, C. D.; Enemark, J. H.; Bruck, M. A.; Kristofzski, J. G. *J. Chem. Soc. Dalton. Trans.* **1987**, 2267–2271. (b) Boyde, S.; Garner, C. D.;

- Enemark, J. H.; Ortega, R. B. *J. Chem. Soc., Dalton. Trans.* **1987**, 297–302. (c) Boyde, S.; Garner, C. D.; Enemark, J. H.; Ortega, R. B. *Polyhedron* **1986**, *5*, 377–379.
8. Rabaça, S.; Almeida, M. *Coord. Chem. Rev.* **2010**, *254*, 1493–1508.
9. (a) Kobayashi, Y.; Jacobs, B.; Allendorf, M. D.; Long, J. R. *Chem. Mater.* **2010**, *22*, 4120–4122. (b) Baudron, S. A.; Hosseini, M. W. *Inorg. Chem.* **2006**, *45*, 5260. (c) Ribas, X.; Dias, J. C.; Morgado, J.; Wurst, K.; Molins, E.; Ruiz, E.; Almeida, M.; Veciana, J.; Rovira, C. *Chem. Eur. J.* **2004**, *10*, 1691. (d) Ribas, X.; Dias, J.; Morgado, J.; Wurst, K.; Almeida, M.; Veciana, J.; Rovira, C. *CrystEngComm* **2002**, *4*, 564. (e) Ribas, X.; MasPOCH, D.; Dias, J.; Morgado, J.; Almeida, M.; Wurst, K.; Vaughan, G.; Veciana, J.; Rovira, C. *CrystEngComm* **2004**, *6*, 589. (f) Takaishi, S.; Hosoda, M.; Kajiwar, T.; Miyasaka, H.; Yamashita, M.; Nakanishi, Y.; Kitagawa, Y.; Yamaguchi, K.; Kobayashi, A.; Kitagawa, H. *Inorg. Chem.* **2009**, *48*, 9048. (g) Ribas, X.; Dias, J. C.; Morgado, J.; Wurst, K.; Santos, I. C.; Almeida, M.; Vidal-Gancedo, J.; Veciana, J.; Rovira, C. *Inorg. Chem.* **2004**, *43*, 3631. (h) Dawe, L. N.; Miglioni, J.; Turnbow, L.; Taliaferro, M. L.; Shum, W. W.; Bagnato, J. D.; Zakharov, L. N.; Rheingold, A. L.; Arif, A. M.; Fourmigué, M. Miller, J. S. *Inorg. Chem.* **2005**, *44*, 7530. (i) Bolliglarla, R.; Das, S. K. *CrystEngComm* **2010**, *12*, 3409–3412.
10. (a) Naraso, Nishida, J.; Kumaki, D.; Tokito, S.; Yamashita, Y. *J. Am. Chem. Soc.* **2006**, *128*, 9598–9599. (b) Naraso, Nishida, J.; Ando, S.; Yamaguchi, J.; Itaka, K.; Koinuma, H.; Tada, H.; Tokito, S.; Yamashita, Y. *J. Am. Chem. Soc.* **2005**, *127*, 10142–10143.
11. (a) Cummings, S. D.; Eisenberg, R. *Inorg. Chem.* **1995**, *34*, 2007–2014. (b) Cummings, S. D.; Eisenberg, R. *Inorg. Chem.* **1995**, *34*, 3396–3403.
12. Bruke, R. W.; Deardorff, E. R. *Talanta* **1970**, *17*, 255–264.
13. Ryabushko, O. P.; Pilipenko, A. T.; Batkovskaya, L. A.; Savin, Y. S. *Ukr. Khim. Zh.* **1988**, *54*, 1172–1176.
14. Baker-Hawkes, M. J.; Billig, E.; Gray, H. B. *J. Am. Chem. Soc.* **1966**, *88*, 4870–4875.

15. Brusso, J. L.; Clements, O. P.; Haddon, R. C.; Itkis, M. E.; Leitch, A. A.; Oakley, R. T.; Reed, R. W.; Richardson, J. F. *J. Am. Chem. Soc.* **2004**, *126*, 8256.
16. Jia, C.; Liu, S.-X.; Tanner, C.; Leiggener, C.; Neels, A.; Sanguinet, L.; Levillain, E.; Leutwyler, S.; Hauser, A.; Decurtins, S. *Chem. Eur. J.* **2007**, *13*, 3804-3812.
17. Zhao, Y.; Su, W.; Cao, R.; Hong, M. *Acta Cryst. E* **2001**, *57*, m229-m230.
18. Bruker. *SADABS*, *SMART*, *SAINT* and *SHELXTL*, **2000** (Bruker AXS Inc., Madison, Wisconsin, USA).
19. Sheldrick, G. M. *Acta Crystallogr. Sect. A* **2008**, *64*, 112-122.
20. More, S. V.; Sastry, M. N. V.; Wang, C.-C.; Yao, C.-F. *Tetrahedron Lett.* **2005**, *46*, 6345-6348.
21. Liu, G.; Botting, C. H.; Evans, K. M.; Walton, J. A. G.; Xu, G.; Slawin, A. M. Z.; Westwood, N. J. *ChemMedChem* **2010**, *5*, 41-45.
22. Bolligarla, R.; Durgaprasad, G.; Das, S. K. *Inorg. Chem. Commun.* **2009**, *12*, 355-358.
23. Shupack, S. I.; Billig, E.; Clark, R. J. H.; Williams, R.; Gray, H. B. *J. Am. Chem. Soc.* **1964**, *86*, 4594.

Synthesis of New Intramolecular Charge Transfer A–D–A Tetrathiafulvalene-Fused Triads Exhibiting Large Solvent Sensitive Emission Behavior

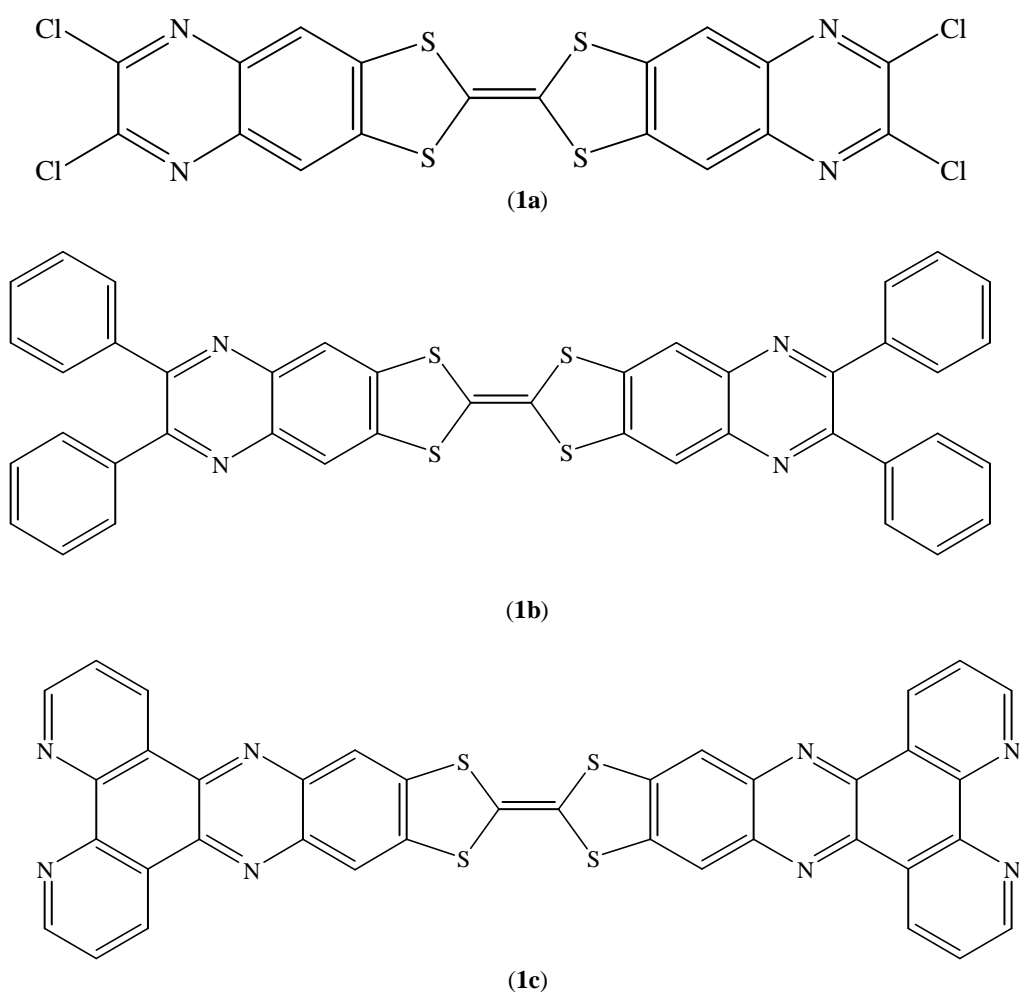
6
Chapter

Abstract:- We have synthesized three new acceptor-donor-acceptor (A–D–A) triads incorporating the donor tetrathiafulvalene (TTF) fused with acceptors quinoxaline and dipyrido[3,2-*a*:2',3'-*c*]phenazine (dppz) systems. Solution emission spectral studies of all these compounds show large solvent sensitive behavior with huge Stokes shifts. The large solvent dependence of the emission indicates that the excited state is stabilized in more polar solvents due to the intramolecular charge transfer. We have also described electrochemical studies of one of the title compounds (compound **1b**) exhibiting two oxidation responses at 1.02 V and 1.31 V *vs* Ag/AgCl, that correspond to the oxidized species of TTF monocation and dication, respectively.

6.1. Introduction

Research interests on tetrathiafulvalene(TTF)–based compounds have remained dynamic in the field of materials science, particularly, in the context of molecular electronics and NLO materials,¹⁻⁶ because this class of compounds can easily form donor-acceptor (D–A) ensembles through facile oxidation of relevant sulfur atoms. Owing to their unique π -donor properties, TTF and its derivatives are successfully used as versatile building blocks for the formation of charge transfer salts giving rise to organic conductors and even super conductors.⁷⁻⁸ Moreover, the molecular systems of D–A diads as well as D–A–D / A–D–A triads, based on TTF derivatives, are of current interest due to their potential applications in molecular electronic devices⁹⁻¹¹ and artificial photo-synthetic systems.¹²⁻¹³ The highly conjugated D–A systems are particularly important in the development of non linear optical materials and in the approach of producing high efficiency solar energy conversion.¹⁴⁻¹⁵ Even though, the intramolecular charge-transfer TTF D–A diads have been explored extensively,¹⁶⁻³⁴ only few examples of TTF-based D–A–D / A–D–A triads have been reported in the literature. To the best of our knowledge, D–A–D triads, such as di-TTF–quionones,³⁵ di-TTF–PI^{23,36-37} (pyromellitic diimide, PI) and di-TTF–TCNAQ (tetracyanoantraquinodimethane, TCNAQ),¹⁶ A–D–A triads, such as TTF–diquionones,^{20,38-39} and Py–TTF–Py⁴⁰ have been described in the literature. Fused A–D–A triad system, incorporating TTF and *p*-benzoquinone molecules, have been synthesized and their opto-electronic properties were investigated by Hudhomme and co-workers.²⁰ Recently, Zhu and co-workers have studied a Py–TTF–Py compound (A–D–A triad)

which exhibits multi-color solvatochromism.⁴⁰ Furthermore, tetrathiafulvalene (TTF) derivatives are promising candidates for semiconductors giving high performance FETs (Field Effect Transistors) because of their self-assembling properties leading to strong intermolecular interactions.⁴¹ However, because of the strong electron-donating properties, the thin films are generally labile to oxygen, resulting in poor FET performance.⁴² Yamashita and co-workers have introduced fused aromatic rings or electron-deficient nitrogen heterocycles to the TTF skeleton to enhance the stability and obtained high hole mobilities in the thinfilms.⁴³ They also have introduced electron-withdrawing halogen groups to the TTF derivative and succeeded in preparing n-type FETs based on them for the first time.⁴⁴ So that our aim is to synthesize the TTF fused quinoxaline based systems by introducing the previously described in our chapter 5 containing 6,7-quinoxaline dithiolate ligands to the TTF core.



Scheme 6.1. Structural representation of newly synthesized A–D–A TTF triads.

In addition, the photo-induced intramolecular charge transfer studies in TTF-dppz molecule (D-A system) have been reported by Liu and co-workers, in which they used electronic absorption, fluorescence emission and electrochemical techniques.⁴⁵ There is considerable interest in the extended dppz-based systems because it's fascinating features include structural planarity, π -extended conjugation and metal-chelating diamine functionality.⁴⁶ However, a system of A-D-A triads, containing TTF-dppz fused molecules, have not yet been reported in the literature. In this chapter, we have described three newly synthesized A-D-A triads (compounds **1a-c**) that contain TTF as donor moiety as shown in Scheme 6.1. Two of them are described as TTF-fused quinoxaline systems [compounds **1a** & **b**] and remaining one can be described as TTF-fused dppz molecule [compound **1c**]. The newly synthesized A-D-A triads exhibit good emission in the visible region with large solvatochromic effects and massive Stokes shifts. We have also described redox properties of the compound **1b** in DCM solution.

6.2. Experimental Details

6.2.1. General Methods

Micro analytical (C, H, N, S) data were obtained with a FLASH EA 1112 Series CHNS Analyzer. Infrared (IR) spectra were recorded on KBr pellets with a JASCO FT/IR-5300 spectrometer in the region of 400-4000 cm^{-1} . ^1H NMR spectra of compounds were recorded on Bruker DRX- 400 spectrometer using $\text{Si}(\text{CH}_3)_4$ [TMS] as an internal standard. Electronic absorption spectra were recorded on a Cary 100 Bio UV-Visible spectrophotometer. The emission spectra for the samples in solutions were recorded at room temperature on a Horiba Jobin Yvon Fluoromax-4 spectrofluorometer. In the measurements of emission and excitation spectra, the pass width was 2 nm. All the measurements were carried out under the same experiment conditions. A Cypress model CS-1090/CS-1087 electro analytical system was used for cyclic voltammetric experiments. The electrochemical experiments were measured in DCM containing $[\text{Bu}_4\text{N}][\text{ClO}_4]$ as a supporting electrolyte, using a conventional cell consisting of two platinum wires as working and counter electrodes, and a Ag/AgCl electrode as a reference. The potentials reported here are uncorrected for junction contributions.

6.2.2. Materials

5,6-Diamino-benzo[1,3]dithiole-2-thione (**5**) is the common precursor for the syntheses of compounds **3a–c**, which was prepared according to literature procedure in two steps starting from *o*-phenylenediamine.^{45,47} Syntheses of TTF compounds were performed under N₂ using standard inert-atmosphere techniques. Solvents were dried by standard procedures.

6.2.3. Synthesis and Characterization

Synthesis of 2-Thioxo-5,8-dihydro-1,3-dithia-5,8-diaza-cyclopenta[*b*]naphthalene-6,7-dione (**4**)

A solution of 5,6-diaminobenzene-1,3-dithiole-2-thione (compound **5**, 100 mg, 0.467 mmol) and oxalic acid (65 mg, 0.515 mmol) in MeOH (15 mL) was refluxed for 24 h under N₂. After filtration, the pale yellow precipitate was washed with cold MeOH, and then air dried. Pale yellow solid; Yield = 66%; IR (KBr, cm⁻¹): 3261 (N–H str), 3049, 2914, 1693, (C=O), 1444, 1379, 1271, 1059 (C=S), 877, 841, 790, 677, 555, 511; ¹H NMR (400 MHz, DMSO-*d*₆): δ 12.22 (s, 2H), 7.48 (s, 2H) ppm; ¹³C NMR (100 MHz, DMSO-*d*₆): δ 213.09 (C=S), 155.29 (C=O), 134.92, 126.95, 108.82 ppm; LC–MS (positive mode): m/z = 269 (M⁺+H)⁺; Anal. Calcd. for C₉H₄N₂O₂S₃: C, 40.28; H, 1.50; N, 10.44%. Found: C, 40.02; H, 1.78; N, 10.56%.

Synthesis of 6,7-Dichloro-1,3-dithia-5,8-diaza-cyclopenta[*b*]naphthalene-2-thione (**3a**)

To a solution of **4** (142 mg, 0.529 mmol) in thionyl chloride (4 mL) was added drop wise DMF (0.05 mL). The reaction mixture was refluxed for 15 h and then concentrated under vacuum. The resulting residue was dissolved in dichloromethane (20 mL) and poured into ice-water. The organic layer was collected, washed with saturated aqueous NaCl, dried over Na₂SO₄, and then evaporated to provide **3a** as a light yellow solid, which was used without further purification in the next step; Yellow solid; Yield = 65%; IR (KBr, cm⁻¹): 1527, 1444, 1257, 1180, 1070 (C=S), 878, 568, 436; ¹H NMR (400 MHz, CDCl₃): δ 8.15 (s, 2H) ppm; ¹³C NMR: We could not record the ¹³C NMR spectrum because of the poor solubility of the compound in common organic solvents; LC–MS (positive mode): m/z = 306 (M⁺+H)⁺, 308 [(M+2)⁺+H]⁺; Anal. Calcd. for C₉H₂N₂S₃Cl₂: C, 35.42; H, 0.66; N, 9.18%. Found: C, 35.22; H, 0.79; N, 9.46%.

Synthesis of 6,7-Dichloro-1,3-dithia-5,8-diaza-cyclopenta[*b*]naphthalen-2-one (2a)

To a solution of 6,7-dichloro-1,3-dithia-5,8-diaza-cyclopenta[*b*]naphthalene-2-thione (**3a**) (90 mg, 0.29 mmol) in chloroform and acetic acid (3:1, v/v, 28.0 mL), Hg(OAc)₂ (332 mg, 1.038 mmol) was added and it was stirred for 15 h at room temperature under N₂ atmosphere. The precipitate was filtered off using celite and washed with chloroform. The filtrate was extracted with saturated NaHCO₃ solution (3×33 mL) and water (50.0 mL). To remove any traces of water anhydrous Na₂SO₄ was added. The solvent was removed in vacuum, which produces pale yellow colored compound **2a** as product. Pale yellow solid; Yield = 95%; IR (KBr, cm⁻¹): 1732 (C=O), 1660, 1523, 1446, 1257, 1147, 999, 862, 561, 435; ¹H NMR (400 MHz, CDCl₃): δ 8.15 (s, 2H) ppm; ¹³C NMR (100 MHz, CDCl₃): δ 187.75 (C=O), 146.20, 138.89, 137.57, 121.57 ppm; LC-MS (positive mode): *m/z* = 290 (M⁺+H)⁺, 292 [(M+2)⁺+H]⁺; Anal. Calcd. for C₉H₂N₂OS₂Cl₂: C, 37.38; H, 0.70; N, 9.69%. Found: C, 37.02; H, 0.78; N, 9.86%.

Synthesis of 6,7,6',7'-Tetrachloro-[2,2']bi[1,3-dithia-5,8-diaza-cyclopenta[*b*]naphthalenyldiene] (1a)

A solution of compound **2a** (32 mg, 0.111 mmol) in triethylphosphite (3 mL) was refluxed at 130-140 °C for 2 h under N₂ atmosphere. After cooling to room temperature, MeOH (20 mL) was added and the resulting orange precipitate was filtered off. Orange solid; Yield = 53%; IR (KBr, cm⁻¹): 1583, 1437, 1259, 1141, 1010, 854, 515, 422; ¹H NMR (400 MHz, DMSO-*d*₆): δ 8.31 (s, 4H) ppm; ¹³C NMR: We could not record the ¹³C NMR spectrum because of the poor solubility of the compound in common organic solvents; LC-MS (positive mode): *m/z* = 546 (M⁺+H)⁺, 548 [(M+2)⁺+H]⁺; Anal. Calcd. for C₁₈H₄N₄S₄Cl₄: C, 39.57; H, 0.74; N, 10.26%. Found: C, 39.51; H, 0.81; N, 10.35%. UV-Vis: λ_{max} = 474 nm (in chloroform, ~ 3×10⁻⁵ M concentration); Fluorescence: λ_{em} = 664 nm (in chloroform, ~ 3×10⁻⁵ M concentration).

Synthesis of 6,7-Diphenyl-1,3-dithia-5,8-diaza-cyclopenta[*b*]naphthalene-2-thione (3b)

A mixture containing 5,6-diaminobenzene-1,3-dithiole-2-thione (**5**) (200 mg, 0.934 mmol), benzil (196 mg, 0.932 mmol) and iodine (10 mol%) in CH₃CN (10.0 mL) was stirred for 30 min. The resulting yellow precipitate was separated by filtration, washed with little CH₃CN, and dried in vacuo. Yield: 83.0%; Yellow solid; IR (KBr, cm⁻¹): 3067, 1531, 1496, 1433, 1392, 1340, 1195, 1059 (C=S), 1020, 966, 877, 769, 696, 545; ¹H NMR

(400 MHz, CDCl₃): δ 8.21 (s, 2H), 7.53 (d, 4H), 7.34-7.43 (m, 6H) ppm; ¹³C NMR (CDCl₃): δ 211.96 (C=S), 154.47, 143.46, 139.64, 138.40, 129.83, 129.38, 128.40, 120.83 ppm; LC-MS (positive mode): m/z = 389 (M⁺+H)⁺; Anal. Calcd. for C₂₁H₁₂N₂S₃: C, 64.92; H, 3.11; N, 7.21%. Found: C, 65.23; H, 3.40; N, 6.96%.

Synthesis of 6,7-Diphenyl-1,3-dithia-5,8-diaza-cyclopenta[*b*]naphthalen-2-one (2b)

To a solution of compound **3b** (210 mg, 0.541 mmol) in chloroform and acetic acid (3:1, v/v, 40 mL), Hg(OAc)₂ (552 mg, 1.73 mmol) was added and it was stirred for 2 h at room temperature under N₂ atmosphere. The resulting suspension was filtered using celite and washed with chloroform. The filtrate was extracted with NaHCO₃ solution (3 × 33 mL) and water (50 mL). To remove any traces of water anhydrous Na₂SO₄ was added. The solvent was removed in vacuum, which produces pale yellow colored compound **2b** as product. Yield: 90.0%; pale yellow solid; IR (KBr, cm⁻¹): 3049, 1734 (C=O), 1651, 1446, 1388, 1336, 1257, 1184, 1097, 1022, 968, 868, 769, 696, 596, 543; ¹H NMR (400 MHz, CDCl₃): δ 8.25 (s, 2H), 8.57 (s, 2H), 7.52 (d, 4H), 7.33-7.41 (m, 6H) ppm; ¹³C NMR (100 MHz, CDCl₃): δ 188.90 (C=O), 154.14, 139.72, 138.48, 135.74, 129.84, 129.27, 128.37, 122.64 ppm; LC-MS (positive mode): m/z = 373 (M⁺+H)⁺; Anal. Calcd. for C₂₁H₁₂N₂OS₂: C, 67.72; H, 3.25; N, 7.52%. Found: C, 67.46; H, 3.59; N, 7.68%.

Synthesis of 6,7,6',7'-Tetraphenyl-[2,2']bi[1,3-dithia-5,8-diaza-cyclopenta[*b*]naphthalenyldiene] (1b)

A solution of compound **2b** (125 mg, 0.336 mmol) in triethylphosphite (3mL) was refluxed at 130-140 °C for 2 h under N₂ atmosphere. After cooling to room temperature, MeOH (20 mL) was added and the resulting orange precipitate was filtered off. Yield: 70.0%; orange solid; IR (KBr, cm⁻¹): 3040, 1658, 1585, 1493, 1450, 1431, 1340, 1253, 1188, 1093, 1055, 1022, 864, 825, 767, 694, 549; ¹H NMR (400 MHz, CDCl₃): δ 8.02 (s, 4H), 7.49 (d, 8H), 7.32-7.37 (m, 12H) ppm; ¹³C NMR (100 MHz, CDCl₃): δ 153.23, 140.93, 140.07, 138.70, 129.79, 128.98, 128.30, 120.23 ppm; LC-MS (positive mode): m/z = 713 (M⁺+H)⁺; Anal. Calcd. for C₄₂H₂₄N₄S₄: C, 70.76; H, 3.39; N, 7.86%. Found: C, 70.61; H, 3.45; N, 7.70%. UV-Vis: λ_{max} = 465 nm (in chloroform, ~ 7×10⁻⁶ M concentration); Fluorescence: λ_{em} = 616 nm (in chloroform, ~ 7×10⁻⁶ M concentration).

Synthesis of compound 3c

A solution of 5,6-diaminobenzene-1,3-dithiole-2-thione (compound **5**, 100 mg, 0.46 mmol) and 1,10-phenanthroline-5,6-dione (102 mg, 0.485 mmol) in MeOH (40 mL) was refluxed for 3h under N₂. After filtration, the precipitate was washed with cold MeOH, and then air dried. Yellow solid; Yield = 80%; IR (KBr, cm⁻¹): 3034, 1585, 1568, 1473, 1440, 1356, 1211, 1122, 1074 (C=S str.), 1028, 887, 846, 806, 738, 613, 513, 416; ¹H NMR (400 MHz, DMSO-*d*₆): δ 6.96 (s, 2H), 7.09 (s, 2H), 7.22 (s, 2H), 7.67 (s, 2H) ppm (because of poor solubility of the compound **3c** we could not get good quality of the ¹H NMR spectrum, however compound **2c** has been synthesized by from this compound **3c** and that (compound **2c**) was characterized by ¹H NMR spectroscopy); ¹³C NMR: We could not record the ¹³C NMR spectrum because of the poor solubility of the compound in common organic solvents; LC-MS (positive mode): m/z = 388 (M⁺+H)⁺; Anal. Calcd. for C₁₉H₈N₄S₃: C, 58.74; H, 2.08; N, 14.42%. Found: C, 58.91; H, 1.99; N, 14.36%.

Synthesis of compound 2c

To a solution of compound **3c** (210 mg, 0.541 mmol) in chloroform and acetic acid (3:1, v/v, 40 mL), Hg(OAc)₂ (552 mg, 1.73 mmol) was added and it was stirred for 2 h at room temperature under N₂ atmosphere. The resulting suspension was filtered using celite and washed with chloroform. The filtrate was extracted with NaHCO₃ solution (3 × 50 mL) and water (50 mL). To remove any traces of water anhydrous Na₂SO₄ was added. The solvent was removed in vacuum, which produces pale orange colored compound **2c** as product. Orange solid; Yield = 98%; IR (KBr, cm⁻¹): 2924, 2852, 1722, 1658 (C=O str.), 1583, 1523, 1473, 1440, 1356, 1259, 1095, 810, 738; ¹H NMR (400 MHz, CDCl₃): δ 7.78 (q, 2H), 8.44 (s, 2H), 9.25 (d, 2H), 9.54 (d, 2H) ppm; ¹³C NMR: We could not record the ¹³C NMR spectrum because of the poor solubility of the compound in common organic solvents; LC-MS (positive mode): m/z = 372 (M⁺+H)⁺; Anal. Calcd. for C₁₉H₈N₄OS₂: C, 61.28; H, 2.17; N, 15.04%. Found: C, 61.13; H, 2.22; N, 15.16%.

Synthesis of compound 1c

A solution of compound **2c** (125 mg, 0.336 mmol) in triethylphosphite (3mL) was refluxed at 140 °C for 2 h under N₂ atmosphere. After cooling to room temperature, MeOH (20 mL) was added and the resulting black precipitate was filtered off. Black powder; Yield = 52%; IR (KBr, cm⁻¹): 3040, 2912, 2841, 1720, 1658, 1585, 1568, 1471,

1439, 1356, 1211, 1072, 1028, 864, 810, 738; ^1H NMR (400 MHz, CDCl_3): δ 7.94(q, 2H), 8.45(s, 2H), 9.45(d, 2H), 9.69(d, 2H) ppm; ^{13}C NMR (100 MHz, CDCl_3): δ 153.01, 148.61, 141.74, 140.74, 137.11, 133.87, 127.22, 124.34, 122.77, 120.31 ppm; LC-MS (positive mode): m/z = 714 ($\text{M}^+ + \text{H}$) $^+$; Anal. Calcd. for $\text{C}_{38}\text{H}_{16}\text{N}_8\text{S}_4$: C, 64.03; H, 2.26; N, 15.72%. Found: C, 64.12; H, 2.33; N, 15.45%. UV-Vis: λ_{max} = 530 nm (in chloroform, $\sim 8.4 \times 10^{-6}$ M concentration); Fluorescence: λ_{em} = 675 nm (in chloroform, $\sim 8.4 \times 10^{-5}$ M concentration)

6.2.4. Single Crystal Structure Determination

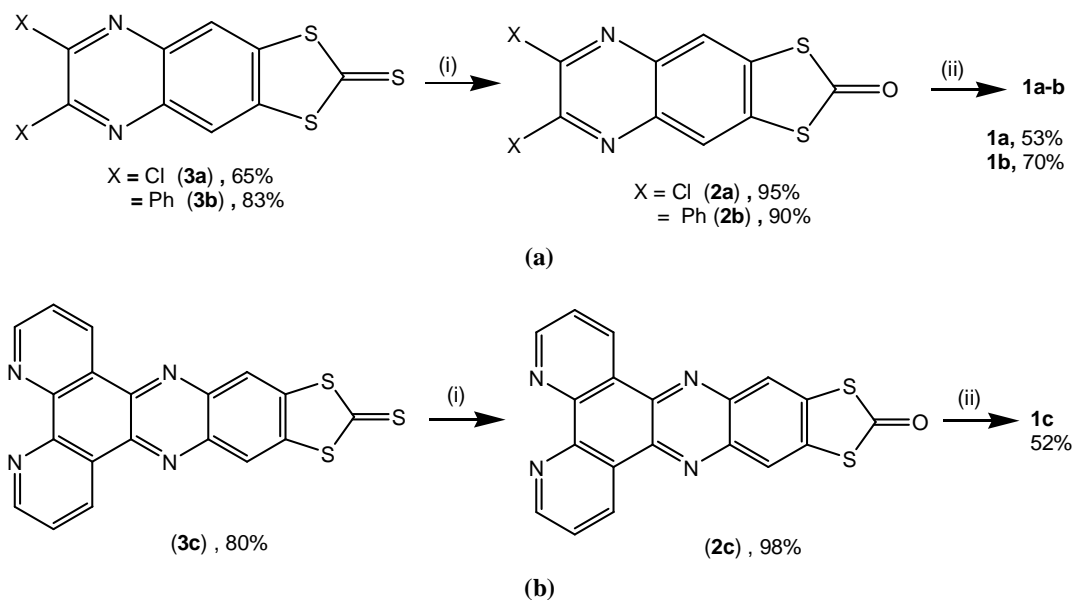
Single crystals suitable for facile structural determination for the compound **1b** was measured on a three circle Bruker SMART APEX CCD area detector system under Mo-K α (λ = 0.71073 Å) graphite monochromatic X-ray beam. The frames were recorded with an ω scan width of 0.3°, each for 8 s, crystal-detector distance 60 mm, collimator 0.5 mm. Data reduction performed by using SAINTPLUS.⁴⁸ Empirical absorption corrections using equivalent reflections performed program SADABS.⁴⁸ The structure was solved by direct methods and least-square refinement on F^2 for the compound **1b** by using SHELXS-97.⁴⁹ All non-hydrogen atoms were refined anisotropically. The hydrogen atoms were included in the structure factor calculation by using a riding model.

6.3. Results and Discussion

6.3.1. Synthesis and Spectroscopic Characterization

Symmetrical TTF-based compounds (**1a–c**) are generally synthesized by the phosphite-mediated (triethylphosphite) self coupling reaction of corresponding 1,3-dithia-2-one derivatives (**2a–c**) at 130-140 °C in good yields (52–70%) as described in Scheme 6.2. The 1,3-dithia-2-one derivatives (**2a–c**) have been prepared from corresponding 1,3-dithia-2-thione derivatives (**3a–c**) by using $\text{Hg}(\text{OAc})_2$ in CHCl_3 : CH_3COOH (3:1) with good yields (90–98%) as presented in Scheme 6.2. 5,6-Diamino-benzo[1,3]dithiole-2-thione (**5**) is the common precursor for the syntheses of compounds **3a–c**, which was prepared according to literature procedure in two steps starting from *o*-phenylenediamine.^{45,47} The 1,3-dithia-2-thione derivatives **3a–c** were prepared by condensation reaction of 5,6-diamino-benzo[1,3]dithiole-2-thione with corresponding diones following the procedures as described in Table 6.1. Compound **3a** has been prepared by the chlorination of 2-

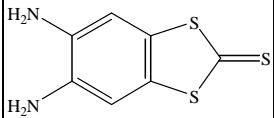
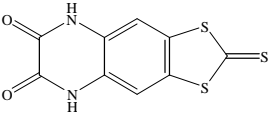
thioxo-5,8-dihydro-1,3-dithia-5,8-diaza-cyclopenta[*b*]naphthalene-6,7-dione (**4**) (di-oxime) with SOCl_2 by using DMF as catalyst with accroding to modified literature procedure.⁵⁰ The di-oxime (**4**) was prepared by condensation reaction between the 5,6-diamino-benzo[1,3]dithiole-2-thione and oxalic acid in MeOH at reflux condition (Table 6.1). Compound **3b** was prepared according to modified literature procedure,⁵¹ which was obtained by a condensation reaction between the 5,6-diamino-benzo[1,3]dithiole-2-thione and benzil by using iodine as catalyst in acetonitrile solution at room temperature. But compound **3c** was isolated by the simple condensation of 5,6-diamino-benzo[1,3]dithiole-2-thione with 1,10-phenanthroline-5,6-dione⁵² in MeOH solution at reflux condition without using any catalyst (Table 6.1).



Scheme 6.2. (a) Synthetic route for compounds **1a** & **b**; (b) compound **1c** from their corresponding 1,3-dithia-2-thione derivatives. Reagents and conditions: (i) $\text{CHCl}_3/\text{CH}_3\text{COOH}$ (3:1), $\text{Hg}(\text{OAc})_2$, RT, 2 h; (ii) $\text{P}(\text{OEt})_3$, 130-140 °C, 2 h.

1 All the synthesized materials have been characterized by NMR spectroscopy including elemental and LC-MS analyses. Molecular structures of the newly synthesized TTFs (**1a–c**) have been determined by ^1H and ^{13}C NMR, LC-MS spectral studies including their elemental analyses and the knowledge of the precursors from which they have been synthesized. Compound **1a** could not be characterized by ^{13}C NMR studies because of its poor solubility in common deuterated solvents. Additionally, compound **1b** has been characterized unambiguously by single crystal structure analysis.

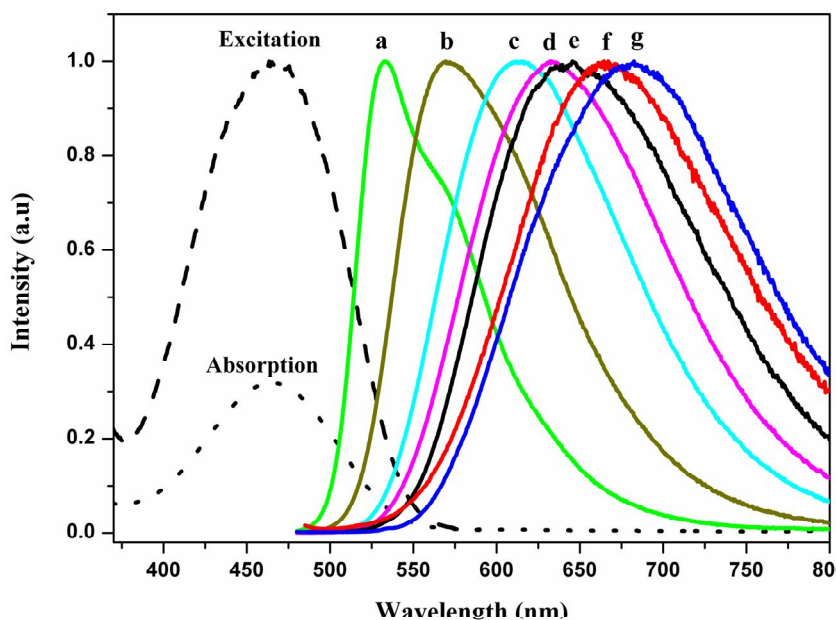
Table 6.1. Syntheses of 1,3-dithia-2-thione derivatives

Entry	Precursor	Reagent	Conditions	Product	Yield %
1	 (5)	Oxalic acid	MeOH, reflux, 24 h	 (4)	66
2	4	SOCl ₂	DMF (cat), reflux, 15 h	3a	65
3	5	Benzil	I ₂ (10 mol%), CH ₃ CN, RT, 30 min	3b	83
4	5	1,10-Phenanthroline-5,6-dione	MeOH, reflux, 24 h	3c	96

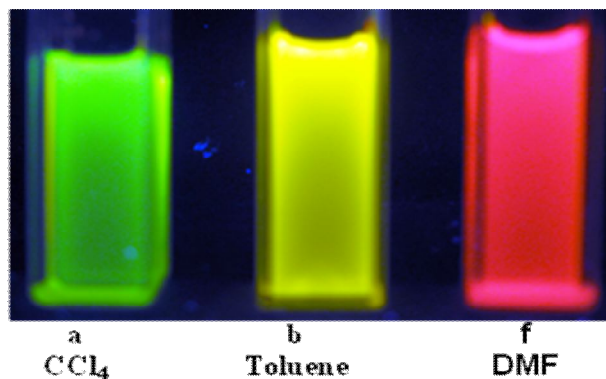
6.3.2. Electronic Spectra

The electronic absorption spectrum of the compound **1b** shows a strong absorption at 465 nm in the visible region in CHCl₃ as shown in Figure 6.1(a). In solutions of other solvents the visible band positions vary with slight change over the region 457–465 nm (Table 6.2). It shows that the absorption band positions do not change much with polarity. Compound **1b** exhibits strong emission in solution at room temperature. In contrast to its electronic absorption spectral behavior in various solvents, the emission spectra of compound **1b** are strongly dependent on polarity of the solvents (Table 6.2). The band maxima shift to red region with increasing the polarity of the solvent as shown in Figure 6.1(a). As shown in Figure 6.1(a), the excitation spectrum of compound **1b** is identical to its absorption spectrum in chloroform and indeed same is true for all the solvents of the series. The emission light of the compound **1b** varies from green to red with increasing the polarity of the solvent (CCl₄ to DMSO). For example, in the solution of non polar solvent, such as CCl₄, this shows green emission and emission maximum is centered at 532 nm [Figure 6.1(b)]. In the solution of moderate polar solvent, such as toluene, it shows yellowish emission as shown in Figure 6.1(b), and the relevant emission maximum centers at 570 nm. On the other hand, in the solutions of relatively more polar solvents, such as DMF and DMSO, this shows red emission and the emission maxima are centered at 665 nm and 682 nm respectively [Figure 6.1(b)]. Thus the solvent dependence of the emission shows that the excited state is stabilized in more polar solvents, which is due to an intramolecular

charge transfer.⁴⁵ Besides, the fluorescence quantum yield of the compound **1b** increases from 4.0% to 12.6% with increasing the polarity of the solvent (CCl₄ to DMF) at room temperature. Notably, the quantum efficiency of the compound **1b** in relatively more polar solvents is ~ 0.1 . This suggests that the compound **1b** is good fluorescent as compared to the other TTF systems of D–A diads as well as D–A–D and A–D–A triads, reported earlier.⁴¹ In the similar fashion, the observed Stokes shifts of compound **1b** increases from 2709 to 7267 cm⁻¹ with increasing the polarity of the solvent (CCl₄ to DMSO).



(a)



(b)

Figure 6.1. (a) Emission spectra (—, $\lambda_{\text{ex}} = 460$ nm) of the TTF triad (**1b**) in different solvents at room temperature, a) CCl₄, b) toluene, c) CHCl₃, d) DCM, e) acetone, f) DMF, g) DMSO, and absorption (----) and excitation spectra (·····, $\lambda_{\text{em}} = 610$ nm) of **1b** in CHCl₃ (excitation and emission spectra are normalized to 1); (b) color response of compound **1b** with different solvents under UV lamp.

Table 6.2. Photophysical properties of A–D–A TTF compounds **1a–c** (A_{\max} and E_{\max} = Absorption and emission maxima respectively, $\Delta\nu_{\text{st}}$ (cm^{-1}) = Stokes shift, Φ_F = fluorescence quantum yield)

Compound	Solvent	A_{\max} [cm^{-1}]	E_{\max} [cm^{-1}]	$\Delta\nu_{\text{st}}$ [cm^{-1}]	Φ_F
1a	Toluene	21097	16474	4623	0.03
1a	CHCl_3	21097	15060	6037	0.05
1a	DMF	21186	13869	7317	0.026
1b	CCl_4	21505	18796	2709	0.04
1b	Toluene	21505	17574	3931	0.063
1b	CHCl_3	21505	16233	5272	0.102
1b	DCM	21739	15797	5942	0.117
1b	Acetone	21834	15503	6331	0.082
1b	DMF	21884	15060	6824	0.126
1b	DMSO	21929	14662	7267	0.097
1c	Toluene	18867	15772	3095	0.024
1c	CHCl_3	18867	14814	4053	0.019
1c	DMF	19047	13315	5732	0.012

Compound **1a** also shows similar absorption band at 465 nm in the visible region in CHCl_3 (Figure 6.2) and it does not change much with the solvent polarity (Table 6.2). The emission spectrum of the compound **1a** is also strongly dependent on the polarity of the solvents (Figure 6.2) as shown by compound **1b**; however, in the case of compound **1a**, emission maxima are further shifted to lower energy in red region as shown in Table 6.2. The absorption spectrum of the compound **1c** in CHCl_3 solution is shown in Figure 6.3. In this case, the absorption band shifts too much low energy region compared to compounds **1a** and **1b**. It absorbs at 530 nm in CHCl_3 solution. The emission spectrum of the compound **1c** is again strongly dependent on the polarity of the solvents (Figure 6.4) as observed in the case of compounds **1a** and **1b**; interestingly, in this case, the emission maxima are further shifted to still low energy region as shown in Table 6.2.

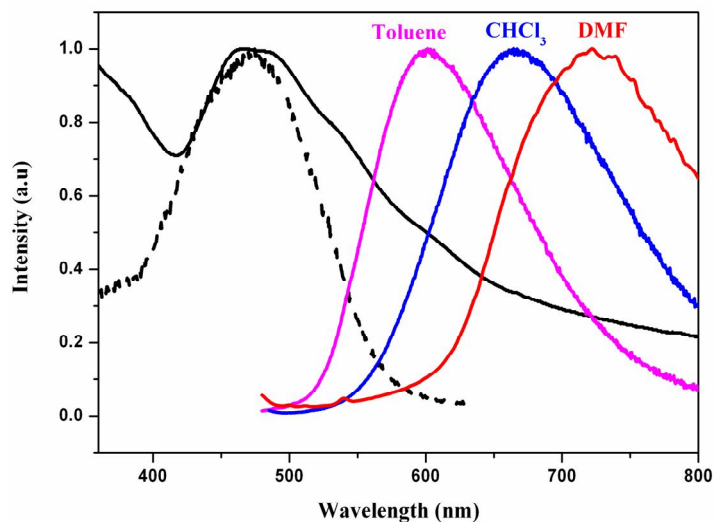


Figure 6.2. Emission spectra (—, $\lambda_{\text{ex}} = 465$ nm) of the TTF triad (**1a**) in different solvents at room temperature, absorption (—) and excitation spectra (---, $\lambda_{\text{em}} = 665$ nm) of **1a** in CHCl_3 (absorption, excitation and emission spectra are normalized to 1).

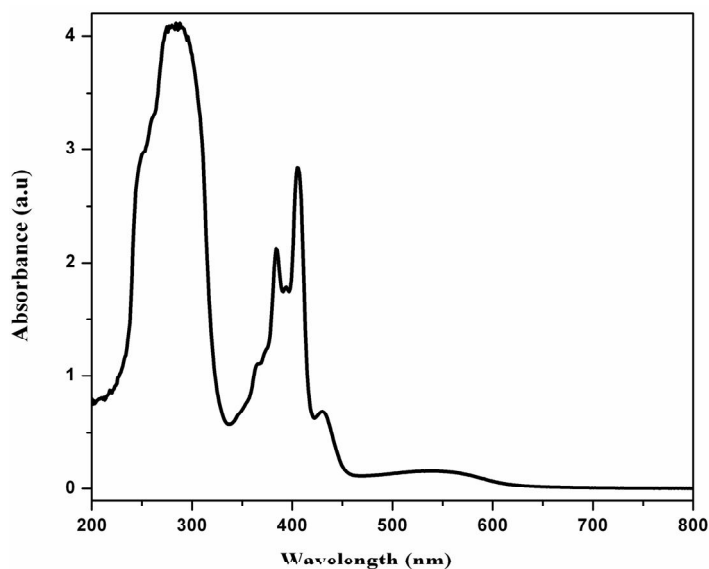


Figure 6.3. Electronic absorption spectrum of compound **1c** in CHCl_3 .

6.3.3. Electrochemistry

We have investigated the electrochemical properties of the compound **1b** in DCM by cyclic voltammetry (CV). CV experiment results revealed that two oxidation responses, corresponding to $E_{1/2}^{\text{ox1}}$ and $E_{1/2}^{\text{ox2}}$, typical for a system. The first single electron oxidation wave appears at 1.02 V vs Ag/AgCl ($\Delta E = 90$ mV) as a reversible wave corresponding to the formation of radical cation (monocation) as shown in Figure 6.5 (blue line). The second oxidation process appears as quasi-reversible wave at $E_{1/2} = 1.31$ V vs

Ag/AgCl($\Delta E = 106$ mV), due to the oxidation of radical cation to the dication as shown in Figure 6.5 (red line). The higher values of oxidation potentials of compound **1b** (that appear at more positive region as compared to those of TTF as such ($E_{1/2}^{\text{ox1}} = 0.41$ V and $E_{1/2}^{\text{ox2}} = 0.71$ V vs Ag/AgCl))⁴⁵ are probably due to an electron withdrawing effect of the fused quinoxaline system with TTF. We could not study the electrochemical properties of the compounds **1a** and **1c** because of their poor solubility.

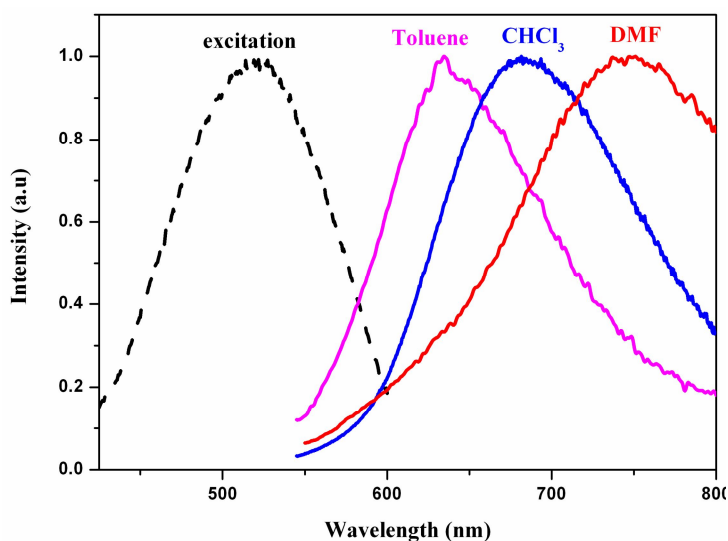


Figure 6.4. Emission spectra (—, $\lambda_{\text{ex}} = 530$ nm) of the TTF triad (**1c**) in different solvents at room temperature, and excitation spectra (---, $\lambda_{\text{em}} = 680$ nm) of **1c** in CHCl_3 (excitation and emission spectra are normalized to 1).

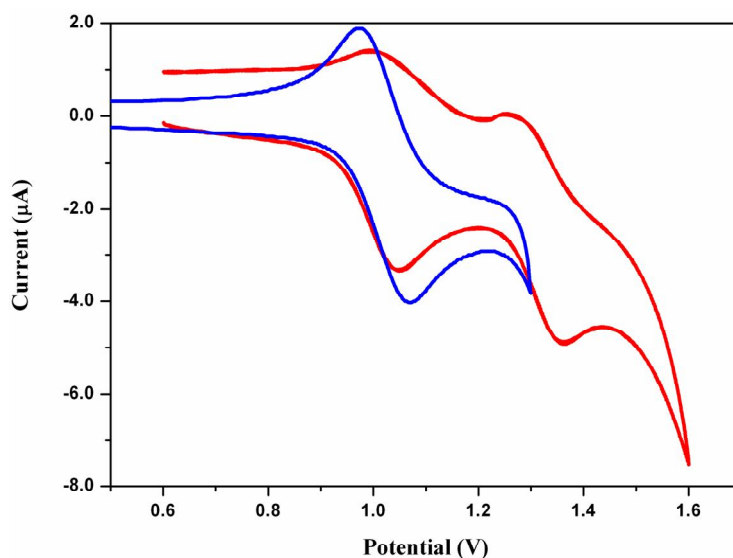
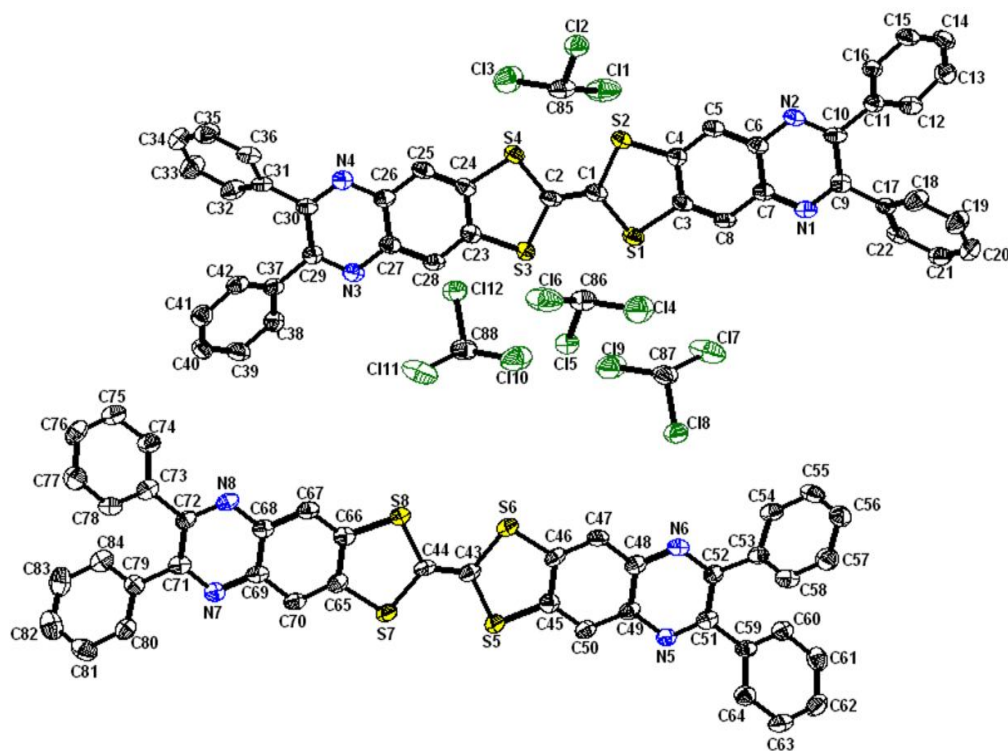
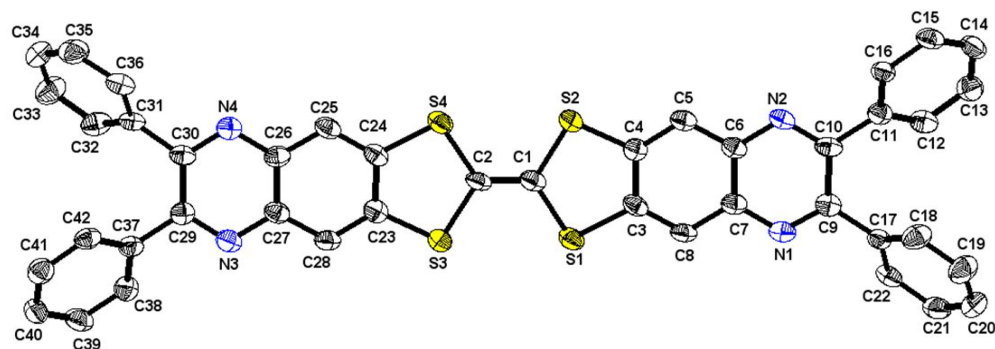


Figure 6.5. Cyclic voltammograms of **1b** in DCM to the monocation (blue line) and to the dication (red line) at a scan rate 0.1 Vs^{-1} , V vs Ag/AgCl.



(a)



(b)

Figure 6.6. (a) Thermal ellipsoidal plot of the asymmetric unit of compound **1b**, the asymmetric unit contain two units of two TTF molecules and four duetrated chloroform solvent molecules. Hydrogen atoms are not shown for clarity (70% probability). (b) Thermal ellipsoidal plot of one of the molecule containing in the asymmetric unit of compound **1b**, Hydrogen atoms are not shown for clarity (70% probability).

6.3.1. X-ray Crystallographic Studies

Crystal Structure Descriptions of Compound **1b**

Single crystals of compound **1b**, suitable for single crystal X-ray analysis were obtained from deuterated chloroform in an NMR tube on slow evaporation over a period of two weeks. The molecule **1b** crystallizes as solvated compound **1b.2(CHCl₃)** in a non-

centrosymmetric monoclinic space group *Cc*. The asymmetric unit contains two molecules of TTF triad **1b** and four molecules of solvent chloroform molecules as shown in Figure 6.6(a). For clarity, one of the molecule present in the asymmetric unit as shown in Figure 6.6(b). As shown in Figure 6.6(b), the skeleton of the molecule is almost planar; excluding the four peripheral phenyl groups. The rms deviation from a least-squares plane through the atoms of the core is 0.027 Å. The phenyl rings are deviated from the plane of skeleton of the molecule with angles in the range from 36.03° to 55.81°. The crystallographic parameters, data collection and structure refinement of the compound **1b** are summarized in Table 6.3. Selected bond lengths and angles for the compound **1b** are listed in Table 6.4. The bond lengths in the TTF moiety are in the range of expected for neutral TTF derivatives.⁵³ Crystal packing diagram of the compound **1b** is characterized by C–H...N weak contacts and noticeable non covalent S...S interactions results in one dimensional alignment as shown in Figure 6.7. The range of S...S intermolecular contacts is 3.710 to 3.731 Å. The relevant hydrogen bonding geometrical parameters of the compound **1b** is listed in the Table 6.5. In addition, six Cl...Cl interactions are present between the solvent molecules resulting in the formation of a one dimensional chloroform tapes, and the Cl...Cl intermolecular contact distances are in the range from 3.263(1) to 3.395(2) Å as shown in Figure 6.8.

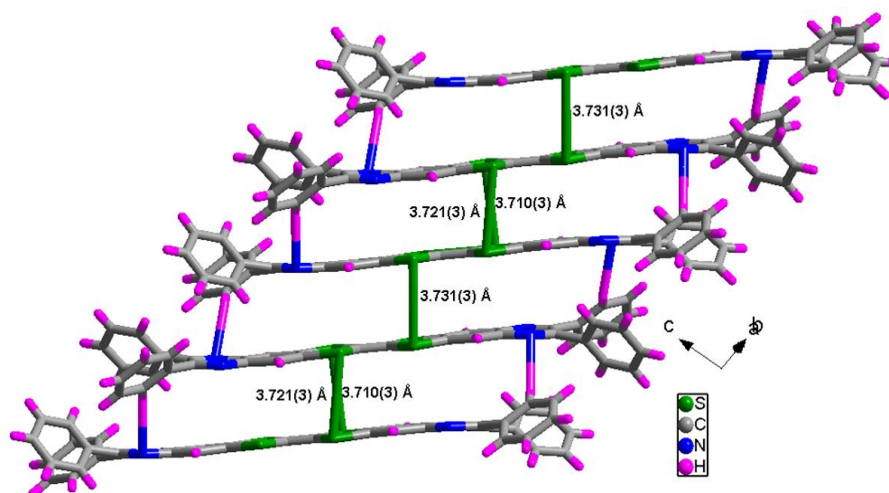


Figure 6.7. View of the crystal packing diagram of compound **1b**, solvent molecules has been omitted for clarity.

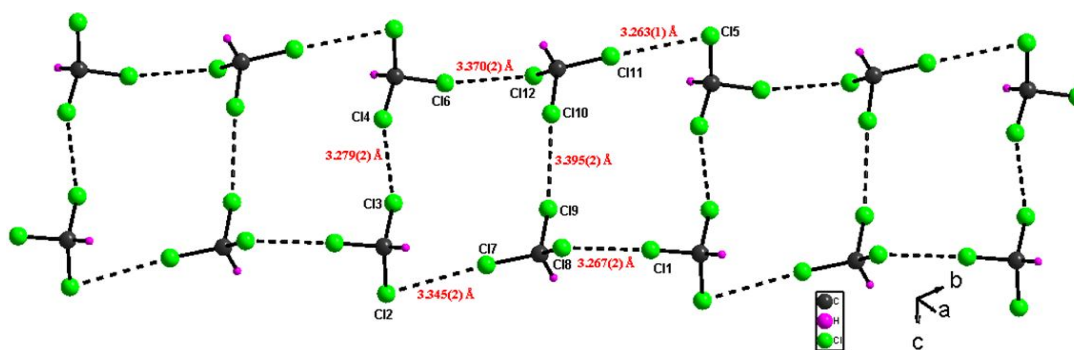


Figure 6.8. The Cl...Cl interactions are between the chloroform solvent molecules to form a one dimensional tape.

Table 6.3. Crystallographic Data and Structural Refinement for Compound **1b**

	1b
Empirical formula	C ₄₄ H ₂₆ N ₄ S ₄ Cl ₆
Formula weight	951.67
Temperature (K)	100(2)
Crystal size (mm)	0.48 x 0.36 x 0.14
Crystal system	Monoclinic
Space group	Cc
Z	8
Wavelength (Å)	0.71073
Unit cell dimensions	
<i>a</i> [Å]	14.5359(11)
<i>b</i> [Å]	14.7543(11)
<i>c</i> [Å]	39.771(3)
β [°]	97.616(2)
Volume [Å ³]	8454.3(11)
Calculated density (Mg/m ³)	0.643
Reflections collected/ unique	43023/16629
R(int)	0.0287
F(000)	3872
Theta range for data collection (deg.)	1.98 to 26.18
Refinement method	Full-matrix least-squares on F ²
Data / restraints / parameters	16629 / 2 / 1045
Goodness-of-fit on F ²	1.071
R ₁ /wR ₂ [I>2σ(I)]	0.0422 / 0.1077
R ₁ /wR ₂ (all data)	0.0436 / 0.1085
Largest diff. peak and hole [e.Å ⁻³]	0.581 and -0.654

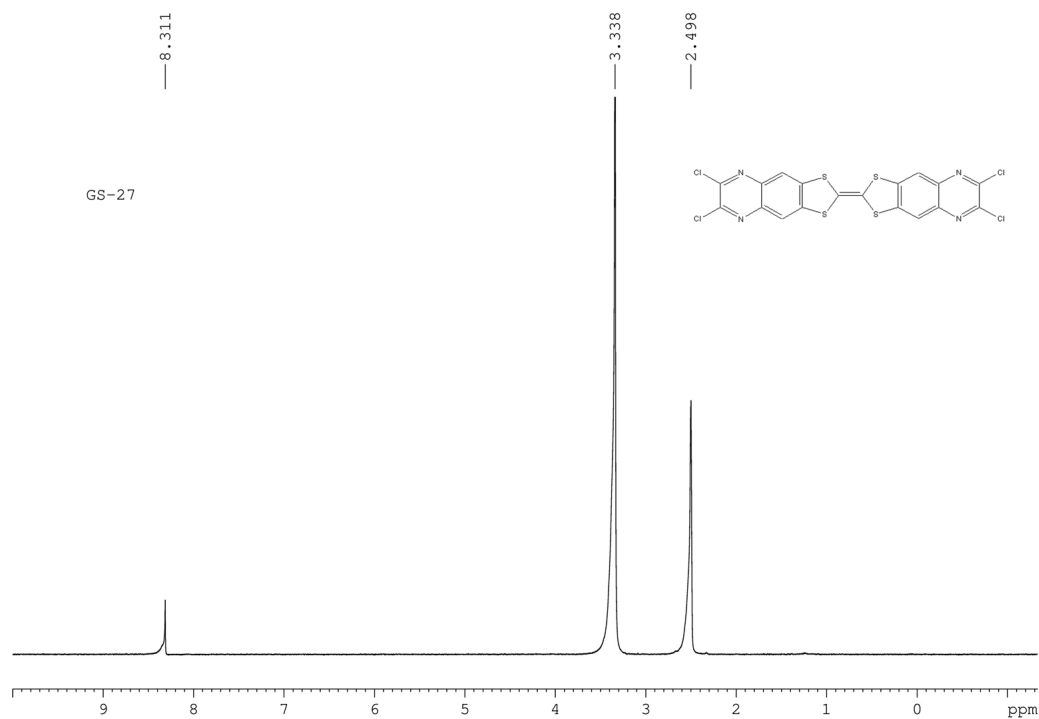
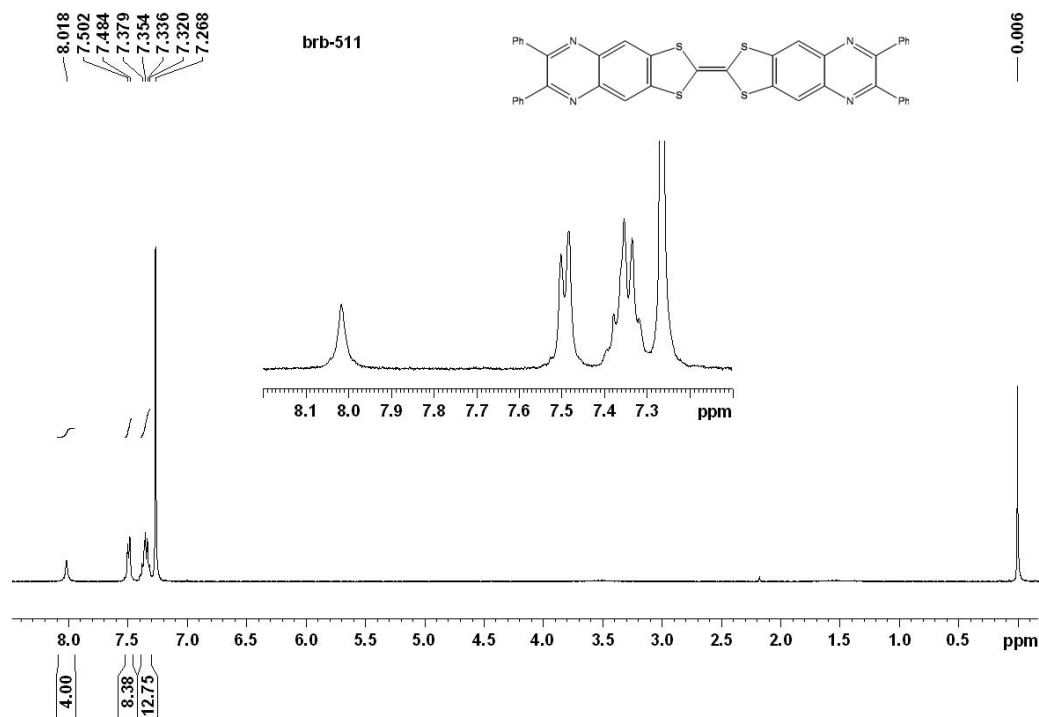
Table 6.3. Selected Bond Length and Bond Angles for Compound **1b**

Bond lengths (Å)			
S(5)-C(45)	1.745(4)	S(5)-C(43)	1.753(3)
S(4)-C(24)	1.743(3)	S(4)-C(2)	1.759(4)
S(8)-C(66)	1.744(4)	S(8)-C(44)	1.754(3)
S(1)-C(1)	1.748(4)	S(1)-C(3)	1.752(3)
S(7)-C(65)	1.748(3)	S(7)-C(44)	1.755(4)
S(3)-C(23)	1.748(3)	S(3)-C(2)	1.756(3)
S(6)-C(46)	1.751(3)	S(6)-C(43)	1.758(4)
S(2)-C(4)	1.749(3)	S(2)-C(1)	1.758(3)
Bond Angles (°)			
C(45)-S(5)-C(43)	96.02(17)	C(24)-S(4)-C(2)	95.88(16)
C(66)-S(8)-C(44)	96.17(16)	C(1)-S(1)-C(3)	95.57(16)
C(65)-S(7)-C(44)	95.98(16)	C(23)-S(3)-C(2)	96.00(16)
C(46)-S(6)-C(43)	95.76(16)	C(4)-S(2)-C(1)	95.70(16)
C(8)-C(3)-S(1)	122.3(3)	C(4)-C(3)-S(1)	116.6(3)
C(44)-C(43)-S(5)	122.6(2)	C(44)-C(43)-S(6)	121.9(2)
S(5)-C(43)-S(6)	115.58(19)	C(5)-C(4)-S(2)	123.4(3)
C(3)-C(4)-S(2)	116.1(3)	C(1)-C(2)-S(3)	122.1(2)
C(1)-C(2)-S(4)	122.5(2)	S(3)-C(2)-S(4)	115.43(19)
C(2)-C(1)-S(1)	122.7(2)	C(2)-C(1)-S(2)	121.3(2)
S(1)-C(1)-S(2)	115.9(2)	C(67)-C(66)-S(8)	123.8(3)
C(65)-C(66)-S(8)	116.0(2)	C(43)-C(44)-S(8)	122.1(2)
C(65)-S(7)-C(44)	95.98(16)	S(8)-C(44)-S(7)	115.6(2)

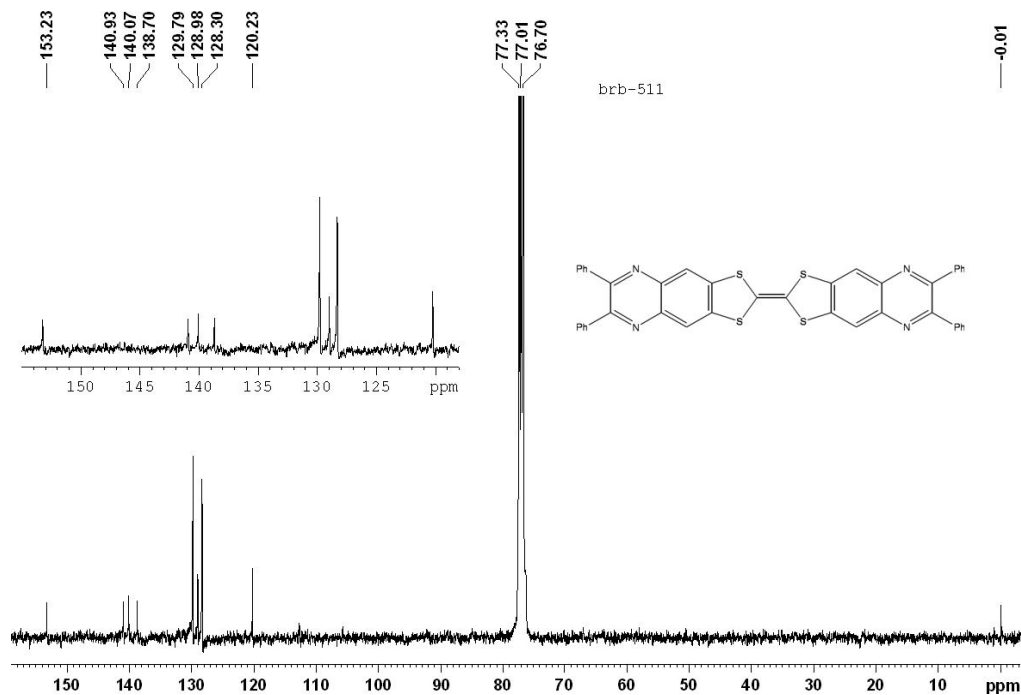
Table 6.5. Hydrogen Bonding Parameters for Compound **1b**

D-H...A	d(D...H)	d(H...A)	d(D...A)	<(DHA)
C(8)-H(8)...Cl(2)#1	0.93	2.94	3.676(4)	137.2
C(85)-H(85)...N(2)#2	0.98	2.31	3.233(5)	155.9
C(12)-H(12)...N(6)#3	0.93	2.61	3.344(4)	135.9
C(86)-H(86)...N(3)#4	0.98	2.29	3.223(5)	157.9
C(88)-H(88)...N(8)#4	0.98	2.28	3.199(5)	155.1
C(87)-H(87)...N(5)#5	0.98	2.32	3.246(5)	156.9
C(42)-H(42)...N(7)#5	0.93	2.61	3.358(4)	137.5
C(60)-H(60)...N(1)#6	0.93	2.63	3.392(5)	139.3
C(78)-H(78)...N(4)#7	0.93	2.62	3.427(4)	145.0

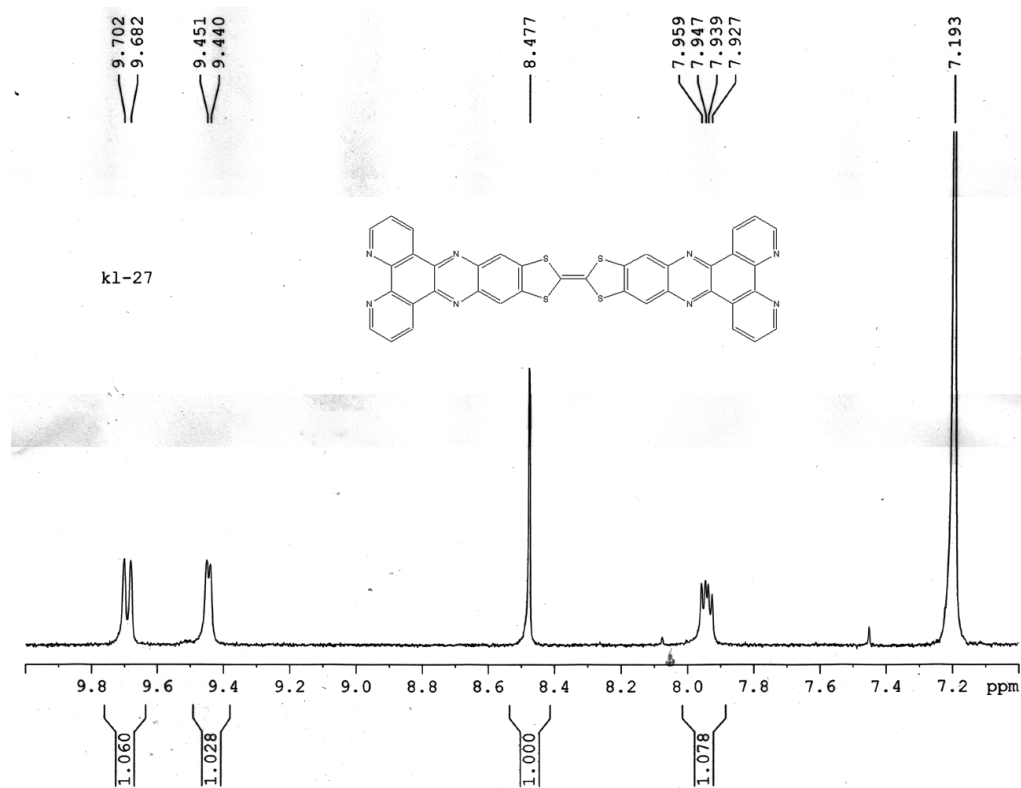
Symmetry transformations used to generate equivalent atoms: #1 $x-1, y, z$; #2 $x+1/2, y+1/2, z$; #3 $x, y-1, z$; #4 $x-1/2, y-1/2, z$; #5 $x+1/2, y-1/2, z$; #6 $x-1/2, y+1/2, z$; #7 $x, y+1, z$

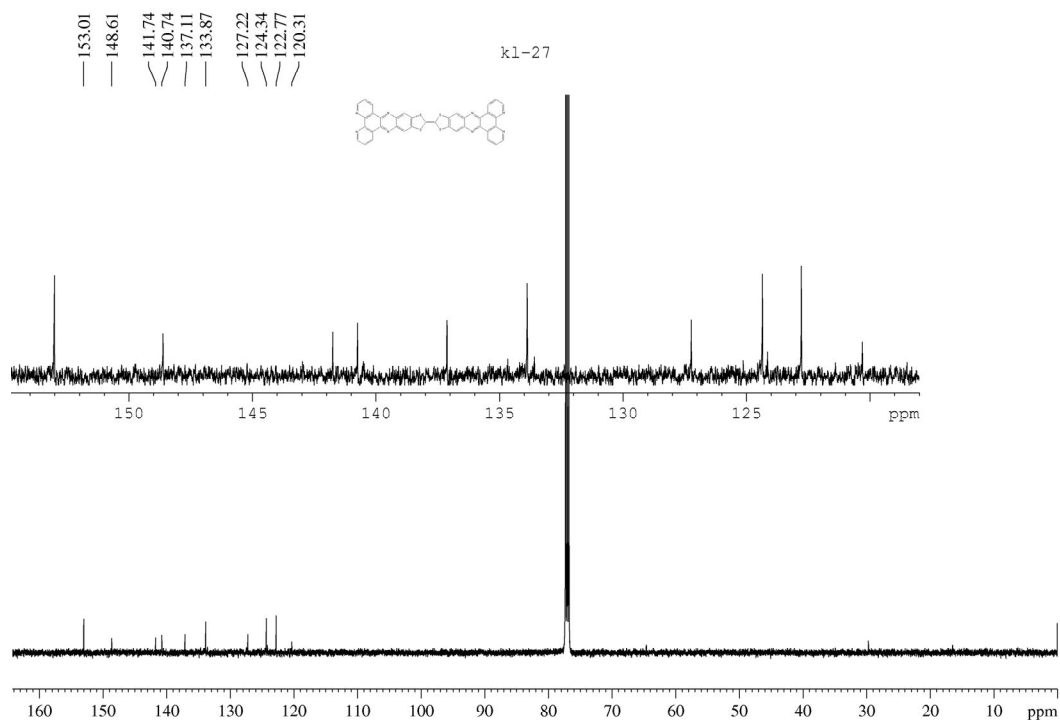
^1H NMR Spectrum of Compound 1a **^1H NMR Spectrum of Compound 1b**

¹³C NMR Spectrum of Compound 1b



¹H NMR Spectrum of Compound 1c



^{13}C NMR Spectrum of Compound 1c**6.4. Conclusion**

In conclusion, we have described the synthesis, characterization and photo physical properties of the three new intramolecular TTF-fused A-D-A triads. All these compounds exhibit good emission in visible region at room temperature. Interestingly, the emission maxima of these triads are largely dependent on the solvent polarity with huge Stokes shifts. Fascinatingly, compound **1b** shows color response with polarity of the solvents under UV lamp. The quantum efficiency of the compound **1b** in more polar solvents is ~ 0.1, which is more emissive as compared to the reported TTF systems of D-A diads as well as D-A-D and A-D-A triads. In addition to this, qdt-based systems have been used in the development of field-effect transistors by introducing the fused qdt-based systems to the TTF-skeleton.^{43,44} So our newly synthesized TTF fused compound **1a-c** may useful in the applications of field-effect transistors. Moreover, the TTF-fused dppz system (compound **1c**) is a good candidate for metal chelation by the coordination of diamine functionality, which is under progress in our laboratory.

6.5. References

- 1 Wudl, F.; Wobschall, D.; Hufnagel, E. *J. Am. Chem. Soc.* **1972**, *94*, 670–672.
- 2 Bendikov, M.; Wudl, F.; perepichka, D. F. *Chem. Rev.* **2004**, *104*, 4891–4945.
- 3 Diaz, M. C.; Illescas, B. M.; Martin, N.; perepichka, I. F.; Bryce, M. R.; Levillain, E.; Viruela, R.; Orti, E. *Chem. Eur. J.* **2006**, *12*, 2709–2721.
- 4 González, M.; Martín, N.; Segura, J. L.; Garín, J.; Orduna, J. *Tetrahedron Lett.* **1998**, *39*, 3269–3272.
- 5 Liu, C.-G.; Guan, W.; Song, P.; Yan, L.-K.; Su, Z.-M. *Inorg. Chem.* **2009**, *48*, 6548–6554.
- 6 Segura, J. L.; Martín, N. *Angew. Chem., Int. Ed.* **2001**, *40*, 1372–1409.
- 7 Yamada, J.; Sugimoto, T. *TTF Chemistry, Fundamentals and Application of Tetrathiafulvalene*, Springer, Berlin, **2004**.
- 8 Otsubo, T.; Takimiya, K. *Bull. Chem. Soc. Jpn.* **2004**, *77*, 43–58.
- 9 Metzger, R. M.; Chen, B.; Höpfner, U.; Lakshmikantham, M. V.; Vuillaume, D.; Kawai, T.; Wu, X.; Tachibana, H.; Hughes, T. V.; Sakurai, H.; Baldwin, J. W.; Hosch, C.; Cava, M. P.; Brehmer, L.; Ashwell, G. J. *J. Am. Chem. Soc.* **1997**, *119*, 10455–10466.
- 10 Imori, T.; Naito, T.; Ohta, N. *J. Phys. Chem. C* **2009**, *113*, 4654–4661.
- 11 Kim, H.; Goddard, W. A.; Jang, S. S.; Dichtel, W. R.; Heath, J. R.; Stoddart, J. F. *J. Phys. Chem. A* **2009**, *113*, 2136–2143.
- 12 Fox, M. A.; Chanon, M. Eds. *Photoinduced Electron Transfer*; Elsevier: Amsterdam, **1988**.
- 13 Kurreck, H.; Huber, M. *Angew. Chem., Int. Ed.* **1995**, *34*, 849–866.
- 14 Michinobu, T.; May, J. C.; Lim, J. H.; Bouden, C.; Gisselbrecht, J. P.; Seiler, P.; Gross, M.; Biaggio, I.; Diederich F. *Chem. Commun.* **2005**, 737–739.
- 15 Thompson, A. L.; Ahn, T. S.; Thomas, K. R. J.; Thayumanavam, S.; Martinez, T. J.; Bardeen, C. J. *J. Am. Chem. Soc.* **2005**, *127*, 16348–16349.
- 16 Miguel, P.; Bryce, M. R.; Goldenberg, L. M.; Beeby, A.; Khodorkovsky, V.; Shapiro, L.; Niemz, A.; Cuello, A. O.; Rotello, V. *J. Mater. Chem.* **1998**, *8*, 71–76.

- 17 Segura, J. L.; Martín, N.; Seoane, C.; Hanack, M. *Tetrahedron Lett.* **1996**, 37, 2503–2506.
- 18 González, M.; Illescas, B.; Martín, N.; Segura, J. L.; Seoane, C.; Hanack, M. *Tetrahedron* **1998**, 54, 2853–2866.
- 19 Tsiperman, E.; Regev, T.; Becker, J. Y.; Bernstein, J.; Ellern, A.; Khodorkovsky, V.; Shames, A.; Shapiro, L. *J. Chem. Soc., Chem. Commun.* **1999**, 1125–1126.
- 20 Dumur, F.; Gautier, N.; Gallego-Planas, N.; Sahin, Y.; Levillain, E.; Mercier, N.; Hudhomme, P. *J. Org. Chem.* **2004**, 69, 2164–2177.
- 21 Wu, H.; Zhang, D.; Su, L.; Ohkubo, K.; Zhang, C.; Yin, S.; Mao, L.; Shuai, Z.; Fukuzumi, S.; Zhu, D. *J. Am. Chem. Soc.* **2007**, 129, 6839–6846.
- 22 Le Paillard, M. P.; Robert, A.; Garrigou-Lagrange, C.; Delhas, P.; Maguerès, P. L.; Ouahab, L.; Toupet, L. *Synth. Met.* **1993**, 58, 223–232.
- 23 Hansen, J. G.; Bang, K. S.; Thorup, N.; Becher, J. *Eur. J. Org. Chem.* **2000**, 2135–2144.
- 24 Murata, T.; Morita, Y.; Yakiyama, Y.; Fukui, K.; Yamochi, H.; Saito, G.; Nakasuji, K. *J. Am. Chem. Soc.* **2007**, 129, 10837–10846.
- 25 Wu, J.; Dupont, N.; Liu, S.-X.; Neels, A.; Hauser, A.; Decurtins, S. *Chem. Asian J.* **2009**, 4, 392–399.
- 26 Goldenberg, L. M.; Becker, J. Y.; Levi, O. P.-T.; Khodorkovsky, V. Y.; Bryce, M. R.; Petty, M. C. *J. Chem. Soc., Chem. Commun.* **1995**, 475–476.
- 27 Goldenberg, L. M.; Becker, J. Y.; Levi, O. P.-T.; Khodorkovsky, V. Y.; Shapiro, L. M.; Bryce, M. R.; Cresswell, J. P.; Petty, M. C. *J. Mater. Chem.* **1997**, 7, 901–907.
- 28 Simonsen, K. B.; Zong, K.; Rogers, R. D.; Cava, M. P.; Becher, J. *J. Org. Chem.* **1997**, 62, 679–686.
- 29 Simonsen, K. B.; Thorup, N.; Cava, M. P.; Becher, J. *Chem. Commun.* **1998**, 901–902.
- 30 Nielsen, M. B.; Nielsen, S. B.; Becher, J. *Chem. Commun.* **1998**, 475–476.
- 31 Devonport, W.; Blower, M. A.; Bryce, M. R.; Goldenberg, L. M. *J. Org. Chem.* **1997**, 62, 885–887.

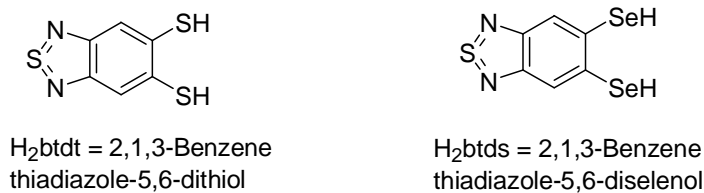
- 32 Levi, O. P.-T.; Becker, J. Y.; Ellern, A.; Khodorkovsky, V. *Tetrahedron Lett.* **2001**, 42, 1571–1573.
- 33 Moore, A. J.; Batsanov, A. S.; Bryce, M. R.; Howard, J. A. K.; Khodorkovsky, V.; Shapiro, L.; Shames, A. *Eur. J. Org. Chem.* **2001**, 73–78.
- 34 Xu, W.; Zhang, D.; Li, H.; Zhu, D. *J. Mater. Chem.* **1999**, 9, 1245–1249.
- 35 Frenzel, S.; Müllen, K. *Synth. Met.* **1996**, 80, 175–182.
- 36 Guo, X.; Zhang, D.; Xu, W.; Zhu, D. *Synth. Met.* **2003**, 137, 981–982.
- 37 Guo, X.; Zhang, D.; Zhang, H.; Fan, Q.; Xu, W.; Ai, X.; Fan, L.; Zhu, D. *Tetrahedron* **2003**, 59, 4843–4850.
- 38 Watson, W. H.; Eduok, E. E.; Kashyap, R. P.; Krawiec, M. *Tetrahedron* **1993**, 49, 3035–3042.
- 39 Gautier, N.; Dumur, F.; Lloveras, V.; Vidal-Gancedo, J.; Veciana, J.; Rovira, C.; Hudhomme, P. *Angew. Chem., Int. Ed.* **2003**, 42, 2765–2768.
- 40 Zhu, Q.-Y.; Huo, L.-B.; Qin, Y.-R.; Zhang, Y.-P.; Lu, Z.-J.; Wang, J.-P.; Dai, J. *J. Phys. Chem. B* **2010**, 114, 361–367
- 41 (a) Mas-Torrent, M.; Durkut, M.; Hadley, P.; Ribas, X.; Rovira, C. *J. Am. Chem. Soc.* **2004**, 126, 984. (b) Mas-Torrent, M.; Hadley, P.; Bromley, S. T.; Crivillers, N.; Veciana, J.; Rovira, C. *Appl. Phys. Lett.* **2005**, 86, 012110.
- 42 (a) Noda, B.; Katsuhara, M.; Aoyagi, I.; Mori, T.; Taguchi, T.; Kambayashi, T.; Ishikawa, K.; Takezoe, H. *Chem. Lett.* **2005**, 34, 392. (b) Katsuhara, M.; Aoyagi, I.; Nakajima, H.; Mori, T.; Kambayashi, T.; Ofuji, M.; Takanishi, Y.; Ishikawa, K.; Takezoe, H.; Hosono, H. *Synth. Met.* **2005**, 149, 219.
- 43 Naraso, Nishida, J.; Ando, S.; Yamaguchi, J.; Itaka, K.; Koinuma, H.; Tada, H.; Tokito, S.; Yamashita, Y. *J. Am. Chem. Soc.* **2005**, 127, 10142–10143.
- 44 Naraso, Nishida, J.; Kumaki, D.; Tokito, S.; Yamashita, Y. *J. Am. Chem. Soc.* **2006**, 128, 9598–9599.
- 45 Jia, C.; Liu, S.-X.; Tanner, C.; Leiggener, C.; Neels, A.; Sanguinet, L.; Levillain, E.; Leutwyler, S.; Hauser, A.; Decurtins, S. *Chem. –Eur. J.* **2007**, 13, 3804–3812.
- 46 (a) Rusanova, J.; Decurtins, S.; Rusanov, E.; Stoeckli-Evans, H.; Delahaye, S.; Hauser, A. *J. Chem. Soc., Dalton Trans.* **2002**, 4318–4320. (b) Ott, S.; Faust, R. *Synthesis* **2005**, 3135–3139.

- 47 Brusso, J. L.; Clements, O. P.; Haddon, R. C.; Itkis, M. E.; Leitch, A. A.; Oakley, R. T.; Reed, R. W.; Richardson, J. F. *J. Am. Chem. Soc.* **2004**, *126*, 8256–8265.
- 48 Bruker. *SADABS*, *SMART*, *SAINT* and *SHELXTL*, **2000** (Bruker AXS Inc., Madison, Wisconsin, USA).
- 49 Sheldrick, G. M. *Acta Crystallogr. Sect. A* **2008**, *64*, 112–122.
- 50 Unciti-Broceta, A.; Pineda-de-las-Infantas, M. J.; Díaz-Mochón, J. J.; Romagnoli, R.; Baraldi, P. G.; Gallo, M. A.; Espinosa, A. *J. Org. Chem.* **2005**, *70*, 2878–2880.
- 51 More, S. V.; Sastry, M. N. V.; Wang, C.-C.; Yao, C.-F. *Tetrahedron Lett.* **2005**, *46*, 6345–6348.
- 52 (a) Paw, W.; Eisenberg, R. *Inorg. Chem.* **1997**, *36*, 2287–2293. (b) Smith, G. F.; Cagle, Jr., F. W. *J. Org. Chem.* **1947**, *12*, 781–784. (c) Guo, W.; Obare, S. O. *Tetrahedron Lett.* **2008**, *49*, 4933–4936.
- 53 (a) Bouguessa, S.; Gouasmia, A. K.; Golhen, S.; Ouahab, L.; Fabre, J. M.; *Tetrahedron Lett.* **2003**, *44*, 9275–9278. (b) Liu, S.-X.; Dolder, S.; Rusanov, E. B.; Stoeckli-Evans, H.; Decurtins, S. *C. R. Acad. Sci. Paris, Chimie* **2003**, *6*, 657–662. (c) Devic, T.; Avarvari, N.; Batail, P. *Chem. -Eur. J.* **2004**, *10*, 3697–3707.

Future Scope of the Present Thesis

Towards the Solid-State Function Materials

Metal coordination polymers are particularly interesting in materials chemistry, and they display remarkable solid state properties in the fields of conducting, magnetic, optical (nonlinear) and gas-storage materials. To accomplish these materials, the use of crystal engineering tools becomes crucial to achieve the adequate packing of the molecules that may lead to the desired properties. In the second chapter of the present thesis, we have described the alkali metal ion based coordination polymers of metal bis(dithiolene) complexes, where simply varying the coordination solvents results in the variation of the structural diversities and dimensionalities. We have demonstrated there the synthesis of sodium metal based coordination polymers of diverse dimensionality (from 1D to 2D through 3D) based on a Metal(III) dithiolene complex anion $[M^{III}(\text{btdt})_2]^{1-}$ [$M = \text{Cu(III)}, \text{Au(III)}$] by changing the solvents of recrystallization. We have shown that dimensionality of a sodium coordination based polymer system, coupled with a Metal(III) (bis)dithiolene complex, can be regulated by the type of hybridization of the central carbon atom of the solvent coordinating to the sodium ion. We believe that in the sodium based coordination polymeric system, octahedral geometry of sodium ion plays an important role in directing the dimensionality of coordination polymers. The electrochemistry of the copper (III) complexes is very interesting in the sense that these complexes get reduced more easily. This indicates that the present system (Cu(III) dithiolate) might act as oxidation catalyst for organic transformations / oxidation reactions of industrial importance. The same methodology can be extended to Ni(III) ions to prepare coordination polymers, in which Ni(III) complexes would show an interesting conducting and magnetic behavior. We would be able to also extend this to diselenolene complexes (Scheme 1). The replacement of sulfur with selenium in the building blocks (metal dithiolene complexes) / tetrathiafulvalenes (TTFs) has been shown to overcome the metal-to-insulator transition, often present in these materials at low temperatures caused by Peierls distortion. The greater spatial extension of Se orbitals compared to S may increase the electronic dimensionality of the system and thus to avoid the undesired transition.



Scheme 1

Very recently, two electro-conductive coordination polymers $Cu[Cu(pdt)_2]$ and $Cu[Ni(pdt)_2]$ have been reported, and these show relatively high electrical conductivity at room temperature with high porosity based on pyrazine bis(dithiolate) building blocks (Figure 1). In addition, the conductivity of $Cu[Ni(pdt)_2]$ has been enhanced through partial oxidation of the its framework. The increasing in counducvity is due to oxidative doping and the resulting framework is a p-type semicounductor. Metal-organic framewoks of these dithiolene based compounds exhibits reletively high elctrical conductivity. In this way, our newly synthesized alkali metal ion based coordination polymers containing alkali cations would be exchanged by transition metal ions such as Cu(1) ions to get good porous conducting materials and the work is going on presently in this direction in our laboratory.

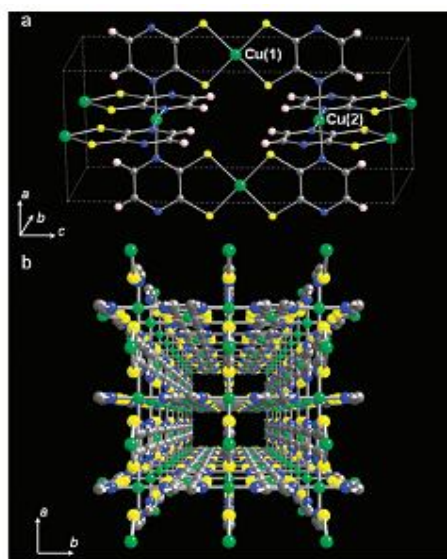


Figure 1. (a) Crystal structure in $Cu[Cu(pdt)_2]$. (b) Perspective view of the crystal structure of $Cu[Cu(pdt)_2]$. Color code: green, Cu; yellow, S; gray, C; blue, N; pink, H.

Towards the biological importance

Dithiolenes play an important role in natural systems. Thus, a dithiolene group is present an integral component of molybdopterin (MPT), the moiety that binds the molybdenum (or tungsten) at the catalytic centre of enzymes that transfer an oxygen atom to or from the

substrate. A wide range of reactions are present in virtually all living systems catalyzed by these enzymes, and many of these enzymes are structurally characterized. Each catalytic centre is shown to involve a single metal atom bound to one or two MPT groups, plus other donor atoms. Spectroscopic information indicates that the oxygen atom transfer reaction takes place at the metal centre, the oxidation state of which changes from M(VI) to M(IV) (or vice-versa). This knowledge should encourage further investigations of dithiolene complexes as catalysts, especially when the process involves a redox change. In this context, particularly qdt (quinoxaline-2,3-dithiolate) ligand and its molybdenum-oxo complexes have been investigated for modeling the active sites of molybdenum hydroxylase enzymes. The newly synthesized ligands $\{6,7\text{-qdt}\}^{2-}$ (quinoxaline-6,7-dithiolate) based ligands, described in chapter 5, $\{\text{btdt}\}^{2-}$ (2,1,3-benzenethiadiazole-5,6-dithiolate) based ligand described in chapter 3, and $\{\text{ppdt}\}^{2-}$ (pyrido[2,3-*b*]pyrazine-2,3-dithiolate) based ligand described in chapter 4, are useful to synthesize the Mo- and W-dithiolene complexes which are related to active sites of many metalloenzymes. The relevant effort has already been underway in our laboratory.

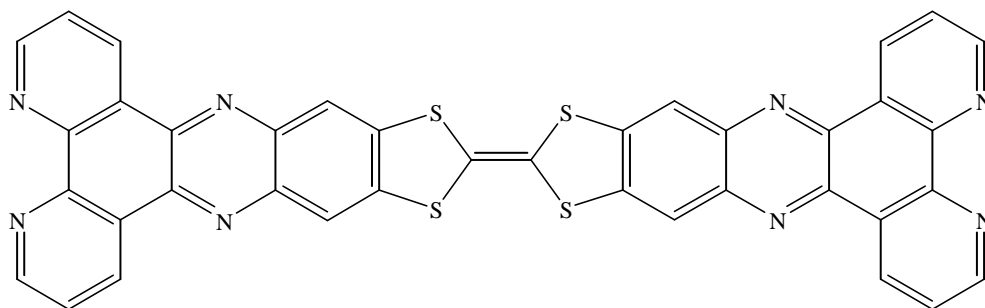
Towards the Field Effect Transistors (FET)

Currently, the generation of field-effect transistors (FET) is of considerable interest in charger carrying semiconductor materials. Recently, qdt-based systems have been used in the development of field-effect transistors by introducing the fused qdt-based systems to the TTF-skeleton. Limited reports have been observed in the literature in this direction. This would be an interesting area in the synthesis of new TTF-fused derivatives with new heterocyclic based ligands in greater extent. The newly synthesized ligands 6,7-qdt based ligands, described in chapter 5, have been used for the synthesis of new acceptor-donor-acceptor tetrathiafulvalene compounds. These compounds may be useful for the applications towards the field effect transistors.

Toward the Coordination Chemistry of dppz-TTF Systems

The significance in the extended dppz compound stems from its fascinating features that include structural planarity, π -extended conjugation, and its metal-chelating diimine functionality. It has been demonstrated that metal complexes containing a dppz ligand, in particular those of ruthenium(II), are good metallo-intercalators. Furthermore, the luminescence properties of dppz-based complexes have led to their application as DNA

“light switches” and probes for long-range DNA-mediated electron-transfer studies. In addition, photochemical behavior of these complexes is interesting in terms of photochemical charge separation. However, the acceptor-donor-acceptor TTF-fused dppz systems have not been reported so far. In this context, our newly synthesized TTF-fused dppz compound (Scheme 2), described in chapter 6 is a good candidate for metal chelation by the coordination of diamine functionality with various metal ions, such as Ru(II), Re(I), Cu(II), Ni(II), Pt(II) and *etc.*, which is under progress in our laboratory.



Scheme 2

List of Publications

1. A Nitrogen Rich Ni(II)-Dithiolate System Exhibiting Acid-Base Behavior: Synthesis, Supramolecular Structure and Spectroscopy of $[\text{Bu}_4\text{N}]_2[\text{Ni}^{\text{II}}(\text{ppdt})_2]$ (ppdt = pyrido[2,3-*b*]pyrazine-2,3-dithiolate).
Ramababu Bolligarla, Gummadi Durgaprasad and Samar K. Das*, *Inorg. Chem. Commun.* **2009**, *12*, 355–358.
2. Design, Synthesis and Discovery of Novel Non-Peptide Inhibitor of Caspase-3 Using Ligand Based and Structure Based Virtual Screening Approach.
P. Jhansi Lakshmi, Suneel Kumar B.V.S, Ravi Shasi Nayana, M. Srinivas Mohan, **Ramababu Bolligarla**, Samar K. Das, M. Uday Bhanu, Anand K. Kondapi Muttineni Ravikumar*, *Bioorg. Med. Chem.* **2009**, *17*, 6040–6047.
3. Acid-Base Behavior of a Simple Metal Bis(Dithiolate) System: Synthesis, Crystal Structure and Spectroscopy of $[\text{Bu}_4\text{N}]_2[\text{M}^{\text{II}}(\text{ppdt})_2]$ (M = Ni, Pt; ppdt = pyrido[2,3-*b*]pyrazine-2,3-dithiolate).
Ramababu Bolligarla, Ravada Kishore, Gummadi Durgaprasad and Samar K. Das*, *Inorg. Chem. Acta* **2010**, *363*, 3063–3069.
4. Dimensionality of Coordination Polymers Decided by the Type of Hybridization of the Central Carbon Atom of the Solvent Molecule that Coordinates to an Alkali Metal Cation: from Discrete to 3-D Networks Based on a Gold(III) Bis(dithiolene) Complex.
Ramababu Bolligarla, and Samar K. Das*, *CrystEngComm* **2010**, *12*, 3409–3412.
5. Hexa Boron-Dipyrromethene Cyclotriphosphazenes: Synthesis, Crystal Structure, and Photophysical Properties.
M. Rajeswara Rao, **R. Bolligarla**, Ray. J. Butcher, and M. Ravikanth*, *Inorg. Chem.* **2010**, *49*, 10606–10616.
6. Synthesis, Molecular Structure and Supramolecular Chemistry of a New Nickel-Quinoxaline Dithiolate System $[\text{Bu}_4\text{N}]_2[\text{Ni}(6,7\text{-qdt})_2]$ (6,7-Qdt = Quinoxaline-6,7-dithiolate) and Comparison of its Electronic and Electrochemical Properties with those of $[\text{Bu}_4\text{N}]_2[\text{Ni}(\text{qdt})_2]$ (Qdt = Quinoxaline-2,3-dithiolate)
Ramababu Bolligarla, Gummadi Durgaprasad and Samar K. Das*, *Inorg. Chem. Commun.* **2011**, *14*, 809-813.

7. Synthesis of New Intramolecular Charge Transfer A–D–A Tetrathiafulvalene-Fused Triads Exhibiting Large Solvent Sensitive Emission Behavior
Ramababu Bolligarla, and Samar K. Das*, *Tetrahedron Lett.* **2011**, 52, 2496–2500.

8. New Square-Planar Bis(Dithiolene) Complexes: Synthesis, Crystallography and Properties of $[\text{Bu}_4\text{N}][\text{M}^{\text{III}}(\text{btdt})_2]$ ($\text{M} = \text{Cu}, \text{Au}$) and $[\text{Bu}_4\text{N}]_2[\text{Pt}^{\text{II}}(\text{btdt})_2]$ ($\{\text{btdt}\}^{2-} = 2,1,3\text{-Benzenethiadiazole-5,6-dithiolate}$)
Ramababu Bolligarla, and Samar K. Das*, *Aust. J. Chem.* **2011**, 64, 550–560.

9. 6,7,6',7'-Tetraphenyl-[2,2']bi[1,3-dithia-5,8-diaza-cyclopenta[*b*]naphthalenyldiene]
Ramababu Bolligarla, Gummadi Durgaprasad and Samar K. Das*, *Acta Cryst. E*, **2011**, (Accepted).

10. Syntheses and Structural Characterization of Potassium Coordination Polymers Based on a Copper-Bis(dithiolato) Complex $[\text{Cu}(\text{btdt})_2]^{1-}$ ($\{\text{btdt}\}^{2-} = 2,1,3\text{-Benzenethiadiazole-5,6-dithiolate}$): Role of Coordinating Solvents and Counter Cation
Ramababu Bolligarla, Bharat Kumar Tripuramallu, Vudagandla Sreenivasulu and Samar K. Das*, *Indian J. Chem. A* **2011**, (Accepted).

11. Synthesis, structural characterization and electrochemical studies of $[\text{Fe}_2(\mu\text{-L})(\text{CO})_6]$ and $[\text{Fe}_2(\mu\text{-L})(\text{CO})_5(\text{PPh}_3)]$ ($\text{L} = \text{pyrazine-2,3-dithiolate}$, quinoxaline-2,3-dithiolate and pyrido[2,3-*b*]pyrazine-2,3-dithiolate): towards modeling the active site of $[\text{FeFe}]$ -Hydrogenase
Gummadi Durgaprasad, **Ramababu Bolligarla**, and Samar K. Das*, (communicated).

12. Dimensionality of Coordination Networks in Terms of the Geometry of Central Carbon of Solvents Through Their Coordination with Sodium Metal ion: Syntheses, Crystal structures and Properties of Coordination Polymers based on $[\text{Cu}^{\text{III}}(\text{btdt})_2]^{1-}$ and $[\text{Au}^{\text{III}}(\text{btdt})_2]^{1-}$
Ramababu Bolligarla, and Samar K. Das*, (communicated).

13. Nature of the Substituent Influences the Electronic and Electrochemical Properties of New Square-Planar Nickel-Bis(Quinoxaline-6,7-dithiolate) Complexes: Synthesis and Crystallographic study
Ramababu Bolligarla, Vudagandla Sreenivasulu and Samar K. Das*, (to be communicated).
14. Oxygenation of $[\text{Ni}(\text{btdt})_2]^{2-}$ (btdt = 2,1,3-Benzenethiadiazole-5,6-dithiolate) Sulphur by Air at an Ambient Conditions: Synthesis, Crystal structure, Properties
Ramababu Bolligarla, and Samar K. Das*, (to be communicated).

Posters and Presentations

1. **Ramababu Bolligarla** and Samar K. Das*, Oxygenation of Nickel Bis(Dithiolato) Sulfur By Air at an Ambient Condition and Nitrogen Rich Metal Bis(dithiolene) Complexes, Poster presentation at “Chemfest-2008 (in-house)” which was held in School of Chemistry, University of Hyderabad, Hyderabad, India on March, 2008.
2. **Ramababu Bolligarla** and Samar K. Das*, Oxygenation of Nickel Bis(Dithiolato) Sulfur By Air at an Ambient Condition and Nitrogen Rich Metal Bis(dithiolene) Complexes, Poster presentation at “NCMC-08” which was held in Gitam University, Visakhapatnam, India on August, 2008.
3. **Ramababu Bolligarla**, Gummadi Durgaprasad, and Samar K. Das*, Nitrogen Rich Metal-Dithiolate System Exhibiting Acid-Base Behavior: Synthesis Supramolecular Structure and Spectroscopy of $[\text{Bu}_4\text{N}]_2[\text{M}^{\text{II}}(\text{ppdt})_2]$ (M = Ni and Pt; ppdt^{2-} = pyrido[2,3-b]pyrazine-2,3-dithiolate), Poster presentation at “Chemfest-2009 (in-house)” which was held in School of Chemistry, University of Hyderabad, Hyderabad, India on March, 2009.
4. **Ramababu Bolligarla** and Samar K. Das*, A New Class of Coordination Polymers Based on a Metal bis(dithiolene) Complex: Synthesis, Crystal Structures and Properties, Oral and Poster presentation at “Chemfest-2010 (in-house)” which was held in School of Chemistry, University of Hyderabad, Hyderabad, India on January, 2010.

5. **Ramababu Bolligarla** and Samar K. Das*, A New Class of Coordination Polymers Based on a Metal bis(dithiolene) Complex: Synthesis, Crystal Structures and Properties, Poster presentation at “CRSI-2010” which was held in Indian Institute of Chemical Technology, Hyderabad, India on February, **2010**.
6. **Ramababu Bolligarla**, Vudagandla Sreenivasulu and Samar K. Das*, Nature of the Substituent Influences the Electronic and Electrochemical Properties of New Square-Planar Nickel-Bis(quinoxaline-6,7-dithiolate) Complexes: Synthesis and Crystallographic Study, Poster presentation at “Chemfest-2011 (in-house)” which was held in School of Chemistry, University of Hyderabad, Hyderabad, India on March, **2011**.

SYNOPSIS

This thesis work entitled with “**Heterocyclic-Based 1,2-Dithiolate Ligands and Their Coordination Complexes with Transition Metals: Synthesis, Characterization and Functional Properties**”, consists of six chapters: (1) Introduction, (2) Self-Assembly of Alkali Metal Based Coordination Polymers of Metal Bis(Dithiolene) Complexes: Role of Coordinated Crystallizing Solvents and Counter Cations in Tuning the Structural Diversity and Dimensionality, (3) New Square-Planar Metal-Bis(1,2-Dithiolene) Complexes Based on 2,1,3-Benzenethiadiazole-5,6-dithiolate ($\{btdt\}^{2-}$) ligand and Nickel Trans-disulfinate Complex: Synthesis, Crystallography and Properties, (4) Acid-Base Behavior of a Simple and Nitrogen Rich Metal Bis(Dithiolene) System: Syntheses, Crystal Structures and Spectroscopy of $[Bu_4N]_2[M^{II}(ppdt)_2]$ ($M = Ni, Pt$; $\{Ppdt\}^{2-} = \text{Pyrido}[2,3-b]\text{pyrazine-2,3-dithiolate}$), (5) Nature of the Substituent Influences the Electronic and Electrochemical Properties of New Square-Planar Nickel-Bis(Quinoxaline-6,7-dithiolate) Complexes and Comparison of These Properties with Those of Existing $[Bu_4N]_2[Ni(qdt)_2]$ ($Qdt = \text{Quinoxaline-2,3-dithiolate}$): Synthesis and Crystallographic study, (6) Synthesis of New Intramolecular Charge Transfer A–D–A Tetrathiafulvalene-Fused Triads Exhibiting Large Solvent Sensitive Emission Behavior. The work described in this thesis, is in the direction towards the synthesis and characterization of late-transition metal (Ni, Pt, Cu, and Au) bis(dithiolene) complexes and studied their electronic and electrochemical properties. Apart from the first chapter (introduction), all the chapters are sub-divided into Introduction, Experimental Section, Results and Discussion and Conclusions followed by References.

Chapter 1

Introduction

This chapter begins with more basic knowledge about dithiolene ligands and their metal complexes, starting from its history. It also reveals brief discussion emphasizing their syntheses, characterization and properties. Some of the important transition metal 1,2-dithiolene complexes are picked up to illustrate their solid state properties, such as, magnetic, conducting, superconducting, and optical properties (NLO, and NIR dyes). The structural, spectroscopic, luminescence, bonding, reactivity, electrochemistry, and catalytic applications of transition metal 1,2-dithiolene complexes are also briefly discussed. In addition, the importance of 1,2-dithiolene ligands and its metal complexes in biology, which are present in active sites of many metalloenzymes are described. Finally, a brief note on the main objectives of this thesis work conversed shortly.

Chapter 2

Self-Assembly of Alkali Metal Based Coordination Polymers of Metal Bis(Dithiolene) Complexes: Role of Coordinated Crystallizing Solvents and Counter Cations in Tuning the Structural Diversity and Dimensionality

This chapter describes the synthesis, structural characterization of properties of alkali metal (Na, and K) based coordination polymers of metal bis(dithiolene) complexes $M(btdt)_2]^{1-}$ ($M = Cu(III)$ and $Au(III)$; $btdt = 2,1,3$ -benzenethiadiazole-5,6-dithiolate). The self-assembly of coordination networks (alkali-metal coordination polymers) are influenced by the coordinating solvents through the coordination with alkali metal ion. In order to investigate the effect of coordinating solvent on the dimensionality of the coordination networks, we have synthesized ten sodium based coordination polymers $\{[Na(CH_3OH)_4][Cu(btdt)_2]\}_n$ (1), $\{[Na(THF)_4][Cu(btdt)_2]\}_n$ (2), $\{[Na(CH_3COCH_3)_2][Cu(btdt)_2]\}_n$ (3), $\{[Na(DMF)_2][Cu(btdt)_2]\}_n$ (4), $\{[Na(CH_3CN)_2][Cu(btdt)_2]\}_n$ (5), $\{[Na(CH_3OH)_4][Au(btdt)_2]\}_n$ (6), $\{[Na(THF)_2][Na(THF)(OH_2)][Au_2(btdt)_4]\}_n$ (7), $\{[Na(CH_3COCH_3)_2][Au(btdt)_2]\}_n$ (8), $\{[Na(DMF)_2][Au(btdt)_2]\}_n$ (9) and $\{[Na(CH_3CN)_2][Au(btdt)_2]\}_n$ (10) by varying the coordinating solvents in respective recrystallization process. The coordination polymers 1–5, based on copper-bis(dithiolene) complex $[Cu^{III}(btdt)_2]^{1-}$, were synthesized from the different solvents by the recrystallization of a black colored-precipitated compound, which was obtained by the reaction of one mole equivalent of $CuCl_2 \cdot 2H_2O$ with two mole equivalents of H_2btdt in MeOH treated with excess amount of NaOH in presence of open atmosphere. The coordination polymers 6–10, based on gold-bis(dithiolene) complex $[Au^{III}(btdt)_2]^{1-}$, were obtained from the different solvents by recrystallizing brown colored-precipitated compound, that was synthesized by the reaction of one mole equivalent of $HAuCl_4 \cdot 3H_2O$ with two mole equivalents of H_2btdt in MeOH treated with excess amount of NaOH in presence of nitrogen atmosphere. In addition to these, a discrete compound $[Na_2(H_2O)_6(\mu-H_2O)_2][Au(btdt)_2]_2$ (11) has been synthesized by the recrystallization of the gold compound in MeOH in open air conditions. In the self-assembly process, the dimensionality of the networks of coordination polymers 1–10 has greatly been influenced by the hybridization of central carbon atom attached to the coordinating solvent atom ('N' or 'O') of the recrystallizing solvents.

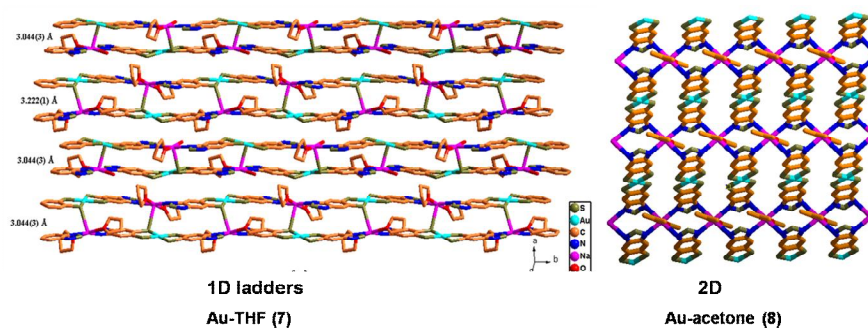
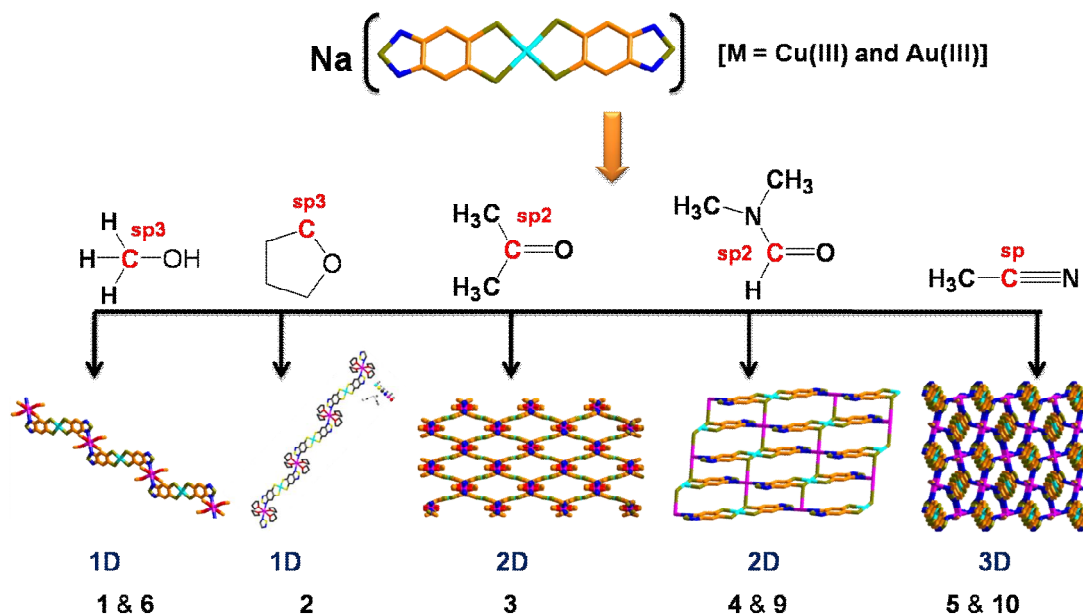


Figure 1. Extended coordination networks observed in the crystal structures of sodium based coordination polymers 1-10.

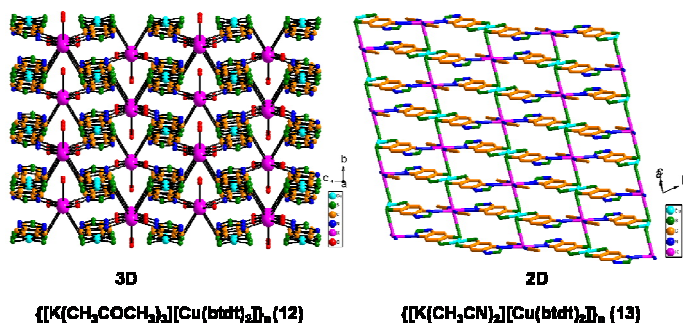


Figure 2. Extended coordination networks observed in the crystal structures of potassium based coordination polymers 12-13.

Recrystallization from sp^3 hybridized central carbon containing coordinating solvent, such as, MeOH and THF solvents lead to the 1D coordination polymers, sp^2 hybridized central

carbon containing coordinating solvents, such as, acetone and DMF solvents lead to the 2D coordination polymers and sp hybridized central carbon containing coordinating solvent (e.g., CH₃CN solvent) results in the formation of 3D coordination polymers are shown in Figure 1. Thus, the shape and space occupied by the hybridized orbitals of central carbon atom attached to the coordinating solvent atoms are the major factors in directing the dimensionality of sodium based coordination polymers of the present system. To study the counter cation effect on the structural diversity and dimensionality, we have synthesized two potassium-based coordination polymers $\{[K(CH_3COCH_3)_3][Cu(btdt)_2]\}_n$ (**12**) and $\{[K(CH_3CN)_2][Cu(btdt)_2]\}_n$ (**13**). Interestingly, compounds **12** and **13** are 3-D and 2-D extended networks respectively observed in their crystal structures which are obtained from recrystallization of acetone and acetonitrile coordinating solvents (Figure 2). Thus potassium-based coordination polymers are in contrast to the sodium-based coordination polymers as far as the dimensionality of the coordination polymers and hybridization of carbon atom of the coordinating solvents are concerned. This is probably due to difference in size of the counter cations (between sodium and potassium). Hence the concept of “dimensionality decided by the hybridization” is limited to sodium based coordination polymers. We believe that in the sodium based coordination polymeric system, octahedral geometry of sodium ion plays a role in directing the dimensionality of coordination polymers compared to the K-based coordination polymers (because of its larger size, coordination number is varying). All these compounds have been structurally characterized unambiguously by single crystal X-ray crystallography. Interestingly, copper compounds **1–5** show two quasi-reversible reduction responses at –0.13 V and –1.10 V vs Ag/AgCl in DMF solutions (Figure 3, representative example). Interestingly, this is a very low reduction potential for a Cu(III)-coordination complex and even it is less than that of reported Cu(III) compound of pds (pyrazine-2,3-diselenote) ligand.

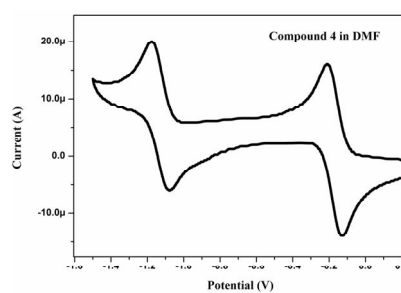


Figure 3. Cyclic voltammetry of complex **4** in DMF with a scan rate 50 mV s⁻¹ (*n*Bu₄NClO₄ as supporting electrolyte).

Chapter 3

New Square-Planar Metal-Bis(1,2-Dithiolene) Complexes Based on 2,1,3-Benzenethiadiazole-5,6-dithiolate ($\{btdt\}^{2-}$) Ligand and Nickel Trans-disulfinate Complex: Synthesis, Crystallography and Properties

In the previous chapter 2, we have described synthesis of alkali metal ion based coordination polymers, based on $\{btdt\}^{2-}$ ligand. This $\{btdt\}^{2-}$ ligand can also be used for the synthesis of “discrete” metal bis(dithiolene) complexes with various transition metal complexes, that will form square-planar dithiolene complexes. In the present chapter, the syntheses, crystal structures and properties of four new coordination complexes $[Bu_4N][M^{III}(btdt)_2]$ [$M = Cu$ (**1**), Au (**2**)] and $[Bu_4N]_2[M^{II}(btdt)_2]$ [$M = Pt$ (**3**), Ni (**4**)] ($\{btdt\}^{2-} = 2,1,3\text{-benzenethiadiazole-5,6-dithiolate}$) have been described. In addition to this, trans-disulfinate complex $[Bu_4N]_2[Ni(btdtO_4)_2] \cdot H_2O$ (**5**) has been synthesized by the air oxidation of the compound **4** in MeOH solutions. Single crystal X-ray structural analyses of complexes **1–5** show that $\{MS_4\}$ chromophores lie in almost square-planar coordination environment in complexes **1** and **4**, whereas in complexes **2**, **3** and **5**, this chromophore has slightly distorted square-planar geometry around the central metal ion. Interactions in the solid-state for all these compounds have been studied by intermolecular contacts, such as, weak hydrogen bonding interactions and non-covalent interactions. Complexes **1–5** show broad absorption bands in the visible region, with that of **3** and **4** are being sensitive to solvent polarity as shown in Figure 4. Blue-colored air-saturated solutions of $[Bu_4N]_2[Ni(btdt)_2]$ (**4**) gradually turn red in the presence of visible light (room light). This transformation requires both oxygen (air) and light. When methanolic solution of complex **4**, under oxygen atmosphere (1 atmospheric pressure) is stirred at room conditions for 1 week, it results in the formation of compound **5**, which was confirmed by 1H NMR and UV-visible absorption spectroscopy. We have recorded the absorption spectra at different intervals of time as shown in Figure 4(c). As shown in Figure 4(c), the CT band at 586 nm gradually decreases with appearance of new absorption band at 485 nm in the blue region. At the same time the band at 360 nm also gradually decreases with the appearance of new band at 310 nm. The appearance of new bands at 485 and 310 nm are due to the formation of compound **5**. The spectral changes are more frequent at the initial intervals / stages of the time as shown in Figure 4(c).

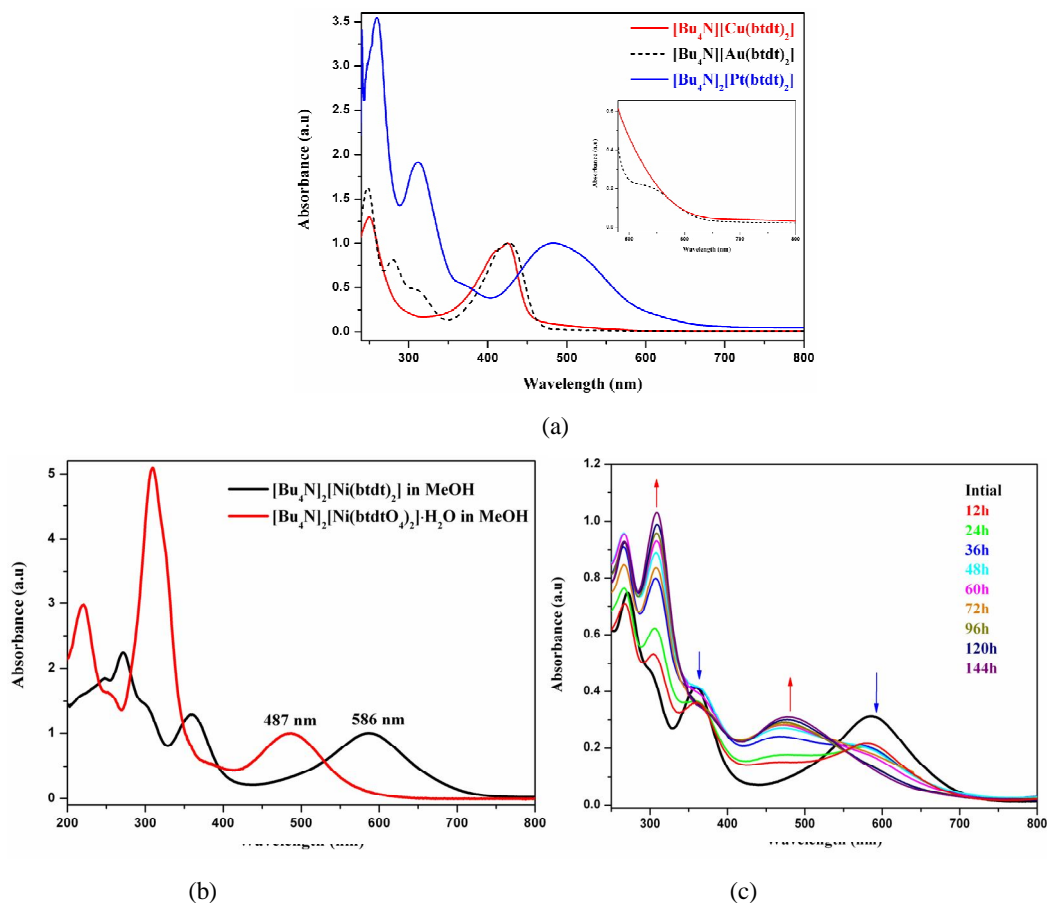


Figure 4. Electronic absorption spectra of compounds (a) **1–3** in acetonitrile solutions; (b) **4** and **5** in methanol solutions; (c) Absorption spectral changes for the methanolic solution of complex $[\text{Bu}_4\text{N}]_2[\text{Ni}^{\text{II}}(\text{btdt})_2]$ (**4**) in oxygen atmosphere at different intervals of time.

Electrochemical properties of all these compounds have been described by cyclicvoltammetric data. The cyclic voltammetric studies of compound **1** shows a Cu(III)/Cu(II) redox couple appearing as a reversible wave at $E_{1/2} = -0.11$ V vs Ag/AgCl ($\Delta E = 74$ mV) in DMF solution as shown in Figure 5(a). Interestingly, this is a very low reduction potential for a Cu(III)-coordination complex and the same type of reduction potentials are observed in the case of previously described cooper coordination polymers in Chapter 2. The platinum complex **3** exhibits two irreversible oxidative responses at 0.45 V and 0.74 V vs Ag/AgCl in MeOH as shown in Figure 5(b). Ni-complex **4** undergoes quasi-reversible oxidation ($\Delta E = 0.10$ V) at $E_{1/2} = +0.16$ V vs Ag/AgCl, that corresponds the $[\text{Ni}(\text{ppdt})_2]^{1+}/[\text{Ni}(\text{ppdt})_2]^{2+}$ redox couple, indicating that Ni(III) complex $[\text{Ni}(\text{ppdt})_2]^{1+}$ is fairly stable in the electrochemical scale. Interestingly compound **4** is oxidized to Ni(III) oxidation state at very low oxidation potentials as shown Figure 5(c).

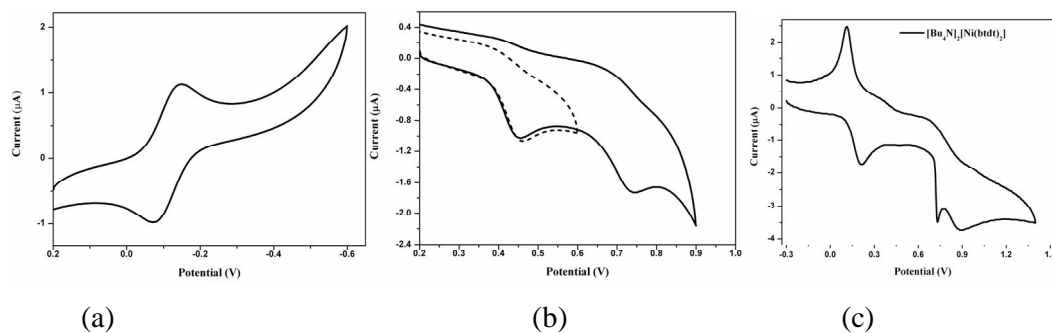


Figure 5. Cyclic voltammograms of complexes (a) **1** in DMF (b) **3** in MeOH and (c) **4** in Methanol, with a scan rate 50 mV s^{-1} ($n\text{Bu}_4\text{NClO}_4$ as supporting electrolyte).

Chapter 4

Acid-Base Behavior of a Simple and Nitrogen Rich Metal Bis(Dithiolene) System: Syntheses, Crystal Structures and Spectroscopy of $[\text{Bu}_4\text{N}]_2[\text{M}^{\text{II}}(\text{ppdt})_2]$ ($\text{M} = \text{Ni}, \text{Pt}$; $\{\text{ppdt}\}^{2-} = \text{Pyrido}[2,3-b]\text{pyrazine-2,3-dithiolate}$)

This chapter describes the syntheses, crystal structures and properties of compounds $[\text{Bu}_4\text{N}]_2[\text{Ni}(\text{ppdt})_2]$ (**1**) and $[\text{Bu}_4\text{N}]_2[\text{Pt}(\text{ppdt})_2]$ (**2**) ($\{\text{ppdt}\}^{2-} = \text{pyrido}[2,3-b]\text{pyrazine-2,3-dithiolate}$) based on more nitrogen containing $\{\text{ppdt}\}^{2-}$ ligand. Compound **1** crystallizes in $P2_1/c$ space group (monoclinic system), whereas compound **2** crystallizes in $C2/c$ space group (monoclinic system). The crystal structures of both compounds **1** and **2** have been characterized by C–H \cdots S and C–H \cdots N hydrogen bonding interactions between cation and anions resulting in 3-dimensional supramolecular networks in the crystals of **1** and **2**, respectively as shown Figure 6. The acid–base behavior of the ground states of both **1** and **2** also the excited state of compound **2** in solutions has been studied by titrating with weak acid-weak bases, and strong acid and strong bases (Figure 7). The pH dependent changes in the charge-transfer absorption and emission spectra are attributed to the protonation on an imine nitrogen of the ppdt ligand. The ground–state basicity constants of the two complexes **1** and **2** have been determined from spectrophotometric analysis by titrating with a weak acid, yielding $\text{p}K_{\text{b1}} = 8.0$ for complex **1** and $\text{p}K_{\text{b1}} = 7.8$ for complex **2**. The excited–state basicity constant $\text{p}K_{\text{b1}}^*$ for complex **2** has been determined by a thermodynamic equation using a Förster analysis yielding the value of 1.8. The complex **1** is electrochemically quasi-reversible with an oxidation potential of $E_{1/2} = +0.46 \text{ V vs Ag/AgCl}$ ($\Delta E = 0.12 \text{ V}$), whereas the complex **2** is electrochemically irreversible with an

oxidation potential of $E_{1/2} = +0.41$ V vs Ag/AgCl in methanol solutions are shown in Figure 8.

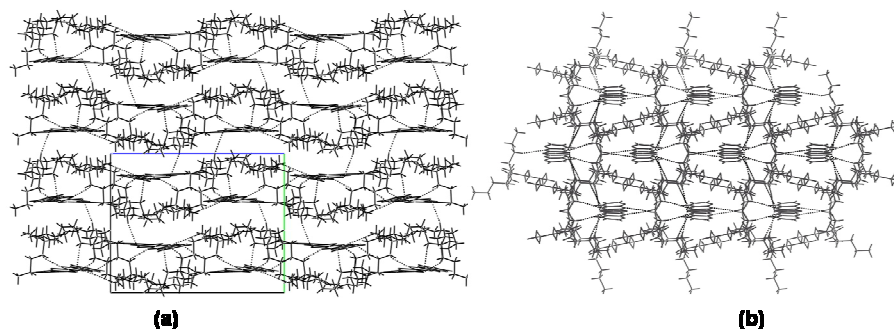


Figure 6. The molecular packing diagrams of (a) $[\text{Bu}_4\text{N}]_2[\text{Ni}(\text{ppdt})_2]$ (**1**) (b) $[\text{Bu}_4\text{N}]_2[\text{Pt}(\text{ppdt})_2]$ (**2**) are characterized by C–H...N and C–H...S weak interactions, when viewed down to the crystallographic a axis.

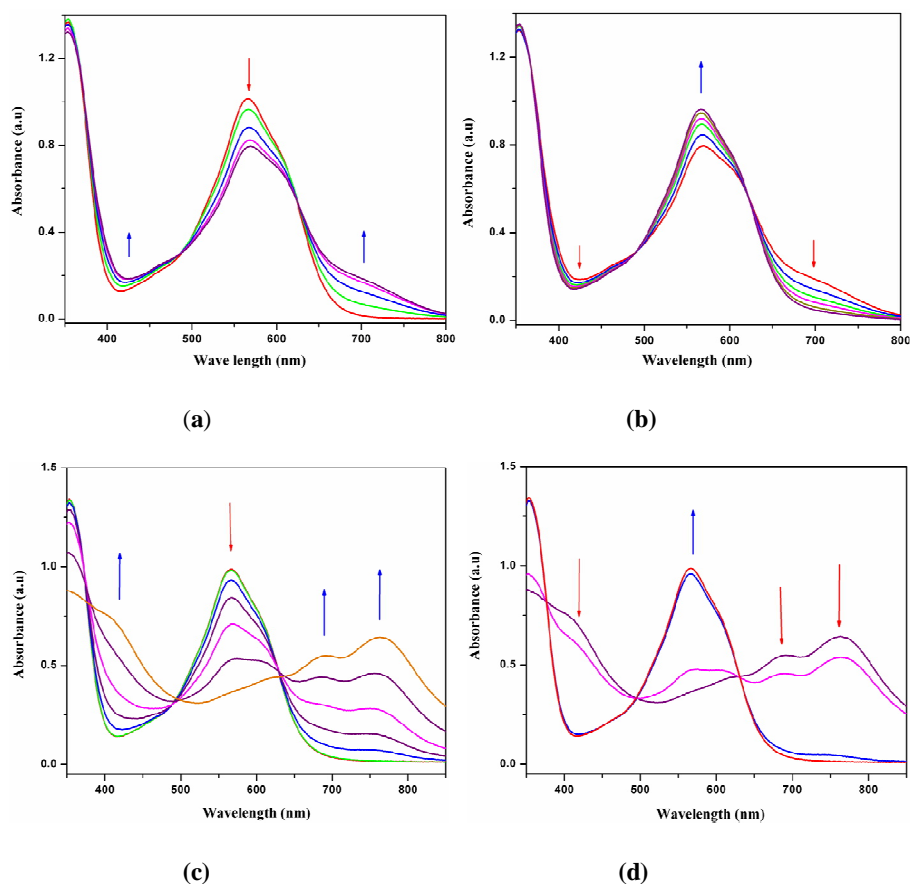


Figure 7. (a) Changes in the absorption spectra of $[\text{Bu}_4\text{N}]_2[\text{Ni}(\text{ppdt})_2]$ (**1**) (4.3×10^{-5} M) upon addition of 10 μL aliquots of dilute CH_3COOH (3.51×10^{-1} M) in methanol. (b) Spectral changes upon addition of 10 μL aliquots of dilute aq. NH_3 (1.068 M) in methanol to the protonated species (blue colored) of **1** (4.3×10^{-5} M). (c) Changes in the absorption spectra of $[\text{Bu}_4\text{N}]_2[\text{Ni}(\text{ppdt})_2]$ (**1**) (4.3×10^{-5} M) upon addition of 10 μL aliquots of dilute HCl (1.13×10^{-1} M) in methanol. (d) Back titration (spectral changes) upon addition of 10 μL aliquots of dilute NaOH (0.1875 M) in methanol to the protonated species (blue colored) of **1** (4.3×10^{-5} M).

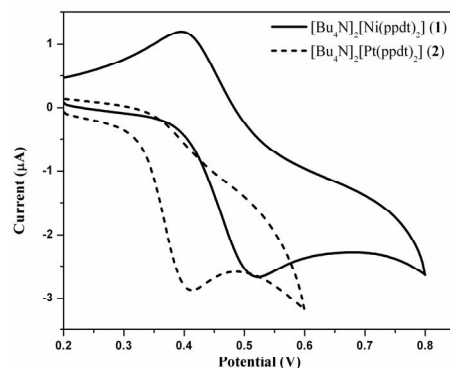


Figure 8. Cyclic voltammograms of compounds **1** and **2** in TBAP/MeOH at a scan rate 50 mV s^{-1} .

Chapter 5

Nature of the Substituent Influences the Electronic and Electrochemical Properties of New Square-Planar Nickel-Bis(Quinoxaline-6,7-dithiolate) Complexes and with Those of Existing $[\text{Bu}_4\text{N}]_2[\text{Ni}(\text{qdt})_2]$ (Qdt = Quinoxaline-2,3-dithiolate): Synthesis and Crystallographic study

Chapter 5 describes mainly the syntheses and crystal structures of a new series of square-planar nickel-bis(quinoxaline-6,7-dithiolate) complexes with the general formula $[\text{Bu}_4\text{N}]_2[\text{Ni}(\text{X}_{2,6,7}\text{-qdt})_2]$, where X = H (**1a**), Ph = phenyl (**2a**), Cl (**3**) and Me = methyl (**4**) [$\{6,7\text{qdt}\}^{2-}$ = quinoxaline-6,7-dithiolate] and comparative studies of their electronic and electrochemical properties. The solution and solid-state electronic absorption spectra and electrochemical properties of these compounds, are strongly dependent on the electron donating / accepting nature of the substituent. Particularly, the CT (charge transfer) transition bands, observed in the visible region, are greatly affected by the electronic nature of the substituent attached to the quinoxaline-6,7-dithiolate ring and the relevant spectra are shown in Figure 9. The CT transition of $[\text{Bu}_4\text{N}]_2[\text{Ni}(6,7\text{-qdt})_2]$ absorb at low energy region in comparison to the CT band of the $[\text{Bu}_4\text{N}]_2[\text{Ni}(\text{qdt})_2]$ in the visible region. In addition to this, the observed CT bands in all the complexes are sensitive to the solvent polarity. Complexes **1a**, **2a**, **3** and **4** undergo reversible oxidation at very low oxidation potentials appears at $E_{1/2} = +0.12 \text{ V}$, 0.033 V , 0.18 V and 0.044 V vs Ag/AgCl, corresponding to the di-anionic complexes to mono-anionic complexes, respectively in MeOH solutions compared to that of $[\text{Ni}(\text{qdt})_2]^{2-}$ ($E_{1/2} = +0.41 \text{ V}$ vs Ag/AgCl) and the concerned CV diagrams are shown in Figure 10. This is probably due to the position of the

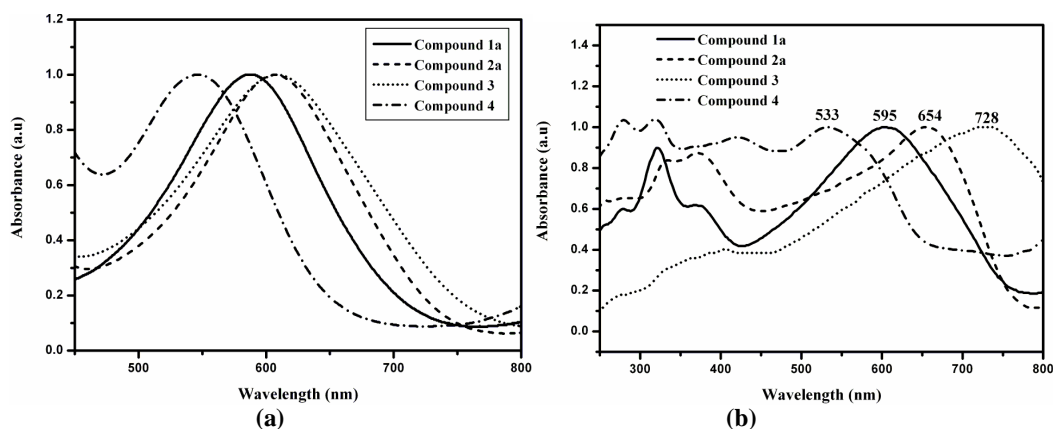


Figure 9. (a) Electronic absorption spectra in solution (MeOH) and (b) diffuse reflectance of solid compounds **1a**, **2a**, **3** and **4**.

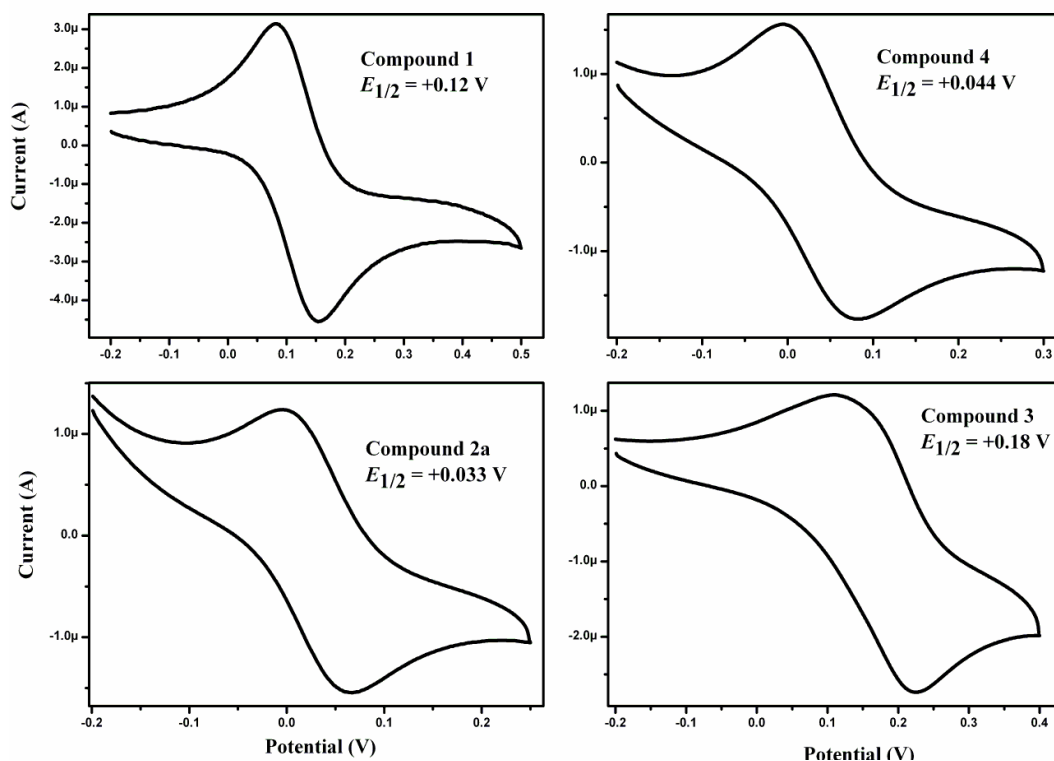


Figure 10. Cyclic voltammograms of compounds **1a**, **2a**, **3** and **4** in MeOH solutions at scan rate 50 mV s⁻¹, V vs Ag/AgCl.

nitrogen atom present in the qdt systems (qdt versus 6,7-qdt), which causes the difference in the withdrawing ability on the electron density in the vicinity of the metal atom. From these results we conclude that the ligand must be participating to a large extent in electron transfer process. In addition to this, [PPh₄]₂[Ni(X₂6,7-qdt)₂] {X = H (**1b**), Ph (**2b**)} complexes also have been described. Compounds **1a**, **1b**, **2b**, **3** and **4** have been

characterized unambiguously by single crystal X-ray structural analysis. The molecular structures of all the compounds exhibit weak C–H...S and C–H...N weak interactions.

Chapter 6

Synthesis of New Intramolecular Charge Transfer A–D–A Tetrathiafulvalene-Fused Triads Exhibiting Large Solvent Sensitive Emission Behavior

Because of the structural similarities between the inorganic “dithiolene” complexes and organic “tetrathiafulvalene” (TTF) molecules, we have aimed to synthesize the TTF fused quinoxaline based systems by introducing the 6,7-quinoxaline dithiolate ligands (described in the previous chapter) to the TTF core. We have synthesized three new acceptor-donor-acceptor (A–D–A) triads incorporating the donor tetrathiafulvalene (TTF) fused with acceptors quinoxaline and dipyrido[3,2-*a*:2',3'-*c*]phenazine (dppz) systems (Figure 11). Solution emission spectral studies of all these compounds show large solvent sensitive behavior with huge Stokes shifts as shown in Figure 12. The large solvent dependence of the emission indicates that the excited state is stabilized in more polar solvents due to the intramolecular charge transfer. Fascinatingly, compound **1b** (structural representation described below) shows color response with polarity of the solvents under UV lamp. The emission light of the compound **1b** varies from green to red with increasing the polarity of the solvent (CCl₄ to DMSO). For example, in the solution of non polar solvent, such as CCl₄, this shows green emission and emission maximum is centered at 532 nm [Figure 12]. In the solution of moderate polar solvent, such as toluene, it shows yellowish emission, and the relevant emission maximum centers at 570 nm. On the other hand, in the solutions of relatively more polar solvents, such as DMF and DMSO, this shows red emission and the emission maxima are centered at 665 nm and 682 nm respectively [Figure 12]. Compound **1b** is additionally characterized by single crystal X-ray crystallography along with IR, NMR spectroscopy including their elemental analysis. Due to the S...S intermolecular contacts (3.710 to 3.731 Å) are between the TTF derivatives of compound **1b** results in the formation of one- dimensional supramolecular chain. We also have described electrochemical studies of one of the title compounds (compound **1b**) exhibiting two oxidation responses at 1.02 V and 1.31 V vs Ag/AgCl, that correspond to the oxidized species of TTF monocation and dication, respectively.

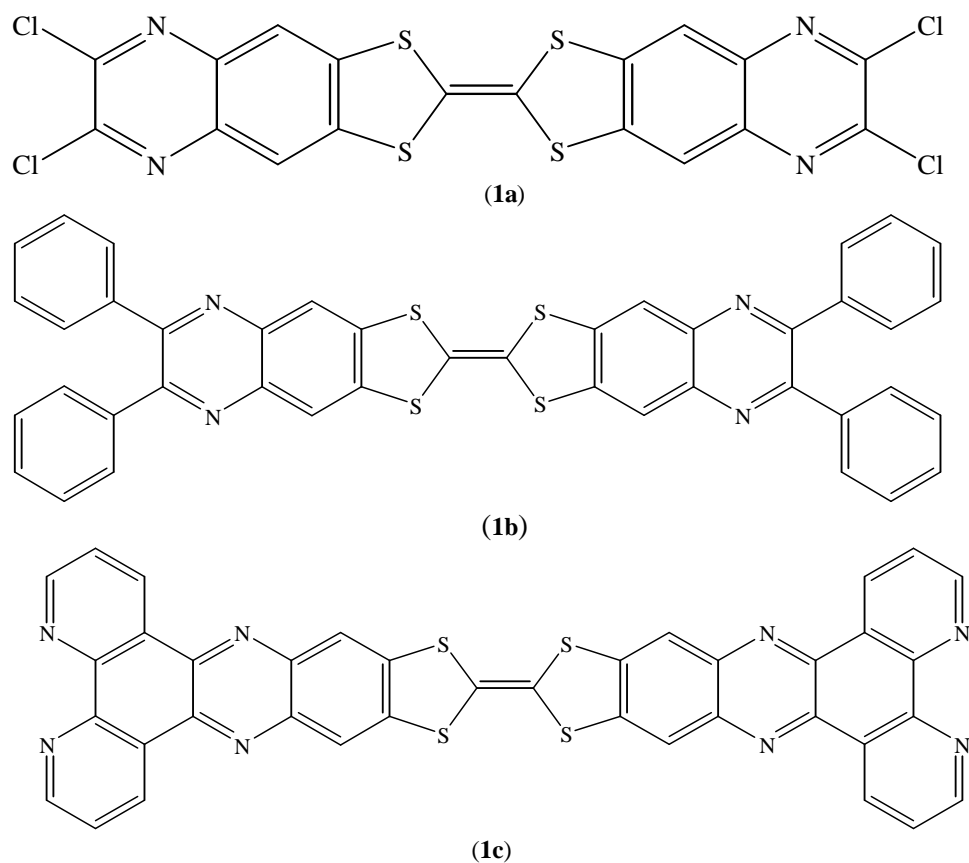


Figure 11. Structural representations of newly synthesized A-D-A TTF triads.

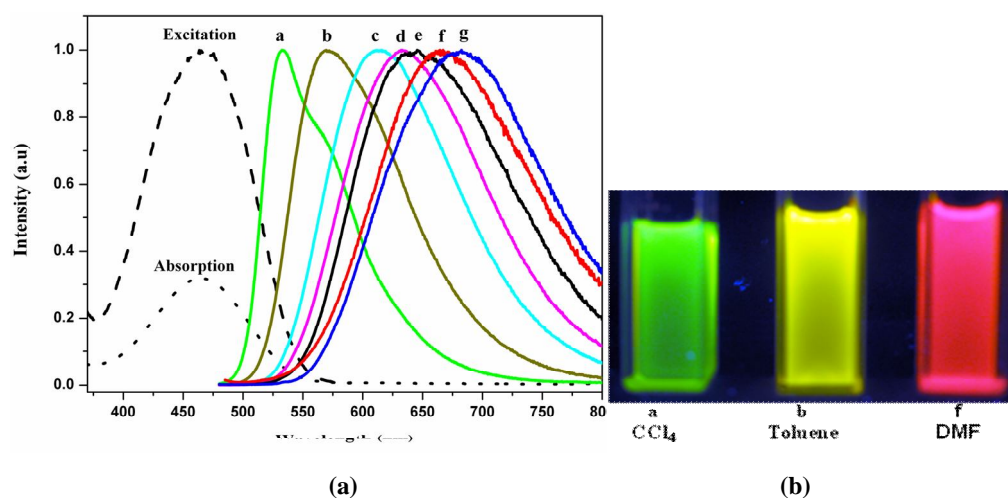


Figure 12. (a) Emission spectra (—, $\lambda_{\text{ex}} = 460$ nm) of the TTF triad (**1b**) in different solvents at room temperature, a) CCl_4 , b) toluene, c) CHCl_3 , d) DCM, e) acetone, f) DMF, g) DMSO, and absorption (---, $\lambda_{\text{em}} = 610$ nm) of **1b** in CHCl_3 (excitation and emission spectra are normalized to 1); (b) color response of compound **1b** with different solvents under UV lamp.

Summary: Future Scope

This part will demonstrate the future scope of this thesis work. In the second chapter of this thesis, we have described the alkali metal ion based coordination polymers of metal bis(dithiolene) complexes, where simply varying the coordination solvents results in the variation of the structural diversities and dimensionalities. This methodology can be extended to Ni(III) ions to prepare coordination polymers, and these Ni(III) coordination polymers will show an interesting conducting and magnetic behavior. We would be able to also extend this to diselenolene complexes. The replacement of sulfur with selenium in the building blocks (metal dithiolene complexes) / tetrathiafulvalenes (TTFs) has been shown to overcome the metal-to-insulator transition, often present in these materials at low temperatures caused by Peierls distortion. The greater spatial extension of Se orbitals compared to S may increase the electronic dimensionality of the system and thus to avoid the undesired transition. In the alkali metal ion based coordination polymers alkali cations would be exchanged by transition metal ions such as Cu(I) ions to get good conducting materials and the work is going on presently in this direction in our laboratory. Currently, the generation of field-effect transistors (FET) is further interest in charge carrying semiconductor materials. Recently, qdt-based systems have been used in the development of field-effect transistors by introducing the fused qdt-based systems to the TTF-skeleton. Based on this, limited reports have been observed in the literature. This would be an interesting area in the synthesis of new TTF-fused derivatives with new heterocyclic based ligands in greater extent. Also N-containing based meta-dithiolene complexes are present in active sites of many metalloenzymes. In this context, particularly qdt (quinoxaline-2,3-dithiolate) ligand and its molybdenum-oxo complexes have been investigated for modeling the active sites of molybdenum hydroxylase enzymes. The newly synthesized ligands 6,7-qdt based ligands, described in the chapter 5, are useful to synthesize the Mo- and W- dithiolene complexes which are related to active sites of many metalloenzymes. The relevant effort has already been underway in our laboratory.

*****End of Synopsis*****